Active Layer Dynamics at Four Borehole Sites in Western Dronning Maud Land, Antarctica

A dissertation submitted in fulfilment of the requirements for the degree of

MASTER OF SCIENCE

of

Rhodes University

by

Camilla Kotzé

December, 2015

Supervisor

Professor K.I. Meiklejohn (Department of Geography, Rhodes University)

Abstract

Permafrost and active layer dynamics in the Antarctic play an important role within terrestrial landscapes and ecosystems and as a climate change indicator. However, they remain less thoroughly researched than their Northern-Hemispheric counterpart. Despite advancements made by ANTPAS on the permafrost and active layer monitoring network in the Antarctic, observational gaps still exist. Western Dronning Maud Land (WDML) has been identified as one of these gaps, necessitating further research on permafrost dynamics and the influence of climate parameters thereon. Such elucidation is critical to both the cryospheric and life sciences. Variations in the surface climate of Antarctica can be seen as a result of inter-annual variations in atmospheric circulation, enhancing permafrost degradation and active layer thickening which directly affects soil processes, such as sorting and cryoturbation. Ground temperatures from four permafrost boreholes from WDML were analysed from 2007 to 2014. The study sites exhibit seasonal freezing, periglacial landforms, and altitudinal variation, ranging between ca. 450masl to ca. 1300masl. Using ground thermal regime and regional climate data, the spatial and temporal variability of the active layer in the Ahlmannryggen and Jutulsessen areas of WDML were characterised. ^{137}Cs tracing has revealed that the active layer and associated landforms have been active over the past half century. Further results show that active layer depths at each site vary inter-annually and are particularly influenced by snow cover, altitude and distance to the ice-shelf. Moreover, a correlation between the SAO (Semi-Annual Oscillation) and measured ground temperatures was found, principally during the transitional season of the SAO in May and September. The relationship between climate and ground thermal regimes, especially the influence of teleconnections thereon, is essential to improving the understanding of permafrost dynamics and landform morphology in continental Antarctica.

Keywords: Antarctic, Western Dronning Maud Land, active layer, ground thermal regime, soil moisture, SAO

Acknowledgements

The author would firstly like to thank her parents and David Cousins for continual support and encouragement throughout her academic career. Thanks and appreciation to Professor Ian Meiklejohn for guidance during the undertaking of this two-year endeavour. Sincerest gratitude is expressed to the NRF (National Research Foundation) whose financial support made the completion of this M.Sc. possible. DEA (Department of Environmental Affair) and SANAP (South African National Antarctic Programme) are thanked for providing logistical support during the fieldwork seasons conducted in the Antarctic. Thanks to SAWS (South African Weather Service) for the provision of data, as well as to the members of the 2009/10, 2010/11, 2011/12, 2012/13, 2013/14, 2013/14 Austral summer relief voyages to SANAE IV that assisted during the fieldwork data collection process. Christel Hansen is especially thanked for her guidance and expertise in the field. Rosie Dwight and Liezel Rudolph are thanked for the provision of some of the data used in this dissertation. Last but not least, Rhodes University is acknowledged for their support throughout the M.Sc. studies.

Table of Contents

Table of Figures

Table of Tables

Table of Equations

List of Abbreviations

3D – Three Dimensional

AAO – Antarctic Oscillation

ACW – Antarctic Circumpolar Wave

ADD – Antarctic Digital Database

AIC – Akaike Information Criterion

Alt. – Altitude

ANTPAS – Antarctic Permafrost and Soils

AP – Antarctic Peninsula

Bh – Direct Normal Radiation

C – Celsius

CALM – Circumpolar Active Layer Monitoring Network

CALM-S – Antarctic Circumpolar Active Layer Monitoring Network

cm –Centimetre

CPT – Circumpolar Trough

Cs – Caesium

D_b – Bulk Density

D_p –Particle Density

DDF – Degree Days of Freezing

DDT – Degree Days of Thaw

DEA – Department of Environmental Affairs

DEM – Digital Elevation Model

DGPS – Differential Global Positioning System

Dh – Diffuse Horizontal Radiation

DJF – December, January, February

DML – Dronning Maud Land

DVDP – Dry Valleys Drilling Project

ESRI – Environmental Systems Research Institute

ENSO – El Niño Southern Oscillation

Ft – Feet

g – gram

Gh – Global Horizontal Radiation

GIS – Geographical Information Systems

GLM – General Linear Model

GMC – Gravimetric Moisture Content

GPS – Global Positioning System

GST- Ground Surface Temperature

GTN-P – Global Terrestrial Network on Permafrost

hPa – Hectopascal

HPGe – Hyper Pure Germanium

IGY – International Geophysical Year

IPA – International Permafrost Association

IPY – International Polar Year

JJA – June, July, August

K – Kelvin

Ka – Kilo-annum (1000 years)

keV – Kiloelectron-volts

L – litres

m – Metres

Ma – Mega-annum (1 000 000 years)

MAAT – Mean Annual Air Temperature

MAGT – Mean Annual Ground Temperature

MAGST – Mean Annual Ground Surface Temperature

MAM – March, April, May

MASL – Metres above sea level

mb – millibar (1 mb = 1 hPa)

MDV – McMurdo Dry Valleys

ml – Millilitre

mm - Millimetre

nf – Freezing N Factor

NH – Northern Hemisphere

NRF – National Research Foundation

NST – Near Surface Temperature

PFTE – Potential Freeze Thaw Events

PPG – Polygonal Patterned Ground

PS – Permafrost Station

PTFE – Polytetrafluoroethylene

s – Standard deviation

SANAE – South African Antarctic Expedition

SANAP – South African National Antarctic Programme

SAWS – South African Weather Service

SCAR – Scientific Committee on Antarctic Research

SAM –Southern Annular Mode

SAO – Semi-Annual Oscillation

SH – Southern Hemisphere

SM – Soil Moisture

SO – Surface Offset

SON – September, October, November

SSA – Specific Surface Area

S_t – Porosity

TAM – Transantarctic Mountains

TDR – Time Domain Reflectometry

TO – Thermal offset

TSI – Thermal Stress Index

TSP – Thermal State of Permafrost

TTOP – Temperature at the top of the Permafrost

UAV – Unmanned Aerial Vehicle

µm – micrometres

VWC – Volumetric Water Content

WDML – Western Dronning Maud Land

w.e. – Water Equivalent

CHAPTER 1: Introduction

1.1. Background, Context and Motivation

A disciplines societal relevance is a measure of its success, which is reflected by the endeavour of Periglacial Geomorphology to understand and contextualise global climate change. Permafrost and ground surface temperature (GST) is fundamental to this as they act as a temperature archive and climate change indicator respectively (French & Thorn, 2006; Guglielmin, 2006). Seasonal and annual variations of GST are recorded by the active layer, which provides an accurate record of present and past changes in surface temperature (Guglielmin, 2004). Therefore, process studies of active layer landforms and monitoring ground temperature profiles in Antarctica is of global significance as it contributes towards obtaining a global perspective on climate-cryosphere interactions. Such research can be used as a proxy for similar periglacial landforms elsewhere, provide foundations for future research on landform-biota interactions, and augment a much broader long-term investigation into periglacial geomorphology and climate change in the Antarctic (Boelhouwers & Hall, 2002; Guglielmin, 2004; Vieira *et al*., 2010). Furthermore, the Southern Hemisphere (SH) permafrost environment differs substantially from the Northern Hemisphere (NH) equivalent, making SH perspectives invaluable to the understanding of driving mechanisms and boundary conditions in permafrost and periglacial processes (Boelhouwers & Hall, 2002). Above all, the fact that permafrost is central to Antarctic terrestrial ecosystem dynamics makes its meticulous characterisation a matter of extreme importance (Vieira *et al*., 2010).

Permafrost is a layer of ground which exists due to extended winters and brief summer thaw period's characteristic of a periglacial environment (French, 2007). The uppermost part of the permafrost that freezes and thaws on an annual basis is known as the active layer (French, 2007). Permafrost has been shown to exist in two primary settings. First is the zone around the poles outside the glacial ice cover, which is a consequence of the negative energy balance generated by the Earths heat and moisture redistribution. It is also known as zonal Arctic or zonal Antarctic permafrost, the latter of which is depicted by black shading in Figure 1 (Bockheim & Hall, 2002; Marchenko & Etzelmuller, 2013). Second are the higher elevations of mountain chains across the world, known as alpine/mountain permafrost (Marchenko & Etzelmuller, 2013). Plateau and marine permafrost also exist (Huggett, 2011).

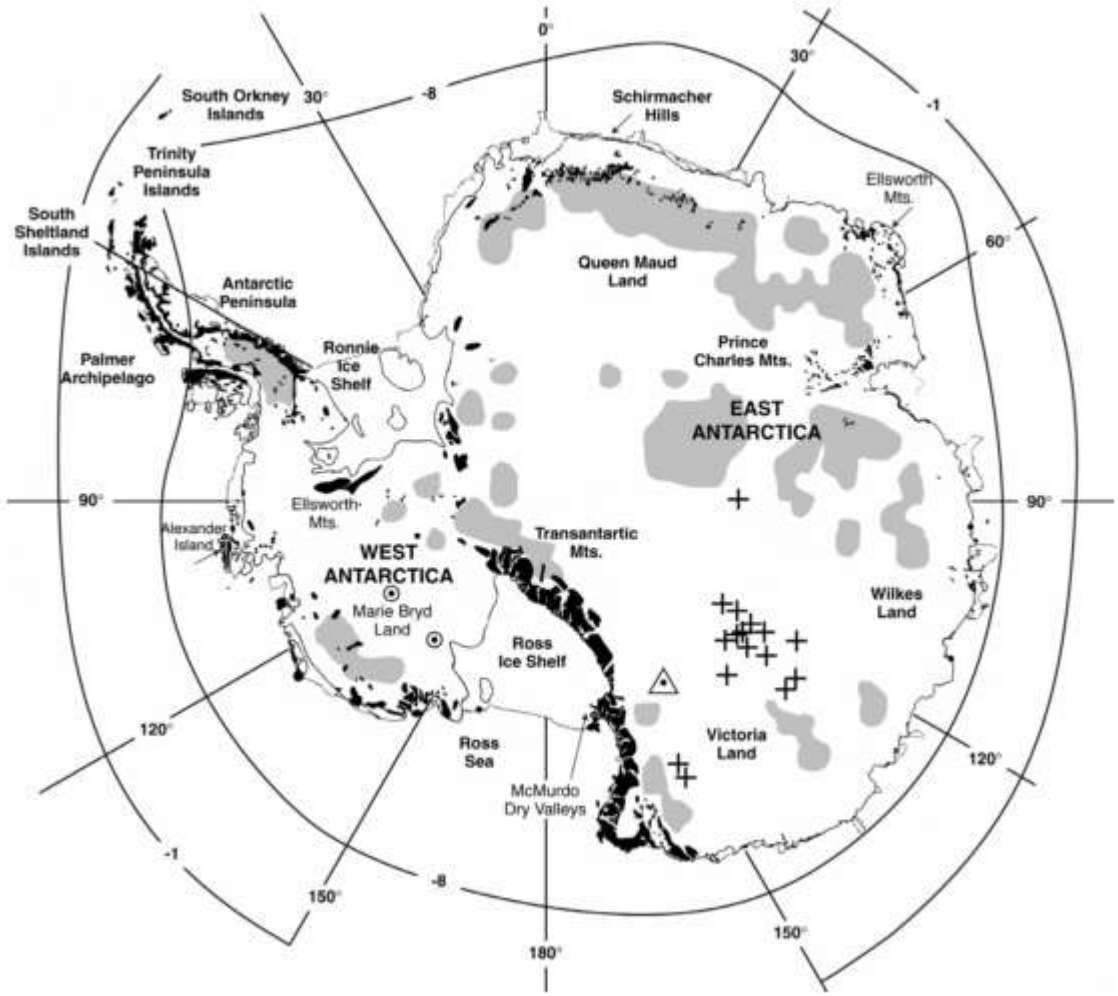

Figure 1: Permafrost distribution in Antarctica (black indicates the existence of permafrost throughout the ice-free areas) (Bockheim & Hall, 2002).

In the 1990's the International Permafrost Association (IPA) established the Global Terrestrial Network for Permafrost (GTN-P), which is currently the primary permafrost and active layer monitoring network (IPA, 2012). The purpose of the GTN-P is to develop a global database of the spatial structure and variability of active layer depth and permafrost temperature (IPA, 2012). Consequently, two supplementary international monitoring networks have been developed by the IPA in cooperation with the Scientific Committee for Antarctic Research (SCAR); the Thermal State of Permafrost (TSP) with the objective of monitoring the long-term thermal state of permafrost in an extensive borehole network, and the Circumpolar Active Layer Monitoring (CALM) network with the goal of monitoring the active layer (IPA, 2012). Over two decades, the IPA through the GTN-P has developed a network of 860 permafrost temperature monitoring boreholes in both hemispheres (Figure 2), a network of more than 200 CALM sites to monitor active layer thickness in both hemispheres (Figure 3), databases and maps providing a snapshot of permafrost temperature and active layer thickness, as well as synthesis papers describing current conditions and recent changes (IPA, 2012).

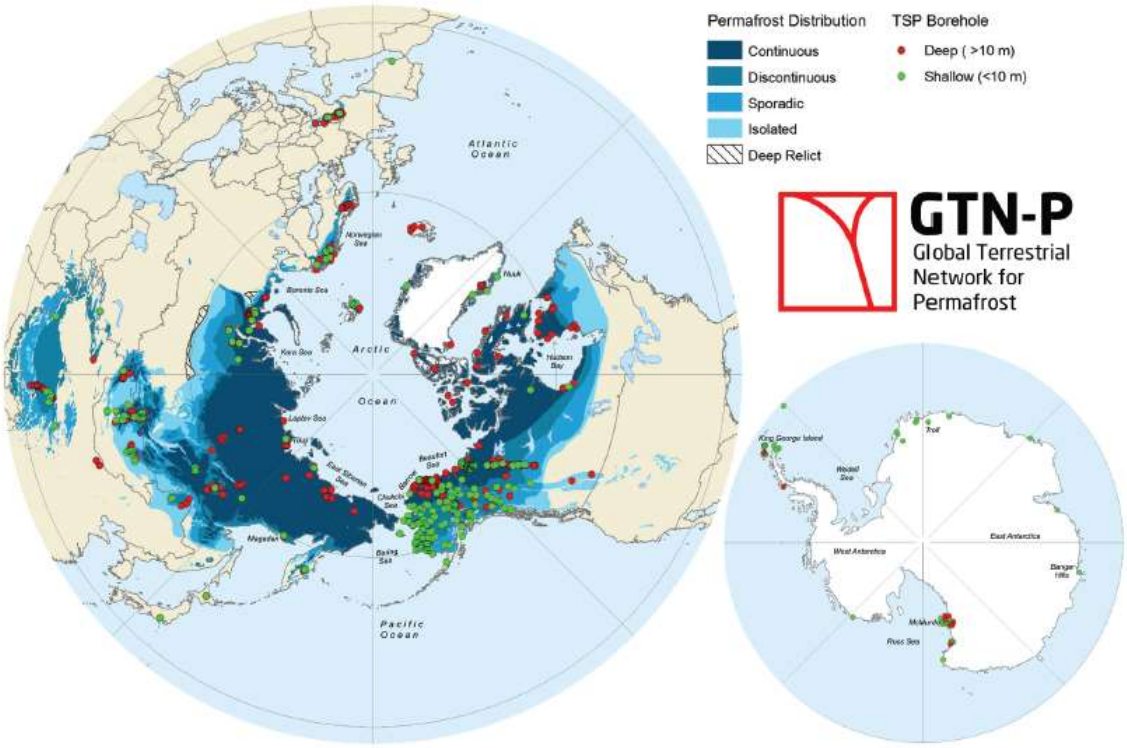

Figure 2: Location of long-term monitoring sites of the TSP in GTN-P (IPA, 2012).

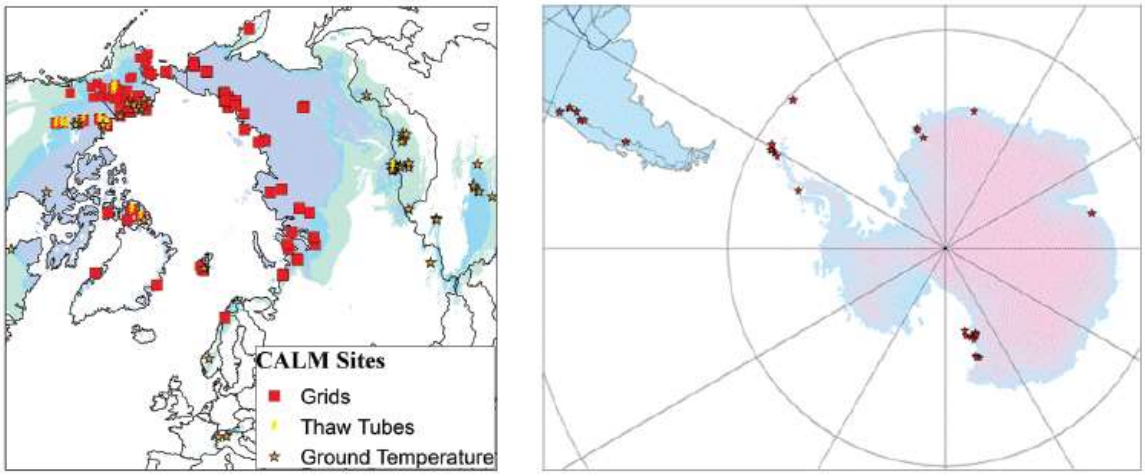

Figure 3: Location of long-term monitoring sites of the CALM network in GTN-P (IPA, 2012).

Both the TSP and CALM networks are predominantly focussed in the circum-Arctic as shown in Figure 2 and Figure 3 (Shiklomanov *et al*., 2008). This is partly a function of it being 'more extensive' (Boelhouwers & Hall, 2002; Bockheim *et al*., 2013). However, this extent is surficial in nature and does not include the potential existence of sub-glacial permafrost in the Antarctic, therefore, permafrost research in the NH can be attributed to other factors such ease of access (French, 2007). Furthermore, human habitation in permafrost areas has generated a need for research into engineering stability solutions and hazard mitigation in response to permafrost warming and active layer thickening (Marchenko & Etzelmüller, 2013).

Various boreholes in the Northern Hemisphere (NH) polar region have been measuring permafrost dynamics over recent decades (Romanovsky *et al*., 2010b); specifically North America (Smith *et al*., 2010), Russia (Romanovsky *et al*., 2010a), and Northern Europe (Christiansen *et al*., 2010). Meanwhile, permafrost research in the Southern hemisphere (SH) has been less systematic and lacks international awareness (Bockheim & Hall, 2002; Vieira *et al*., 2010; Bockheim *et al*., 2013). Permafrost and active layer insight is absent in most of Antarctica, exempting the McMurdo Dry Valleys (MDV) and the maritime Antarctic where some records of ground thermal regimes exist (Ramos *et al*., 2007; Vieira *et al*., 2010).

There are several factors buttressing the dearth of permafrost awareness, knowledge and monitoring in Antarctica. These include the remoteness of Antarctica, which results in logistic and maintenance difficulties (Ramos *et al*., 2008); the fact that glacier and ice-shelve monitoring have until recently taken priority over permafrost and ground thermal regime monitoring (Ramos *et al*., 2007); the limited financial and human resource capacity of SH countries (Boelhouwers & Hall, 2002); permafrost research developing in seclusion from the scientific endeavours and debates of the NH (Boelhouwers & Hall, 2002); the rare advancement of permafrost research through dedicated programmes underpinned by the perception that permafrost and seasonally frozen ground in the circum-Antarctic is absent in the context of the extensive glaciation (Hedding, 2006); and a lack in harmonised efforts to monitor permafrost properties and active layer dynamics external from individual countries and researchers in the vicinity of their own research stations (Vieira *et al*., 2010).

In preparation for the International Polar Year (IPY) 2007-2008, the Antarctic Permafrost and Soils (ANTPAS) project was developed by the IPA and SCAR, with the aim of addressing the research bias and promoting research through a dedicated programme with the integration of existing datasets on permafrost, ground ice, active layer dynamics and soils in Antarctica; and by implementing borehole, active layer, periglacial process and soil monitoring networks as the Antarctic component of the TSP and of the CALM (CALM-S) (Guglielmin, 2006; Ramos *et al*., 2007; Vieira *et al*., 2010; Guglielmin & Vieira, 2014). The TSP monitoring network increased to 73 boreholes at the end of the IPY from a total of 21 in 2004 (Vieira *et al*., 2010). Under the TSP umbrella, the CALM-S network increased from 18 boreholes in 2004 to 28 post IPY. However, due to difficult terrain, the CALM-S network altered its monitoring protocol from the use of 100m grids to the use of smaller grids and shallower boreholes; leading to a lack of standardization as they may or may not include permafrost borehole sites or the monitoring of other environmental parameters (Vieira *et al*., 2010).

Despite advancements on the permafrost and active layer monitoring network made by the IPY project ANTPAS, it has been noted by Viera *et al*. (2010) that observational gaps still exist in most of Antarctica. Dronning Maud Land (DML) has specifically been identified as an area where an increase in permafrost and active layer monitoring efforts are required (Vieira *et al*., 2010). Additionally, more in depth research of the thermal and physical properties of Antarctic permafrost are required, incorporating links to pedogenesis, hydrology, geomorphic dynamics, and response to global change (Vieira *et al*., 2010). The most pertinent to this project are geomorphic processes within the active layer related to ground freezing and thawing dynamics, as well as meteorological influences such as those brought about through teleconnections (French & Thorn, 2006; Marchenko & Etzelmüller, 2013).

This project falls under periglacial geomorphology, a sub-discipline of geomorphology (French & Thorn, 2006). Periglacial geomorphology encompasses geocryology, the combination of which results in studies focussed on perennial and seasonal ground ice processes and landforms, as well as thermal associations of the terrain respectively (French & Thorn, 2006; Berthling *et al*., 2013). According to Berthling *et al*. (2013), the term cryogeomorphology has recently been adopted to define the geomorphology of cold regions. Historically, descriptive and non-quantitative models have been assigned to cold-climate terrain (French & Thorn, 2006). However, the discipline has evolved and is reaching new frontiers with quantitative science and techniques in order to characterize landscapes and landscape change (Murray *et al*., 2009). At the centre lies the monitoring of thermal regimes as periglacial landforms and processes are dependent on cryotic temperatures; this is underpinned by the rapid advance of the permafrost research community (Berthling *et al*., 2013).

Barsch (1993) identified four key study foci within periglacial geomorphology; areas in the vicinity of glacier or snow covered terrain which is governed by a geomorphic relevant frost climate, the climatic conditions influencing landform development, the geomorphic processes, as well as the landforms and sediments created by the geomorphic processes. Therefore, this dissertation encompasses all of the above in order to generate knowledge and understanding of active layer dynamics and landform morphology resulting from seasonal freezing and thawing in a polar desert environment. The focus is on the rocky nunataks of the Ahlmannryggen-Borgmassivet Mountains in Western Dronning Maud Land (WDML), Antarctica (SANAP, 2009). DML is located between 20°W and 45°E in East Antarctica. Chang *et al*. (2015) topographically defined the western part of DML as the area along the grounded ice margin from north of 75°25′S to the Prime Meridian, terminating at the Jutulstraumen ice stream. However, for the purpose of this study, the area up until 3° E of the prime meridian is also included in the definition of WDML.

This dissertation is comprised of six chapters. The current chapter provides a backdrop to the project, details the study area, as well as outlines the aims and objectives. A more comprehensive discussion is given in Chapter 2; Chapter 3 itemises data requirements and adopted methodologies; the findings are analysed and discussed in Chapter 4; Chapter 5 provides a summary of the findings and examines future research avenues as well as limitations to the study; and lastly the dissertation concludes with Chapter 6, which includes a list of reference material used throughout the study.

1.2. Aims and Objectives

This project takes on an investigative approach in line with the Newtonian Paradigm, whereby the landscape is directly observed, measured and interpreted with the aid of numerous statistical analyses (Mikulecky, 2001; Church, 2010). Accompanying a strong empirical framework, a holistic rather than reductionist approach is adopted (Huggett, 2011; Church, 2013). Underpinned by the fact that geomorphology is a system science, this dissertation aims to promote understanding surrounding the relationships between climate, active layer dynamics and associated landforms in coastal East Antarctica. Most importantly, it provides a basis for contributing to and answering the 42nd key question posed by the SCAR Antarctic and Southern Ocean Science Horizon Scan (Kennicutt *et al*., 2014a; 2014b): 'How will permafrost, the active layer and water availability in Antarctic soils and marine sediments change in a warming climate, and what are the effects on ecosystems and biochemical cycles?'. The overall aim may be broken down into four key objectives. These are listed below:

1. To characterize ground thermal and moisture regimes on selected nunataks in WDML.

2. To investigate the relationship between active layer thickness and ground thermal regimes with climate parameters such as pressure, temperature and radiation. As well as to elucidate the role that teleconnections may play thereon.

3. To reveal whether active layer related landforms, such as sorted circles and solifluction terraces, have been active since the 1960's using ^{137}Cs tracing.

4. To reveal the spatial distribution of periglacial features indicative of active layer environments and permafrost such as terraces, mudboils, patterned ground (sorted and unsorted), thermal contraction polygons and rock glaciers.

1.3. Setting and Study Sites

Antarctica is the fifth largest continent, with an area of 14 million km² that doubles in size during winter due to sea ice (Bockheim & Hall, 2002; Huggett, 2011; Turner & Marshall, 2011). It is an ice-bound continental mass, isolated by an extensive cold ocean and the fact that it has had no terrestrial connections with other continents for over 25Ma (Bargagli, 2005; Convey *et al*., 2013). Antarctica has mostly been within the glacial phase of a glacial-interglacial cycle over the last 800 000 years, however, it is currently within an interglacial phase which has resulted in more than 2% of the continent and its islands being snow and ice-free (Bargagli, 2005; Convey *et al*., 2013). Antarctica has also been defined as the driest, windiest, highest, and coldest continent, with the thickest and largest ice sheet (Bockheim & Hall, 2002; Bargagli, 2005; Huggett, 2011; Masson-Delmotte, 2013).

The volume of ice sheet is 30 million km³, which is 80% of the earth's terrestrial water and more than 86% of the world's total ice-area (Hughes, 2013; Masson-Delmotte, 2013). Conversely, the Antarctic atmosphere contains approximately one tenth of the water vapour found in the temperate latitudes (Rafferty, 2011). Cold temperatures and the sinking motion associated with the polar cell results in the dissipation of clouds, which in turn results in a very low average annual precipitation (Bargagli, 2005; Turner *et al*., 2009; Huggett, 2011; Cassano, 2013). According to Bargagli (2005), altitude and precipitation are inversely proportional, therefore, precipitation increases in magnitude from the interior to the coast. Over the polar plateau, an average of only 50mm is received per year. Most precipitates as snow along the continental margin, such as the coastal region of the south-eastern Bellingshausen Sea which receives more than 800mm annually (Bargagli, 2005; Rafferty, 2011). With scarce biota, low temperatures and less than 250mm of annual precipitation, Antarctica has earned the title of the largest cold desert in the world (Bargagli, 2005; Cassano, 2013).

There is a large temperature disparity between the coastal and interior regions, with the coast experiencing just above 0ºC during summer and −15ºC during winter, and the interior experiencing approximately −30°C during summer and −65°C during winter (Cassano, 2013). This can be attributed to the geometry of the sun-earth relationship, effectively the amount of incoming solar radiation received at the Antarctic's surface (Cassano, 2013; Rafferty, 2011). During summer, more than 80% of solar radiation is lost to space in conjunction with the surface emitting long-wave radiation; the result is a net loss of energy from the ground and cooling of the surface (Cassano, 2013). This effect is heightened during winter months when no solar radiation reaches the ground; resulting in the ground cooling the air to the point that a temperature inversion develops whereby temperature increases from the surface to 1000ft (Cassano, 2013; Rafferty, 2011).

The mean annual wind speed in Antarctica varies from approximately 4 to 20m.s^{-1} (Block, 1994). Stations situated at the plateau edge exhibit the highest wind speeds due to katabatic winds, which are a result of cold air near the surface and the sloping terrain characterising most of the continent (Block, 1994; Cassano, 2013). Tectonically, Antarctica has occupied a stable position during the last 100Ma as a result of its distal proximity to plate margins and location within an expanding lithospheric plate (Bargagli, 2005).

The Transantarctic Mountains (TAM) divide Antarctica into East Antarctica, characterized by high elevation and the East Antarctic Ice Sheet, and West Antarctica, which is an archipelago buried by the West Antarctica Ice Sheet (Bockheim & Hall, 2002). For the past 15Ma, Antarctica has been continuously covered by these ice sheets, leaving less than 0.34 % of the underlying rock exposed (including nunataks, cliffs and seasonally snow and ice free areas) (Huggett, 2011; Convey *et al*., 2013; Masson-Delmotte, 2013). Nunataks are mountain peaks protruding from the glaciers, mostly on the continents periphery (Huggett, 2011). According to Bargagli (2005), roughly 330,000km^2 of the Antarctic surface is free of ice and snow during the Austral summer. The western Antarctic Peninsula (AP) contains a decent portion of the ice-free areas and the continent contains the rest in the form of scattered coastal areas, nunataks, and the TAMs steep slopes (Bargagli, 2005). The TAM have the largest ice-free area at 55%, followed by the AP and its offshore islands with 14%, Marie Byrd Land with 12%, Dronning Maud Land with 4.8%, maritime East Antarctica with 4.6%, the Prince Charles Mountains with 4.4%, and lastly the Ellsworth Mountains with 3.1% (Bockheim & Hall, 2002; Turner & Marshall, 2011).

The South African National Antarctic Programmes' (SANAP) base, SANAE IV was opened on the 19th of January 1997 on the Vesleskarvet Nunataks inland of the Princess Martha coast in WDML (Bargagli, 2005; Hansen, 2013; Figure 4). The construction of SANAE IV was preluded by the signing of the Antarctic Treaty on the 1st of December 1959 and the joining of the Scientific Committee on Antarctic Research (SCAR) following the International Geophysical Year (IGY) of 1957-1958, which was a prime contributor to the development of the Antarctic Treaty (Orheim, 2013; Summerhayes, 2013; Walton, 2013). SANAE IV experiences an average minimum and maximum air temperature (recorded between 2009-2014) of –39°C and 4°C respectively. Average ambient air temperatures in the Austral summer (DJF) and Austral winter (JJA) months are –8.6°C and –22.8°C respectively, with a temperature range of 34.5 °C. The weather conditions for Robertskollen and Flårjuven are assumed to be similar to that of Vesleskarvet on account of their close proximity. Temperatures at Robertskollen have, however, been recorded as mild due to its proximity to the coast and altitude (Ryan *et al*., 1989). Troll station (Nonshøgda) experiences a similar mean annual temperature to Vesleskarvet, at –14.3°C (Lee *et al*., 2013).

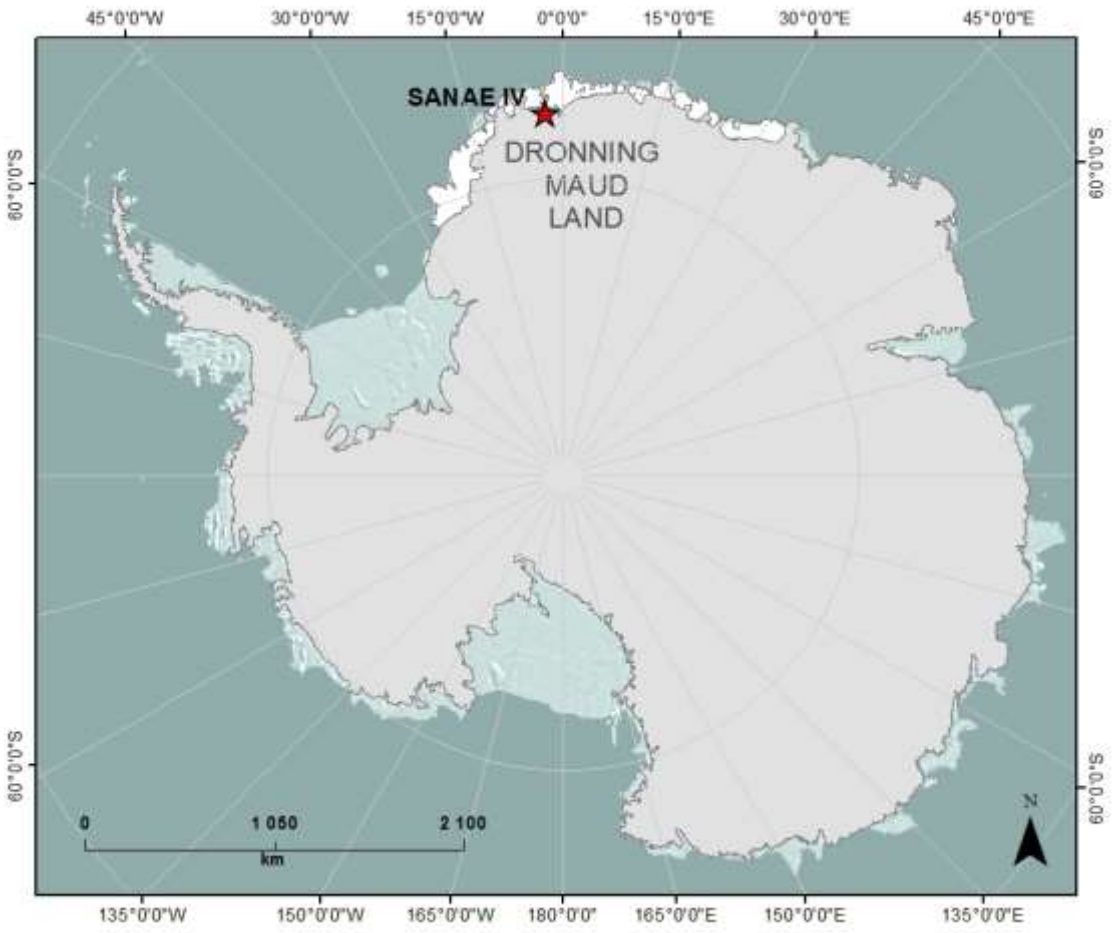

Figure 4: Map of Antarctica showing the location of SANAE IV in Western Dronning Maud Land.

In winter, the air temperature is especially variable, which is a consequence of large meridional and vertical temperature gradients (Kärkäs, 2004). Passing low pressure systems advecting maritime air to the south lead to changes in temperature in conjunction with changes in wind speed and direction (Kärkäs, 2004). The dominant wind direction is from the East, averaging a speed of 11m.s^{-1} (Kärkäs, 2004; Hansen *et al*., 2013). Katabatic winds and those produced by ephemeral eastward travelling cyclones, play a role in the dynamic of the near surface climate (Kärkäs, 2004). Snow is the primary source of precipitation on the DML plateau, originating in the northeast from the Weddell Sea according to Kärkäs (2004). Coastal areas receive 150-200mm water equivalent (w.e.) annually, whilst WDML receives between 55-81mm w.e. annually (Reijmer & van den Broeke, 2001; Hansen, 2013). The mean accumulation rate for WDML, according to medium and deep ice cores studied by Reijmer and van den Broeke (2001), is 62mm w.e. per year. Conversely, Noone *et al*. (1999) have identified the mean accumulation rate as 80-100mm w.e. per year according to short ice core data. The coast is characterised by cyclonic and frontal snowfall which is episodic in nature, whilst snowfall in the high interior originates orographically (Kärkäs, 2004).

As mentioned previously, the areas of investigation in this study are the scattered rocky nunataks situated on the Ahlmannryggen-Borgmassivet Mountains and areas surrounding Robertskollen and Troll Base (Jutulsessen) in WDML (Figure 5; Meiklejohn, 2012; Hansen *et al*., 2013). According to Marshall *et al* (1995), the Ahlmannryggen is a northeast trending ridge flanked by the Jutulstraumen glacier in the east and the Schyttbreen glacier in the west. Due to the northward flow of the glaciers, the nunataks have developed steep northern cliffs and gentle southern slopes via snow build-up (Marshall *et al*., 1995).

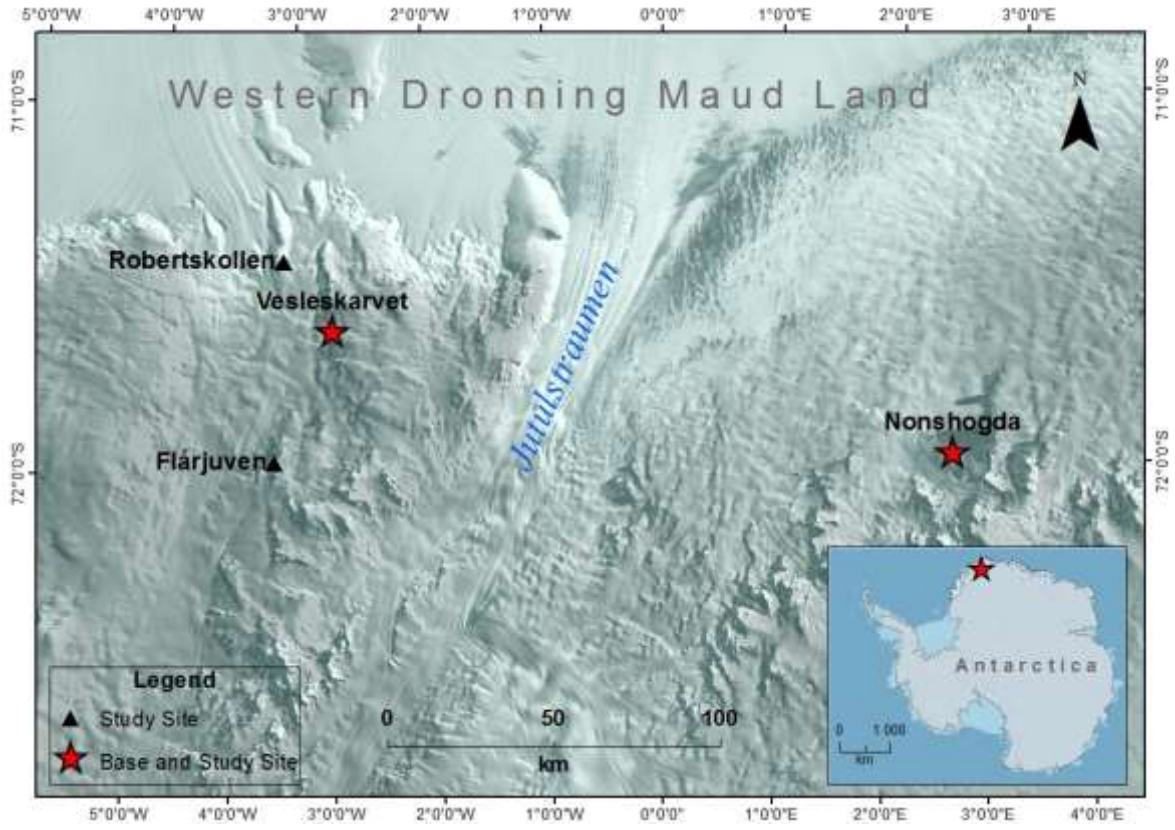

Figure 5: Study sites in Western Dronning Maud Land, Antarctica.

The nunataks belong to the Mesoproteorozoic Ritscherflya Supergroup, which were intruded by the Borgmassivet Suite 1107Ma years ago (Grosch *et al*., 2007). This suite is typified by 400m thick ultramafic, mafic and intermediate sills and dykes (Marshall *et al*., 1995). According to Grosch *et al*. (2007), the mafic sills intruded into the northeastern and southwestern part of the Maud belt approximately 600Ma years ago. The WDML nunataks, particularly Vesleskarvet, are primarily comprised of the homogenous mafic igneous rocks of the Borgmassivet Intrusions (SASCAR, 1984). Robertskollen, however, contains a large amount of meta-olivine gabbronorites and gabbro in both its lower ultramafic unit and overlying mafic unit (Ryan *et al*., 1989; Dwight, 2014). Parts of the Slettfjell nunatak belong to the Schumacherfjellet Formation, which is typified by quartzites and arkoses, interfingered with siliceous siltstone (Meiklejohn, 2012). Jutulsessen, separated from the doleritic and dioritic sills of WDML by the Jutulstraumen glacier, is comprised of high-grade

metamorphic granulite and gneisses. Granitic intrusions began deformation at ca.1000-1200 million years ago under high-grade metamorphic conditions, resulting in gneissosity and migmatization (Dallmann *et al*., 1990).

According to Vieira *et al*. (2010), DML experiences cold permafrost with temperatures as low as −17.88°C on nunataks. In terms of soils, they have a low organic content, are poorly developed, and are predisposed to cryoturbation (Convey *et al*., 2013). Weathering on these nunataks is poorly developed and is dominated by 'frost shattering' according to Marshall *et al*. (1995), which has led to the development of a blocky boulder surface in flat-lying areas. However, the mechanism of frost shattering remains disputed amongst the scientific community, especially in light of other physical weathering processes at play which are often compounded by chemical weathering (Hall, 2013). Hall (2013) elucidates that freeze-thaw weathering not only involves the repeated crossing of a freezing point but is also a consequence of wetting and drying, chemical weathering, thermal stresses, and potentially salt weathering.

Within the study area, a total of four nunataks have been chosen as the central focus of this dissertation; Flårjuven, Robertskollen, Nonshøgda (Troll) and Vesleskarvet. Their main characteristics are outlined in Table 1 with site descriptions below adapted from Meiklejohn (2012) and the SANAP 2012/2013 takeover report (Meiklejohn *et al*., 2014). The sites have been chosen as they spatially represent the study area (WDML) well, and exhibit topographic variation as indicated by the distance to ice-shelf and altitude. Furthermore, cryoturbation within the active layer is one of the main reasons for selecting these nunataks as it produces various types of patterned ground (Hjort & Luoto, 2009). Cryoturbation is the process of soil movement resulting from frost action such as frost heave and sorting, thaw settlement, as well as temperature induced expansion and contraction from temperature changes (Hjort & Luoto, 2009).

Table 1: Study area characteristics.

Study Area	**Coordinates**	**Logging Duration (years)**	**Logger Depth (cm)**	**Altitude (masl)**	**Distance to ice-shelf (km)**
Robertskollen	S 71°29'28.6" W 3°14'03.72"	2013-Present	60	468	120
Vesleskarvet	S 71°40'12.7" W 3°50'32.5"	2009-Present	60	848	140
Flårjuven	S 72°01'26.4" W 3°22'47.6"	2008-Present	60	1278	174
Nonshøgda	S 72°00'40.6" E 2°32'00.2"	2007-Present	200	1283	220

1. *Vesleskarvet:*

   SANAE IV base is situated on the Southern buttress of a flat-topped mountain called Vesleskarvet, which also comprises of a northern buttress where data for this study were collected. It exhibits sorted patterned ground in minor depressions. Since February 2009 to present, the 60cm borehole has recorded data (Figure **6**).

Figure 6: PACE XR5 logger at Vesleskarvet (top left), view of Vesleskarvet nunatak with the Northern and Southern buttress respectively (top right), and a panoramic view of the active layer borehole site on the Northern buttress of Vesleskarvet.

2. *Flårjuven:*

   Flårjuven is one of the most suitable locations for conducting research on active layer dynamics in the entire Ahlmannryggen region as it is characterised by large exposed areas and numerous patterned ground features. It is a flat-topped mountain approximately 44km south-west of Vesleskarvet. The old 60cm borehole logger used in this dissertation has recorded from January 2008 to present (Figure 7), whilst the new 60cm borehole data logger began recording in January 2013.

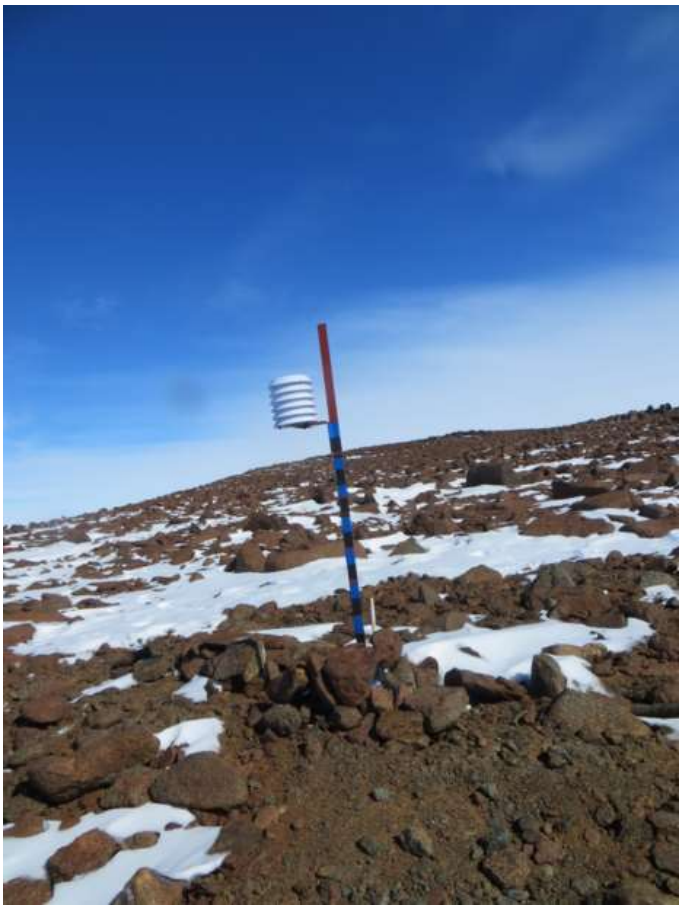

Figure 7: Active layer borehole site at Flårjuven

3. *Robertskollen:*

   Robertskollen is situated approximately 25km Northeast of SANAE IV and is situated around the margin of an ice-rise. It is one of the most northerly outcrops in WDML ranging in altitude and size, between 200masl and 500masl and 100m^2 and 12 5000m^2 respectively (Ryan *et al*., 1989). Robertskollen has substantial geomorphological research potential as it exhibits numerous geomorphological features indicative of active layer dynamics. The presence of sorted patterned ground, unsorted patterned ground, and lobes have been verified. The borehole (60cm) has been logging since January 2013 (Figure 8).

Figure 8: Active layer borehole site (top) at Robertskollen, closer view of the active layer borehole site (bottom left), and the adjacent hillside to the right of the logger (bottom right).

4. Nonshøgda (Troll Station):

Troll lies 190km across the Jutulstraumen glacier, making it the furthest study site from SANAE IV base. It forms part of a coastal mountain chain at between 1000m and 3000m elevation at approximately 200km from the edge of the ice shelf (Dallmann *et al*., 1990) Within this study area, large areas of non-sorted polygons dominate due to contraction of the ground during freezing events which resulted in cracks in the permafrost (Lee *et al*., 2013). According to Bockheim *et al*. (2013), infiltrating sands into the cracks may broaden and deepen them as repeated expansion-contraction takes place. The diameters of the polygons at Troll range from 5m to 30m in diameter, bordered by cracks which are almost as deep as they are wide, measuring 0.1m to 0.3m and 0.1m to 0.5m respectively (Lee *et al*, 2013). Dallmann *et al*. (1990) has documented patterned ground, particularly stone pits, at a general slope angle of 15° and below. The old 2m borehole used in this dissertation has been logging data since February 2007 until present (S72°00'40.6", E2°32'00.2", alt. 1283m) (Figure 9). Whilst a new 2m borehole (S72°00'39.66", E2°31'28.8", alt. 1290m) has been logging data from January 2013 on account of a hut that was placed too close to the previous logger. However, data from the old logging site has proven to be reliable.

Figure 9: Zoomed out (left; logger circled in yellow) and zoomed in (right) view of the active layer borehole site at Nonshøgda.

CHAPTER 2: Literature Review

The following chapter is divided into four parts. First, progress and the current state of permafrost and active layer monitoring sites which are obtained from Viera *et al*. (2010), unless otherwise stated. Second, the occurrence and properties of permafrost and the active layer in the Transantarctic Mountains (TAM), Antarctic Peninsula (AP), and East Antarctica which encompasses WDML. Third, surface manifestations of permafrost in WDML will be discussed. Last, teleconnections and subsequent meteorological influences on the study area are provided.

2.1. Progress and Current Status of TSP and CALM-S Sites

The Antarctic permafrost borehole network has grown considerably since the haphazard ground thermal monitoring of the 1960's. The IPY (2007-2008) being the main driver, increased the spatial coverage of the borehole network from 21 sites in 2004 to 73 by 2009. Of the 73 sites, 39 are permafrost boreholes and 34 are CALM-S boreholes, of which 6 were recorded inactive by Vieira *et al*. (2010). CALM-S sites are responsible for recording spatial variation with depth and temperature in the active layer in relation to various environmental factors. According to Viera *et al*. (2010), the TAM have the most CALM-S sites at 15, followed by the AP with eight, DML with four and one in the Vestfold Hills. The eight regions of Antarctica relevant to active layer research can be seen in Figure 10 (Vieira *et al*., 2010).

It has been estimated that the Transantarctic Mountains (TAM) contain approximately half of the 0.33% (46000km^2) of bare ground in Antarctica, with the MDV hosting the most (6000km^2). The rest of the ice-free areas in the TAM are dispersed between coastal areas and valley heads spanning 2500km across Antarctica from Northern Victoria Land to the Pensacola Mountains (Campbell & Claridge, 2006). Subsequently, the TAM has the longest record of systematic permafrost research, beginning in the early 1970's with the establishment of the Dry Valley Drilling Project (DVDP). The record was further solidified with the installation of a permafrost borehole network in 1999. Additionally, it has one of the most extensive networks as most boreholes were installed pre-IPY. It currently possesses 23 boreholes; 11 active and 5 inactive CALM-S boreholes, as well as 7 permafrost boreholes. Majority of the work in the TAM is concentrated on monitoring the position of the permafrost table, as well as meteorological factors such as air temperature, relative humidity, wind speed and direction. Solar radiation, soil moisture and snow thickness are also measured at a few sites in the TAM. Significant work has been done by Adlam *et al*. (2010), Bockheim *et al*. (2007), Campbell and Claridge (2006), and McLeod *et al*. (2008).

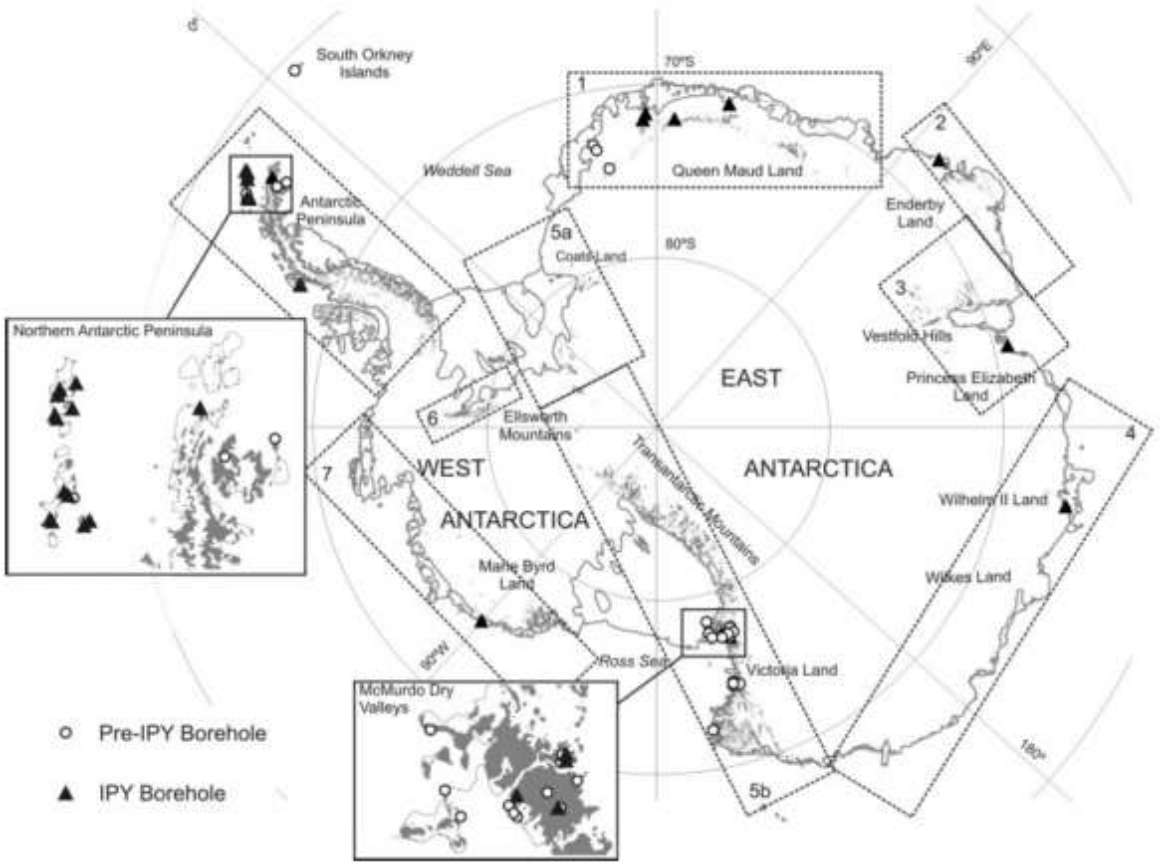

Figure 10: Antarctic permafrost monitoring boreholes (pre-IPY and IPY installations) in relation to Antarctic regions (Vieira *et al*., 2010).

On account of receiving a greater focus during the IPY, the Antarctic Peninsula (AP) has the largest borehole network in the Antarctic as evidenced by the expansion from five to 39 boreholes. The network consists of 16 CALM-S borehole (15 active and one inactive), as well as 23 permafrost boreholes which are largely situated in the South Shetland Islands, markedly on Deception Island where shallow boreholes and mechanical probing have been implemented in the pyroclastic terrain and sedimentary infills. Boreholes on the eastern coast and interior of the AP are absent. With focus centralized around the AP and TAM during the IPY, the Vestfold Hills received a single CALM-S, whereas Enderby Land and Wilkes Land received their first and only permafrost borehole. Additionally, Marie Byrd Land currently has two permafrost boreholes, one of which was received during the IPY.

Ground temperatures in DML are currently monitored on the Basen, Flårjuven, Grunehogna, Novolozarevskaya, Robertskollen, Schumacherfjellet, Slettfjell, Troll, Valterkulten and Vesleskarvet nunataks. The Basen and Troll nunataks have been monitored the longest, since 2004 and 2007 respectively. Collaboration between Sweden and South Africa during the IPY led to the installation of an additional borehole at Vesleskarvet, and new boreholes at Troll and Flårjuven. The Russian Antarctic programme also drove the installation of a new borehole at

Novolozarevskaya during the IPY, which is also the only formal CALM-S site in DML. It is apparent that installation procedures are not standardized on account of logistic and terrain constraints. The outcomes of which include the combination of a CALM-S site with a permafrost borehole site, a permafrost borehole site being installed without CALM-S grids, or the installation of an active layer borehole without the monitoring of other environmental parameters.

During the 2012/2013 Antarctic take-over, 60cm active layer boreholes were installed on seven nunataks in DML (Meiklejohn, 2012). Valterkulten, Slettfjell, Schumacherfjellet, Grunehogna, and Robertskollen received their first and only shallow active layer borehole, whilst Nonshøgda (Troll) and Flårjuven each received a 60cm active layer borehole to accompany the boreholes installed during the IPY. Overall, DML has a total of 10 loggers on 8 nunataks (Troll, Flårjuven, Valterkulten, Slettfjell, Schumacherfjellet, Grunehogna, Robertskollen and Vesleskarvet). Other boreholes that exist in DML are based on the Fossilryggen and Svea nunataks, however, they are currently inactive (Vieira *et al*., 2010). The scope of this project will include the comparative analysis of four nunataks (Vesleskarvet, Robertskollen, Flårjuven and Troll (Nonshøgda)), selected according to topographical, geological, and climatological heterogeneity.

2.2. Active Layer and Permafrost Occurrence and Properties

Huggett (2011) provides the modern-day definition of periglacial, whereby proximity to a glacier is disregarded and a wider range of cold, non-glacial conditions are embraced, characterised by intense frosts during winter and snow-free ground during summer months (Huggett, 2011). According to Barsch (1993, pg.142), "periglacial is accepted as the term to name special processes, landforms and environments under cold climates in the high latitudes and altitudes". French (2007) identified permafrost and ground freezing/thawing as the key physiognomies of a periglacial environment whereby frost action and pre-sort-related processes dominate. Furthermore, he thermally defined the periglacial domain as regions where the mean annual air temperature (MAAT) is less than 3ºC; which was further split into periglacial environments where frost action dominates with a MAAT of less than –2ºC (such is the case with Antarctica), and those where frost action is present but not dominant with a MAAT between –2 ºC and 3ºC (French, 2007).

Permafrost is also thermally defined such that formation takes place when the ground is subjected to a negative energy budget at the surface and the mean annual ground surface temperature (MAGST) remains below 0ºC for two consecutive summers (Riseborough *et al*., 2008; Rafferty, 2011; Marchenko & Etzelmüller, 2013). According to Marchenko and Etzelmüller (2013), the global permafrost distribution is an outcome of two circumstances. The first of which was the cryogenic development of the Earth's crust over the last 2 million years (Late Eo-Pleistocene,

Pleistocene, and Holocene), which provided the basis for present permafrost conditions. The second being the energy balance at the ground surface and the thermo-physical properties of the ground. The energy balance is influenced by local controls on the environment, such as solar radiation, air temperature, topography, bodies of water, the interior heat of the earth, soil moisture, hydrology, glacial and snow cover, sediment properties, age of the geomorphic surface, vegetation, and climate (Bockheim & Hall, 2002; Turner *et al*., 2009; Marchenko & Etzelmüller, 2013).

The environmental factors listed above also influence permafrost thickness which too is a consequence of the thermal balance, reliant on the MAAT and geothermal gradient which generally increases by 1ºC for every 30-60m of depth (Rafferty, 2011). According to Guglielmin *et al*. (2011), climate variations at different time scales induce certain responses in the permafrost and active layer thermal regime. The first of which is on a seasonal level with fluctuations of air temperature around the mean annual ground temperature (MAGT) from winter to summer, reflected in the upper few metres of the ground which diminish with depth (Figure 11). Almost immediately below, lies the level of zero annual amplitude where temperature fluctuations have reached a thermal equilibrium (maximum depth of annual variation) (Williams & Smith, 1989; Rafferty, 2011; Figure 11). Lastly, from years to millennia at progressively greater depth. Therefore, it is clear that permafrost distribution and thickness is ruled by energy exchange dynamics at the earth's atmosphere–land surface boundary, and is regulated strongly by global climatic conditions (Marchenko & Etzelmüller, 2013).

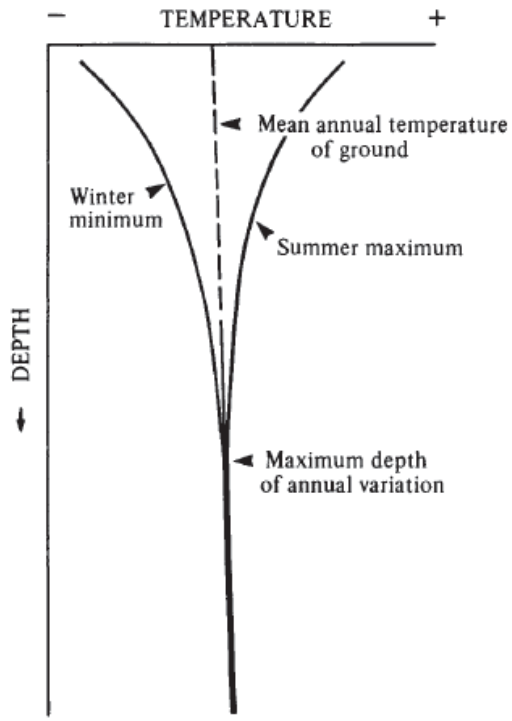

Figure 11: Diagram showing summer maxima and winter minima about the mean annual ground temperature as a function of depth (Williams & Smith, 1989).

Continuous and discontinuous zones of permafrost exist in periglacial environments, underlying as more than 22% of the Earth's land surface (Huggett, 2011; Rafferty, 2011). Permafrost is surficially less extensive in the Antarctic compared to the Arctic due to the presence of large ice sheets (Turner *et al*., 2009). Nine tenths of the world's glacial ice and 37% of the world's permafrost is found in Antarctica (Bockheim & Hall, 2002). However, permafrost only occupies 0.36% (49,800km^2) of the Antarctic region and is pervasive throughout ice-free terrain on both the continent and offshore islands, as well as under most active layer sites with the exception of low maritime elevations and sub-Antarctic islands (Bockheim, 1995; Vieira *et al*., 2010; Guglielmin & Cannone, 2012). Permafrost grows by freezing from the ground surface downward, resulting in the transition of soil moisture to ice (ice-cemented permafrost) or soils into the frozen state where soil moisture is lacking (dry permafrost) (Bockheim & Hall, 2002; Marchenko & Etzelmüller, 2013). The level of how moist or dry permafrost is determined by the chemical composition (dissolved mineral salts) of the water and the depression of the freezing point by capillary forces (Barry & Yew Gan, 2011; Rafferty, 2011). A zero curtain effect is created during freezing through the release of latent heat, leading to the stabilization of ground close to 0°C (Barry & Yew Gan, 2011).

According to Bockheim and Hall (2002), the Antarctic Peninsula and maritime East Antarctica are the only areas relevant to the concept of an active layer as the rest of Antarctica, predominantly the interior, contains dry permafrost. Dry permafrost has a gravimetric moisture content of 3% and lower, whereas ice-bonded permafrost averages 40% (Bockheim, 2002; Campbell & Claridge, 2006; Bockheim *et al.*, 2007; Turner *et al*., 2009). In order for ice-cementation to occur in coarse-textured sediments, a minimum gravimetric moisture content of 5-7% is required (Bockheim & Hall, 2002; Campbell & Claridge, 2006; Rafferty, 2011). Bockheim and Hall (2002) and Bockheim *et al*. (2007) indicated that dry permafrost may be unique to Antarctica as it has not been reported in the NH. This makes it difficult to characterize SH permafrost environments as it cannot be compared with the NH equivalent which experiences ice-bonded permafrost, additionally frost processes in the circum-Antarctic could be very different to those in the circum-Arctic (Boelhowers & Hall, 2002). The nature, occurrence, and origin of dry permafrost in Antarctica are explored by Bockheim and Tarnocai (1998a). Marchenko and Etzelmüller (2011) point out that Antarctica is dominated by cold permafrost conditions (< −10ºC), except for the AP which is characterised by a more maritime climate and therefore warmer permafrost temperatures surrounding 0ºC. At low elevations in the South Shetland Islands, permafrost temperatures are slightly below 0ºC and decrease with height. At 270masl and at 25m depth, permafrost has a temperature of −1.8ºC (Vieira *et al*., 2010; Guglielmin, 2012). Thermophysical properties also play a role in permafrost distribution, such as on Deception Island where ice-rich permafrost is found down to sea level as a result of the high insulation provided by volcanic-sedimentary substratum (Vieira *et al*., 2010).

Victoria Land exhibits permafrost temperatures between −14ºC and −24ºC. Higher temperatures are associated with Northern Victoria Land and coastal sites, whilst lower temperatures are associated with the MDVs and the Ross Sea region (Vieira *et al*., 2010). For example a permafrost temperature of −1.8°C was recorded at Wright Valley (Guglielmin, 2012). Novolozarevskaya and Troll Station in DML experiences permafrost temperatures of −8.3ºC and −17.8ºC respectively, with elevation accounting for the large difference in temperature between the two. In Enderby Land, a permafrost temperature of −9.8ºC was recorded, whereas a temperature of −8.5ºC was documented for the Vestfold Hills which is similar to coastal temperatures in DML. Lastly, Marie Byrd Land exhibited a permafrost temperature of −10.48ºC (Vieira *et al*., 2010).

Permafrost thickness ranges from 100m to 1km in continental Antarctica according to Bockheim (1995) and from 240m to 900m thick according to Turner *et al*. (2009). It has been suggested that Antarctic permafrost developed approximately 40 million years ago following the final breakup of Gondwana and the initiation of glaciers at the Eocene-Oligocene boundary which is why it is able to reach depths of up to 1km (Turner *et al*., 2009). According to Vieira *et al*. (2010), the thickness of permafrost in the TAM varies between 250m to 970m. The McMurdo Dry Valleys experience thicknesses between 240m to 970m overlain by a shallow active layer (10-70cm), whereas North Victoria Land experiences a range between 400m to 900m (Turner *et al*., 2009; Ball *et al*., 2011). The South Shetland Islands experience sporadic permafrost that is on average continuous above 100-150masl whilst lower down it becomes discontinuous (Turner *et al*., 2009). Seymour and James Ross Island on the northeastern section of the Antarctic Peninsula experience an elevation dependent permafrost thickness which ranges from 15m to 180m (Turner *et al*., 2009).

The TAM exhibit ice-cemented permafrost, dry permafrost, permafrost intermediate between ice-cemented and dry permafrost, saline permafrost, and permafrost underlain by thermally heated ground in volcanic regions (Campbell & Claridge, 2006). Ice-cemented permafrost is characterised by hard ice bonded permafrost overlain by an active layer of variable depth. It is abundant on younger land surfaces, particularly near the coast where the ice content is the greatest (Campbell & Claridge, 2006). At the coast, ice-bonded permafrost was found to have a mean gravimetric water content of approximately 40%, whereas a value of 34% was recorded in ice-bonded permafrost at higher coastal elevation sites (Campbell & Claridge, 2006). Dry permafrost has a very low water content ranging from 0.5% to 5%, which is consequential of the xerous climate and pre-late Quaternary (>115ka) sediments with which it is predominantly associated (Bockheim & Hall, 2002; Campbell & Claridge, 2006; Bockheim *et al*., 2007). Dry permafrost occupies 43% of the MDV, ice-cemented permafrost occupies 55%, and the remaining 2% is occupied by ground and buried ice (Bockheim *et al*., 2007). Overall, permafrost in the TAM is significantly influenced by the environment and age of the land surface (Campbell & Claridge, 2006).

Over the last half century, increasing air temperatures have led to the disappearance of permafrost sites on the Antarctic Peninsula (AP). The mean annual air temperature and mid-winter temperature along the western AP have increased by 3.4°C and 6.0°C respectively, making the AP a climate warming hotspot (Turner *et al.*, 2009; Bockheim *et al*., 2013). Permafrost depths reached 25m to 35m in ice-free areas near Palmer Station before 1980, now permafrost is absent in the upper 14m of the highest ice-free areas (Bockheim *et al*., 2013). Thermokarst features such as active layer detachment slides and debris flows are present in places such as the South Shetland Islands due to permafrost thawing and increasing active layer thickness (Bockheim *et al*., 2013). The AP has also been the focal point of investigating the relationship between vegetation and permafrost, specifically the influence of vegetation on the ground thermal regime and active layer thickness (Guglielmin *et al*., 2008).

Temperature, thickness, structure, and active layer thickness are the main countenances of permafrost (Marchenko & Etzelmüller, 2013). The active layer has been defined by Muller (1947), as cited by Burn (1998, pg.411), as the 'layer of ground above permafrost which thaws in summer and freezes in winter'. The suprapermafrost layer contains the active layer, named on account of the fact that it is the most active part in an Antarctic landscape. It is host to majority of biological and hydrological processes, and can be likened to membrane which allows the exchange of heat, moisture and gas between the atmospheric and terrestrial components of the Antarctic landscape (Barsch, 1993; Anisimov *et al*., 2001; Huggett, 2011).

The MAGT decreases with depth in the active layer due to the fact that thawed soils have a lower thermal conductivity than frozen soils (Marchenko & Etzelmüller, 2013). In Antarctica seasonal thawing is at a maximum in early February (Turner *et al*., 2009). Between November and February, the active layer in the Northern Foothills reaches depths between 20cm to100cm (French & Guglielmin, 2000). The depth of an active layer varies between 10cm and 3m and is thicker in well-drained gravels compared to well-drained organic sediment (Huggett, 2011; Rafferty, 2011). Continental Antarctica exhibits an active layer that ranges from 20cm to 70cm, whereas coastal sites are typified by higher values at > 90cm and high elevation sites are characterized by lower values at <10cm (Vieira *et al*., 2010). The Antarctic Islands active layer ranges between 40cm and 150cm (Vieira *et al*., 2010; Tuner & Marshall, 2011). The thickness of the active layer in Maritime East Antarctica ranges from 60cm to 150cm, however, this may be an overestimation due to the presence of dry permafrost (Bockheim & Hall (2002).

Long-term records of active layer thickness are rare, nevertheless, the existing records have shown variations within the active layer on multiple temporal scales which are regulated by climatic trends and local conditions at the surface and in the substrate (Anisimov *et al*., 2001; Turner *et al*., 2009; Guglielmin *et al*., 2011). Thickness and thermal regimes have been the centre focus of active layer

studies in the Antarctic, particularly the influence of air temperature (Ramos & Vieira, 2003; Guglielmin, 2004; Cannone *et al.*, 2006; Conovitz *et al*., 2006; Guglielmin, 2006; Bockheim *et al*., 2007; Ramos *et al*., 2007; Ramos *et al*., 2008; Adlam *et al*., 2010; Guglielmin *et al*., 2011; Guglielmin *et al*., 2012). Several other factors also impact on the thickness of the active layer, such as vegetation type and density (Cannone *et al*., 2006; Guglielmin *et al*., 2008; Cannone & Guglielmin, 2009; Guglielmin *et al*., 2012; Almeida *et al*., 2014), snow-cover (Guglielmin, 2004; Guglielmin, 2006; Guglielmin *et al*., 2011; Guglielmin & Cannone, 2012; de Pablo *et al*., 2013), thermal properties of the substrate (de Pablo *et al*., 2013), incoming radiation (Adlam *et al*., 2010; Guglielmin & Cannone, 2012), and moisture content (Ikard *et al*., 2009; Seybold *et al.*, 2010; Michel *et al.*, 2012). Summaries of active layer research in Antarctica have been provided by several authors (Bockheim & Hall, 2002; Vieira *et al*., 2010; Guglielmin, 2012; Guglielmin & Vieira, 2014). Active layer research has only taken place on the Antarctic Peninsula and the Transantarctic Mountains (particularly Victoria Land and the McMurdo Dry Valleys), leaving observational gaps throughout the rest of the continent, including WDML.

Daily fluctuations in active layer thickness hinge on diurnal temperatures and other external factors such as cloud cover, vegetation, and snow as they affect the vertical temperature profile (Bockheim & Hall, 2002; Guglielmin, 2012). For instance, temperature gradients in the active layer profile are greatest during cloud-free days (Bockheim & Hall 2002). According to Guglielmin (2012), the effects of micromorphology on active layer thickness have been uncovered by several authors (Cannone *et al*., 2006; Guglielmin, 2006; Guglielmin *et al*., 2008; Cannone and Guglielmin, 2009, 2012). In the TAM, the effects of microclimate on active layer depths are apparent according to Bockheim *et al*. (2007). The depth of the active layer varies from 45cm to 70cm in coastal areas, 20cm to 45cm in interior valleys, and <20cm along the polar plateau (Bockheim *et al*., 2007). It has also been found that diurnal variations in temperature are a lot less pronounced at lower elevation sites compared with higher elevation sites. Therefore, active layer thickness is indirectly proportional to elevation as well as diurnal temperature variations (Campbell & Claridge, 2006).

The active layer is strongly linked to fluctuations in air temperature, especially during the summer season (Bockheim *et al*., 2007; Turner *et al*., 2009). Marble Point provides a strong case for this as active layer thickness doubled from 30cm in 2001 to 60cm in 2002 due to the combined result of anomalously high summer temperatures and flooding (Turner *et al*., 2009). Snow-cover, surface albedo and solar radiation have also been identified as drivers of variability in active layer depth in the TAM, however, more on a local scale (Guglielmin & Vieira, 2014). Three years (1997-1999) of active layer monitoring at Boulder Clay in Northern Victoria Land presented by Guglielmin (2004) revealed large variations in summer temperatures, a lacking zero curtain effect, and most importantly a strong correlation between air temperature fluctuations and active layer variations.

Additionally, the GST was found to be lower than air temperature during summer and often during winter, which has been attributed to the buffering effect of snow which prevents heating when warmer sea air reaches the continent (Guglielmin, 2004; Guglielmin, 2006). During the summer of 2002/03, the GST of snow free areas showed significant variability with recordings between 4.8°C and 17.7ºC. However, the GST of snow-covered areas remained constantly below 0ºC (Guglielmin, 2006). For the past decade and a half, Boulder Clay has been experiencing a 0.3cm increase in the active layer per year as a result of increasing solar radiation, despite stable annual and summer mean air temperatures (Guglielmin & Vieira, 2014). Conversely, temperature at the permafrost table is decreasing by 0.1ºC per year in relation to decreasing air temperature and snow cover in winter (Turner *et al*., 2009).

The active layer is host to numerous frost processes, a consequence of changes in the thermal properties of soil due to seasonal freezing and thawing cycles (French & Thorn, 2006; French, 2007; Marchenko & Etzelmüller, 2013). These processes involve cryotubation, frost creep, solifluction, and particle-size sorting which give rise to geomorphic features such patterned ground and viscous flow features (French, 2007).

2.3. Surface Manifestations of Permafrost and the Active Layer

2.3.1. Patterned Ground

According to majority of the literature, when the air temperature drops below 0ºC, ground freezing occurs along a freezing front from the area of maximum energy loss in the presence of soil and water, producing geometric patterns on the ground (Warburton, 2013). However, as mentioned earlier, the depression of the freezing point is underpinned by the chemical composition of the water which does not necessarily coincide with the 0°C isotherm (French, 2007). Slope, sorting, and patterning processes are essential to the formation of patterned ground as seen in the Venn diagram in Figure 12 (Warburton, 2013).

Circles and mudboils are the most common features of the active layer, whilst polygons and stripes are associated with seasonally frozen ground (French, 2007). Circles, polygons, stone nets, and stripes are common in periglacial environments due to seasonal freezing and thawing (Huggett, 2011; Rafferty, 2011). They can occur in sorted or unsorted forms, generally with a relief ranging from 10cm to 30cm and dimensions of 1m to 2m (Barry & Yew Gan, 2011). According to Barry and Yew Gan (2011), sorting is a consequence of frost heave, fine particle migration and mechanical processes under the influence of gravity. The morphometry and distribution of sorted ground is dependent on frost susceptibility according to Feuillet *et al*. (2012), which in turn is a factor of thermal conductivity, water content, microtopography, hydrostatic pressure, and regolith texture.

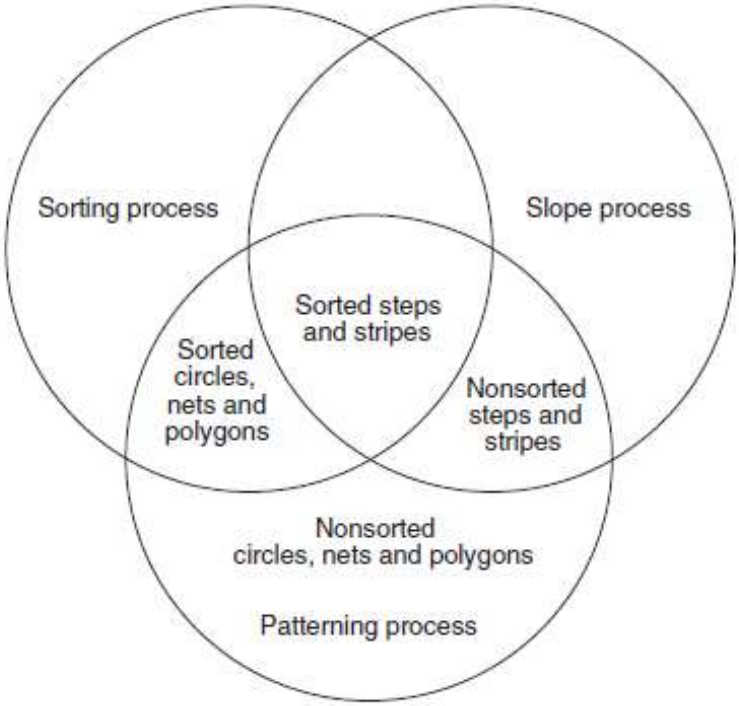

Figure 12: Venn diagram indicating the linkages between sorting, slope and patterning processes in patterned ground formation (Warburton, 2013, pg.302).

French (2007) credited cryoturbation as the responsible mechanism for producing circular forms of patterned ground, non-sorted circles being the most abundant. They have been recorded to reach half a metre in height and alternate between 0.5m to 3m in diameter (French, 2007). Cryoturbation is a process involving all soil movements owing to frost action/freeze-thaw processes (Bockheim & Tarnocai, 1998b). Accordingly, it is most common in fine-grained, frost susceptible soils (French, 2007). The volume expansion of water during freezing is 9%, however, this value is dependent on the lithology and hydrological regime of soils and can, therefore, be as much as 50% (Williams & Smith, 1989; Warburton, 2013). This expansion produces strong mechanical forces (frost heaving and thrusting), also known as cryoturbation, owing to cryostatic capillary suction caused by pore pressure in freezing soils (Christopherson, 2009; Barry & Yew Gan, 2011). Freezing of moisture in the active layer occurs on an annual basis during autumn to produce frost heave which sorts sediment vertically and laterally; ground displacements have been measured at generally 2cm to 5cm (French, 2007; Barry & Yew Gan, 2011; Warburton, 2013).

Four models have been put forward for cryoturbation, the ‘cryostatic’ model, the ‘convective cell equilibrium’ model, the ‘differential collapse model’, and the ‘differential frost-heave model’. The first involves the movement of two freezing fronts in opposite directions, downward to the permafrost table and upward to the surface. The second involves a heave-subsidence process whereby material at the bottom moves upward and inward and material from the top of the active layer moves downward and outward (Bockheim & Tarnocai, 1998b). The differential collapse model has been applied to the development of mud boils whereby unstable bulk-density profiles

coupled with the viscous nature of wet soils encourage the flow of soil by diapirism (Bockheim, 2007). Lastly, the differential frost-heave model is based on the non-homogeneity of sediments and uplifting due to the presence of ice lenses within the active layer (Bockheim, 2007). French (2007) has also suggested two models for frost heaving in the active layer, the "frost-pull" and "frost-push" mechanism. The first mechanism arises from the stones being raised by the advancing freezing plane, whilst the second is attributed to ice formation beneath the stones due to their greater thermal conductivity, which forces them upwards (French, 2007). The frost pull and push mechanism is responsible for stone sorting (Warburton, 2013).

The most pertinent patterning processes in periglacial environments are frost cracking by thermal contraction and dilation cracking by heaving which plays an important role in sorting (Huggett, 2011). The continuous expansion and contraction during the freeze-thaw process results in the movement of soil particles and small boulders through heaving, whereby the "self-organization' process begins under mechanical and gravitational forces (Christopherson, 2009; Warburton, 2013). Whilst unsorted patterns show no segregation of particle sizes, sorted patterns are distinguished by fine sediments (silt particles) being located in the centre and the coarser sediments surrounding located on the periphery. This is attributable to the fact that fine particles migrate under a wider range of freezing rates than coarser particles (Wynn-Williams, 1990; French, 2007). According to Rafferty (2011), for this process to occur, fine-grained sediments and soil moisture are imperative (Huggett, 2011). Figure 13 illustrates the convective sorting process within the active layer that gives rise to sorted circles (Warburton, 2013).

The downward soil motion occurring at the margins is made evident by a domed centre of fines and a ridge of coarse sediments on the periphery (Rafferty, 2011; Feuillet, 2012; Warburton, 2013). According to Rafferty (2011), the more circular forms of patterned ground develop when sorting is dominant due to stone confinement by frozen soil domains.

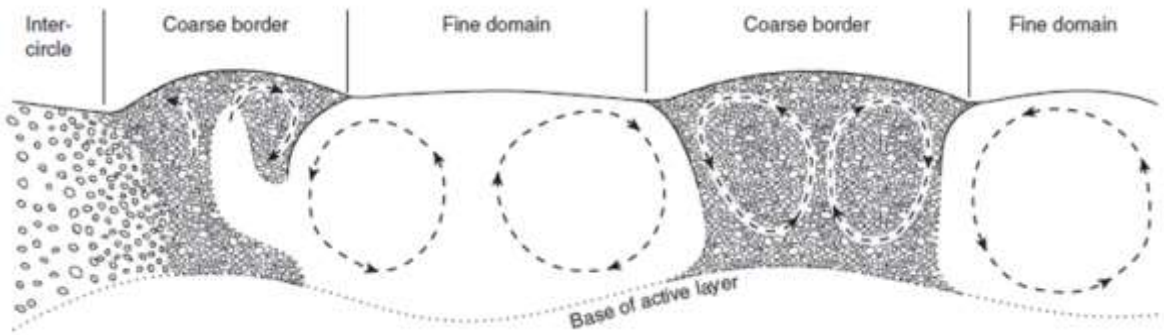

Figure 13: Surface soil displacement in sorted circles (Warburton, 2013, pg.305).

Mudboils are also a common feature of the active layer and arise due to the development of locally high hydraulic potentials due to water being trapped between a surficial carapace and the underlying permafrost (French, 2007). Owing to over saturation of the sediments, the mud is able to flow effortlessly through the relief of internal stresses by the bursting of the mud through the semi-rigid carapace. Mudboils are indicative of poorly sorted mud/diamict that is significantly silty or clayey (French, 2007). Furthermore, the process is most common in late summer where the thickness of the active layer reaches its greatest extent, which is concurrently when the most moisture is available due to the thawing of the transient layer (French, 2007).

Polygonal patterned ground (PPG) also known as thermal-contraction-crack polygons, frost-fissure polygons, tundra polygons, or ice/sand-wedge polygons, have been described by French (2007) as the most widespread, visible, and characteristic features of permafrost terrain. It arises as a result of transecting networks of shallow troughs delineating areas between 3m to 30m in diameter according to Rafferty (2011) or 15m to 40m in unconsolidated sediments and 5m to 15m in bedrock according to Barry and Yew Gan (2011). They develop through the accommodation of stress in expanding and contracting soils as a result of freeze-thaw processes through the development of crack filigree (Godfrey *et al*., 2008). Thermal contraction occurs while the permafrost is cooling, leading to tensile stress parallel to the ground surface. The stress is abruptly relived through a fracture, leading to a network of vertical cracks. In other words, cracks develop when the cooling of the ground surpasses the tensile strength of the frozen soil (Hallet *et al*., 2011). They form with ground surface temperatures of about –15°C to –25°C (French, 2007). The conditions favourable to cracking include a GST of ~ –15°C to –25ºC, as well as a ~1.8°C.d $^{-1}$ air temperature decrease over a four day interval (Barry & Yew Gan, 2011).

Soil, ice and rock debris accumulate in the cracks which open during cold periods, preventing full closure of the cracks during warm periods (Godfrey *et al*., 2008; Hallet *et al*., 2011). During the thaw periods, deformation and uplift occur along the crack, eventually leading to warping on both sides of the crack to form symmetrical ridges separated by a trough over the crack (Hallet *et al*., 2011). The cracks progressively grow larger and deeper, expanding laterally after each consecutive season due to infilling, effectively creating a wedge of vertically laminated sediments, or sediments and ice, or just ice depending on the climate of the region (Black, 1976; Godfrey *et al*., 2008; Levy *et al*., 2008; Hallet *et al*., 2011). Sand wedges are characteristic of arid polar regions and require relatively snow free winters to form whereby moisture from the cracks sublimate to the air, whilst the opposite holds true for ice wedges as moisture is gained from the air (Black, 1976). PPG serves as a strong geological marker of climate stability in the Antarctic (Levy *et al*., 2006). According to French & Guglielmin (2000), thermal contraction polygons are the most widespread permafrost-related landforms in the Northern Foothills, Victoria Land and are currently active under today's

climatic regime. They are 15m to 20m in diameter, bordered by shallow inter-polygon furrows that extend to a depth of 10cm to 30cm and have a breadth of 10-100cm. Surficially, the furrows contain gravel and sand which may be underlain by ice veins that are 50cm to 100cm deep and have the same width as the furrow (French & Guglielmin, 2000).

In Beacon Valley, non-sorted sand-wedge polygons were examined by Bockheim *et al* (2009). The polygons range from 9m to 16m in diameter, and the sand wedges range from 0.2m to 2.5m in width. Some were classed as composite wedges as they were found to contain ice veins up to 1cm in width. Sletten *et al*. (2003) stated that surface reworking of the wedges is apparent due to how wide, active, and closely spaced they are. Spasmodic cracking and continued addition of sand within the wedge, up to a depth of more than five metres, reveals surface reworking. The origin of the sand has been identified as external via wind-blown sediment and local via adjoining polygons (Sletten *et al*., 2003). Furthermore, it was found that more defined polygons were observed on younger surfaces (ca. 117Ka), whilst older surfaces (ca. >1.1Ma) conveyed poorly expressed polygons. Bockheim *et al*. (2009) attributed this degenerating development to the sublimation of ice-bonded permafrost post thermal cracking. Levy *et al*. (2008) points out that thermal contraction crack polygons are widespread in the McMurdo Dry Valleys. They are generally composite-wedge polygons as the wedges contain alternating lenses of ice and sand.

The borders of sorted polygons consist of stones with interstitial fines, whereas the borders of non-sorted polygons originate from furrows or cracks (Huggett, 2011). According to Williams and Smith (1989), the size of the surface materials has a strong correlation to the size of the sorted polygons. Non-sorted circles, also known as stony earth circles, are also common in these environments. They can reach up to three metres in diameter and 0.5m in height, and are characterised by a relatively flat, stony surface (French, 2007). They appear in response to frost heave and are restricted to windblown, exposed ground (Williams & Smith 1989). According to French (2007), the interaction of circles with one another result in a net.

A relationship between slope processes and patterned ground exists. Christopherson (2009) and Huggett (2011) highlighted that flat areas/lesser slopes are associated with sorted polygons, circles and nets whilst greater slopes resulted in non-sorted polygons, circles and nets. Similarly, stripes also develop on steeper slopes with the sorted variety consisting of alternating coarse and fine stripes as one progresses downslope (French, 2007; Rafferty, 2011). Huggett (2011) points out that these various forms of patterned ground have a tendency to connect with one another as they transition downslope under the influence of gravity, forming steps and eventually stripes. Steps may become lobate as they elongate downslope, alternately, they run parallel to hillside contours and the risers are edged with larger stones in sorted forms (French, 2007; Huggett, 2011).

2.3.2. Viscous-flow Features

Active and inactive viscous-flow features in Antarctica have been documented in the MDV, North Victoria Land, DML, the Patriot Hills, the South Shetland Islands and on James Ross Island (Bockheim, 2014). According to Bockheim (2014), the term viscous-flow features encompasses solifluction/gelifluction landforms, as well as rock glaciers. The presence of frozen ground during solifluction is not presumed and, therefore, the term gelifluction is alternately used as it incorporates permafrost (Ridefelt & Boelhowers, 2006; Millar, 2013). In summary, solifluction includes frost creep which may occur in association with diurnal frost, whilst gelifluction is a function of melt out during spring (Ridefelt & Boelhouwers, 2006). In view of the fact that both solifluction and gelifluction produce similar landforms, solifluction will be used as the inclusive terms so as to avoid confusion (Millar, 2013).

Gravitational force is a primary role player in slope processes and subsequent events such as collapse, talus, land sliding, stone streams, rapid flows, solifluction and more (Yershov, 1998). Due to the fact that permafrost exhibits poor drainage, the regolith and active layer become saturated during seasonal thaw which results in progressive downslope movement (solifluction) (Christopherson, 2009; Berthling *et al.*, 2013). Material can easily be transported over low angle slopes and are augmented by freeze-thaw cycles which drive frost creep. According to French (2007), frost creep arises from frost heaving and settlement upon thawing, producing a ratchet-like downslope movement of particles. Solifluction on the other hand is influenced by the presence or absence of permafrost and snow cover, as well as soil properties including texture and moisture, and air and ground temperatures (Millar, 2013). Slope steepness, soil thawing depth, terrain type, and composition of deposits are also important factors defining solifluction (Yershov, 1998). According to Yershov (1998), clays and sands that are silty and contain rudaceous materials provide a more conducive environment for solifluction. If large clasts are present in solifluction deposits, they are generally oriented parallel to the direction of movement (French, 2007). These factors in conjunction with the mechanism of movement dictate the type of solifluction landform produced such as lobes, fans, sheets or terraces (Huggett, 2011; Rafferty, 2011; Millar, 2013). According to Matsuoka (2001), solifluction features are linked with lower gradients due to the fact that the overturning in the surficial soil layer loses velocity as it progresses downslope. In Antarctica, this process occurs within the top 10cm to 15cm of regolith during diurnal freeze-thaw regimes which are restricted to summer periods which provide moisture via snowmelt, activating the process (Matsuoka, 2001).

Solifluction lobes are tongue-shaped features which reach can reach extents of up to 50m in diameter, 100m in length and 1.5m in height (Huggett, 2011; Rafferty, 2011). Stone-banked lobes arise when a lobe's outer margins are abundant in clasts as a result of frost sorting processes.

Soilfluction lobes without a concentration of clasts on the periphery are termed turf-banked lobes (Huggett, 2011). According to French (2007) and Matsuoka (2001), cold regions that have the advantage of high elevation and latitude, result in defined lobate forms due two-sided freezing which induces a plug-like flow. Conversely, the aridity of the polar deserts may favour the development of soilfluction sheets with small riser heights as thaw depths are shallow (Matsuoka, 2001; French, 2007). Solifluction sheets are essentially widespread solifluction lobes, and generally develop on low slope gradients (1° to 3°) (Huggett, 2011). Similarly, terraces also develop on lower valley slopes and can also be sub-divided into turf-banked and stone-banked terraces (Matsuoka, 2001). Solifluction terraces have been documented extensively in Victoria Land and areas in the adjacent vicinity such as McMurdo Sound (Speden, 1960; Mccraw, 1967; Selby, 1971; Cannone & Guglielmin, 2012; Bockheim, 2014).

Rock glaciers are lobes of angular rock mixed with interstitial ice, and are found in high mountain environments (Huggett, 2011; Rafferty, 2011). Permafrost and a sufficient supply of debris from talus slopes or adjacent moraines are essential to formation (French, 2007). Rock glaciers move as a result of flowing interstitial ice or creeping via frost action, according to Rafferty (2011), they can move more 150cm per year. French (2007) highlights that movement rates can vary between a few centimetres to several metres annually and according to Barry and Yew Gan (2011), are dependent on ground temperature, surface slope, composition and internal structure, as well as thickness of the ice horizon. Huggett (2011) stated that active rock glaciers contain an ice core which constitutes 50-90% of its volume. A cold climate, abundant rock debris and a slope are required for the formation of a rock glacier, which occurs in one of three ways. A glacier can be buried by debris, or meltwater and rain can sink into debris to form interstitial ice, or environments with a MAAT of less than 0ºC create the perfect ratio of precipitation and debris input (Huggett, 2011). Vieira *et al*. (2012) provides a list of identified and documented rock glaciers around the Antarctic, including the coast and sub-Antarctic islands, the Transantarctic Mountains and the McMurdo Dry Valleys.

Variations in the surface climate of Antarctica can be seen as a result of inter-annual variations in atmospheric circulation, particularly temperature, precipitation and wind stress (Carleton, 2003). This in turn impacts landscape and geomorphic processes, particularly through permafrost degradation and active layer thickening which directly affects soil processes such as sorting and cryoturbation (Guglielmin, 2012). According to van den Broeke (2000b), the circulation system/teleconnection that plays the largest role in influencing Antarctic temperatures is the semi-annual oscillation (SAO). Therefore, it is important to define the link between variations in the SAO and active layer dynamics in WDML.

2.4. Teleconnections

When a statistical link, positive or negative, is found in the global atmospheric circulation over sizeable and spatially non-contiguous locations, it is known as a teleconnection (Bridgman & Oliver, 2006; Trenberth *et al*., 2007). They express large-scale patterns in atmospheric pressure, which are reflected by the surface climate and variations in wind which play a role in temperature and moisture advection at specific locations within that pattern (Carleton, 2003; Trenberth *et al*., 2007). Furthermore, the poleward flux of heat, moisture and momentum between the atmosphere and earth's surface is a dominant driver in their formation (Carleton, 2003; Trenberth *et al*., 2007).

Acting from 50ºS, extending poleward, are the sub-Antarctic and Antarctic teleconnections which include the Semi-Annual Oscillation (SAO), Southern Annular Mode (SAM), El Niño Southern Oscillation (ENSO) and Antarctic Circumpolar Wave (ACW) which exist on inter-seasonal, annual, inter-annual, and inter-decadal time scales respectively (Carleton, 2003). It is essential to differentiate between the SAO and SAM as they both involve modes of pressure variation in the mid-to-high-southern latitudes. The SAO is the longitudinal expression of surface pressure which is reflected in annual pressure data by two distinguished peaks and troughs in the form of a half-yearly wave (Russell & McGregor, 2010; van den Broeke, 2000a). Therefore, the SAO shows longitudinal variation in amplitude and phase of pressure within the regions it affects. Whilst the SAM also exhibits longitudinal variability, it describes the pressure gradient between 40°S and 65°S (Russell & McGregor, 2010). An abundance of literature refers to the SAM as the Antarctic Oscillation (AAO) (Carleton, 2003; Marshall, 2007; Stammerjohn *et al*., 2008; Russell & McGregor, 2010; Turner & Marshall, 2011), care must thus be taken to avoid confusion.

The SAM is most aptly defined by Gong and Wang (1999, pg.459) as the "the alternation of atmospheric mass between the mid-latitude and high-latitude surface pressure", for instance, lower pressures over the Antarctic translate to stronger westerlies in the sub-Antarctic (Carleton, 2003). It is the leading mode of annual cycle variability in the SH (Sexton, 2001; Fogt & Bromwich, 2006; Stammerjohn *et al*., 2008). According to Marshall (2007), it accounts for approximately 35% of southern hemispheric climate variability. Similarly, according to van den Broeke (1998a), the second harmonic for the annual cycle of surface pressure (i.e. the semi-annual variation associated with the SAO) is the most dominant in SH high latitudes as it accounts for approximately 80% of the total variance in surface temperature. The fact the SAO plays a dominant role in the development of climatological variables (surface air pressure, precipitation, sea ice cover, wind speed and cloudiness) (van den Broeke, 2000d), makes it more pertinent to this dissertation as the seasonal and inter-seasonal dynamic between the atmosphere and ground thermal regime is important to active layer research in WDML.

2.4.1. Semi-Annual Oscillation

The Semi-Annual Oscillation (SAO) materializes from a twice-yearly expansion and contraction of the circumpolar trough (CPT) on account of baroclinity and storm activity peaking during the equinoctial seasons, this arises from a seasonal differential in heat storage between Antarctica and the Southern Ocean (Meehl, 1991; van den Broeke, 2000a; van den Broeke, 2000b; Carleton, 2003; Stammerjohn *et al*., 2008; Russell & McGregor, 2010). The half-yearly wave associated with the SAO experiences a peak at 45-50ºS, a minimum at 60ºS, and a second peak over coastal Antarctica (van den Broeke, 1998a). Meehl (1991) highlights that summer temperature maximums and winter temperature minimums in Antarctica are delayed by heat storage in the ocean. This gives rise to very short transitional seasons whereby rapid changes in temperature occur just before and after winter (King & Turner, 1997). On account of the atypical climate experienced in Antarctica, the seasons have been redefined. Summer ranges from late November to the end of February, autumn includes March and April, winter is from May to early October, and spring extends from mid-October to mid-November (King & Turner, 1997).

The SAO is characterized at the surface by the CPT which is found between 60°S and 70°S, a zone inhabited by an abundance of low pressure cells (King & Turner, 1997; Bargagli, 2005). The trough expands and weakens from March to June and September to December, and contracts and intensifies from June to September and December to March (Meehl, 1991). The latitudinal location of the CPT highlights the variations in the SAO, as it is defined seasonally through the shifting of the trough equatorward in January and July and poleward in March and September (Carleton, 2003). Logically, the trough is most pronounced in the intermediate seasons (February/March and September/October) when it is furthest south, and weaker during summer (December/January) and winter (July/August) when it's further north (King & Turner, 1997). During maximum contraction of the CPT in early winter and spring, low pressure areas migrate towards the continent, bringing in a net transport of air. The expansion phase in late winter and summer results in a net export of atmospheric mass to lower latitudes (King & Turner, 1997; van den Broeke, 2000a).

The presence of the SAO has been identified in Antarctic surface temperatures at Antarctic coastal stations as a "coreless winter" whereby a well-defined temperature mean is missing (Carleton, 2003). The cause, according to Meehl (1991), is an amplification of the trough and enhanced meridional flow in winter in conjunction with the effects of radiative forcing. This process (amplification of the wave-3 structure) directly links the SAO to Antarctic surface temperatures (van den Broeke, 1998a). The decadal variability of the SAO impacts temperature trends on longitudinal scales in Antarctica which is why temperature trends at Antarctic stations differ. This can be through changes in wind speed and cloudiness or as a direct result of alterations in warm air advection (van den Broeke, 2000a, 2000c).

Russell & McGregor (2010) substantiate the role that the SAO plays in temperature trends throughout the Antarctic. For instance, the Antarctic Peninsula has warmed by 2.5°C over the last 40 years whilst East Antarctic stations are experiencing cooling (van den Broeke, 2000c). According to van den Broke (1998a), seasonal cooling is significantly reliant upon the presence and strength of a temperature inversion at the surface owing to the amplification of the wave-3 structure of circulation. The inversion is supported by radiative cooling of the surface and lower atmosphere, and occurs only when horizontal advection is lacking (King & Turner, 1997; van den Broeke, 2000c). Its strength is determined by the temperature disparity between the surface of the earth and the highest temperature within the lower troposphere. Spatially, the inversion is strongest in the continental interior during winter. Temporally, inversions are almost omnipresent throughout the year in the coastal regions (King & Turner, 1997). Inversion strength varies between 2K in coastal localities to 25K over the east Antarctic plateau (van den Broeke, 2000c). During the presence of an inversion, cloud cover and wind speed which impact longwave radiation and sensible heat flux respectively, have a significant impact on near surface temperatures. Thus, a positive correlation exists between mean temperature and wind speed/cloudiness, such as that experienced by Halley and possibly SANAE (van den Broeke, 2000c). Conversely, stations lacking a significant inversion are privy to other climatological influences, such as a sea ice extent feedback, experienced by Faraday and Dumont d'Urville (van den Broeke, 2000c).

Bridgman and Oliver (2006) emphasize the relationship between sea ice extent and variations in the CPT, which is embodied well by Dumont d'Urville (a coastal station closest to the CPT). The strength of westerlies, as well as atmospheric precipitation between 40°S to 60°S are altered with variations in the CPT, the former being due to changes in the near surface wind direction over the ocean (King & Turner, 1997; Carleton, 2003; Bargagli, 2005; Trenberth *et al*., 2007). Westerlies in the SH are maintained by the meridional transport of westerly momentum (Meehl, 1991). Stronger westerlies are synonymous with deeper lows and an intensification of the CPT during intermediate months south of 50ºS, whilst weaker westerlies occur during solsticial months north of 50ºS; this has consequences for the advancement and retreat of sea ice (Meehl, 1991). According to Meehl (1991), more than 50% of the variance in sea level pressure can be accounted for by the SAO. Shifting westerlies, in accordance with the poleward migration of the CPT between June and September, result in the rapid advancement of sea ice (Carleton, 2003). During October when the CPT is furthest south and pressure is at its minimum, maximum sea ice is experienced (Bridgman & Oliver, 2006). Conversely, the equatorward migration of the CPT during later spring and in early summer leads to ice retreat (Carleton, 2003). According to van den Broeke (1998), the spring time phase of the SAO has been retarded to November as a result of heightened sea surface temperatures in the tropical eastern Pacific associated with frequent El Niño events; this anomaly manifested during the 1970s.

CHAPTER 3: Materials and Methods

Permafrost and active layer dynamics have been more extensively studied in the NH (Smith *et al*., 2010; Romanovsky *et al*., 2010a; Christiansen *et al*., 2010), in comparison to the Southern hemisphere (SH) where research has been less systematic; lacking international awareness despite its role within terrestrial landscapes/ecosystems and as a climate change indicator (Bockheim & Hall, 2002; Vieira *et al*., 2010; Bockheim *et al*., 2013). Therefore, insight into permafrost and active layer regimes is needed in those parts of Antarctica, aside from the McMurdo Dry Valleys (MDV) and the maritime Antarctic, which have been neglected (Ramos *et al.*, 2007; Vieira *et al*., 2010). Research conducted on ground-atmosphere coupling, will further strengthen the understanding of landform and landscape development (Vieira *et al*., 2010).

The fieldwork component of this study was undertaken since the conception of the 'Geomorphology and Climate Change' project in 2006 which was changed over to the 'Landscape Processes in Antarctic Ecosystems' project in 2011. Numerous field assistants contributed to the collection of data for the automated logging station and landscape subsections detailed on pg.35 and pg.43 respectively. The ^{137}Cs fieldwork was conducted during the 2014/15 Austral Summer. Methods were standardised and equipment (particularly the loggers) were calibrated after each download to minimize error. The accuracy of fieldwork data collection determines the accuracy of statistical analyses which augment the fieldwork component (Till, 1985). Large datasets on multiple parameters were required and included the soil temperature and soil moisture regimes, air temperature, radiation and pressure. Majority of data were acquired through fieldwork and the loggers, which was followed and extended by laboratory analyses. The Analysis Tool Pak plug-in of Microsoft® Excel was utilised to do a large proportion of statistical analysis, followed by R Statistical Software®. The contouring of the temperature in respect to time and depth was plotted using linear interpolation in Surfer 8.0®. Although methods in the field were aligned with project requirements, methods described in literature were followed as closely as possible to reduce subjectivity and bias. The same was followed for laboratory and statistical methods.

To achieve Objective 1 (pg.6), appropriate loggers in the field were used to obtain data on soil temperature and moisture dynamics. Objective 2 on the ground-atmosphere interface required the collection of air temperature, pressure and radiation data from SAWS and Meteonorm®. Objective 3 (pg.6) aims to determine the degree to which the ground is active involving the mechanism of cryoturbation. For this, soil samples were collected from sorted circles at numerous locations and analysed using Gamma Ray Spectrometry and a Malvern Mastersizer 3000. GIS were employed to map active layer related landforms in accordance with Objective 4 (pg.6). Table 2 provides a list of

data collection and instruments according to the objectives, which are discussed in greater detail in the relevant sections of this chapter.

Table 2: Data requirements and instruments used during field and laboratory work.

Measurement/ Observation	Instrument	Date/Season	Objective	Source
Permafrost/active layer dynamics	• XR5 data logger • Decagon EC-5 Soil Moisture Sensor	2006-2012 2010	1	Fieldwork
Climate data (ambient temperatures, pressure, radiation)	• N/A	2015	2	SAWS Meteonorm®
Particle size analysis & corrections	• Endecott test • Malvern Masterizer 3000	2015	3	Laboratory analysis
^{137}Cs analysis	• Ortec Gamma Ray Photon Detector	2015	3	Laboratory analysis
Location	• GIS & GPSmart 60CSx GARMIN	2009/10-2014/15	3 & 4	Fieldwork

This chapter is sub-divided into field, laboratory, and statistical methodology. These sections along with their sub-sections may be found under Field Methods (pg.35), Laboratory Methods (pg.43), and Statistical Analyses and Preparation (pg.48) respectively.

3.1. Field Methods

3.1.1. Automated Logging Stations

The implementation of CALM networks in Antarctica is different to the strategy used in the Arctic as the rocky terrain inhibits mechanical probing and the use of 100m by 100m grids (Vieira *et al*., 2010). Therefore, the active layer is monitored with the use of smaller grids and shallow boreholes (less than 2m from the surface) which forms part of the Antarctic permafrost borehole network (Vieira *et al*., 2010). The purpose of the Antarctic Circumpolar Active Layer Monitoring (CALM–S) sites is to record the spatial variations in depth and temperature of the active layer in relation to environmental parameters (Vieira *et al*., 2010).

In February 2007, a systematic investigation of permafrost landforms was initiated in WDML whereby study sites were identified in areas surrounding SANAE IV and Troll. By the end of the 2014 Austral Summer, ten boreholes on eight nunataks had been installed. Majority of the boreholes were installed at a depth of 60cm (thermistors were placed at 1cm, 15cm, 30cm, 45cm, and 60cm), whilst only one was installed to a depth of 2m (thermistors were placed at 1cm, 0.5m, 1m, 1.5m, and 2m). The borehole depth was limited by the presence of ice-cemented ground. At the selected sites, a borehole was dug into permafrost. The five thermistors were attached to a rod and placed in the borehole; arranged in a vertical array at different depths below the surface. At one centimetre depth, a Decagon EC-5 soil moisture sensor was installed. The thermistors and soil moisture sensor were connected to a PACE XR5 data logger which records data according to the protocols suggested for ANTPAS with measurements at hourly intervals (Viera *et al*. 2010). Once the boreholes were installed, a two week period was allowed for the ground to settle, thereafter, logging commenced. Caution was practised when covering the pit in order to return the site as much as possible to its original condition, and protect the sensors from being disturbed. Protected by a radiation shield at one metre above the ground, ambient air temperature was also measured by the logger. The setup of the logger is depicted in Figure 14 below (adapted from Meiklejohn, 2012).

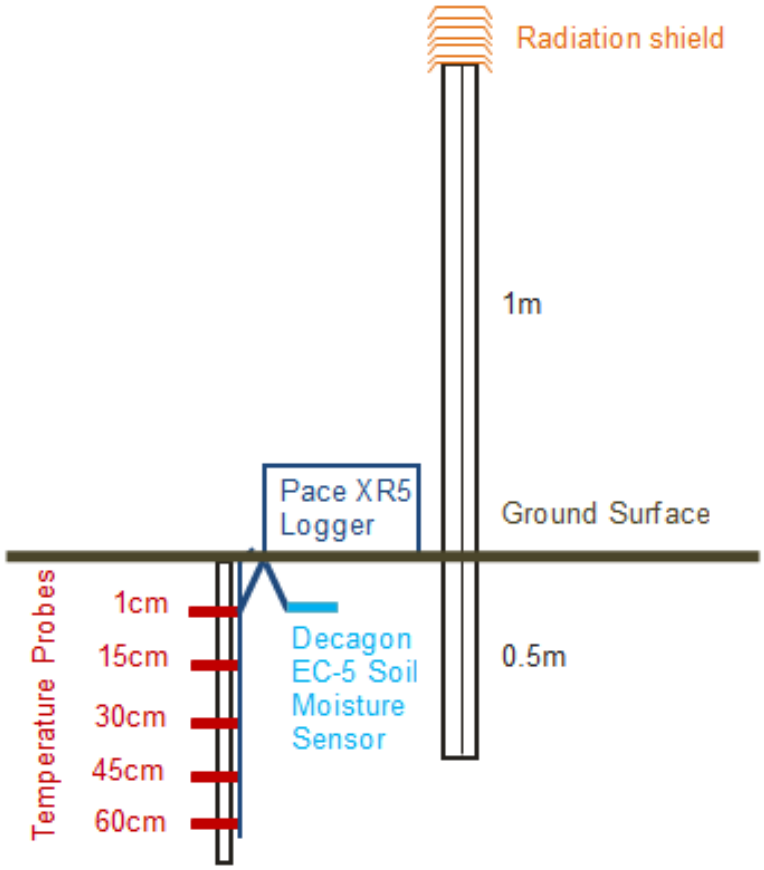

Figure 14: Set-up of a data logging system (adapted from Meiklejohn, 2012).

Ground thermal profiles and monitoring of temporal variation in the active layer are examined up to a depth of up to 60cm at Flårjuven (72°01'S, 3°24'W), Vesleskarvet (71°40'S, 2°51'W), and Robertskollen (71°29'S, 3°13'W); and up to a depth of 2m at Nonshøgda; i.e. Troll (72°01'S, 02°32'E). The temporal and spatial variability at and between these four sites are analysed in depth to form part of Objective 1. Numerous factors impact on the thickness of the active layer, such as vegetation type and density (Almeida *et al*., 2014), snow-cover (Guglielmin *et al*., 2014b), thermal properties of the substrate (de Pablo *et al*., 2013), moisture content (Seybold *et al*., 2010) and incoming radiation *(*Adlam *et al*., 2010). The influence of air temperature, specifically during the summer, on the thickness and thermal regimes has been the central focus of active layer studies in Antarctica (Guglielmin, 2004; Cannone *et al*., 2006; Conovitz *et al*., 2006; Guglielmin, 2006; Bockheim *et al*., 2007; Adlam *et al*., 2010; Guglielmin *et al*., 2011, 2012, 2014b).

Therefore, the aim of Objective 2 was to understand the annual and seasonal variability of the ground thermal regime and active layer thickness in WDML, and the influence of climate parameters thereon such as air temperature, incoming radiation and pressure. Temperature was measured in degrees Celsius (°C), pressure in hectopascals (hPa), and radiation in kWh/m^2. All parameters were observed on the hour. Vesleskarvet was chosen for this objective as it is where the South African base is located along with the SAWS station, making the climate data more accessible and location specific. Table 3 provides information regarding the SAWS weather station.

Table 3: Metadata on the SAWS weather station (Hansen, 2013).

Description	Value
Climate Number	00000024
Latitude	71° 40’ 48’’ S
Longitude	02° 51’ 00’’ W
Height	849m

With the help of continuous ground thermal records at 1cm, 15cm, 30cm, 45cm and 60cm below the surface, active layer thickness was determined by the graphical interception of the 0°C axes by the annual maximum temperature exhibited at each depth (Guglielmin *et al*., 2003; Adlam *et al*., 2010; Guglielmin and Cannone, 2012; Guglielmin *et al*., 2014a). For a better understanding of the nature of relationship between ground thermal regimes and air temperatures the following were quantified: thawing and freezing hours, degree days of freezing (DDF, sum of mean daily ground surface temperatures below 0°C), degree days of thawing (DDT, sum of mean daily ground surface temperatures above 0°C), thermal stress index (TSI, daily maximum− daily minimum), the freezing n-factor (*nf* , as the ratio of the freezing degree-day sum at the soil surface to that in the air for the thawing period), surface thermal offset (SO, difference between NST and air temperature), and potential freeze-thaw events (PFTE, number of times that hourly mean temperature crossed the threshold of 0 °C) (Guglielmin *et al*., 2014b; Wilhelm *et al*., 2015). Since the logger does not

record ground surface temperatures (GST, 2cm depth), near surface temperatures (NST, 1cm depth) were used for the calculation of the thermal indices. Moreover, PFTE, DDF and DDT were calculated using freeze thaw events for the whole year, contrary to the standard of a seasonal time period (Farbrot *et al*., 2013).

Whilst ground thermal data were obtained from the PACE XR5 data logger, air temperatures were analysed using the SAWS meteorological station located at SANAE (± 300m away from the logger site). Since the elevation of the study site and meteorological station were the same, lapse rate corrections were unnecessary. Although wind speed is one of the major determinants in active layer depth, it was not looked at for this study as the data corresponding to the timeline of this research were not available. Meteonorm® (v 7.0) was used to obtain radiation data which is calculated using the hemispherical potential incoming radiation with stochastic models which generate hourly values at any desired location (Remund *et al*., 2014). Two primary types of radiation values are output by Meteonorm® (v 7.0), direct normal radiation (Bn) and global horizontal radiation (Gh) (Gh = direct radiation (Bn) + diffuse horizontal (Dh) radiation). Similarly to Guglielmin and Cannone (2012), global radiation values were used for this study, more importantly because the Meteonorm®(v 7.0) uncertainty ranges were less than that of direct normal radiation (Gh = 2-10% uncertainty; Bn= 3.5-20% uncertainty) (Remund *et al.*, 2014). Neumayer, Novolazarevskaya and Showa Station (224km, 533km and 1579km from the study site) were used as radiation interpolation locations by Meteonorm® (v 7.0) to create the data. The climatological data available for radiation was 1991-2010, which was the period analysed by Meteonorm® (v 7.0). Because the outputted data for the 19 year period is averaged by Meteonorm® (v 7.0), analysis undertaken regarding the relationships between radiation, temperature and ground thermal data were done for 2010. It is pertinent to note that based on the remoteness of the study sites and lack of locally measured radiation, Meteonorm was used as first approach to the estimation of solar radiation. Although the data is interpolated, the errors are typically within the variations of climate from one year to the next according to Remund *et al*. (2014)

For the purpose of Objective 2, the Austral summer was defined as DJF (December, January, and February), the Austral winter as JJA (June, July, and August), the Austral autumn as MAM (March, April, May) and the Austral spring as SON (September, October, November). Knowledge of climate-cryosphere interactions will provide a foundation for bridging the knowledge gap of permafrost and active layer dynamics in WDML as stressed by Viera *et al*. (2010). A borehole was set up in 2009 to measure ground temperatures and soil moisture at Vesleskarvet, presenting six years of air and ground temperature measurements with a particular focus on 2010 to discuss the relationship between the ground-atmosphere interfaces.

3.1.2. Soil Moisture Calibration

In the Antarctic, the duration and presence of soil moisture are underpinned by snow and ice melting or sublimating (Seybold *et al*., 2010). Soil moisture in the Antarctic holds importance for numerous soil processes such as erosion, chemical exchange, microbial activity, as well as landform development via moisture migration and freeze-thaw cycles within the active layer (French, 2007; Navas *et al*., 2008). Soil moisture is essential for the formation of patterned ground as it facilitates particle migration under freezing fronts (Wynn-Williams, 1990; French, 2007).

The presence, abundance and diversity of biota on the exposed terrestrial areas of Antarctica are constrained by the availability of moisture, as well as the duration of moisture, particularly in terms of seasonal variability (Kennedy, 1993; Seybold *et al*., 2010). Maximum soil moisture content has been shown to be the most significant variable in the microbial content of soils (Kennedy, 1993; Chown *et al*., 2015). Lee *et al.* (2013) indicated that soil moisture is responsible for up to 80% of the variance in mite abundance in the Jutulsessen.

Soil moisture can be measured volumetrically (volume of soil water per unit of total volume) or gravimetrically (weight of soil water per unit weight of dry soil). The most common methods of monitoring soil moisture include capacitance or time domain reflectometry (TDR). Both measure the dielectric constant, with an output relating to VWC (Cobos & Chambers, 2009; Francesca *et al*., 2010). The Decagon EC-5 sensor was used in this study, it is a capacitance soil water content sensor based on a wireless network that provides in situ measurements with a high spatial and temporal resolution output (Figure 15; Bogena *et al.*, 2007). It was chosen over other Decagon devices such as the ECH20 sensor as it measures at a higher frequency which lessens its sensitivity to variation in texture and electrical conductivity Moreover, it is more applicable to a smaller sampling volume (i.e. one sensor at a site as opposed to a network) (Campbell 2009; Francesca *et al*., 2010). However, this does increase the possibility of error due to non-homogeneity of the soil.

Soil moisture of the upper 2cm of the ground surface was determined gravimetrically using a Decagon EC-5 soil moisture probe connected to a PACE XR5 logger at each study site. The dimensions of the EC-5 probe are 8.9cm by 1.8cm, typified by two sharp geometric prongs at 5cm length which facilitate easy insertion into the soil (Francesca *et al*., 2010). General installation techniques involved placing the sensors into an augured hole with the flat side vertically in order to avoid pooling or air gaps (Campbell 2009; Refer to Recommendations on pg.118). However, the prongs were inserted horizontally, parallel to the soil surface, in order to expose the prongs to as much soil surface area as possible.

The EC-5 has a volume influence of 0.3L, and measures VWC by averaging the results over its entire length (Campbell, 2009). The calibration equation applied to the EC-5 probe prior to logging was that used for mineral soils (Francesca *et al*., 2010; Equation 1):

Equation 1: Calibration for Mineral Soils

$$U(\%Vol) = 0.119\,mV - 40.1$$

Figure 15: EC-5 soil moisture probe (8.9cm by 1.8cm).

Variability and inaccuracies in the sensor readings stem from multiple sources such as sensor-sensor variability, supply voltage affecting sensor reading, and dependency of the sensor reading on electrical conductivity and temperature (Bogena *et al*., 2007; Francesca *et al*., 2010; Rosenbaum *et al*., 2010). The remaining errors which are pertinent to this study are directly dependent on the in-situ site characteristics such soil texture, bulk density, clay mineralogy, and salinity which alter the soils electrical properties. The standard mineral soils calibration for EC-5 results in approximately ± 3-4% error, which has the potential to be decreased to ± 1-2% with soil- specific calibration (Cobos & Chambers, 2009; Francesca *et al*., 2010). Therefore, the EC-5 sensor underwent a soil-specific calibration for each of the four permafrost borehole sites.

For the purpose of soil-specific calibration, sediment samples were taken next to each of the four logging sites using a bulk density square. This was done so that amounts would be standardized for the calibration process, as well as to obtain important measures such as bulk density and porosity. Further information is available under laboratory methods (pg.43). The samples were taken as close to the loggers as possible in order to get an accurate representation of the sediment housing the sensors. Care was taken not to disturb the loggers.

3.1.3. ^{137}Cs Analysis

Recently there has been an emergence of research into the investigation of cryoturbation rates in the active layer using radioactive isotope tracers (Lacelle & Vasil'chuk, 2013). Convective processes, powered by freeze-thaw cycles in soils containing moisture results in the movement of soil. However, knowledge of soil movement rates in the active layer are quite poor (Lacelle & Vasil'chuk, 2013). Therefore, ^{137}Cs will be used to trace soil movement within the active layer at

selected sites in WDML. Ceasium-137 is an anthropogenic radioactive isotope which was introduced into the environment during the nuclear weapon testing period of the 1960's, and during various nuclear accidents, the most recent of which was the Fukushima nuclear disaster in 2011 (Lacelle & Vasil'chuk, 2013). It has a half-life of 30.17 years with a high affinity for soil particles, making it an ideal tracer of soil movement within the active layer (Kachanoski, 1993; Lacelle & Vasil'chuk, 2013).

According to Mabit *et al*. (2008), ^{137}Cs tracing has proved useful in tracking sediment movement post 1958 which will aid in the determination of patterned ground/bioturbation processes. The horizontal and vertical tracing of patterned ground provided by ^{137}Cs will allow a three-dimensional analysis of sediment movement. According to preliminary investigations of sorted patterned ground on the Slettfjell Nunatak in WDML by Meiklejohn (2012), a concentration of ^{137}Cs in the coarse boundary was found, suggesting movement of material from the fine centres towards coarse boundaries.

Twelve surface (0–5cm) soil samples were collected from three different patterned ground locations. According to Mabit *et al*. (2008), the upper ca. 5cm of the soil profile contains a near-constant concentration which decreases with depth in undisturbed soils. Sorted circles at Robertskollen, Flårjuven, Slettfjell were identified by broken boundaries and surficial microtopography characteristic of cryoturbated horizons (Jelinski, 2013). The most suitable looking circles, closest to the loggers, with clear boundaries were used for sampling. Moreover, the centre and edge of the sorted circle were chosen for sampling in order to characterize maximum variability (Jelinski, 2013). Three circles were chosen at Robertskollen to sample (Figure 16). Pit excavation was limited to the depth of a hand tool (bulk density square) on account of impenetrable lithic material (Jelinski, 2013). A bulk density square was filled with surface sediment from three different sorted circles centres (indicated by the X in the centre in Figure 16). The same was done from the crack of each sorted circle (indicated by the X on the circle boundary in Figure 16). Overall, a single profile was excavated across three cycles at one location with strong patterned ground expression to provide a complete "snapshot" of variability. The same process was applied to the sorted circles at Slettfjell and Flårjuven.

Figure 16: Sorted circle sampling at Robertskollen (a-axis= ~16cm, b-axis = ~13cm).

During the field season of January 2014, two field assistants (Dave Scott and Elizabeth Rudolph) took sediment samples from the terrace treads (B1-B7) and risers (M1-M7) at Flårjuven (Figure 17; Table 4). The position of the terraces were marked using a Garmin GPSmap 60CSx. For the purpose of ^{137}Cs analysis, the sediment samples of the treads and risers from the base, middle and top sections of the terraces were analysed. This make a total of 6 samples from Flårjuven, highlighted in blue on Table 4.

Figure 17: Terraces at Flårjuven (area = ~1283m^2).

Table 4: Sediment sample ID, location and elevation taken from the Flårjuven terraces.

Sample ID	Latitude	Longitude	Elevation (masl)
B 1	-72.012183	-3.381484	1261.846680
B 2	-72.012235	-3.381374	1261.365967
B 3	-72.012284	-3.381231	1264.730469
B 4	-72.01236	-3.380931	1267.614258
B 5	-72.012416	-3.380846	1269.537354
B 6	-72.012564	-3.380682	1273.863037
B 7	-72.012615	-3.38042	1277.708252
M 1	-72.012204	-3.381391	1260.404541
M 2	-72.012281	-3.381241	1265.211182
M 3	-72.012319	-3.381104	1265.451416
M 4	-72.012409	-3.380949	1269.777588
M 5	-72.012463	-3.380703	1271.219482
M 6	-72.012587	-3.380499	1276.506592
M 7	-72.012656	-3.380278	1280.111572

3.1.4. Landscape Mapping

According to the Initial Environmental Evaluation by Meiklejohn (2012), a spatially referenced database has been established for WDML of topography, selected imagery, borehole temperatures, as well as a spatial network of ground temperature and moisture, together with derived themes, surface materials, landforms, and vegetation. Objective 4 has supplemented the database with new periglacial landforms. The spatial inventory of periglacial landforms began in 2006, successively being added to each Austral Summer by the each year's respective team until January 2014. The landforms positions were recorded using either a Garmin GPSmap 60CSx, a differential GPS (DGPS), or both. Each team member during each Austral summer was supplied with their own Garmin to record landforms as they came across them in the landscape. My contribution was made during the 2014/15 Austral Summer. The purpose of this objective was to spatially demonstrate the presence of periglacial landforms at the separate study areas to give an indication of permafrost and active layer dynamic activity.

3.2. Laboratory Methods

Laboratory analysis involved particle size analyses, gamma ray spectrometry and soil moisture calibrations. The same laboratory using the same equipment was used for all laboratory methods. Samples were weighed to the nearest 100^{th} of a gram (0.01g). For each of the sediment samples, the weight before, dry weight, bowl weight, and net weight were recorded and total water loss was calculated during the drying process. The methods are detailed below.

3.2.1. Soil Moisture Calibrations

The following section details the laboratory methods employed to achieve Objective 1 (pg.6). Cobos & Chambers (2009) provided detailed calibration techniques for decagon devices, which was followed as closely as possible. Once the samples were collected in the field using a volumetric sampler (bulk density square), they were oven-dried for 24 hours in a Labcon Forced Circulation oven at 105ºC to remove any available moisture (Carter & Gregorich, 2008). The samples were weighed before and after drying in order to calculate bulk density, volumetric water content (VWC) and gravimetric moisture content (GMC) (Francesca *et al*., 2010)

Large stones were removed from the sample which was then disaggregated using a pestle and mortar. Thereafter, the soil was packed into a container using the total sample obtained to maintain the field bulk density. The sensor was connected to a laptop running Log XR software and inserted horizontally into the container, ensuring the sensor tines were straight to avoid air gaps between the sensor and sediment. The software was calibrated to log according to mineral soils with an offset of

40.1. First a dry sensor reading was taken and the raw data recorded. This process was repeated a few times to get an average and make sure the sensor had stabilized in the medium. Thereafter, 1ml of distilled water was added at a time, followed by a thorough mixing of the sample to ensure incorporation of all the fines. The process of adding 1ml at a time was repeated until there was free moisture present in the container. This yielded over 60 calibration points for each sample, which were plotted on a scatter graph and fit with a polynomial curve to obtain the calibration equation (Refer to Appendix A, pg.136 for the calibration curves and associated graphs).

The bulk density of each sample was then determined to identify the nature of the soil (Briggs, 1977a). First, the sample volume was determined using Equation 2 (Briggs, 1977a), followed by the bulk density shown in Equation 3 (Ashman & Puri, 2002). Bulk density (D_b) is simply defined by Chesworth (2008, pg.74) as the "mass of a unit volume of dry soil". It is used in conjunction with particle density (D_p) to determine soil porosity (S_t) as shown in Equation 4 below (Carter & Gregorich, 2007). The average particle density of mineral soils is 2.65g.cm^{-3} (Carter & Gregorich, 2007; Chesworth, 2008).

Equation 2: Volume

$$V = h\pi r^2$$

Equation 3: Bulk density (D_b)

$$D_b = \frac{Mass\ of\ soil\ (g)}{Volume\ of\ bulk\ density\ square\ (cm^3)}$$

Equation 4: Soil Porosity (S_t)

$$\%\ S_t = \left[1 - \frac{D_b}{D_p}\right] * 100$$

Particle size and textural analysis was done after the bulk densities of sediment samples were determined. The samples were weighed, disaggregated with a mortar and pestle and sieved in a sieve stack for ten minutes at the Rhodes University sedimentology laboratory (Briggs, 1977a). Sediment in each sieve was weighed separately to determine the dry mass proportion of sediment within each size class. For particle size analyses the percentage dry mass for each class was calculated in terms of the total mass of the sample, followed by plotting the values as a cumulative

percentage (fine to coarse), representative of each sieve class. Additionally, phi (ø) sorting was used an indication of the degree of dispersion in sediments (analogous to the standard deviation of a sample), calculated using Equation 5 below (Briggs, 1977b). Well-sorted soils are associated with low sorting values, and vice versa.

Equation 5: Phi (ϕ) Sorting

$$\frac{\phi 84 - \phi 16}{2}$$

3.2.2. ^{137}Cs Analysis

3.2.2.1. Sample Preparation

The sediment samples were weighed, oven dried at 105 °C over a 24hour period, and reweighed to determine moisture content (Claridge *et al*., 1999). The samples were then gently manually disaggregated using a pestle and mortar and sieved in a sieve stack for ten minutes (Briggs, 1977b; Foster *et al*., 2007). A sieve analysis allows for the determination of a soils particle size distribution (gradation) between 0.05mm-5.0mm (Das, 2002). Samples were sieved to <63µm, conforming to common practice in sediment provenance studies with the added intention of minimising the potential impacts of differences in particle size on tracer concentration (Koiter *et al*., 2013). Once the sieving process was complete, the sediment in each sieve was weighed separately to determine the dry mass proportion of sediment within each size class.

Due to insufficient fines present in the <63µm and 63µm class in most of the samples, the lowest four sediment classes (250µm, 125µm, 63µm, and <63µm) were combined for all samples in order to acquire enough sediment for analysis, as well as to keep the measurement procedure standardised for all twelve samples. From this point forward the fine earth fraction is defined as sediment between <63µm and 250µm. This remained consistent with the methods used by Jelinski (2013), where a fine earth fraction of >2mm in diameter is required for ^{137}Cs activity analyses by gamma spectrometry. Consequently, by not limiting the analysis to the <63um particle size fraction of the sediment, particle size corrections had to be made to negate the effects of particle size distribution on an accurate ^{137}Cs analysis (Pulley, 2014). This was done by normalising tracer measurements to the specific surface area (SSA) of the sediment samples; the method is explained further on pg.46.

3.2.2.2. Radionuclides

Spontaneous change within the nucleus of an atom leads to radioactive decay, resulting in electromagnetic radiation in the form of alpha particles, beta particles and gamma rays (Gilmore, 2008). Radionuclides within the sediment emit energies which interact with the germanium in the detector to produce a spectrum of emission accounts plotted against radionuclide energies (Wallbrink *et al*., 1997). Therefore, the activity concentrations of ^{137}Cs are easily measured using its decay energies (Pulley, 2014). Radionuclide activity in this study was measured using an Ortec hyper-pure germanium (HPGe) coaxial well photon detector, similarly to Foster *et al*. (2007). The detector measures an internal diameter of 10mm and a 40mm active depth which is retained in 10cm thick lead shielding with a copper and carbon fibre lining (Foster *et al*., 2007).

For all twelve samples, approximately 3g of the fine earth fraction of sediment were packed to a depth of 4cm into clean, pre-weighed 7×1cm PTFE cylinders in order to match the geometry of the 'well' detectors used for measurement (Foster *et al*., 2007). The sample pots were re-weighed before they were sealed with a rubber turnover cap (Foster *et al*., 2007). On account of the low ^{137}Cs inventories in the SH, a greater count time in excess of 160,000 seconds was required for gamma analyses in order to increase the accuracy of the measurements (Mabit *et al*., 2008). The resulting spectra were analysed by calculating the number of photon counts at each decay energy (the measured decay energy for ^{137}Cs is 661.7Kev). Ortec Gamma Vision software, version 6.08, was used to manually identify each peak, from which the net area and live count times were recorded. The net area value of each radionuclide decay peak was accompanied by an error value which was used to determine the measurement error of the tracer. Before this was done, the results were corrected for detector efficiency, background interference, sample mass, surface area and storage time. The data were also smoothed twice to increase the accuracy of manually identifying the peaks.

3.2.2.3. Organic Enrichment and Particle Size Corrections

Once the ^{137}Cs analysis was complete, the sediment (<63µm - 250µm) samples contained in the PTFE cylinders were removed to undergo organic enrichment and particle size corrections. The fine earth fraction (<63µm - 250µm) of the sediment for each sample was measured using specific surface area (SSA). SSA is a measure of the surface area of the combined effects of particle of the whole particle size distribution, on the assumption that all particles are spherical ($m^2.g^{-1}$) (Santamarina *et al*., 2002). According to Pulley (2014), this measurement has been used as an accuracy tool in multiple provenance studies owing to the linear relationship between particle size and tracer quantity.

The nature of particles are dynamic, ranging from being a certain kind of material with homogenous properties to an aggregation of multiple smaller particles with different properties bonded together (Loveland & Whalley, 2000). In order to correct for the effects of particle-particle interaction, it is imperative that organic matter within the sediment is destroyed and that the sediment is well dispersed in an electrolyte (Loveland & Whalley, 2000). This is necessary as the presence of organic matter is a precursor to particle aggregation which may lead to the underestimation of fine particle size fractions and have an overall effect on the absolute particle size distribution of the sample (Di Stefano *et al.*, 2010). The method used involved adding 10ml of 30% hydrogen peroxide to ~ 0.1g of sediment (Collins *et al*., 1997). After 24 hours at room temperature, the mixture was heated at 70°C until the bubbling had stopped and all the hydrogen peroxide dissolved (Pulley, 2014). The sediment was further dispersed by 5ml of 3% sodium hexametaphosphate solution for 2 minutes before conducting particle analysis (Gray *et al.*, 2010).

The sedimentation technique used to measure the particle size distribution of the sediment sample was laser light scattering (i.e. laser granulometry) using the Malvern Mastersizer 3000. Laser granulometry is the most advantageous method to use for the purpose of this dissertation as it is available at Rhodes University, cost-effective, requires no manual calibration, has a fast analysis time (<5 minutes per sample), and precise at quantifying a wide range of different sized particles (Blott & Pye, 2006). The only drawback is that the estimates of SSA may underestimate the clay particle size fraction on account of the assumption that all particles are spherical (Blott & Pye, 2006; Pulley, 2014). Loveland & Whalley (2000, pg.282) stated, "Few natural particles are spheres, and often the smaller they are, the greater is the departure from sphericity".

The Malvern Mastersizer 3000 is based on Stokes' equation whereby particles in a fluid settle under the influence of gravity (Briggs, 1977b;

Equation **6**). The basic premise of Stokes' Law is that the heavier the particle, the faster it falls. The sediment samples were added to 500ml of pure water in the Malvern Mastersizer 3000 unit. Before analysis, the sample underwent two minutes of ultrasonic dispersion before being measured for a minute at 8-12% obscuration (Pulley, 2014). The process was repeated another two consecutive times for each sample in order to increase accuracy.

Equation 6: Stokes' Law

t = the time in seconds for a particle to fall h cm once reaching terminal velocity, ρ = particle density (g cm^{-3}), ρ_0 = density of the suspending medium (g cm^{-3}), g = acceleration due to gravity (cm s^{-2}), d = particle diameter (cm), and η = viscosity of the liquid (Loveland & Whalley, 2000).

$$t = \frac{18\eta h}{(\rho - \rho_0) g d^2}$$

3.3. Statistical Analysis and Preparation

Atkinson *et al*. (2003) highlights the need for geomorphologists to apply the concept of spatially non-stationary analysis to their work in response to relationships that change on spatial and temporal scales. This is a concept known as spatial auto-correlation, a measure of the similarity between samples for a given variable as a function of spatial distance (Diniz-Filho *et al*., 2003). It is an important concept to apply in the field of geomorphology, as it reveals spatial associations among geographic units even if only evidence of causality and not the causality itself is provided (Miller, 2004).

Consequently, this dissertation applies methods for analysing spatial variation between active layer thicknesses and controlling factors. This method is generalised linear modelling (GLM) which facilitates a regression relation between a response variable and multiple explanatory variables. GLM is preferable to general linear regression as it is inclusive of categorical variables and do not require parameters to be normally distributed about their mean (Atkinson *et al.*, 2003). In addition, classical statistical analysis (non-spatial regression) is used to complement geographical (spatial regression) statistical methods as it augments the validation of results (Miller, 2012). The methods employed are detailed in the section titled Statistical Methods (pg.49).

3.3.1. Data Preparation

Raw data were captured in Microsoft® Excel. All data collected (except radiation values) were recorded hourly and ranged from eight years to two years depending on the objective in question. Before statistical analysis was carried out, raw data were cleaned by removing outliers. This was done by determining population means and standard deviations (s) to compute z-scores. Z-scores standardize data values by quantitatively representing how it is from the mean in terms of standard deviation (Walford, 2011). Consequently, any values exceeding the value of three z-scores were deemed outliers and removed from the population (Williams *et al*., 2007). The cleaned data were then statistically analysed in Microsoft® Excel which was used as the platform to create charts and graphs, as well as R v3.0 whereby files were saved in the .csv format. Descriptive statistics and statistical inference were used to determine linkages between the collected data, primarily those existing between ground thermal regimes and climate parameters. A confidence interval of 0.95 corresponding to a probability of 0.05 ($\alpha = 0.05$) are the most accepted certainty and significance parameters in earth sciences and are used for this project (Till, 1985; Walford, 2011).

3.3.2. Statistical Methods

3.3.2.1. Descriptive Statistics

Ground thermal dynamics and moisture regimes were recorded using XR5 data loggers and compared to climate data (pressure, radiation and ambient temperatures) for the same period. Once data were normalized using z-scores, null or missing values (observed for pressure and ambient temperatures) were excluded when conducting analyses. Descriptive statistics are based on measures of centre and variations within a dataset (Weiss, 2012). The mean, median and skewness were calculated for each dataset in order to determine the shape of the distribution which is also important for the removal of outliers to the data set using z-scores. A skewness value of 0 is indicative of a normal distribution, and values of 1.62 and -1.62 indicate highly skewed distributions to the right and left respectively (Hansen, 2013, Williams *et al*., 2007; Refer to Appendix B for descriptive terms and ranges used for skewness classes, pg.140). This was done for both the ground thermal dynamics as well as the soil moisture calibrations.

To increase the accuracy of the soil moisture calibration process, the datasets were reduced to only the summer months (DJF) as it is only during this period that air temperatures are high enough for melting to take place. Where clear breaks were visible in the soil moisture regime over the logging period, the dataset was sub-sectioned to be normalized and calibrated individually (Figure 18). For each dataset outlined in Table 5, the mean and standard deviations were used to standardize the soil moisture values, normalizing the distribution. The normalized values descriptive statistics revealed a standard deviation of 1. Aside from Flårjuven 2, which was finely negatively skewed, all the sites were positively to highly positively skewed (Table 5). The polynomial equation generated from the lab work (Appendix A, pg.136) for each logger sediment sample was calculated using an intercept of −1, which is the standard deviation found for all datasets normalized values. The polynomial equations were applied to the normalized values of each dataset using an intercept of −1 (Table 6).

Table 5: Descriptive statistics of soil moisture (mean, median, skewness) at the four borehole sites.

	Mean	**Median**	**Skewness**
Vesleskarvet	1.44	1.02	1.41
Robertskollen 1	-6.29	-6.54	2.85
Robertskollen 2	-1.54	-1.81	2.78
Robertskollen Combined	-4.22	-5.59	0.32
Flårjuven 1	-4.55	-4.65	1.89
Flårjuven 2	-4.61	-4.57	-0.25
Flårjuven 3	-3.95	-3.92	1.25
Flårjuven 4	-3.46	-3.56	1.34
Flårjuven 5	-3.51	-3.63	1.46
Flårjuven Combined	-3.92	-3.99	1.36
Nonshøgda	-1.19	-1.31	2.21

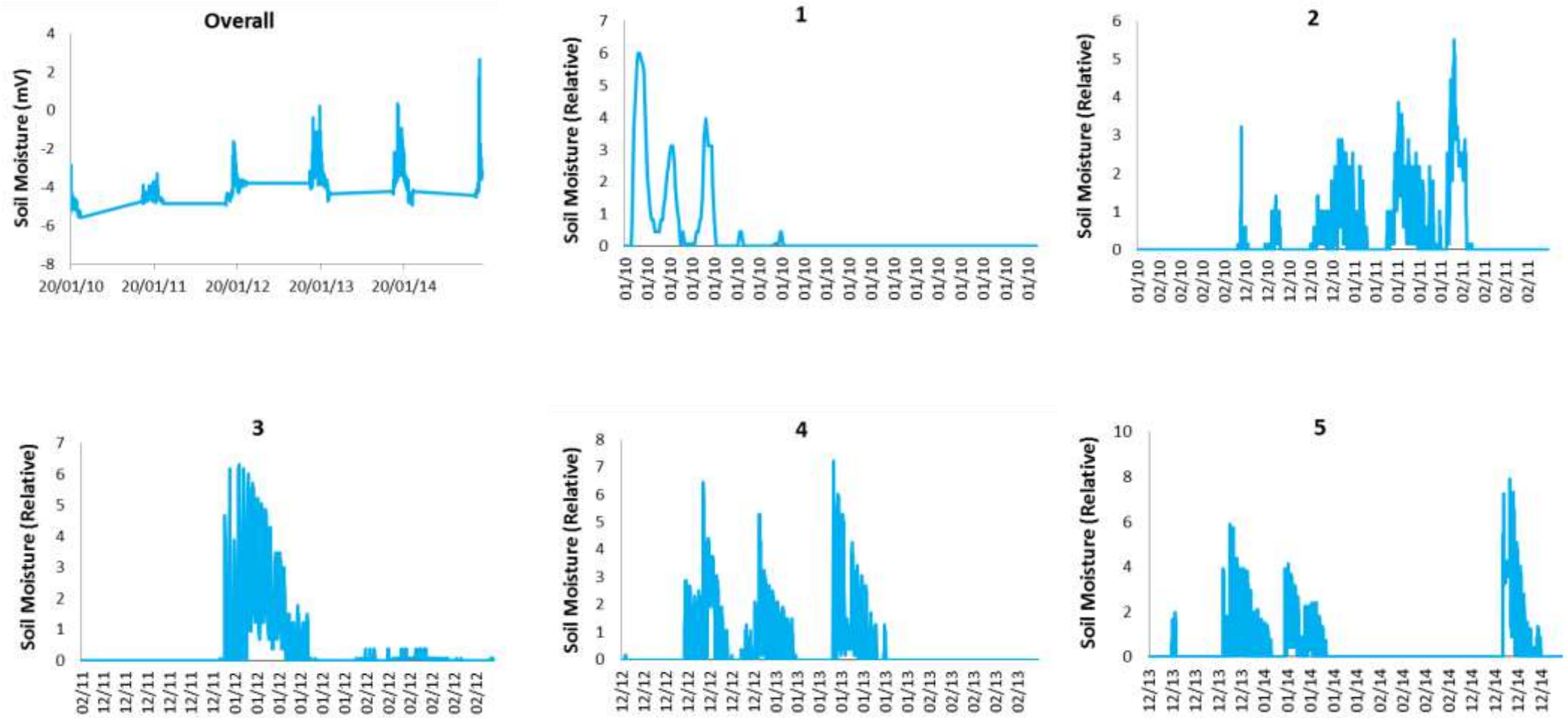

Figure 18: Seasonal summer (DJF) soil moisture for Flårjuven (2010-2014).

For each dataset outlined in Table 5, the mean and standard deviations were used to standardize the soil moisture values, normalizing the distribution. The normalized values descriptive statistics revealed a standard deviation of 1. Moreover, it is clear that aside from Flårjuven 2, which was finely negatively skewed, all the sites were positively to highly positively skewed (Table 5). The polynomial equation generated from the lab work (Appendix A, pg.136) for each logger sediment sample was consequently calculated using an intercept of −1, which is the standard deviation found for all datasets normalized values. The polynomial equations were then applied to the normalized values of each dataset using an intercept of −1 (Table 6). This gave a soil-specific calibration for each site.

Table 6: Polynomial equations applied to each logger dataset.

	Polynomial Equation
Vesleskarvet	$y = -8E09x^6 + 2E - 06x^5 - 0.002x^4 + 0.0092x^3 - 0.2146x^2 + 2.0735x - 1$
Robertskollen	$y = -1E - 05x^3 + 0.0032x^2 + 0.2351 - 1$
Flårjuven	$y = -4E - 05x^4 + 0.0051x^3 - 0.1805x^2 + 2.3284x - 1$
Nonshøgda	$y = -3E - 10x^6 - 4E - 08x^5 + 2E - 05x^4 - 0.0041x^3 + 0.0489x^2 - 0.3089 - 1$

3.3.2.2. Statistical Inference

Statistical inference used for the project comprises of the Pearson's correlation coefficient, regression analyses, and GLM. These were used to identify correlations between ground and climate data for each individual data series as well as the global data set. Linear regression was also utilised to attach a level of importance to the individual climate parameters. In addition, linear regression was used to determine the role/importance of individual climate parameters.

In linear regression, the least-squares line of best-fit method was applied to a set of observations (Till, 1985). Independent variables were modelled against dependent variables to determine the relative influence of the former (e.g. pressure) on the latter (soil temperatures) (Till, 1985). The Pearson's product-moment coefficient of linear correlation (*r*) is a bivariate technique founded on covariance in which the degree of dispersion of two variables for a group of observations is measured (Walford, 2011). The value of the coefficient (*r*) indicates the strength of the relationship using positive and negative values (−1 = negative relationship; +1= positive relationship) (Bluman, 2009). An *r* value close to zero is denotes no observed trend between populations (Williams *et al.*, 2007).

The square of r (r^2) indicates the amount of total variance explained by the linear relationship (Till, 1985; Walford, 2011), however, the remaining percentage of the variance remains unattributed. The use of general linear models is, therefore, required for a more in depth statistical analysis. Processes responsible for the active layer thermal regimes and thickness in WDML remain undocumented, necessitating the use of GLM. This will generate a scope for making predictions and providing explanations for observed geomorphological processes (Atkinson *et al*., 1998; Miller, 2012). According to Atkinson *et al*. (1998), the binary form of the GLM lends itself to use across numerous fields in geography, especially geomorphology as variables are required to be quantified on a categorical rather than continuous scale.

GLMs were run in order to investigate the relationships between active layer thermal regimes, pressure, air temperature and radiation for the 2010 dataset. This was done in R v3.0.1, by using the "glm" function. The spdep, MuMIn and ncf packages were run. Thereafter, the results were ranked according to their Akaike information criterion (AIC) using the dredge function from the MuMIn library (Marmion *et al*., 2008). The model with the lowest AIC was chosen as the model with the best fit, and rerun with only the most significant parameters. The pseudo r^2 was applied once modelling was completed to determine the fit of the model.

3.3.2.3. Mapping

Mapping using GIS techniques allows a visual representation of spatial data, aiding researchers in interpreting their findings. The majority of data were collected in the field. Additional data were obtained from Antarctic Digital Database (ADD). ESRI's ArcGIS suite of products was used for the creation and display of selected spatial data. WGS84 was used as the geographical coordinate system, and then projected to Transverse Mercator with 3°W as the central meridian for Flårjuven, Robertskollen and Vesleskarvet, as it preserves shape without over compromising on distance and area accuracy. For Nonshøgda, the Transverse Mercator projection using 3°E as a central meridian was used. Maps were standardised in terms of symbology, colour use, font type, size and weight as well as features such as the north arrow and scale bar.

CHAPTER 4: Results and Discussion of Findings

This chapter details the results for each objective, and provides a discussion based on these results. Each of the four sections represents the results corresponding to an objective set out in chapter one.

4.1. Objective 1: Active Layer Dynamics

4.1.1. Soil Moisture Regimes

Due to the variability of soil moisture sensors on account of a wide variety of in situ site characteristics, soil specific calibration of sensors at each of the four logging sites were done. Figure 19 and Figure 20 reveal large differences between respective pre and post calibration at the sites, Robertskollen in particular experienced a substantial amount of heave during the 2013/14 summer which resulted in the displacement of the Decagon EC-5 soil moisture sensor. Relative soil moisture for Robertskollen in 2014 should therefore be disregarded, however, the amount present post calibration was so low that the effects remain negligible. As mentioned previously, soil moisture was calibrated for the summer months (DJF). In both Figure 19 and Figure 20, the soil moisture for all four sites is plotted on the same axis for an inter-site comparison. Flårjuven and Vesleskarvet have the most abundant soil moisture, followed by Robertskollen and lastly Nonshøgda which has no recorded soil moisture (Figure 20: Soil moisture post soil-specific calibration; Appendix A, pg.136).

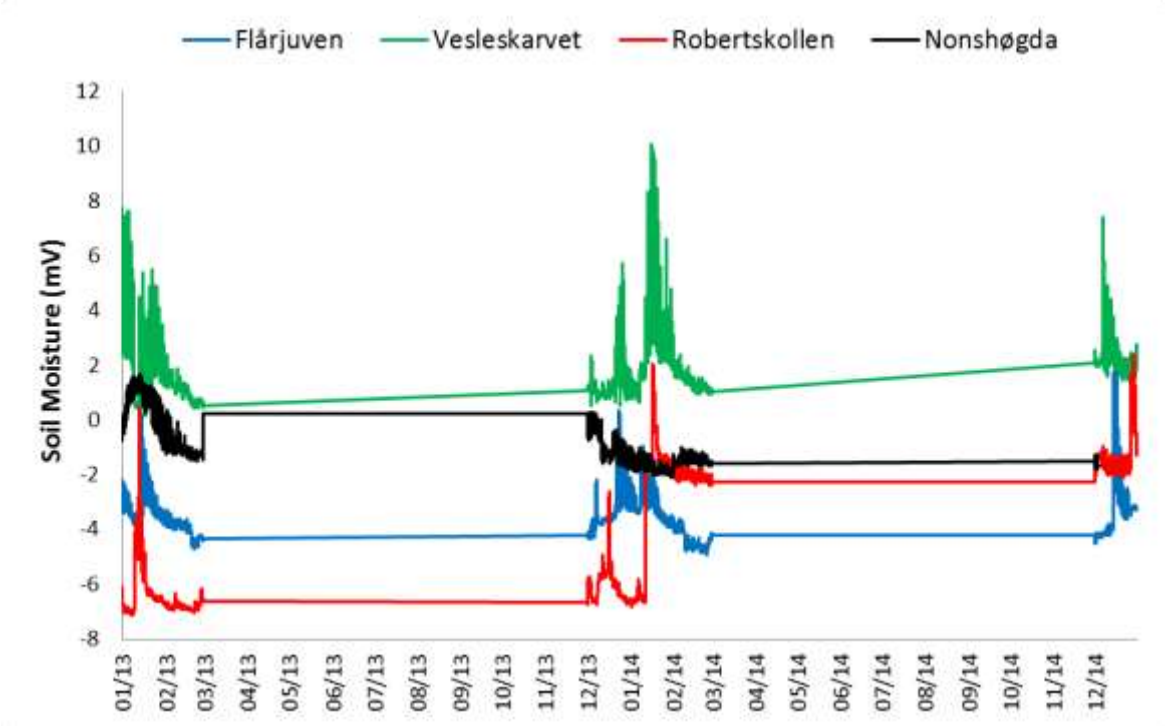

Figure 19: Soil moisture before soil-specific calibration.

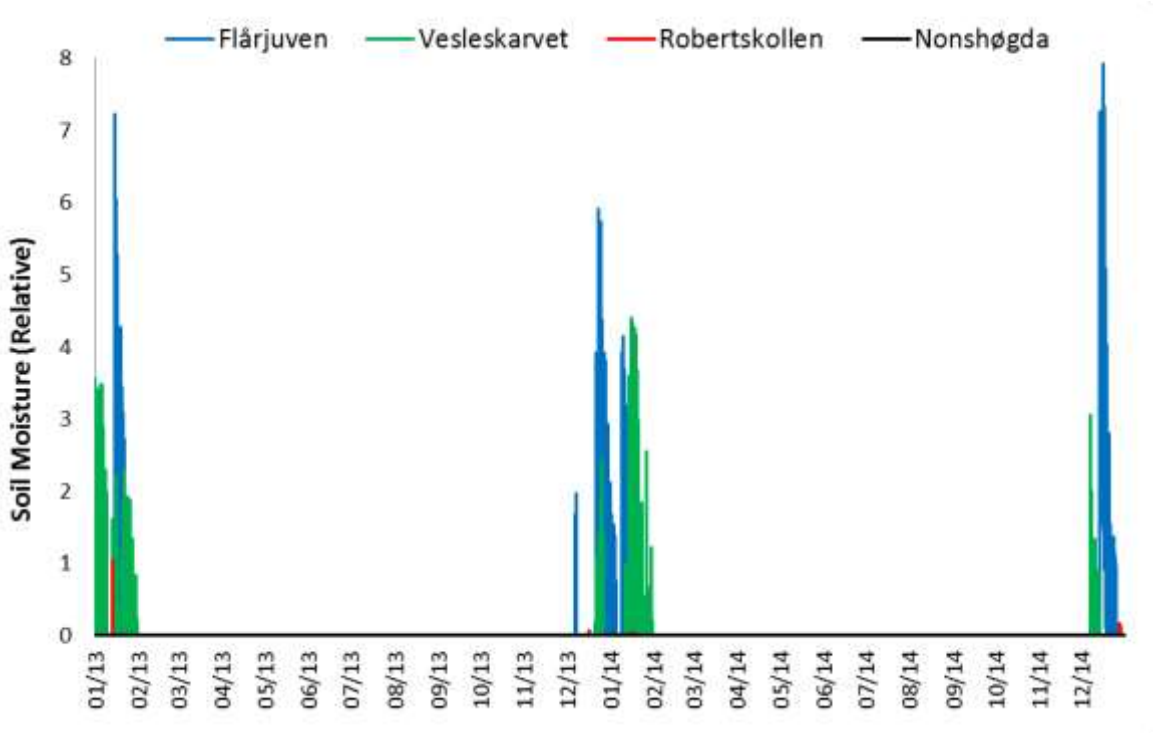

Figure 20: Soil moisture post soil-specific calibration.

4.1.1.1. Soil Physical Analysis

Table 7 shows the weights of the samples before and after drying, as well as bulk density, porosity volumetric water content (VWC), and phi sorting. Mineral soils have a bulk density between 1.00 g.cm^{-3} and 2.0 g.cm^{-3}, with an average bulk density of 1.25g.cm^{-3} (Briggs, 1977a). Soil at the study sites have little to no organic content which substantiates higher bulk density values falling close to 2.0 g.cm^{-3}. The bulk density values for Vesleskarvet were consistent with the findings by Hansen (2013) of bulk densities between 1.84 and 1.99 g.cm^{-3}. The gravimetric moisture content (GMC) of the active layer (<60cm) was below 5% for all sites except Vesleskarvet. Below this, ice-cemented permafrost is found, indicating that the soils may be <18,000 years old (Bockheim & Tarnocai, 1998a).

Table 7: Physical soil values for at each permafrost borehole.

Logger Site	**Wet soil mass (g)**	**Dry soil mass (g)**	**Mass & volume of water (cm^3)**	**Bulk Density (g/cm^{-3})**	**Porosity S_t**	**VWC (cm^3/cm^3)**	**Phi sorting (ϕ)**
Vesleskarvet	492.55	458.50	34.05	1.97	0.26	0.15	1.5
Flårjuven	407.86	394.74	13.12	1.69	0.36	0.06	1.5
Nonshøgda	475.42	475	0.42	2.04	0.23	0.00	3.3
Robertskollen	433.33	425.90	7.43	1.83	0.31	0.03	2

Figure 21 shows the dry mass proportions per sample, expressed as a percentage of total sample weight. As can be seen from Figure 21, all but one of the samples recorded majority of their weight for coarse sand and fine gravel. The largest proportion in terms of weight of particles for Vesleskarvet, Flårjuven and Robertskollen is for coarse sand to fine gravel particles between 1000µm and 2000µm (Refer to Appendix B for size grades of sedimentary particles, pg.140). Whilst weight proportions are similar throughout the profile for Nonshøgda, the largest proportion is medium gravels at 8000µm (Figure 21). The phi sorting values indicate that all sites have poorly sorted soils to very poorly sorted soils (Refer to Appendix B (Table 41) for sorting classes).

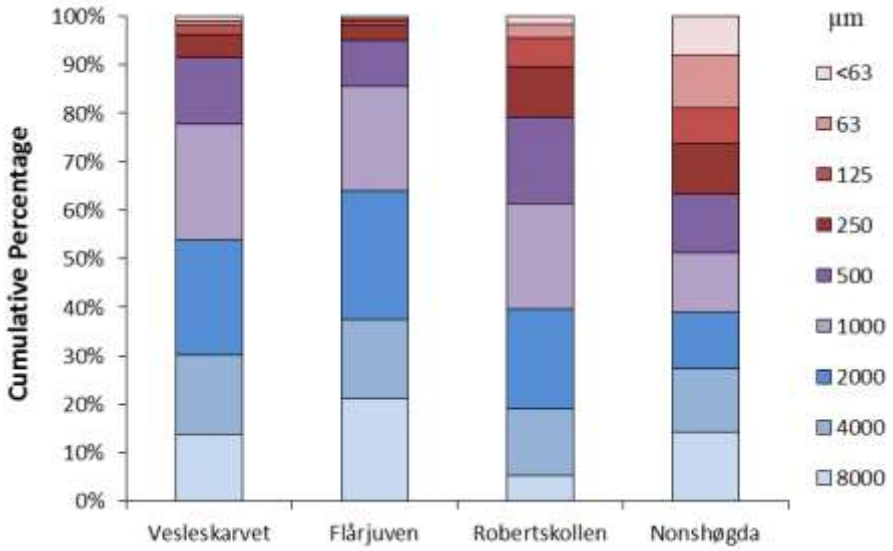

Figure 21: Particle size proportions for each study site.

The almost non-existent VWC of 0.0018 (GMC=0.01%) reflects the lack of soil moisture recorded at Nonshøgda as evident by Figure 20. This is substantiated by high bulk density and low porosity values which reduces the water holding capacity of the soil. However, soil moisture presence increased with depth in the active layer until ice cement was reached (pers.obs). This could be due to grain size decreasing with depth in the active layer, which increases the soils capacity to hold moisture (Haeberli *et al*., 2006). Seybold *et al*. (2010) found an increase in soil moisture with depth in the active layer, concentrated at the margin of permafrost. Conversely, the sediment at Flårjuven showed the lowest bulk density of all sites consistent with the highest porosity, which underpins the high soil moisture content displayed in Figure 20. This is not reflected by the VWC for Flårjuven (GMC=3%) which is substantially lower than that of Vesleskarvet (Table 7). The higher VWC (GMC=7%) at Vesleskarvet may be a function of the blockfield coupled with substantial snow cover, encouraging the development of meltwater pools through heat absorption by the dark surfaces of the rock (Hansen *et al*., 2013). It is important to recognize that the quantity of soil moisture measured is not only dependent on the physical characteristics of the soil, but more so on the local climate and presence of potential water sources such as snow during the sampling period.

The low altitude and warmer climate associated with Robertskollen anticipates a wetter soil moisture regime in comparison to the other sites. However, it had the second lowest soil moisture content (GMC=1.7%; Figure 20). This may be related to the absence of snow cover during the 2013/14 summer which could be attributed to sublimation before infiltration could take place or by wind redistributing the snowfall. Despite low soil moisture levels, the active layer was significantly deeper (58cm) than the three other sites. This is partially a product of higher temperatures, however, low thermal conductivity due to low soil moisture values does not account for the depth of the active layer. From personal observations during the 2013/14 summer, water pools were found in areas of low elevation several meters from the logging site. This flow is not supplied by glacial melt, and therefore, must be derived from snow patches, permafrost, buried glacier ice or groundwater from the subsurface (Harris *et al*., 2007). Ryan *et al*. (1989) noted an abundance of meltwater streams during a biological survey.

There are three possible explanations for low surface soil moisture accompanied by a thick active layer at Robertskollen. First, it is plausible that strong pressure potentials between soil pores facilitates the transport of moisture from these pools through the active layer over distances of several metres (Ikard *et al*., 2009). Harris *et al*. (2007) has documented occurrences of groundwater reaching the soil surface have during warm summer seasons. The soil moisture augmented by the pools has the capacity to increase conductive heat transfer in the subsurface regardless of changes to the surface energy balance, effectively creating a deep active layer (Ikard *et al*., 2009). Second, any water infiltrating from snowmelt on the elevated logger site is effectively drained into the meltwater pools, leaving little detectable soil moisture behind. Lastly, a snow-covered hillside adjacent to the logger may result in heat transfer as a result of subsurface meltwater percolating from the slope, effectively deepening the active layer. A combination of these explanations may be plausible, as multiple authors have demonstrated how local topography influences the depth of the active layer (Cannone *et al*., 2008; Adlam *et al*., 2010).

4.1.1.2. Soil Moisture and Air Temperature

From analysis of the ground thermal regimes recorded by the PACE XR5 logger at the four sites, it is clear that air temperature influences the soil moisture regime and NST, particularly during summer (DJF). Williams and Smith (1989) highlight how seasonal fluctuations of solar radiation and air temperature is reflected by ground surface temperature and soil moisture, evident as a wave that proliferates down into the ground. These fluctuations are also seen diurnally in soil moisture which is a function of climate, as well as through the slight dependency of the electronic devices on temperature.

Pearson's correlation coefficients of soil moisture with air and near surface ground temperatures are shown in Table 8 (pg.58). Nonshøgda correlation coefficients are null as no soil moisture is present at this site (Table 10; Figure 22). Figure 22 shows pre-calibrated soil moisture values with air temperature at Nonshøgda over the study period. During January 2013, a peak in soil moisture is evident due to the construction of a hut in the vicinity of the logger. However, it has been disregarded as this was not a natural moisture input (Figure 22). Moreover, it is clear from Figure 22, that the "soil moisture" regime at Nonshøgda closely follows air temperature. This is substantiated by strong and positive relationships (significant at 95%) between original soil moisture and air temperature, and original soil moisture and near surface temperature, at 0.72 and 0.83 respectively. The sensor is in fact picking up and measuring variations in temperature and not soil moisture. According to Campbell (2006), although probes are effective at shallow depths, there is a higher risk of temperature dependence. This has an effect on the permittivity of water, the soils electrical conductivity, as well as the amount of water bound to the mineral surface (Francesca *et al*., 2010).

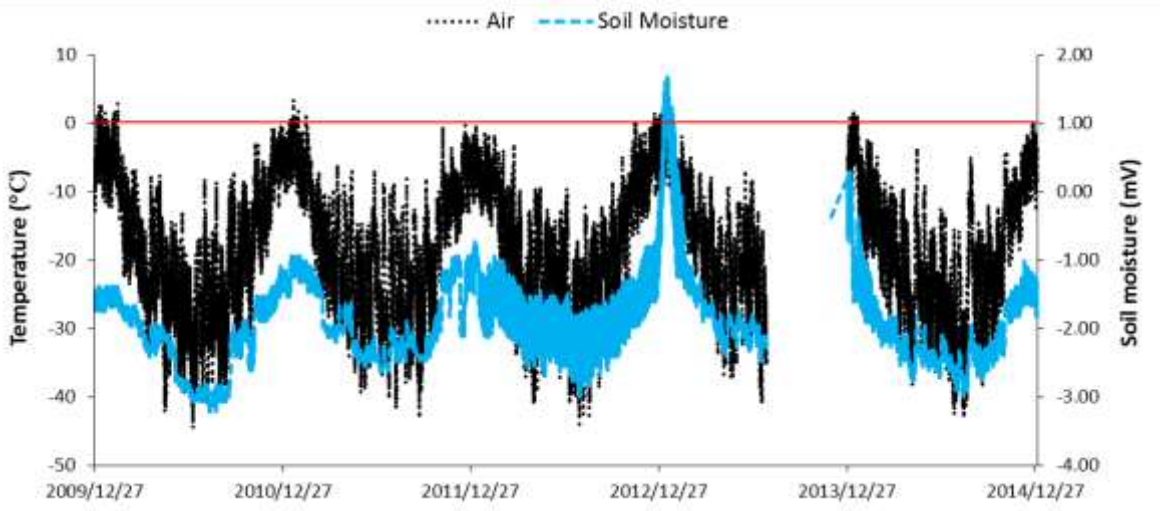

Figure 22: Soil moisture and air temperature data for Nonshøgda (2009-2014).

Soil moisture and air temperatures have a moderate and positive relationship at Vesleskarvet and Flårjuven (see Appendix B for descriptive terms and ranges used for correlation coefficients, pg.140). Robertskollen showed a weak relationship between temperatures and soil moisture. At Vesleskarvet, the relationship between soil moisture and NST is stronger than the relationship between soil moisture and air temperature. The opposite is found for soil moisture at Flårjuven and Robertskollen. The results are not as statistically significant as anticipated, with p-values greater than 0.05. This is due to the fact that all summers have been combined to obtain the results in Table 8, reducing the correlation coefficient as each summer experiences a different moisture regime.

Table 8: Pearson's correlation coefficients between calibrated soil moisture and temperature (°C) (air and near surface) observed during each nunataks recording period.

	Air Temperature	Near Surface Temperature
Vesleskarvet	0.45	0.47
Flarjuven	0.53	0.49
Robertskollen	0.25	0.23
Nonshogda	0.00	0.00

Table 9 shows the correlation co-efficient of soil moisture values with air and near surface temperature for the summers at Vesleskarvet. Summer 2009/10 has the lowest correlation coefficient concurrent with the fact that this summer had the lowest soil moisture content overall. Conversely, the summer of 2012/13 experienced the highest soil moisture volumes, relating to higher correlation values. The same principle can be applied to Robertskollen, as this site received the least soil moisture overall (Table 8). Table 10 shows the link between the percentage of soil moisture during the 2013/14 summer, with correlation coefficients calculated between soil moisture and near surface temperature, significant at 95%. It is clear that less soil moisture present yields much lower correlation values.

Table 9: Pearson's correlation coefficients between calibrated soil moisture and temperature (°C) (air and near surface) observed during each summer (DJF) at Vesleskarvet.

	Air Temperature	Near Surface temperature
2009/10	0.14	0.21
2010/11	0.52	0.56
2011/12	0.36	0.39
2012/13	0.58	0.58
2013/14	0.38	0.34

Table 10: Pearson's correlation coefficients between NST (°C) and calibrated soil moisture observed during the 2013/14 summer (DJF) at Vesleskarvet, Flårjuven and Robertskollen.

	% Soil Moisture	Correlation Coefficient
Vesleskarvet	10.75	0.34
Flarjuven	21.48	0.42
Robertskollen	0.79	0.12

It is important to note from these findings that soil moisture varies on an annual basis, as can be seen by the variability during summer at Vesleskarvet in Table 9. Moreover, soil moisture is unique to each nunatak and the fact that correlation values are not significant between air and near surface temperatures and soil moisture at each site indicates the relative nature of soil moisture. Although correlation values do not indicate strong relationships, the relationship between soil moisture and climate variables such as radiation, cloud cover, snow frequency and air temperature persist. The relationship is heightened in summer when higher temperatures facilitate the melt out of snow, as well as by the delay in soil moisture peaks following peaks in air and near surface temperatures.

Mineral soils exhibit a thermal diffusivity that increases with water content when water content in the soil is low. Similarly, when water contents in the soil are high, thermal diffusivity decreases (Seybold *et al*., 2010). Therefore, at the four study sites which all contain relatively little soil moisture in comparison to Arctic environments, small increases in water contents lead to an increase the thermal diffusivity, allowing deeper penetration with consecutive wetting events (Seybold *et al*., 2010). This leads to an increased deeper thaw depth and duration (Adlam *et al*., 2010; Seybold *et al*., 2010). This is supported by the findings through the correlation coefficients calculated between soil moisture and average NST, particularly for Vesleskarvet and Flårjuven; larger amounts of moisture generate higher observable ground temperatures due to increased thermal conductivity, i.e. a deeper active layer (Adlam *et al*., 2010). The exception is Robertskollen which is also influenced by topography, which is not a determining factor for the other three study sites as they are located on a generally flat surface.

4.1.2. Annual Ground Thermal Regimes

The average annual amplitude of air temperature at Vesleskarvet was 47.6°C, with a mean of −15.9 °C (Table 11). The air temperature range at Flårjuven was lower at 43.7°C, with the lowest overall mean of −18.2°C. Interestingly, Flårjuven showed the same modal temperature throughout the ground thermal profile, and was the only site to do so. Nonshøgda has the highest range in air temperature at 58.6°C, and a mean of −17.7°C. The high range in temperature at Nonshøgda would be exaggerated in the ground due to the nature of the coarse-grained rocks and sediment which contains a relatively high amount of mafic minerals (Dallmann *et al*., 1990)

Robertskollen has the lowest range in air temperature at 38.7°C and highest overall mean of −13.8°C, this is due to its low altitude and proximal distance to the ice-shelf compared to the other sites. The large air temperature ranges displayed by the four sites, with maximum air and near surface temperatures as high as 8.76°C and 18.22°C respectively, provides the perfect conditions for the development of active layer related landforms when coupled with an adequate supply of soil moisture. The temperature ranges in both the air and ground allows the active layer to become a weathering agent, aiding in soil formation due to thermally induced stresses (Singh *et al*., 2011).

The air temperature at Vesleskarvet and Robertskollen was finely positively skewed, at Nonshøgda it was finely negatively skewed, and Flårjuven displayed a symmetrical distribution. Near surface temperature regimes displayed the largest standard deviation for all the sites. For all four sites, the ground thermal regimes displayed finely positive to positive distributions. Overall, Nonshøgda displayed the most normally distributed dataset of all. Skewness values for all sites were suitable to assume a near-normal distribution as well as to allow for standardisation of values. Refer to Appendix B, pg.140, for a description of terms used.

Table 11: Summary statistics calculated on GTR (°C) and soil moisture for the Vesleskarvet PACE XR5 data logger, during 2009-2014.

	Air	Near Surface	15cm	30cm	45cm	60cm
Mean	-15.88	-16.08	-16.05	-16.22	-16.03	-16.14
Standard Error	0.04	0.04	0.03	0.03	0.03	0.03
Median	-16.29	-17.20	-17.42	-17.68	-17.59	-17.59
Mode	-21.18	-23.78	-21.18	-21.18	-20.78	-21.18
Standard Deviation (*s*)	7.37	7.85	6.90	6.62	6.16	5.90
Sample Variance	54.31	61.64	47.57	43.89	38.00	34.82
Kurtosis	-0.56	-0.44	-0.82	-0.92	-0.92	-0.94
Skewness	0.11	0.39	0.38	0.39	0.42	0.43
Range	47.55	52.02	34.08	31.72	27.52	25.50
Minimum	-40.78	-38.95	-33.96	-31.98	-29.64	-28.56
Maximum	6.77	13.07	0.12	-0.26	-2.12	-3.06
n = 5 years; 8 months						

Table 12: Summary statistics calculated on GTR (°C) and soil moisture for the Flårjuven PACE XR5 data logger, during 2008-2014.

	Air	Near Surface	15cm	30cm	45cm	60cm
Mean	-18.15	-17.28	-17.70	-17.80	-17.91	-18.11
Standard Error	0.04	0.04	0.03	0.03	0.03	0.03
Median	-18.46	-18.79	-19.40	-19.70	-19.80	-19.93
Mode	-23.10	-23.10	-23.10	-23.10	-23.10	-23.10
Standard Deviation (s)	7.17	8.95	7.76	6.96	6.57	6.33
Sample Variance	51.36	80.15	60.26	48.48	43.16	40.03
Kurtosis	-0.60	-0.12	-0.75	-0.90	-0.92	-0.93
Skewness	0.06	0.56	0.46	0.49	0.52	0.53
Range	43.68	59.12	40.24	30.28	26.05	25.31
Minimum	-41.38	-40.90	-35.74	-31.48	-29.14	-29.10
Maximum	2.30	18.22	4.50	-1.20	-3.09	-3.79
n = 6 years; 9 months						

Table 13: Summary statistics calculated on GTR (°C) and soil moisture for the Robertskollen PACE XR5 data logger, during 2013-2014.

	Air	Near Surface	15cm	30cm	45cm	60cm
Mean	-13.79	-13.07	-13.15	-12.98	-12.86	-12.78
Standard Error	0.06	0.08	0.07	0.06	0.06	0.05
Median	-14.42	-14.99	-15.57	-15.65	-15.32	-15.32
Mode	-18.64	-20.57	-19.98	-19.69	-20.37	-0.07
Standard Deviation (s)	7.43	10.03	8.64	7.95	7.47	7.04
Sample Variance	55.22	100.67	74.59	63.16	55.81	49.61
Kurtosis	-0.82	-0.59	-0.91	-1.01	-1.05	-1.07
Skewness	0.15	0.51	0.48	0.50	0.52	0.53
Range	38.67	48.87	43.58	34.51	28.39	24.47
Minimum	-32.73	-32.99	-28.78	-26.30	-24.59	-23.49
Maximum	5.94	15.88	14.80	8.21	3.80	0.98
n = 2 years						

Table 14: Summary statistics calculated on GTR (°C) and soil moisture for the Nonshøgda PACE XR5 data logger, during 2007-2014.

	Air	Near Surface	50cm	100cm	150cm	200cm
Mean	-17.70	-17.15	-17.02	-16.89	-16.92	-17.06
Standard Error	0.04	0.04	0.03	0.03	0.02	0.02
Median	-17.06	-19.12	-18.98	-18.09	-17.72	-17.46
Mode	-26.68	-24.71	-21.18	-21.18	-22.88	-19.59
Standard Deviation (s)	9.26	9.33	7.66	6.61	5.71	4.98
Sample Variance	85.84	87.11	58.65	43.76	32.57	24.79
Kurtosis	-0.75	-1.04	-1.21	-1.28	-1.32	-1.34
Skewness	-0.25	0.33	0.31	0.25	0.20	0.13
Range	58.55	42.30	29.20	24.16	19.96	17.15
Minimum	-49.79	-36.14	-31.24	-28.42	-26.42	-25.42
Maximum	8.76	6.16	-2.04	-4.26	-6.46	-8.27
n = 7 years; 2 months						

From Figure 23 to Figure 26, the seasonality of air temperature, ground thermal regimes, and soil moisture are clearly depicted by the peaks and troughs of summer and winter maximums and minimums respectively. During winter months, air temperature becomes more observable as near surface temperatures show reduced variations in response to increasing snow cover (PermaNet, 2011). At Vesleskarvet, Flårjuven and Robertskollen, air temperature and ground temperatures fluctuate slightly from one another during winter which is attributable to the insulating effects of snow, increasing NST by several degrees above the ambient mean annual air temperature on a frequent basis (Zhang *et al*., 1996; Ishikawa, 2003).

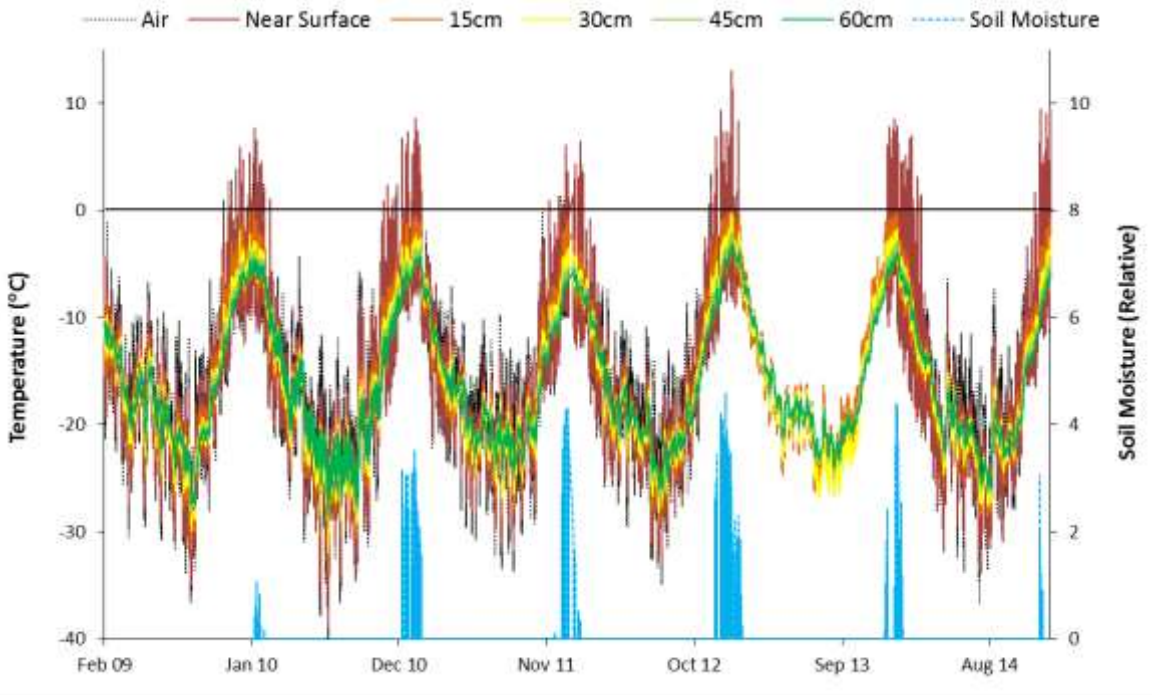

Figure 23: Air, ground temperature and soil moisture data for Vesleskarvet, 2009-2014 (air and near surface temperature data missing from January 2013 – January 2014 due to logger malfunctions).

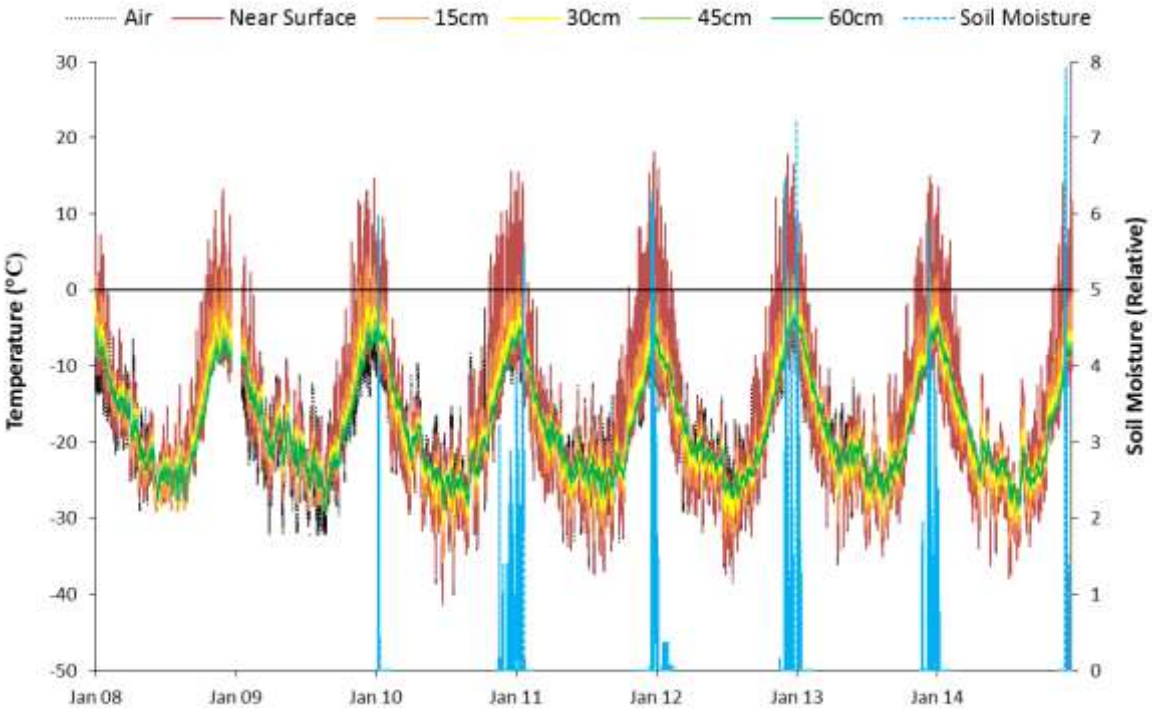

Figure 24: Air, ground temperature and soil moisture data for Flårjuven, 2008-2014 (air temperature data missing from June 2008-January 2009 and from January 2013-December 2014) due to logger malfunctions).

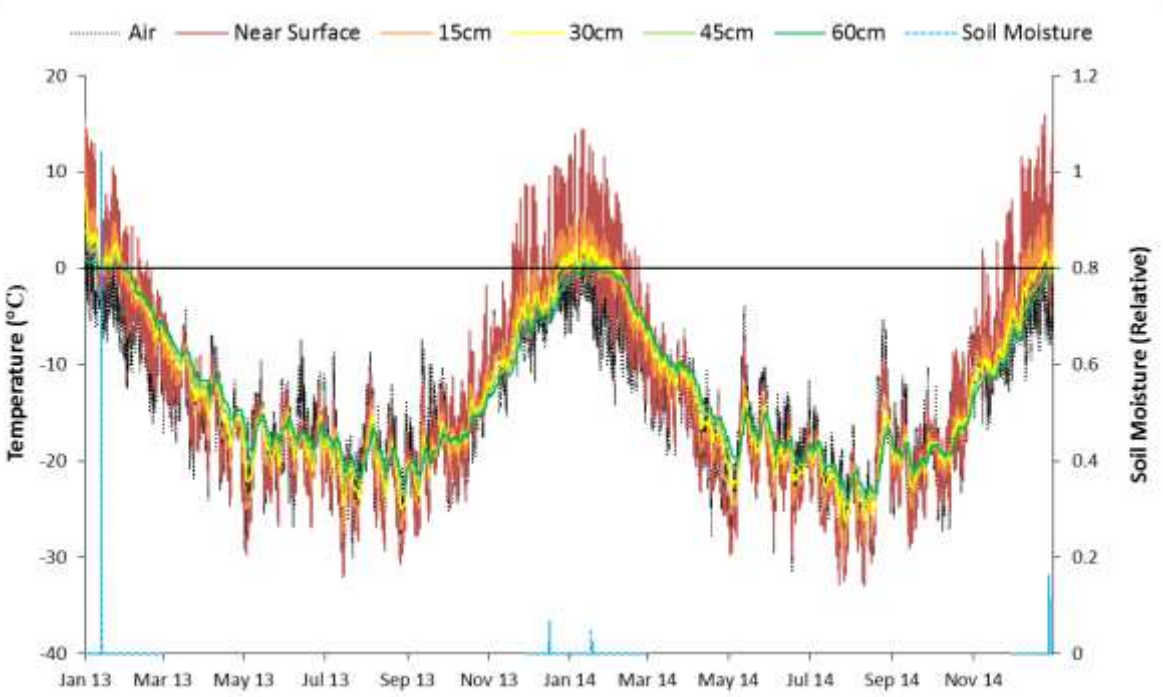

Figure 25: Air, ground temperature and soil moisture data for Robertskollen, 2013-2014.

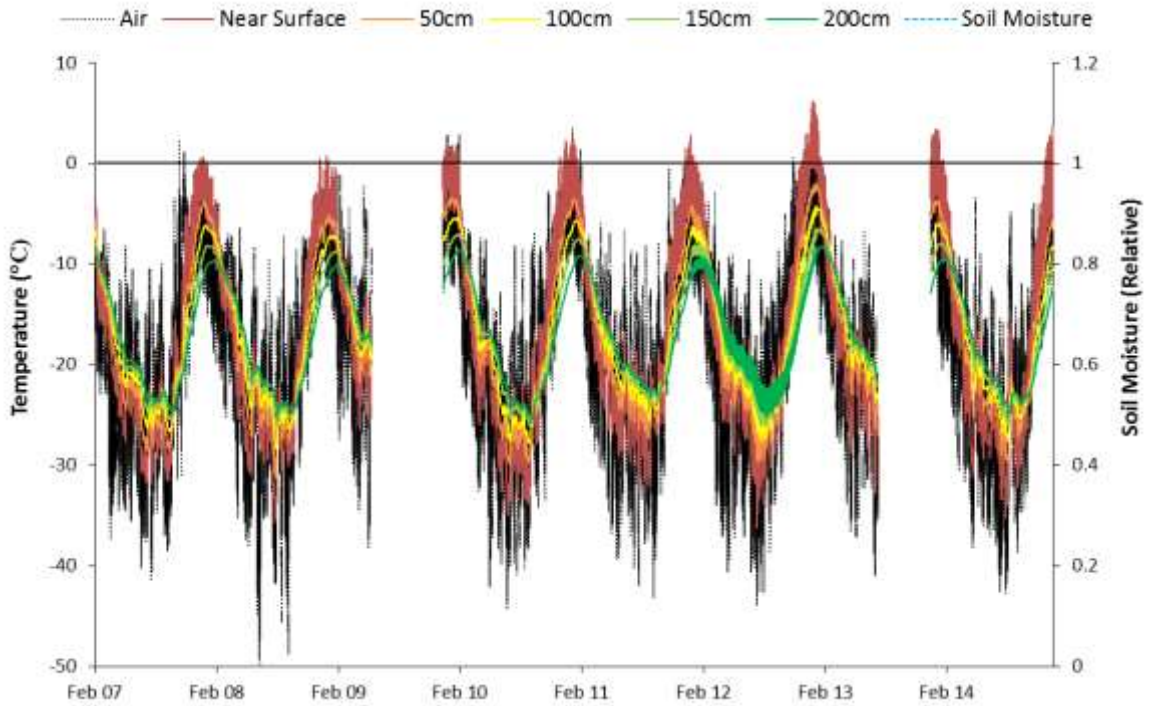

Figure 26: Air, ground temperature and soil moisture data for Nonshøgda, 2007-2014 (missing data from May-December 2009 and July-November 2013 due to logger malfunctions).

The disparity between air and ground temperatures are more pronounced at Nonshøgda (Figure 26). Despite a reduction in the magnitude of ground temperature fluctuations at Nonshøgda, it is hypothesized that either a thin snow layer or lack of snow completely, facilities an overcooling of ground temperatures, manifested as air temperature being drastically higher than ground temperature (PermaNet, 2011). Overall, during winter, the lack of solar radiation allows the thermal insulating effects of snow to be exceeded by the net balance of the longwave radiation leading to higher air temperatures than ground temperatures (Guglielmin *et al*., 2014b).

During summer, attenuations in NST cease as a result of its strong relationship with air temperature from late spring to autumn when the site is snow free, allowing larger observable daily fluctuations in NST (PermaNet, 2011). Moreover, the effect of solar radiation on ground thermal temperatures is equally important to air temperature as more energy is absorbed through heating of the surface (Guglielmin *et al*., 2011; Guglielmin *et al*., 2014a). This is evident for all four sites (Figure 23; Figure 24; Figure 25; Figure 26).

4.1.2.1. Active Layer Depth

Active layer depths for each year were calculated using the intercept of the maximum ground thermal regimes with the 0°C isotherm, also known as the cryofront which serves as a boundary between cryotic and noncryotic ground (Singh *et al*., 2011). The following depth profiles visually indicate the yearly depth of the cryofront. At Vesleskarvet, the 0°C isotherm threshold was crossed annually around 15cm depth exempting 2013, indicating the typical depth of the active layer (Figure 27; Table 15). The average active layer depth for the six year period was approximately 16cm; with the maximum active layer depth in 2013 at approximately 24cm (Figure 27). The summer of 2012/13 was also the warmest of all summers with an active layer depth of 20cm (Table 15). Minimum ground thermal regimes exhibit a large inter-annual variability, with 2011 and 2013 showing the warmest minimum temperatures, and 2009 and 2010 the coldest minimum temperatures (Figure 28). Overall, the NST (near surface temperature) minima varied between −40°C to approximately −30°C between 2009 and 2014, showing an increasing trend in temperature. The same trend is apparent for maximum annual ground thermal regimes; the warmest maximum temperatures were experienced in 2013 and 2014. Near surface maxima increased from approximately 10°C to 30°C during the period monitored at Vesleskarvet (Figure 27).

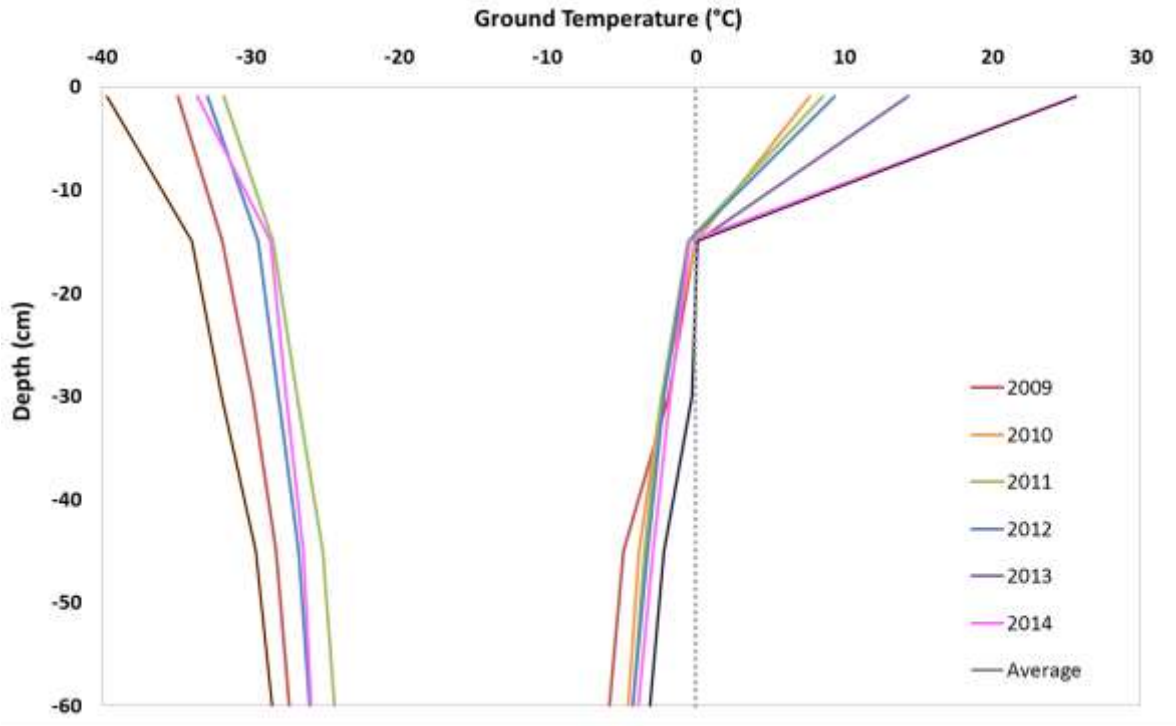

Figure 27: Yearly minimum (left) and maximum (right) ground thermal regimes with depth at Vesleskarvet, 2009-2014 (2013 minimum excluded due to logger malfunctions experienced during winter).

Table 15: Maximum active layer depth and date (d/m/y) of the deepest measured melting (0°C) during summers at Vesleskarvet.

Summer	Date	Thickness (cm)
2009-10	19/01/10	15.40
2010-11	21/01/11	14.10
2011-12	30/01/12	13.45
2012-13	08/01/13	20.20
2013-14	12/01/14	14.60

At Flårjuven, the cryofront reached depths between 22cm and 26cm annually (Figure 28; Table 16). The average active layer depth for the six year period was approximately 24cm; with the maximum active layer depth in 2008 and 2009 at approximately 26cm. The summer of 2009/10 and 2012/13 were the warmest of all summers with an active layer depth of approximately 25cm. The minimum ground thermal regimes exhibit a larger inter-annual variability than the maxima, with 2009 showing the warmest minimum temperatures, and 2010 the coldest minimum temperatures (Figure 28). Overall, the NST minima varied between −40°C to approximately −30°C between 2009 and 2014, however, no increasing trend in temperature is evident. Near surface maxima varied from approximately 12°C to 20°C during the period monitored (Figure 28).

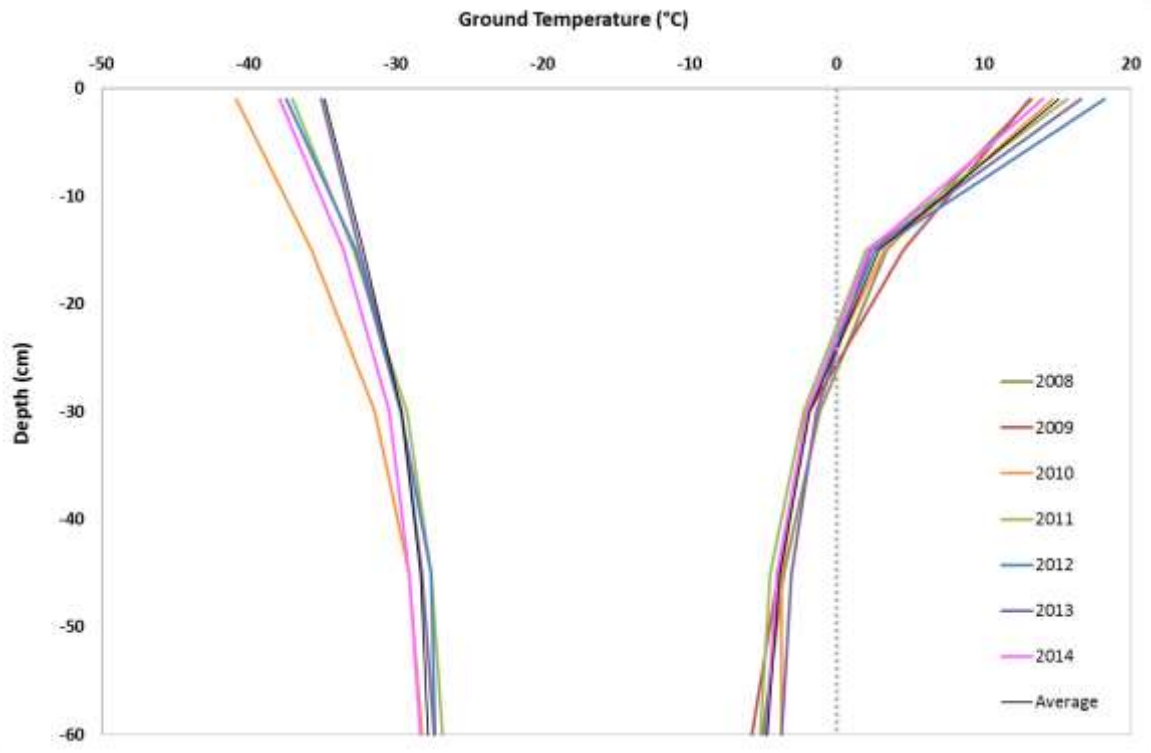

Figure 28: Yearly minimum (left) and maximum (right) ground thermal regimes with depth at Flårjuven, 2008-2014 (2008 & 2009 minimum excluded due to logger malfunction).

Table 16: Maximum active layer depth and date (d/m/y) of the deepest measured melting (0°C) during summers at Flårjuven.

Summer	Date	Thickness (cm)
2008-09	14/12/2008	23
2009-10	22/12/2009	26
2010-11	21/01/2011	22
2011-12	10/01/2012	22
2012-13	20/12/2012	25
2013-14	27/12/2013	23

At Robertskollen, the cryofront reached a depth of 58cm in the summer of 2013/14, which was the same maximum depth reached in 2014 (Figure 29; Table 17). However, the depth of the logger was not adequate enough to allow the determination of the 2013 active layer thaw depth. This indicates that a 2m rather than 60cm borehole is required at Robertskollen since it is the warmest site with the deepest active layer. Minimum ground thermal regimes exhibit a lower inter-annual variability than the maxima which is contradictory to the other sites. This could be due to a change in the thermal diffusivity of the ground following the warm summer of 2012/13 as freeze-thaw cycles progress (Ikard *et al.*, 2009). Overall, the NST minima varied between −35°C to approximately −30°C, whilst near surface maxima for the two years coincided at approximately 15°C (Figure 29).

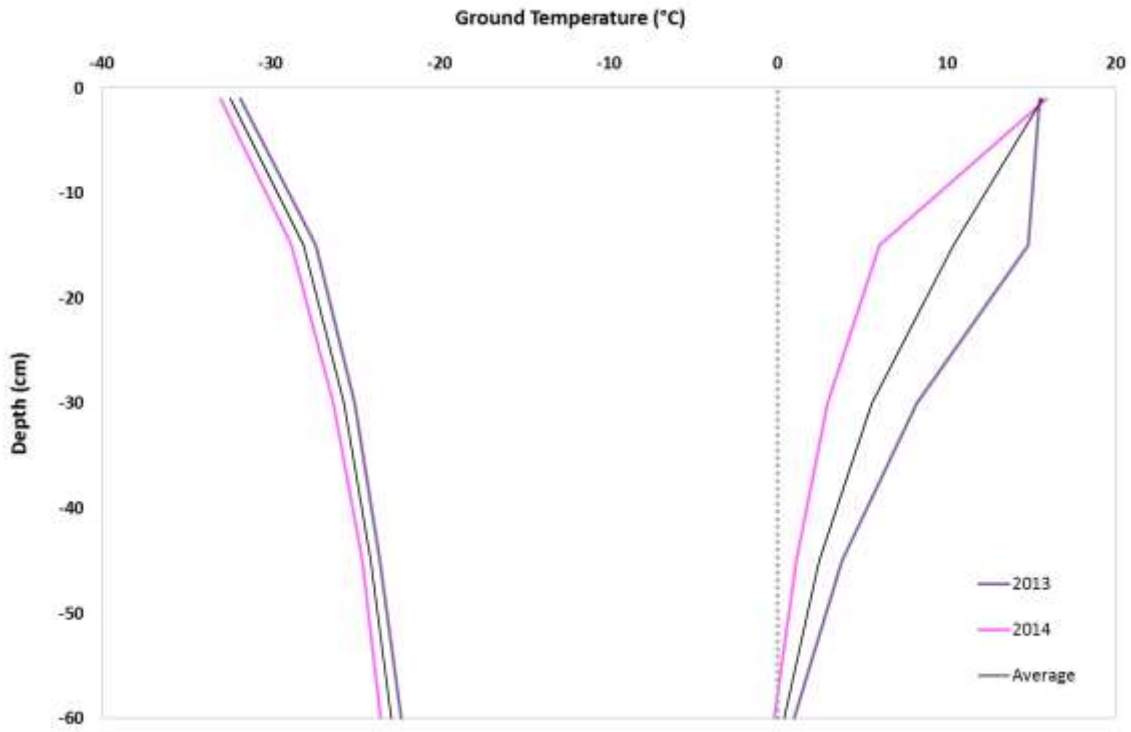

Figure 29: Yearly minimum (left) and maximum (right) ground thermal regimes with depth at Robertskollen 2013-2014.

Table 17: Maximum active layer depth and date (d/m/y) of the deepest measured melting (0°C) during summers at Robertskollen.

Summer	Date	Thickness (cm)
2013-14	13/01/2014	58

At Nonshøgda, the cryofront reached an average active layer depth of 18cm for the eight-year period, with the maximum active layer depth during 2013 at approximately 37.5cm (Figure 30). The summer of 2012/13 was by far the warmest of all summers with an active layer depth of approximately 38cm (Table 18). A larger inter-annual variability is exhibited by both the minimum and maximum ground thermal temperatures. The years 2007, 2008, and 2009 had the coldest maximum near surface temperatures, with active layer depths to match at approximately 2cm, 7cm and 7cm respectively. Overall, the NST minima varied between –37°C to approximately –32°C between 2007 and 2014, however, no increasing trend in temperature is evident. Near surface maxima varied from approximately 0.04°C to 6°C during the period monitored, with an increasing trend in temperature maxima (Figure 30).

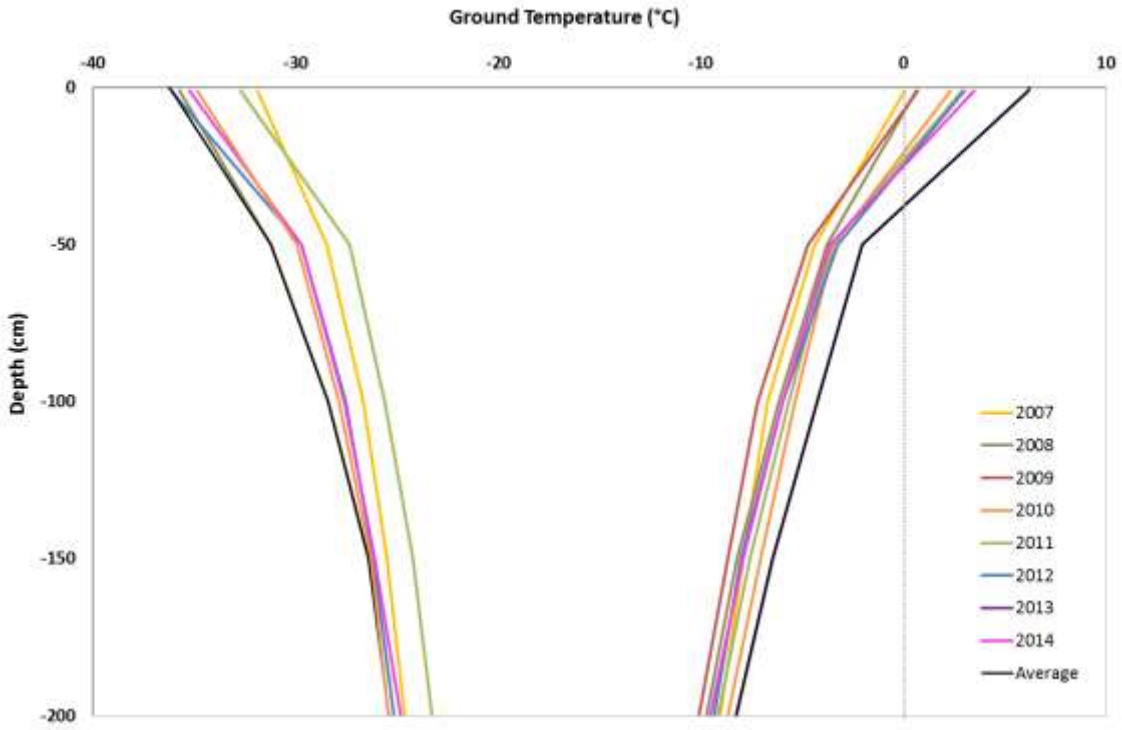

Figure 30: Yearly minimum (left) and maximum (right) ground thermal regimes with depth at Nonshøgda 2007-2014 (2009 & 2013 Minimum Data not recorded; logger did not function from May-December & July-November respectively).

Table 18: Maximum active layer depth and date (d/m/y) of the deepest measured melting (0°C) during summers at Nonshøgda.

Summer	Date	Thickness (cm)
2007-08	04/01/2008	8
2008-09	10/01/2008	7
2009-10	09/01/2010	18
2010-11	18/01/2011	23
2011-12	07/01/2012	21
2012-13	07/01/2013	38
2013-14	12/01/2014	24

From the depth profiles, barring Robertskollen, it is clear that ground thermal regimes experience a larger variability in minimum temperatures compared to maximum temperatures. This can be ascribed to air temperature during winter months fluctuating more than during summer (Figure 31). This has to do with meridional and vertical temperature gradients in winter being larger than in summer, which is why we see such high standard deviations at this time (Figure 31). These temperature gradients arise from advection, inversions and katabatic winds. Large changes in air temperature stem from passing low pressure systems advecting relative warm and moist maritime air to the south, which also brings about changes in wind speed and direction (French & Burns, 2004; Reijmer & van den Broeke, 2001).

When horizontal advection is absent during winter, a near surface temperature inversion develops through a balance reached between warming by the turbulent downward transport of sensible heat and cooling by longwave radiation as a result of a deficit in surface radiation (van den Broeke 2000; Pavelsky *et al.* 2011). Changes in wind speed and cloudiness disturb the inversion, reflected by changes in near surface temperature which are sensitive to these disturbances (van den Broeke 2000; Schneider *et al.* 2004). Moreover, from Figure 31, it is apparent how the standard deviations increase from Robertskollen, the lowest elevation site, through to Nonshøgda, the highest elevation site. This indicates how geographical location creates a meridional gradient with increasing continentality due to differences in convective heat exchange of the atmosphere with the lithosphere (Yershov, 1998). The result is increasing amplitude of temperature as one move from the coast to the continent.

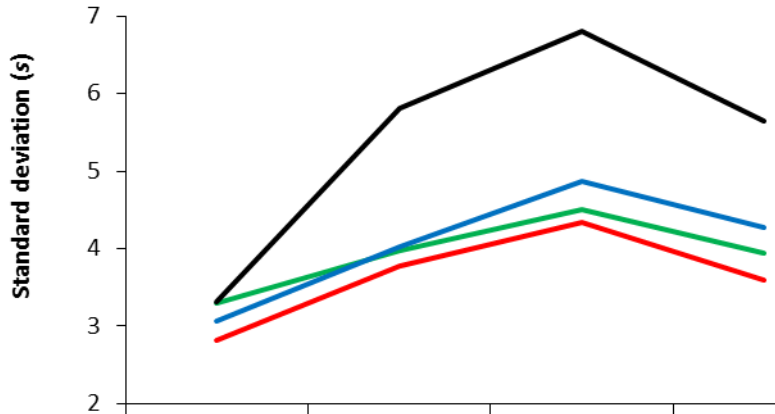

	DJF	MAM	JJA	SON
Vesleskarvet	3.30	3.98	4.50	3.94
Flårjuven	3.06	4.03	4.87	4.28
Robertskollen	2.82	3.77	4.35	3.59
Nonshøgda	3.32	5.81	6.80	5.64

Figure 31: Seasonal standard deviations in air temperature (total dataset for each site used).

From the depth profiles and accompanying tables it has become increasingly clear that a temporal variation of the maximum active layer depth at the four sites was observed between summers. This was evident by the intercept of ground temperatures with the 0°C isotherm, which mostly varied inter-annually within the month of January (Table 19). The date of deepest measured thawing for both Nonshøgda and Vesleskarvet was very similar, occurring on 7 and 8 January 2013 respectively. The date of the deepest measured thawing at Robertskollen was on 1 January 2013, reaching 1°C at 58cm depth which penetrated beyond the scope of the logging depth. Flårjuven was the only site that experienced active layer thickness maxima in December (Table 19). Owing to the fact that all sites varied on a summer-to-summer basis in terms of date of maximum thaw, specific site factors such can be ruled out on influencing variability which is more likely a result of summer weather patterns (Adlam *et al*., 2010).

Table 19: Date (d/m/y) of the deepest measured melting (0°C) during summer for all sites.

Summer	Nonshøgda	Flårjuven	Vesleskarvet	Robertskollen
2007-08	04-Jan-08	-	-	-
2008-09	10-Jan-09	14-Dec-08	-	-
2009-10	09-Jan-10	09-Jan-10	19-Jan-10	-
2010-11	18-Jan-11	21-Jan-11	21-Jan-11	-
2011-12	07-Jan-12	10-Jan-12	30-Jan-12	-
2012-13	07-Jan-13	20-Dec-12	08-Jan-13	-
2013-14	12-Jan-14	27-Dec-13	12-Jan-14	13-Jan-2014

From Figure 32 increasing or decreasing trend of active layer depth was observed over the examined period for Vesleskarvet and Flårjuven. Therefore, continued monitoring is necessary to identify any long-term trends in active layer depth. However, with Nonshøgda recording temperatures over a longer timescale, a definite trend of increasing active layer thickness is apparent with an r^2 value of 0.68. The trend cannot be attributed to increasing ambient air temperatures with an r^2 value of 0.0029, and therefore, may be a function of increasing solar radiation. Guglielmin (2012) briefly mentioned the same phenomenon occurring at Boulder Clay in northern Victoria Land, where an active layer thickening of 1cm per year between 1997 and 2009 was found despite stable air temperatures. Guglielmin and Vieira (2014) emphasized that in the absence of air warming, active layer thickening in continental Antarctica over the last 15 years has been a function of increasing solar radiation, which is seen by an increase of thawing degree days (Guglielmin, 2012; Figure 33).

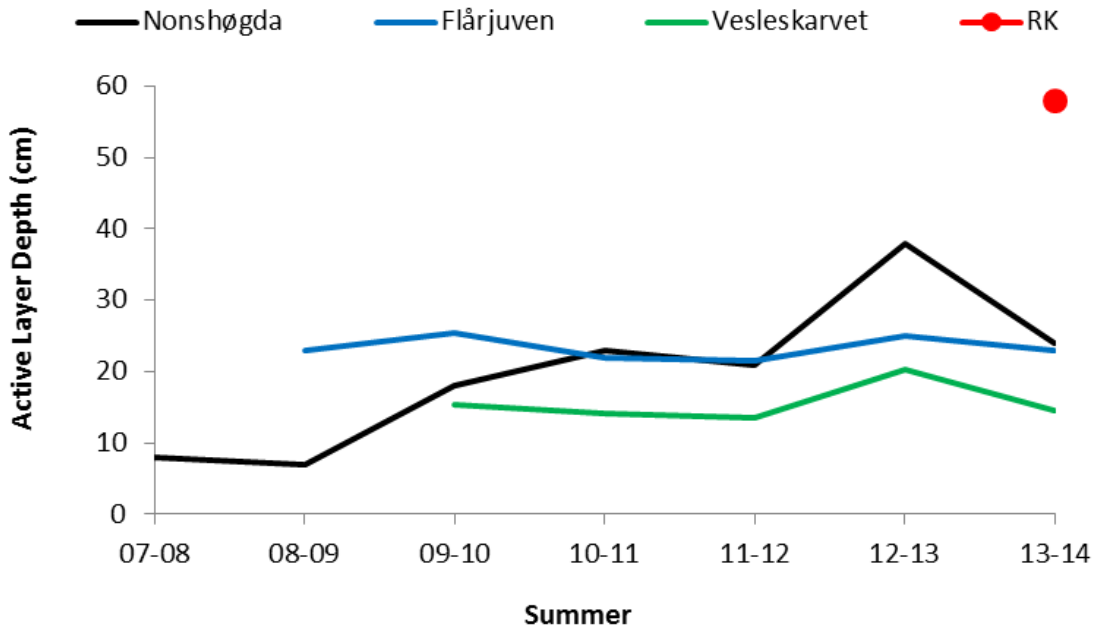

Figure 32: Active layer depths over seven summers at the four study sites.

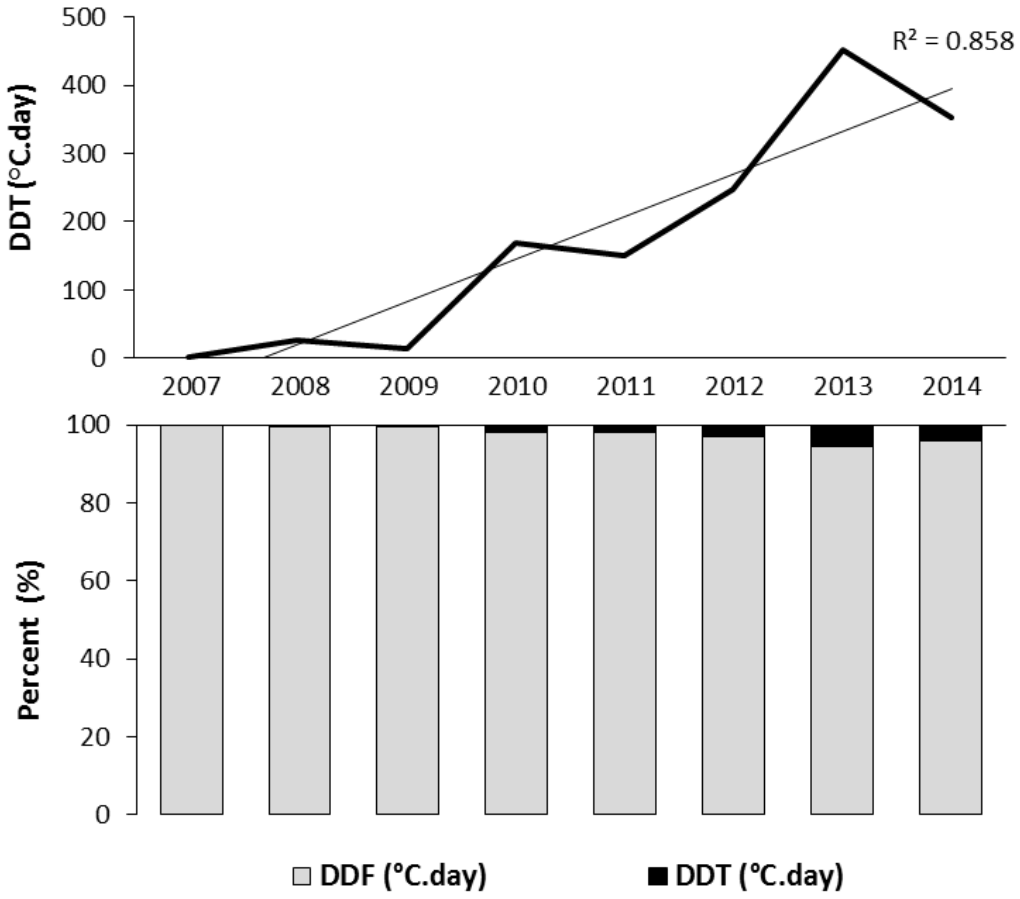

Figure 33: Percent degree-days of freezing and thawing annually at Nonshøgda with accompanying straight-line graph of degree-days of thawing.

All sites experienced heightened active layer depths during the summer of 2012/13 (Figure 32). The above average active layer depths of the 2012/13 summer coincided with one of the warmest summers on record in the Antarctic (Bothale *et al.* 2014). Bothale *et al.* (2014) conducted a study on the dynamics of ice melt over the Amery ice shelf and observed high melt conditions concurrent with above freezing temperatures in summer 2012/13. Conversely, cold conditions were experienced during summers 2010/11 and 2011/12 (Bandoro *et al.* 2014). Bandoro *et al*. (2014) showed that higher amounts of springtime ozone extend the duration of the polar vortex, consequently strengthening the summertime SAM. This is applicable to the anomalously hot Austral summer of 2012/13, a result of high ozone concentrations in November 2012 *(*Bandoro *et al*., 2014). The summer of 2013/14 saw a drop in air temperature as well as active layer depth following the warm summer of 2012/13, previous studies found that this could be due to an enhanced surface layer inversion and stronger katabatic drainage flow from the interior (Turner, 2004).

4.1.2.2. Active Layer Depth and Air Temperature

The mean annual air temperatures recorded at the four permafrost sites (PS) were synchronous with air temperature recorded by the South African Weather Service (SAWS) weather station on the northern buttress of Vesleskarvet (Figure 34). A relatively close correlation was found despite the four sites being separated by distance and altitude (Table 20). However, some specific differences can be identified in that the air temperature recorded at the permafrost site (PS) at Vesleskarvet, which records closer to the surface than the SAWS weather station, was usually warmer by an average of 1.1°C (Figure 35).

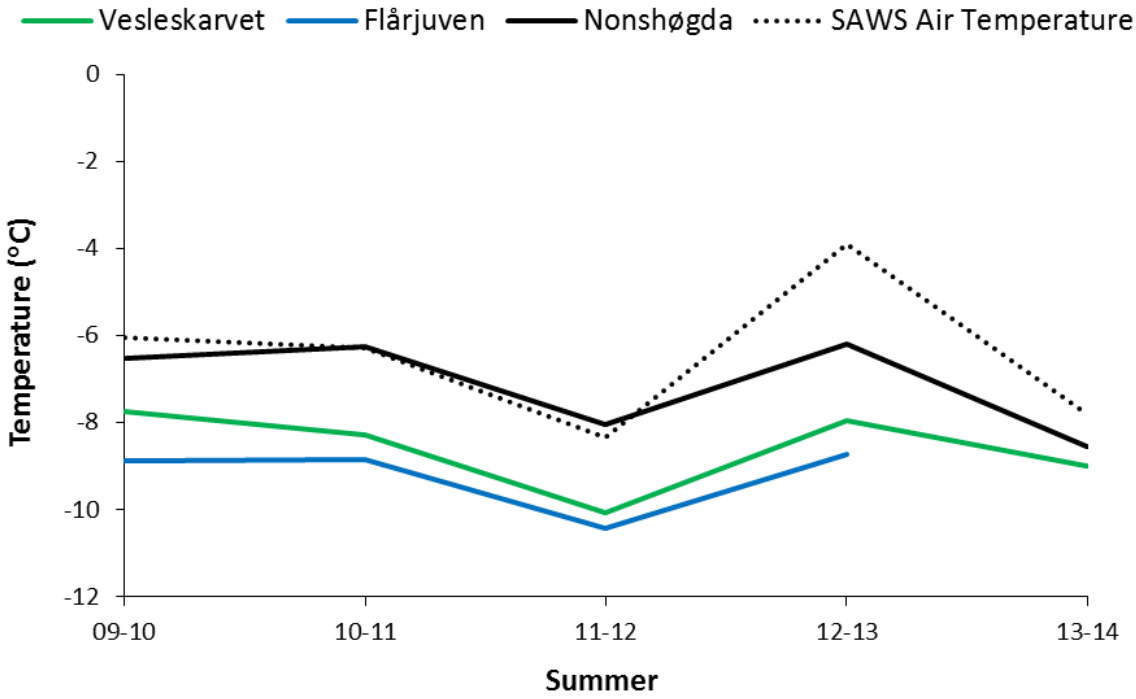

Figure 34: Mean summer ambient SAWS air temperature and permafrost site air temperature at three sites from 2009-2014 (summer of 2013/14 excluded for Flårjuven due to missing data).

Table 20: Linear regressions between the daily mean air temperatures measured at SAWS and the four permafrost sites.

	Linear regression	**R^2**
Vesleskarvet	y= 1.0205x + 1.6516	0.9782
Flårjuven	y=1.0138air - 1.5499	0.9503
Nonshøgda	y= 1.2115x + 3.0403	0.8759
Robertskollen	y= 1.049x + 4.1965	0.9639

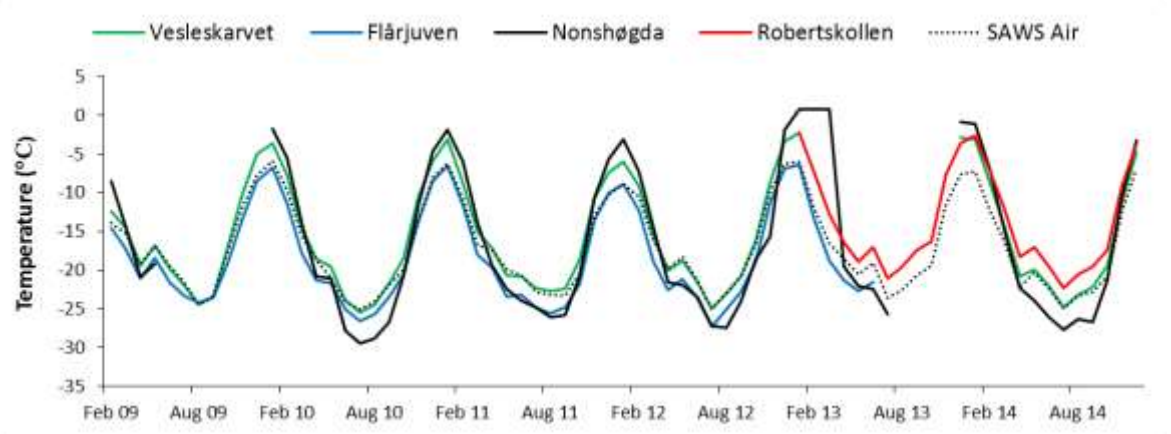

Figure 35: Example of differences between monthly mean daily air temperatures recorded by the permafrost sites and SAWS.

The strong linear regressions between NST and air temperature at the four sites indicate that NST follows the temporal pattern of the air temperature (Table 21 and Table 22). At Vesleskarvet, NST was slightly lower than the air temperature except during the spring and summer months, giving a mean annual ground temperature roughly equal to the MAAT (-17°C and −17.6 °C respectively). In all cases, ground temperatures were higher than air temperatures except in winter when solar radiation was at a minimum (Figure 36). Air temperature was consistently lower than the NST at all four sites during the summer, while it was close to the NST at Vesleskarvet and Robertskollen during winter and higher than the NST at Flårjuven and Nonshøgda during the winter (Figure 36). Air temperature and NST at the four locations were the least correlated at Nonshøgda as its furthest away (Table 21; Table 22). Despite, a higher correlation of 0.0425 between PS air temperature and NST at Nonshøgda compared to when the SAWS air temperature was used, Nonshøgda still had the lowest correlation with air temperature compared to the other sites (Table 22). This reveals the potential significance of solar radiation at Nonshøgda which is augmented by the absence of cloud cover as evidenced by satellite observations. Cloud cover decreases significantly from the coast towards the continent as highlighted by Bridgman and Oliver (2006).

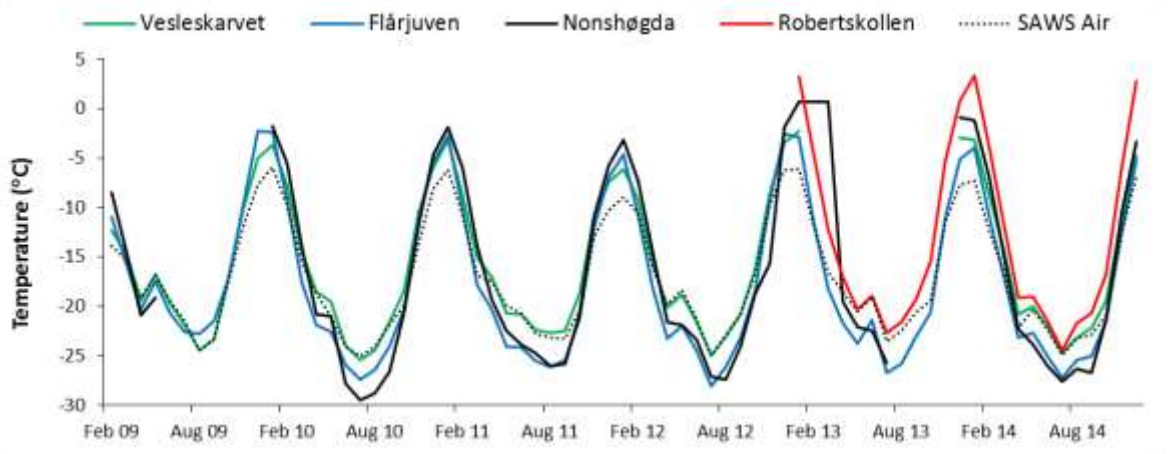

Figure 36: Monthly mean air temperature (SAWS) and near surface temperatures (NST) at the four permafrost sites.

Table 21: Linear regressions between daily mean SAWS air temperature and near surface temperature at the permafrost sites.

	Linear regression	**r^2**
Vesleskarvet	y= 1.0706x + 2.2261	0.9552
Flårjuven	y=1.194x +2.2739	0.9274
Nonshøgda	y= 1.239x + 4.0773	0.8277
Robertskollen	y= 1.3684x + 10.294	0.9096

Table 22: Linear regressions between daily mean permafrost site air temperature and near surface temperature at the permafrost sites.

	Linear regression	**r^2**
Vesleskarvet	y= 1.0504x + 0.5257	0.9755
Flårjuven	y=1.167x +3.7539	0.9632
Nonshøgda	y= 0.9516x -0.2852	0.8702
Robertskollen	y= 1.3289x + 5.2678	0.9544

The differences among the four permafrost sites are further illustrated in Table 23 which shows annual and seasonal means of NST and air temperature, and temperature indices at the four sites. The small brackets in the table heading denote whether the indices were calculated using air or near surface temperatures (NS), as well as whether ambient air temperature from the permafrost site (PS) was used. The n-factor (*nf*) and surface offset (SO) was calculated using the logger air temperature (PS) as it provides a more accurate representation of the degree of decoupling between air and NST. This is due to the dependency of the relationship between air and near surface temperature on the height above the surface that the air temperature is measured (Karunaratne, 2002). The air temperature measured by the logger measures closer the ground at a height of 1m in comparison to air temperature measured by the SAWS at 1.5m above the ground.

Defining the link between air and ground temperatures can be done using surface offsets (SO) and seasonal n-factors (*nf)* (Lacelle *et al*., 2015). The surface offset (SO) between air temperature and NST varied annually for each site. According to PermaNet (2011), the surface offset is used determine the effect of the snow cover timing and duration (Zhang *et al*., 2005; Guglielmin, 2006; Guglielmin *et al*., 2014b). When determining the annual surface offset, the difference between the mean near surface temperature and mean surface air temperature, a positive offset (ground warmer than air) may be due to the insulating effects of a thick snow cover whilst a negative offset (ground colder than air) may be related to an overcooling effect for a shallow snow cover (Farbrot *et al*., 2013). In WDML, the mean daily air temperatures remain below 0°C throughout the year which is why the freezing *nf* was used. A freezing *nf* value of 1 is interpreted as air and soil NST being equal, whilst an $nf > 1$ or < 1, is interpreted as soil NST being colder than or warmer than air temperature respectively (Lacelle *et al*., 2015).

Table 23: Annual and seasonal means of near surface temperature and SAWS air temperature, accompanied by temperature indices at the four sites. (At Vesleskarvet, air and near surface temperature data missing Jan to mid-Feb 2009, and from mid-January to mid-December 2013 (*); At Flårjuven, air temperature data is missing from mid-June 2013 to the end of 2014 (*); At Nonshøgda, data at all depths is missing from June to December 2009 and from the end of July to the end December 2013 (*)).

	ANNUAL (°C)	**MAM (°C)**	**JJA (°C)**	**SON (°C)**	**DJF (°C)**	**Thaw(NS) (Hours)**	**Freeze (NS) (Hours)**	**DDF(NS) (°C.day)**	**DDF(air) (°C.day)**	***nf* (°C.day)**	**PFTE(NS) (n)**	**TSI(NS) (°C.day)**	**SO(PS) (°C)**
2009													
Vesleskarvet	-17*	-16.9	-22	-16.9	n.d.	71*	7599*	5448*	5350*	1.02*	11*	1361*	-0.3*
Flårjuven	-16	-17.8	-22	-16.1	-7.3	265	7844	5254	6092	0.86	33	2579	1.2
Nonshøgda	-12.8*	-18.1	n.d.	n.d.	-6	13*	3582*	1720*	1831*	0.94*	4*	389*	1.1*
Air	-17.6	-17.1	-21.8	-17.5	n.d.	8	7662	n.d.	6404	n.d.	4	1789	n.d.
2010													
Vesleskarvet	-16.3	-17.6	-24.6	-16.8	-5.5	185	8571	5933	5791	1.02	44	2384	-0.4
Flårjuven	-17.9	-20.7	-26.6	-18.4	-4.6	429	8300	6590	6776	0.97	73	2677	0.5
Nonshøgda	-17.8	-18.6	-26.5	-21	-3.7	169	8591	6493	6569	0.99	32	1052	0.2
Air	-17.5	-18.4	-24.4	-18.5	-7.8	25	8731	n.d.	7214	n.d.	6	2071	n.d.
2011													
Vesleskarvet	-15.9	-17.6	-22	-17.3	-6	182	8578	5800	5692	1.01	33	1776	-0.3
Flårjuven	-18.1	-20.8	-25.3	-19.6	-6.1	331	8429	6606	6814	0.97	58	2862	0.6
Nonshøgda	-16.9	-18.6	-24.9	-26	-4.2	150	8610	6151	6297	0.97	26	970	0.4
Air	-17	-18.1	-22.2	-18.9	-8.3	23	8736	n.d.	7046	n.d.	9	2315	n.d.
2012													
Vesleskarvet	-16	-18.2	-23.2	-15.2	-7.6	230	8291	5701	5583	1.02	44	1746	-0.3
Flårjuven	-17.6	-21.1	-26.2	-17	-7.4	457	8327	6494	6721	0.96	72	2919	0.8
Nonshøgda	-16.8	-19.4	-26	-19.5	-5.4	247	8538	6139	6301	0.97	42	1371	0.4
Air	-16.7	-18.1	-23.1	-15.8	-9.9	52	8467	n.d.	6819	n.d.	9	1859	n.d.
2013													
Vesleskarvet	-2.18*	n.d.	n.d.	n.d.	-2.9*	152*	8607*	54*	71*	0.76*	21*	252*	1*
Flårjuven	-17.7	-21.3	-24.6	-18.2	-5.6	365	8396	6467	2753*	2.35*	64	2601	0.7*
Nonshøgda	-15.1*	-13.6	-24*	n.d.	-0.2*	452*	7526*	3183*	3459*	0.92*	68*	596*	1.5*
Robertskollen	-12.9	-16.5	-21.1	-13.4	n.d.	1063	7681	4856	4891	0.99	61	1855	0.6
Air	-16.5	-18.6	-21.7	-17.2	-8.1	3	8756	n.d.	6960	n.d.	3	1926	n.d.
2014													
Vesleskarvet	-16.23	-18.3	-23.5	-17.6	-4.9	351	8410	5916	5864	1.00	66	2386	-0.1
Flårjuven	-18.3	-20.9	-25.9	-19.7	-6.6	340	8420	6693	n.d.	n.d.	68	2867	n.d.
Nonshøgda	-17.6	-20.3	-26.7	-19.5	-8	353	8403	6441	6712	0.96	44	1270	0.5
Robertskollen	-13.3	-16.6	-22.5	-14.5	0.1	1267	7494	5057	5174	0.97	73	2141	0.9
Air	-18.5	-19.6	-23.5	-18.6	-9.1	28	8732	n.d.	6836	n.d.	3	1771	n.d.

All sites except for Vesleskarvet revealed positive annual surface offsets between PS air temperatures for the study period, meaning that the ground temperatures are warmer than air temperatures for majority of the year (Table 23). This is supported by the freezing *nf* of less than 1 for Flårjuven, Robertskollen and Nonshøgda; a low freezing *nf* is associated with insulation by snow cover (Klene *et al*., 2001). It is important to note that all the *nf* values are only marginally greater than or less than 1, showing the strong relationship between air and near surface ground temperatures (Table 23).

Vesleskarvet shows negative surface offsets for every year except 2013, indicating that air temperatures are marginally warmer than ground temperatures for majority of the year. The same was found for the freezing *nf* which was consistently above 1 at Vesleskarvet, except for 2013, and at exactly 1 during 2014 which indicates equal annual air and NST values (Table 23). Overall at Vesleskarvet, soil NST is generally slightly colder than air temperature. This could be due to the presence of blocky deposits over Vesleskarvet, which have been shown to increase cooling in the ground as a result of the blocks advecting cold air drainage (Harris & Pedersen, 1998; Ishikawa, 2003; Marchenko & Etzelmüller, 2013). However, the blocky deposits may not be large enough to support this hypothesis, therefore, a cooler NST than air temperature could be due to the combined effects of an intermittent snow cover or the high emissivity of the blockfield which enhances radiative cooling.

Surface offsets at Robertskollen were 0.6°C and 0.9°C during 2013 and 2014 respectively. Whilst offsets between −0.1°C and −0.4°C, 0.5°C and 1.2°C, and 0.2°C to 0.5°C were experienced for Vesleskarvet, Flårjuven and Nonshøgda respectively (Table 23). Robertskollen showed the only positive mean NST during the summer (DJF) of 2013/2014 at 0.1°C, which is 8.1°C warmer than Nonshøgda, the coldest site during the summer. Thawing hours, PFTE, TSI and SO were also substantially higher at Robertskollen during 2014 than 2013. The average NST at Robertskollen during 2013 and 2014 were similar around −13°C, however, the mean annual air temperature differed by 2°C between 2013 and 2014, giving 2014 the higher surface offset.

In 2009, Flårjuven and Nonshøgda had the largest surface offset between NST and air temperature at 1.2°C and 1.1°C respectively, as well as the lowest *nf*. Additionally, the lowest overall thawing hours, PFTE, and TSI were also experienced in 2009, suggesting that this year potentially had the thickest and most prolonged snow cover of all the years. Year 2012 was warmest for Flårjuven with the one of the highest average near surface temperatures in conjunction with the highest thawing hours, PFTE and TSI, and a surface offset of 0.8°C (Table 23). Barring 2013, Nonshøgda experienced the highest reading of DDT and PFTE in 2014.

Similarly to Nonshøgda, Vesleskarvet also had higher recordings of DDT, PFTE and TSI during 2014. A thermal offset of −0.1°C at Vesleskarvet in 2014 indicates that ground temperatures are marginally colder than air temperatures and that the presence of snow cover is non-existent (Table 23).The TSI was also extremely high in 2010, concurrent with the finding that 2010 had both the highest maximum and lowest minimum air temperatures of all the years, at 6.77°C (22/12/2010) and −40.78°C (07/07/2010) respectively. The annual near surface temperature range in 2010 matched the range in air temperature measured by the permafrost station at approximately 47°C. If data for 2013 at Vesleskarvet and Nonshøgda were complete, the results would have showed this being the warmest year overall.

Overall, Flårjuven had the highest thawing hours for the study period from 2009-2013, whilst Nonshøgda had the most DDT during 2014. Flårjuven had the largest TSI every year, followed by Vesleskarvet and then Robertskollen. In 2014, the TSI at Flårjuven was roughly 44% higher than the TSI recorded at Nonshøgda (Table 23). In conjunction with having the largest TSI, Flårjuven also had the largest amount of freeze-thaw cycles except during 2013 and 2014 when Nonshøgda and Robertskollen had the most PFTE respectively. Flårjuven also has the lowest annual NST of all the sites, followed by Nonshøgda, Vesleskarvet and then Robertskollen (Table 23). It is clear that Flårjuven is the coldest site overall with the most dynamic active layer seen by high TSI and PFTE. Conversely, Robertskollen is the warmest site overall, accompanied by a high amount PFTE.

Majority of the temperature indices (thawing hours, DDF air, DDF NS, and TSI) are consistent with Nonshøgda having a deeper and more prolonged period of snow cover relative to the other sites (Guglielmin *et al*., 2014b; Table 23), particularly from 2009 to 2012. This is because snow cover has the ability to reduce the potential for freeze–thaw events and thermal stress. Additionally, the higher DDF in air temperature compared to near surface temperature is a sure indicator that it was insulated by snow (de Pablo *et al*., 2013). Conversely, DDF indicated that Vesleskarvet experienced no snow cover for all years which it contrary to field observations. The anomalous result at Vesleskarvet could be explained by the block field as mentioned previously.

Focusing on the summer months which are central to active layer dynamics, the mean summer air temperature showed synchronicity with variability in active layer depths (Figure 37). Table 24 provides the seasonal temperature indices in the near surface ground regime. The thawing and freezing hours of the air compared to the near surface ground temperatures, validated higher near surface temperatures than air temperature (Klene *et al*., 2001; Karunaratne & Burn, 2004). This is confirmed by positive thermal offsets ranging from 0.37°C to 0.93°C and a freezing *nf* below 1, (Figure 37; Table 24). NST were approximately 3°C warmer than air temperature at Flårjuven, Robertskollen and Nonshøgda, and 0.8°C at Vesleskarvet (averaged over the summers). This is due to solar heating of the bare ground surface according to Lacelle *et al*. (2015).

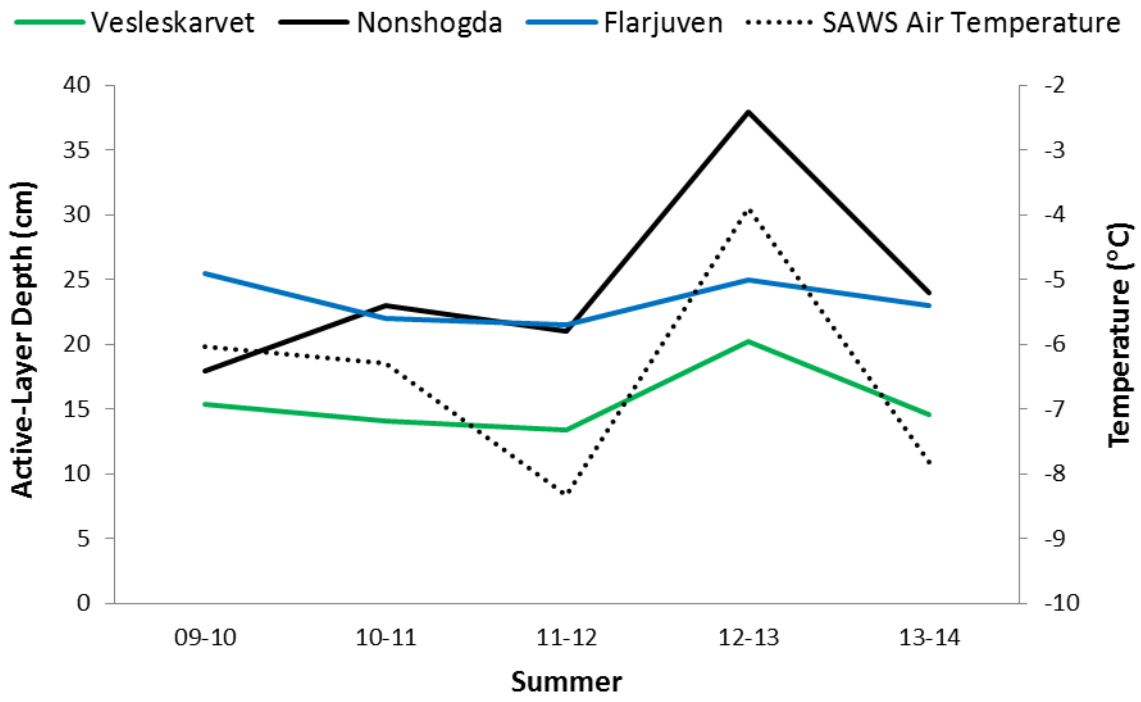

Figure 37: Summer active layer depths with SAWS air temperature (Robertskollen excluded due to insufficient data).

At Vesleskarvet the summer of 2011/12 exhibited the lowest thawing hours, PFTE and TSI overall, with the highest thermal offset. The same was evident with the thawing hours, *nf* and PFTE for Flårjuven and Nonshøgda. Additionally the air temperature recorded by SAWS over that summer was the lowest on average at −13.6°C. Both Flårjuven and Nonshøgda experienced the highest TSI in summer 2011/12. These results reveal that for all sites during the 2011/12 summer, snowfall was definitely present, insulating ground temperatures and reducing PTFE. The high TSI reveals the variability of the snow cover at Flårjuven and Nonshøgda (Table 24).

NST during the summer of 2012/13 had the highest thawing hours, *nf* and PFTE for Vesleskarvet and Nonshøgda, and the second highest for Flårjuven (first highest was the summer of 2009/10) (Table 24). If the 2012/13 dataset was complete, a higher TSI and more PFTE would be observed. This is concurrent with air temperature measured by SAWS being the highest during the 2012/13 summer at −11.2°C, coming close to the summer of 2009/10 with an air temperature of −11.4°C which is why the sites display such high *nf*.

At Vesleskarvet, the summers of 2012/13 and 2013/14 had the highest average thermal offset between PS air temperature and NST of 0.9°C and 1.6°C respectively. This is consistent with a larger snowpack than previous summers (pers.obs). Whilst the summers of 2009/10, 2010/11, and 2011/12 exhibit a more synchronous active layer depth with air temperature, with average thermal offsets of 0.6, 0.4 and 0.6 respectively (Figure 37). Summer 2011/12 exhibited a marginally lower active layer depth despite a marked decrease in air temperatures.

The opposite was true for the summer of 2012/13 with a sharp increase in active layer depth accompanied by a sharp rise in air temperature. The difference between active layer thickness and air temperatures during the summer could be attributed to one of the many properties of snow cover.

Table 24: Seasonal means of thawing and freezing hours, *n-factor*, potential freeze thaw events, thermal stress index, and the surface offset illustrated over five summers (2009-2014). (At Vesleskarvet, air and near surface temperature data missing Jan to mid-Feb 2009, and from mid-January to mid-December 2013 (*); At Flårjuven, air temperature data is missing from mid-June 2013 to the end of 2014 (*); At Nonshøgda, data at all depths is missing from June to December 2009 and from the end of July to the end December 2013 (*)).

	Thawing (Hours)	**Freezing (Hours)**	***nf* (SAWS) (°C.day)**	***nf* (PS) (°C.day)**	**PFTE (n)**	**TSI (°C.day)**	**SO (PS) (°C)**
2009/10							
Vesleskarvet	202*	4162*	0.52*	0.90*	39*	715*	0.6*
Flårjuven	515	3852	0.64	0.70	64	988	3
Nonshøgda	647*	872*	0.24*	0.53*	28*	226*	3.1*
Air	6	4358	n.d.	n.d.	4	475.9	n.d.
2010/11							
Vesleskarvet	218	4150	0.55	0.93	43	687	0.4
Flårjuven	381	3987	0.56	0.68	69	1125	2.9
Nonshøgda	762	1701	0.38	0.66	34	371	2.1
Air	14	4354	n.d.	n.d.	6	435.5	n.d.
2011/12							
Vesleskarvet	76	4053	0.62	0.92	26	609	0.6
Flårjuven	304	4088	0.67	0.71	59	1253	3.1
Nonshøgda	419	1766	0.49	0.67	17	399	2.7
Air	48	4081	n.d.	n.d.	5	381.5	n.d.
2012/13							
Vesleskarvet	295	4075	0.17	0.79	40	466	0.9
Flårjuven	467	3902	0.54	0.65	70	755	3.3
Nonshøgda	1277	882	0.25	0.42	93	240	4
Air	7	4361	n.d.	n.d.	6	256.6	n.d.
2013/14							
Vesleskarvet	239*	4128*	0.31*	0.80*	47*	765*	1.6*
Flårjuven	352	4016	0.57	–	70	870	n.d.
Nonshøgda	670*	823*	0.23*	0.45*	28*	342*	4.8*
Robertskollen	1188	3182	0.14	0.37	73	824	4.6
Air	0	4367	n.d.	n.d.	0	343	n.d.

4.1.2.3. Active Layer Temperature at the four sites, 2014

Vesleskarvet

The highest mean monthly soil temperature from Vesleskarvet was −3.2°C (Table 25), registered for the near surface soil layer in January 2014, whilst the highest mean daily air temperature was 4.3°C recorded on 16 January. Relative soil water content ranged from approximately 0.5 in summer to nothing in winter (Table 25; Figure 38). Mean annual temperatures of −16.3°C, −16.2°C, −16.2°C, −16.1°C and −16.3°C were found for the increasing depths (1cm, 15cm, 30cm, 45cm and 60cm, respectively). The maximum and minimum temperatures (hourly records) for the bottommost layer (depth of 60cm) were -3.9°C and −25.9°C, respectively (Table 25). Positive mean monthly temperatures occur at the depth of 1cm and near positive temperatures at 15cm depth. However, these layers did not present positive mean monthly temperatures, indicating that, even during summer, it remained close to freezing. Mean monthly air temperature was colder than near surface temperature from January to March and November to December, and warmer than NST from April to September.

Table 25: Monthly mean temperature (°C) and relative soil moisture at each horizon, Vesleskarvet; an annual synthesis is provided at the bottom with mean, maximum, minimum, and standard deviation calculated from hourly data.

	Air	**NS**	**15cm**	**30cm**	**45cm**	**60cm**	**SM**
Jan. 14	-5.3	-3.2	-3.9	-4.2	-4.6	-5.2	0.5
Feb. 14	-9.9	-8.7	-8.7	-8.6	-8.4	-8.5	0.0
Mar. 14	-14.4	-14.3	-13.8	-13.7	-13.3	-13.2	0.0
Apr. 14	-20.2	-20.8	-19.2	-18.7	-17.9	-17.5	0.0
May. 14	-19.0	-20.0	-19.8	-19.8	-19.5	-19.5	0.0
Jun. 14	-20.8	-22.1	-21.5	-21.3	-20.8	-20.6	0.0
Jul. 14	-23.6	-24.8	-23.7	-23.3	-22.7	-22.4	0.0
Aug. 14	-21.9	-23.2	-23.1	-23.2	-23.1	-23.2	0.0
Sep. 14	-21.3	-22.2	-22.0	-22.0	-21.7	-21.6	0.0
Oct. 14	-19.6	-19.5	-19.9	-20.2	-20.3	-20.5	0.0
Nov. 14	-11.6	-11.3	-12.0	-12.6	-13.2	-13.8	0.0
Dec. 14	-6.2	-4.7	-6.2	-7.0	-7.8	-8.6	0.1
Mean	-16.4	-16.3	-16.2	-16.2	-16.1	-16.3	0.1
Min	-36.7	-33.6	-28.6	-27.6	-26.4	-25.9	0.0
Max	4.3	9.5	-0.4	-1.7	-2.9	-3.9	4.4
St dv	7.2	8.2	7.1	6.8	6.4	6.1	0.4

The active layer thickness estimated was 14cm, reaching a maximum thickness on 31 December 2014. According to mean monthly maximums, negative temperatures for the uppermost layer become more abundant in March, marking the beginning of the thermal autumn. Amidst numerous temperature fluctuations, the last positive temperature using hourly values was seen on 7 March; thereafter temperatures begin to drop rapidly. Soil temperature dropped to a minimum of −26.42°C at 45cm and −25.92°C at 60cm in August, as an effect of the winter season, which lasted until October.

Thawing started at the end of November, when the upper layer presented positive temperatures on the 27th. Despite rapid thaw in the upper layer (1cm), temperature below 15cm depth remained negative until the following January. During the course of the year, the temperature amplitude between the surface and bottom soil layers (1cm and 60cm respectively) were low at an average 0.01°C, with extremes of −10.03°C on 2014/05/03 and 18.71°C on 2014/12/10. There were 351 thawing hours at near surface, and none were evident at deeper layers. Thawing and freezing cumulative degree days provide an estimate of the net energy flux in the studied sites (Michel *et al*., 2012). January and December were the only months to show thawing degree-days of 2.3°C.day and 2.4°C.day respectively. Comparing the near surface thawing degree-days (4.64 °C.day) and freezing degree-days (-5915.9 °C.day) for the soil at Vesleskarvet indicated predominantly freezing conditions.

The contouring of temperature in respect to time and depth illustrates the seasonality within the active layer and the speed at which freezing and thawing take place (Figure 39). The white area in the surfer plot outlined in black denotes the penetration depth of the 0°C isotherm. This soil presents one-sided freezing, from the ground surface downwards. A deeper borehole is necessary to capture the full extent of the seasonal freezing within the active layer. It may be that two-sided freezing occurs as it has been commonly associated with in continuous permafrost zones (French, 2007). Although, two-sided freezing has mainly recorded in the Arctic, Michel *et al*. (2012) documented two-sided freezing in King George Island (Guglielmin, 2012). The penetration of the cryofront is only visible in January and December with temperatures during these times fluctuating between −5°C and −10°C. By the end of February, the ground is −15°C and decreases further to −20°C by April. Thereafter, winter temperatures between −25°C and −30°C are interfingered by warm periods of −20°C.

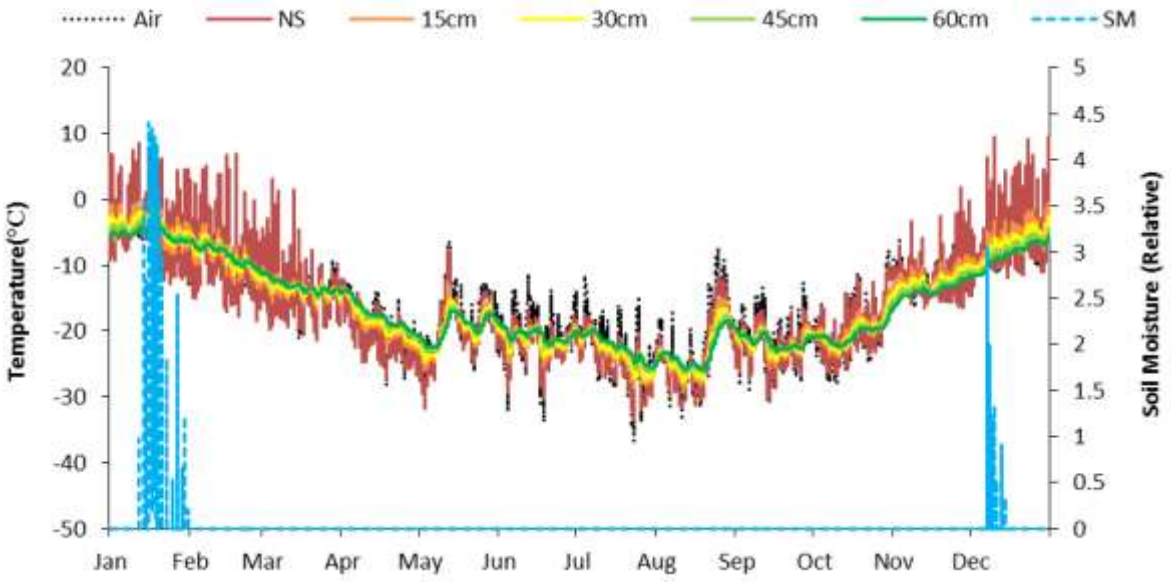

Figure 38: Soil water content, air temperature and ground temperatures at Vesleskarvet, 2014.

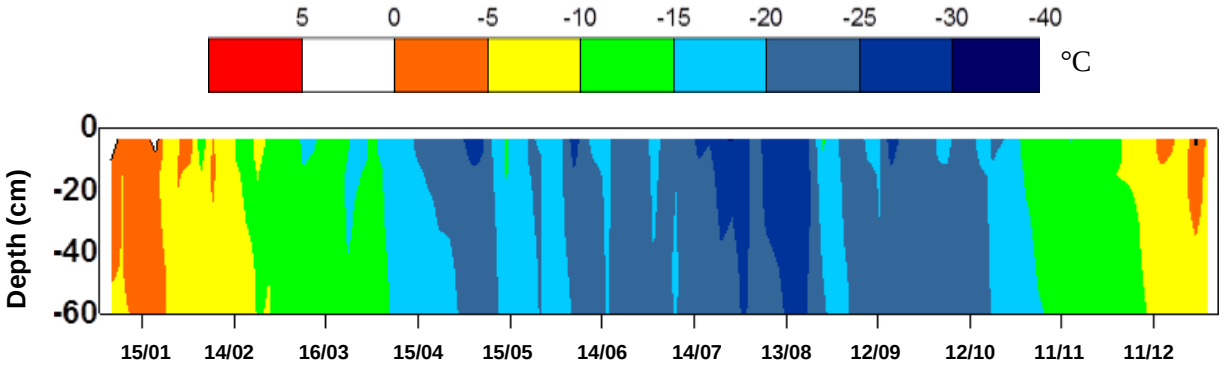

Figure 39: Thermal regime of the active layer at Vesleskarvet from January to December 2014.

Flårjuven

The highest mean monthly soil temperature from Flårjuven was −3.9°C (Table 26), registered for the near surface soil layer in January 2014, whilst the maximum mean near surface temperature was 14°C recorded on 10 December. Relative soil water content ranged from approximately 0.6 in summer to nothing in winter (Table 26; Figure 40). Mean annual temperatures of −18.3 °C, −18.5 °C, −18.5 °C, −18.4 °C and −18.3 °C were found for the increasing depths (1cm, 15cm, 30cm, 45cm and 60cm, respectively). The maximum and minimum temperatures (hourly records) for the bottommost layer (depth of 60cm) were −4.7°C and −28.4°C, respectively (Table 26). Positive temperatures occur at a depth of 1cm and 15cm. However, these layers did not present positive mean monthly temperatures, indicating that even during summer it remained close to freezing. The estimated active layer thickness was 23cm, reaching a maximum thickness on 31 December 2014.

Table 26: Monthly mean temperature (°C) and relative soil moisture at each horizon, Flårjuven; an annual synthesis is provided at the bottom with mean, maximum, minimum, and standard deviation calculated from hourly data (air temperature missing due to logger malfunctions).

	NS	**15cm**	**30cm**	**45cm**	**60cm**	**SM**
Jan. 14	-3.9	-5.0	-5.6	-5.9	-6.1	0.5
Feb. 14	-10.8	-11.2	-10.7	-10.2	-10.0	0.0
Mar. 14	-16.9	-16.8	-16.1	-15.5	-15.1	0.0
Apr. 14	-23.2	-22.1	-20.9	-20.1	-19.6	0.0
May. 14	-22.7	-22.5	-22.3	-22.1	-21.9	0.0
Jun. 14	-25.0	-24.6	-24.0	-23.6	-23.2	0.0
Jul. 14	-27.2	-26.5	-25.5	-24.9	-24.5	0.0
Aug. 14	-25.4	-25.4	-25.5	-25.6	-25.5	0.0
Sep. 14	-25.0	-25.0	-24.8	-24.6	-24.4	0.0
Oct. 14	-21.5	-22.0	-22.4	-22.7	-22.8	0.0
Nov. 14	-12.6	-13.6	-14.8	-15.9	-16.3	0.0
Dec. 14	-5.2	-7.0	-8.5	-9.5	-10.1	0.6
Mean	-18.3	-18.5	-18.5	-18.4	-18.3	0.1
Min	-37.9	-33.6	-30.5	-29.1	-28.4	0.0
Max	14.0	2.2	-2.0	-4.1	-4.7	7.9
St dv	9.1	7.8	7.1	6.7	6.5	0.5

According to mean monthly maximums, the last positive temperatures for the uppermost layer are seen on 19 February 2014, marking the beginning of the thermal autumn. Soil temperature dropped to a minimum of −29.14 °C at 45cm and −28.35°C at 60cm in August, as an effect of the winter season, which lasted until October (Table 26). Thawing started at the end of November, when the upper layer presented positive temperatures on the 29th. Thereafter, 22 of the 31 days in December experienced positive temperatures according to daily averages. The difference in the temperature between the surface and bottom soil layers were low at an annual average of 0.02°C, with extremes of 25.1°C on 10 December 2014 and −14°C on 4 June 2014. There were 340 thawing hours at near surface, 41 thawing hours at 15cm depth and none in the other layers. Comparison of the near surface thawing degree-days (7 °C.day) and freezing degree-days (-6711.5°C.day) for the soil at Flårjuven indicated chiefly freezing conditions. The sum of 7°C.day corresponded with January 2014, which was the only month to experience positive degree-days. Similarly to Vesleskarvet, the freezing front originated only from the surface downwards (Figure 41). A deeper penetration of the cryofront is evident in January and December in comparison to Vesleskarvet. However, the −5°C isotherm is not as prevalent in January and December in comparison to Vesleskarvet, decreasing by as much as 5°C nearing the 60cm and 30cm depth respectively. Temperatures of −15°C are reached much sooner in February and quickly change into much colder temperatures during winter. In July, temperatures of −30°C and less penetrate almost 20cm into the active layer, increasing and deepening the freezing into August (Figure 41).

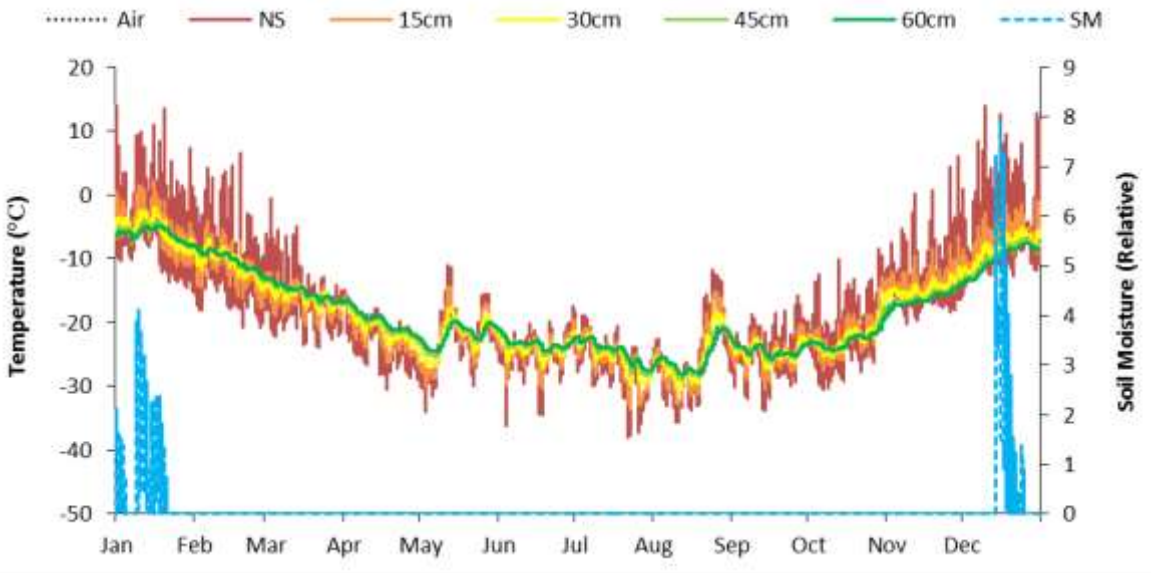

Figure 40: Soil water content, air temperature and ground temperatures at Flårjuven, 2014.

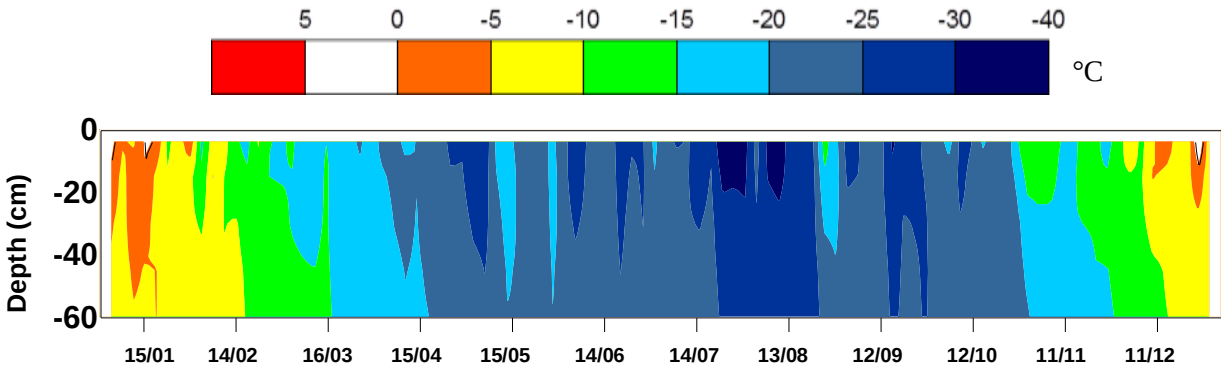

Figure 41: Thermal regime of the active layer at Flårjuven from January to December 2014.

Robertskollen

The highest mean monthly soil temperature from Robertskollen was 3.4°C (Table 27), recorded for the near surface soil layer in January 2014, whilst the highest mean daily air temperature was 1.7°C recorded on 10 January. Relative soil water content ranged from approximately 0.2 in summer to nothing in winter (Table 27; Figure 42). Mean annual temperatures of −13.3°C, −13.4°C, −13.2°C, −13.1°C and −13°C were found for the increasing depths (1cm, 15cm, 30cm, 45cm and 60cm, respectively). The maximum and minimum temperatures (hourly records) for the bottommost layer (depth of 60cm) were –0.2°C and −23.5°C, respectively (Table 3). Positive mean monthly maximum temperatures are found from a depth of 1cm to 45cm. However, these layers only present positive mean monthly temperatures in January and only to a depth of 15cm in December, indicating that majority of the year remained close to freezing (Table 27).

Table 27: Monthly mean temperature (°C) and relative soil moisture at each horizon, Robertskollen; an annual synthesis is provided at the bottom with mean, maximum, minimum, and standard deviation calculated from hourly data.

	Air	**NS**	**15cm**	**30cm**	**45cm**	**60cm**	**SM**
Jan. 14	-2.6	3.4	1.7	0.9	0.2	-0.5	0
Feb. 14	-7.2	-3.8	-3.7	-3.1	-2.9	-2.8	0
Mar. 14	-12.1	-11.7	-10.9	-10.0	-9.4	-9.0	0
Apr. 14	-18.3	-19.2	-17.4	-16.0	-14.9	-14.2	0
May. 14	-17.0	-19.0	-18.6	-18.0	-17.6	-17.2	0
Jun. 14	-19.6	-21.5	-20.7	-19.9	-19.2	-18.6	0
Jul. 14	-22.3	-24.5	-23.2	-22.0	-21.1	-20.5	0
Aug. 14	-20.5	-21.7	-21.7	-21.5	-21.3	-21.1	0
Sep. 14	-19.5	-20.7	-20.4	-20.0	-19.7	-19.5	0
Oct. 14	-17.5	-16.8	-17.4	-17.5	-17.6	-17.7	0
Nov. 14	-9.2	-6.0	-8.2	-9.4	-10.3	-11.0	0
Dec. 14	-3.8	2.7	0.0	-1.7	-2.9	-3.9	0
Mean	-14.2	-13.3	-13.4	-13.2	-13.1	-13.0	0
Min	-32.7	-33.0	-28.8	-26.3	-24.6	-23.5	0
Max	5.9	15.9	6.0	2.9	1.1	-0.2	0.2
St dv	7.6	10.5	8.9	8.2	7.6	7.2	0

Air temperature was colder than NST from January to March and October to December, and warmer than NST from April to September. The ALT estimated was 58cm, reaching a maximum thickness on 13 January 2014. According to mean monthly maximums, the last positive temperatures are seen at 45cm on 30 January 2014. Soil temperature dropped to a minimum of −24.6 °C at 45cm and −23.5 °C at 60cm at the end of July and mid-August respectively, as an effect of the winter season which lasted until October (Table 27). Thawing started early November, when the upper layer presented positive temperatures on the 8th according to averaged daily data. Thereafter, 28 of the 31 days in December experienced positive temperatures in the uppermost layer. During the year, the temperature amplitude between the surface and bottom soil layers was low at −0.2°C, with extremes of 19°C on 2014/12/07 and −11°C on 2014/06/18. There were 1267 thawing hours at near surface, 1121 at 15cm depth, 895 at 30cm, and 523 at 45cm, and no thawing hours found at 60cm depth. Comparison of the near surface thawing degree-days (216°C.day) and freezing degree-days (5056.7°C.day) indicate primarily freezing conditions.

Contrary to Vesleskarvet and Flårjuven, there is a double-sided freezing front (Figure 43). In January and December, positive temperatures are evident by the red and white which correspond to the 5°C and 0°C isotherms respectively. The cryofront is deepest in January at 58cm. By the end of January, cooling from below is evident, as seen by the movement of the 0°C isotherm between 55cm and 40cm depth. Colder temperatures begin in early march at −15°C, which decrease further into the winter months, reaching a minimum of −30°C in early May, and between June and August (Figure 43).

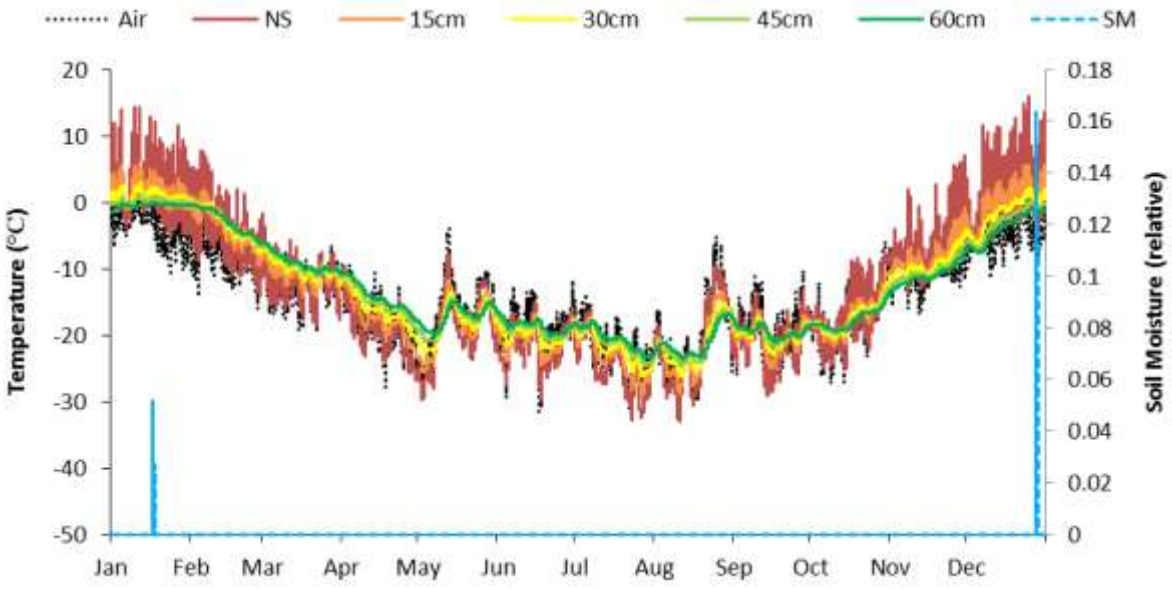

Figure 42: Soil water content, air temperature and ground temperatures at Robertskollen, 2014.

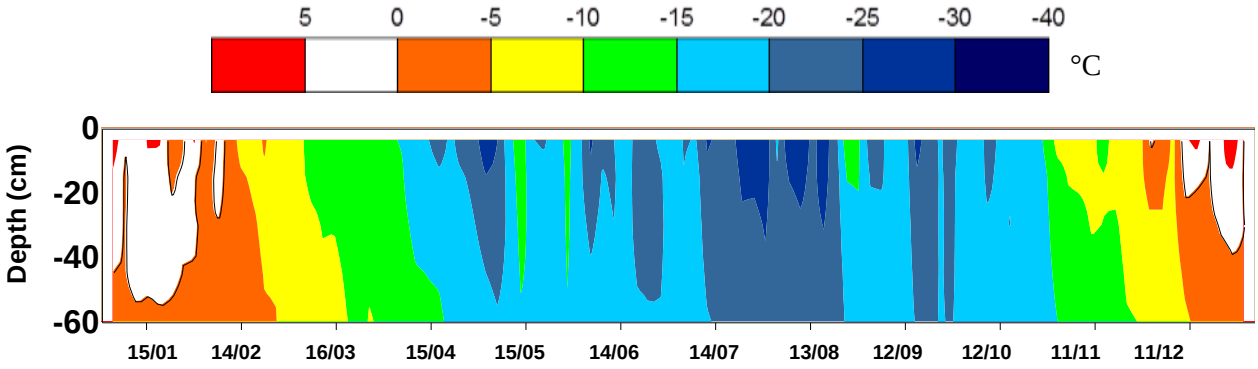

Figure 43: Thermal regime of the active layer at Robertskollen from January to December 2014.

Nonshøgda

The highest monthly mean soil temperature from Nonshøgda was −1.2°C (Table 28), registered for the near surface soil layer in January 2014, whilst the highest mean daily air temperature was −1.57°C recorded on 10 January. No soil moisture was present in the near surface soil layer at Nonshøgda (Table 28; Figure 44). Mean annual temperatures of −17.6°C, −17.7°C, −17.6°C, −17.7°C and −17.8°C were found for the increasing depths (1cm, 50cm, 100cm, 150cm and 200cm, respectively). The maximum and minimum temperatures (hourly records) for the bottommost layer (depth of 200cm) were −9.6°C and −24.8°C, respectively (Table 28). Positive temperatures are only found at the near surface, and positive mean monthly temperatures are not presented, indicating a predominantly frozen year. Air temperature was colder than near surface temperature from January to March and November to December, and warmer than NST from May to October.

Table 28: Monthly mean temperature (°C) and relative soil moisture at each horizon, Nonshøgda; an annual synthesis is provided at the bottom with mean, maximum, minimum, and standard deviation calculated from hourly data.

	Air	**NS**	**50cm**	**100cm**	**150cm**	**200cm**	**SM**
Jan. 14	-16.9	-1.2	-16.3	-16.3	-16.4	-16.7	-
Feb. 14	-11.3	-6.9	-7.3	-7.8	-8.7	-9.8	-
Mar. 14	-16.8	-14.8	-13.1	-12.3	-11.9	-11.9	-
Apr. 14	-22.3	-22.3	-18.8	-17.0	-15.9	-15.1	-
May. 14	-22.3	-23.9	-22.2	-20.9	-19.8	-18.8	-
Jun. 14	-25.2	-26.1	-24.0	-22.5	-21.4	-20.4	-
Jul. 14	-28.5	-27.7	-25.3	-23.9	-22.9	-22.0	-
Aug. 14	-24.2	-26.4	-26.2	-25.6	-24.9	-24.0	-
Sep. 14	-24.7	-26.7	-25.3	-24.3	-23.7	-23.2	-
Oct. 14	-20.6	-21.3	-22.7	-22.9	-23.0	-23.0	-
Nov. 14	-11.9	-10.6	-14.5	-16.4	-18.0	-19.2	-
Dec. 14	-6.4	-3.3	-8.0	-10.5	-12.8	-14.6	-
Mean	-18.4	-17.6	-17.7	-17.6	-17.7	-17.8	-
Min	-42.7	-35.3	-29.7	-27.6	-26.1	-24.8	-
Max	1.8	3.5	-3.6	-6.0	-7.9	-9.6	-
St dv	9.3	9.9	7.7	6.6	5.7	5.0	-

The active layer thickness estimated was 25cm, reaching a maximum thickness on 31 December 2014. According to mean monthly maximums, the last positive temperatures are seen at 1cm depth on 5 February 2014. Soil temperature dropped to a minimum of −26.1°C at 150cm and −24.8°C at 200cm on 20 August. The cold winter temperatures lasted until October, after which thawing started early December, marking the start of the thermal summer. The first positive temperatures occurred in the uppermost layer on 7 December 2014 according to daily averages. Positive temperatures in the uppermost layer were experienced on 18 of the 31 days in December. During the year, the difference in the temperature between the surface and bottom soil layers (1cm and 200cm depth) was low at 0.12°C, with extremes of 16°C in 2014/12/31 and −14°C on 2014/05/03. There were 353 thawing hours at near surface, and none in the rest of the array. Comparison of the near surface thawing degree-days (4°C.day) and freezing degree-days (-6441.5°C.day) for the soil in Nonshøgda over 2014 indicated predominantly freezing conditions. The sum of 4°C.day corresponded with January 2014, which was the only month to experience positive degree-days.

Comparably to the Vesleskarvet and Flårjuven, the freezing front originated only from the surface downwards (Figure 45). The cryofront can be seen in early January and late December, accompanied by lower temperatures of −5°C which surpass 50cm depth in January. By mid-April, temperatures below −20°C begin penetrating into the active layer from the surface until the lowest temperatures (−40°C) are experienced in August (Figure 45).

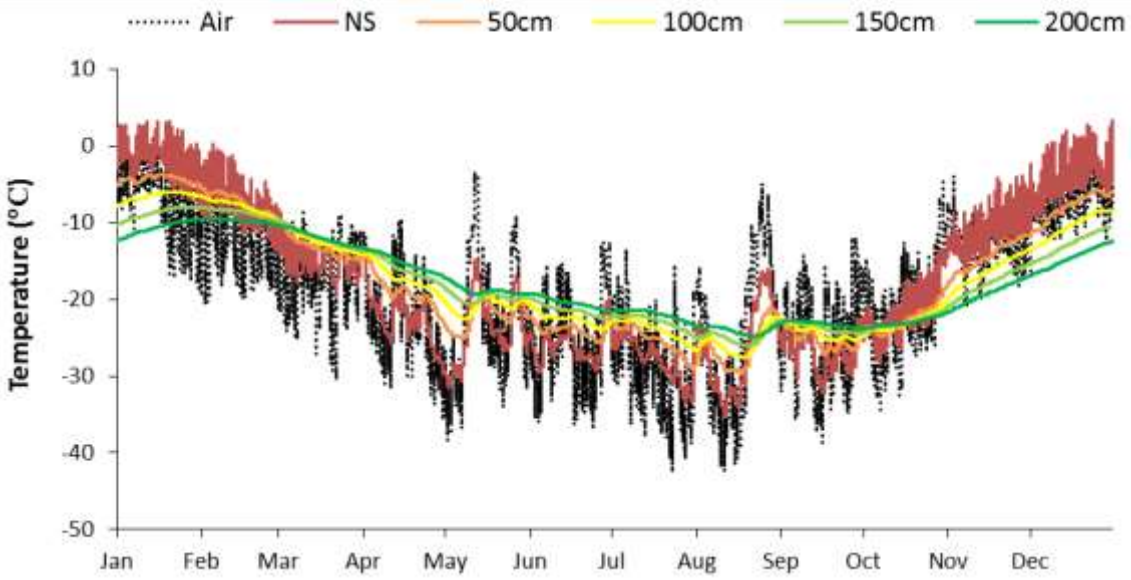

Figure 44: Soil water content, air temperature and ground temperatures at Nonshøgda, 2014.

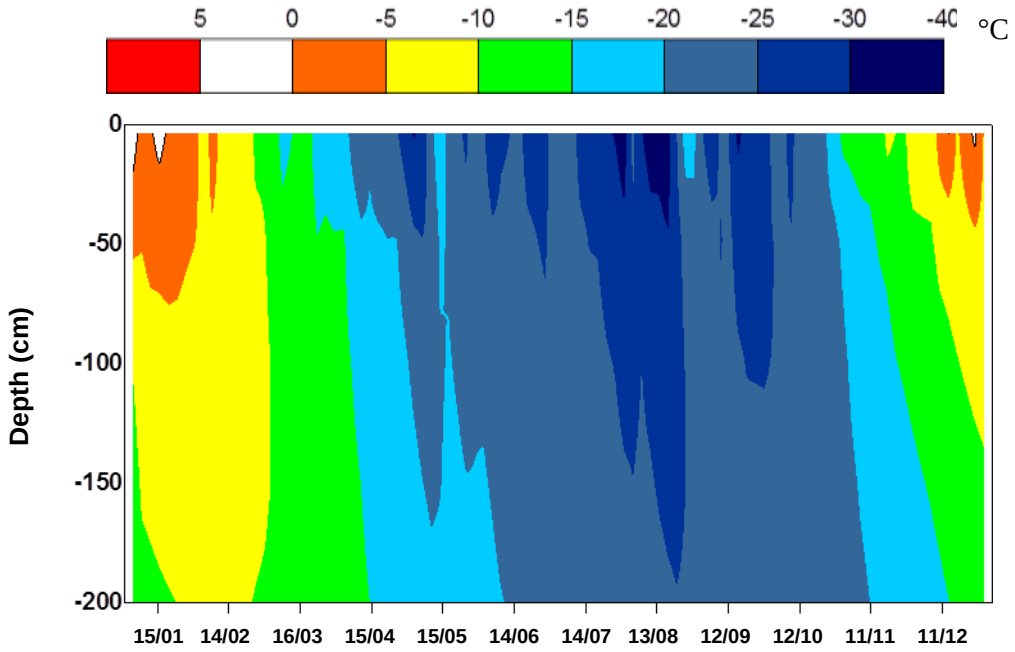

Figure 45: Thermal regime of the active layer at Robertskollen from January to December 2014.

Inter-site comparison

Despite the fact that all four sites were different in terms of latitude, altitude, and distance to coast, which were reflected in the soil thermal regimes of 2014, patterns found within the thermal regimes share similarities.

Nonshøgda experienced a sharper meridional gradient as evident by the high standard deviation in air temperature in comparison to other sites. This is due to its position in the transition zone between the coast and inland ice plateau, situated on the slope of the ice sheet (Hansen *et al*., 2009). Therefore, it would have a harsher climate compared to the more coastal sites that are Vesleskarvet, Flårjuven and Robertskollen. Moreover, the topography facilitates wind direction and speed, which influence ground thermal regimes by reducing temperatures (Karunaratne 2002; Adlam *et al*., 2010). Winds blow from NE-ESE during winter, with strong winds reaching an hourly mean of $>15ms^{-1}$, whilst there is no favoured directionality during summer (Hansen *et al.*, 2009) .

The contrasting behaviours in water content between the four sites could be attributed to differences in sediment texture. The soil at Nonshøgda has a coarser texture being derived from granitic gneiss. Therefore, it has a higher macroporosity in conjunction with infiltration rates (Michel *et al*. 2012). This is evident by its high bulk density of 1.89 g/cm^3. Whilst the soil at Flårjuven has a finer texture which results in higher soil moisture content, this is substantiated by the lowest bulk density of all sites with the highest porosity (see pg.54). All sites experienced predominantly freezing conditions throughout the year; however, differences in the degree of freezing are evident at sites. Cumulative thawing degree-days were similar Vesleskarvet, Flårjuven and Nonshøgda at 5, 7 and 4 degree-days in the near surface. Robertskollen had 216 thawing degree-days at 1cm depth. Flårjuven and Nonshøgda expressed the most similar quantity of FDD (6711 and 6441 thawing degree-days, respectively) and most abundant FDD overall.

The contouring of the temperature in respect to time and depth illustrated by the surfer plots, highlights the differences and similarities in thermal regime between sites (See Appendix C for annual and summer surfer plots for each site, pg.142). Temperature drops and increases more rapidly at Vesleskarvet, not reaching values as extreme as those found at Robertskollen, where absolute values have lower standard deviations for all depths compared to other sites (Table 25). All sites show lower standard deviation with depth as variation in the near surface as meteorological effects diminish with depth. All sites, except Robertskollen, represent one-sided freezing with rapid temperature drops in surface temperatures. Vesleskarvet winter temperatures, as seen on the surfer plot, do not drop as low as those reached at Nonshøgda and Flårjuven, this could be due to the ameliorating effect of the blockfield which is also seen by the low standard deviations in temperature at all depths. Flårjuven and Nonshøgda share similar altitude which could be a determinant of why the contouring of the temperature in respect to depth is the most similar to each other than in comparison with other sites, especially with minimum temperatures (<−40°C) peaking over the same time in July/August. Nevertheless, during winter all sites display similar trends of warming and cooling of the ground thermal regime in response to passing cyclonic events.

Overall, the effects of altitude are probably a main driver for the differing thermal regimes in the active layer, which may be compounded by the thermo-physical properties of the soil. The effects of altitude are evident by looking at the contouring of the temperature profile with depth during the 2013/14 summer in a transect from Flårjuven to Robertskollen (Figure 46; Figure 47). It is clear that Robertskollen is warmer than Vesleskarvet and Flårjuven, and that Vesleskarvet is warmer than Flårjuven. Most importantly, there is an up to 8°C difference in temperature between site's that are in a relatively close proximity to one another. This highlights the uniqueness of each site's active layer characteristics, which has implications for monitoring the effects of climate change as well as the impact it may have on soil development, local biodiversity and ecosystem functioning (Seybold *et al*., 2010).

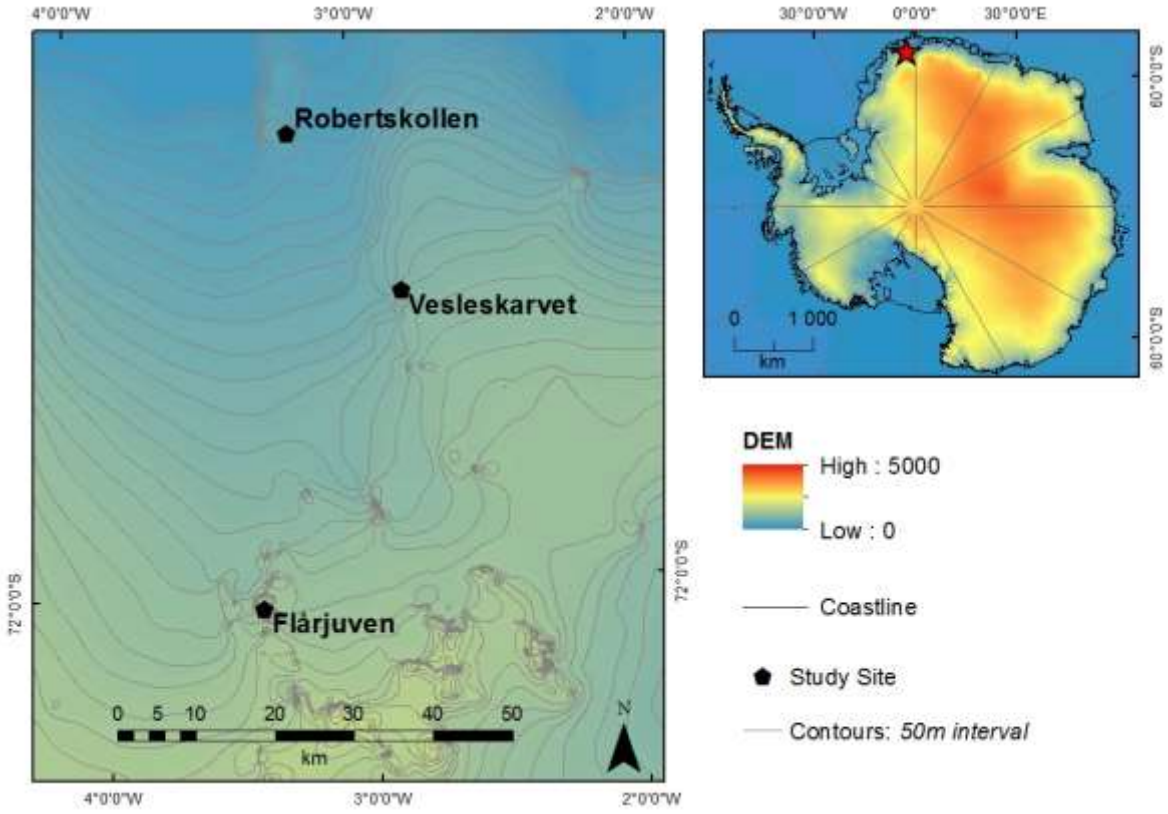

Figure 46: Transect decreasing in altitude and increasing in distance to the ice shelf from Flårjuven to Robertskollen.

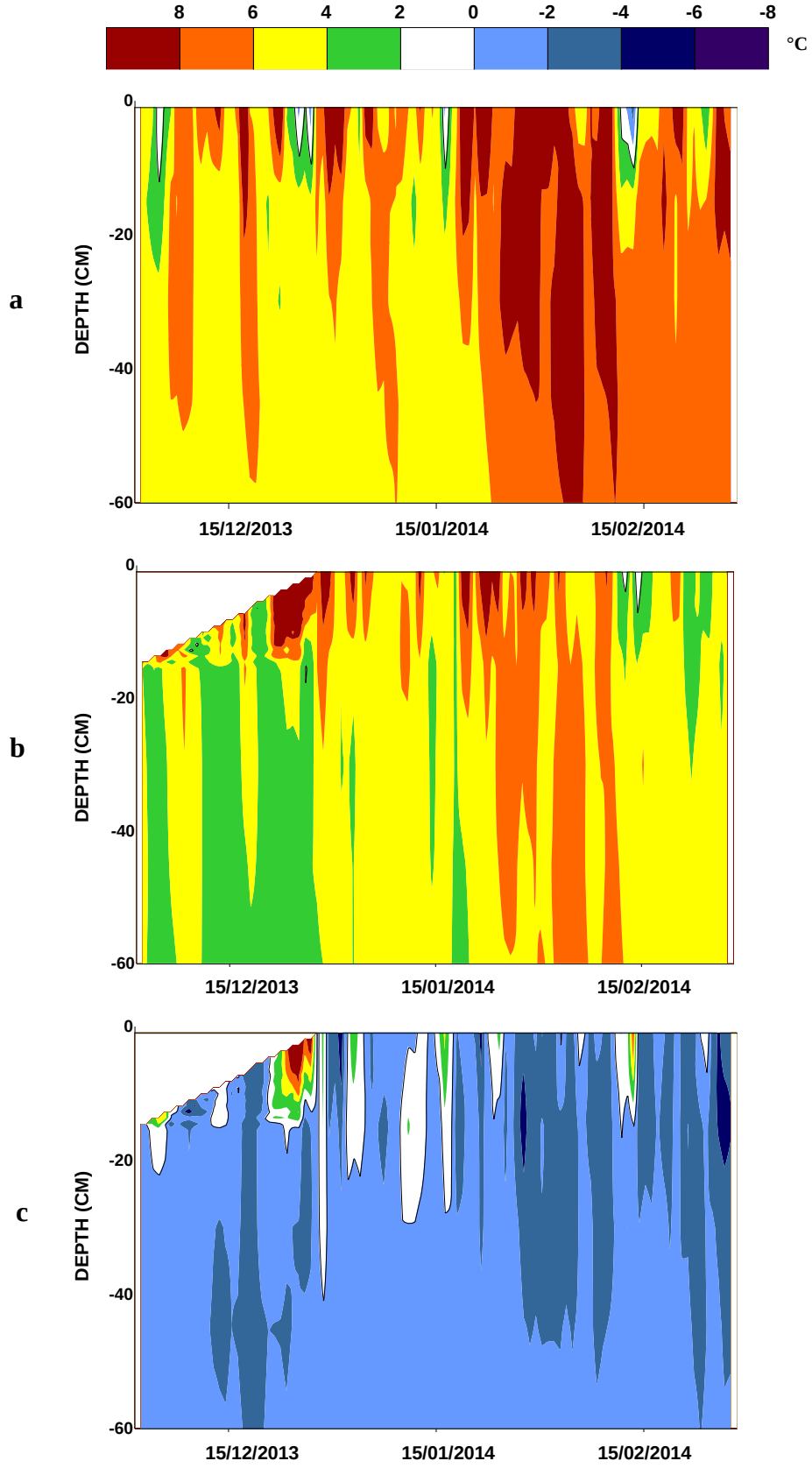

Figure 47: Differences in the thermal regime of the active layer between Robertskollen and Flårjuven (a), Robertskollen and Vesleskarvet (b) and Flårjuven and Vesleskarvet (c), from December 2013 to February 2014.

4.2. Objective 2: Ground Atmosphere Interface –Vesleskarvet Case Study

To elucidate the role of synoptic events on the active layer dynamics at Vesleskarvet, meteorological variables were compared with the observed ground thermal regime. A number of authors have highlighted the role of climate parameters on the active layer, i.e. GST dynamics. During the summer season (DJF), the influence of air temperature and radiation have been documented to have a strong influence on the depth of the active layer and its thermal regimes (Guglielmin *et al*., 2011; Guglielmin & Cannone, 2012; Guglielmin *et al*., 2012; Guglielmin, *et al*., 2014b). Adlam *et al*. (2010) confirmed that the role of radiation and ambient temperature exerts the greatest influence on the active layer, i.e. GST dynamics. Guglielmin *et al*. (2011) noted a strong relationship between ground surface and air temperature at Wright Valley (r^2=0.96) and Marble point (r^2=0.94) in southern Victoria Land. A similar relationship between ground surface temperature and incoming radiation was showcased by Guglielmin and Cannone (2012) in northern Victoria Land whereby a trend of active layer thickening (1cm per year) was identified. Pressure has also been used in studies involving the interaction between the active layer and the climate (Ling and Zhang, 2003; Cannone *et al*., 2006; Guglielmin *et al*., 2008).

Pressure was finely negatively skewed and temperature was symmetrical (Appendix B, pg.140). These distributions are sufficiently low to assume a normal distribution and allow for standardisation of raw data (Table 29). The average pressure observed over the study period was 881.76 hPa, compared to the average summer pressure of 888.6 hPa (refer to Table 31 pg.93 for the seasonal pressure of the study site). The lowest ambient temperature recorded was –39.40°C while the highest temperature is 4.1°C. This yields a range of 43.50°C (Table 29).

Table 29: Summary statistics for pressure (hPa) and temperature (°C) at Vesleskarvet, December 2009-December 2010.

	Pressure	Temperature
Mean	881.76	-16.70
Standard Error	0.10	0.08
Median	882.05	-16.90
Mode	889.80	-7.50
Standard Deviation(s)	9.92	7.87
Sample Variance	98.42	61.89
Kurtosis	0.24	-0.94
Skewness	-0.27	-0.07
Range	75.10	43.50
Minimum	837.50	-39.40
Maximum	912.60	4.10
n=1 year; 1 month		

Average, median and modal near air temperatures recorded by the logger (–6.04°C, –5.90°C and –5.22°C respectively) fall within a 0.82°C to each other. Whilst average, median and modal near surface temperatures recorded (–5.43 °C, –5.46°C and –6.21 °C respectively) fall within a 0.7°C to each other (Table 30). Average ambient temperatures measured by the logger are, therefore, lower than average near surface temperatures recorded. The range and variance of NST are higher than air temperatures, indicating a more variable and dynamic regime.

Table 30: Summary statistics for permafrost station air temperature (°C), ground thermal regimes (°C) and relative soil moisture (SM) for the 2009/10 summer at Vesleskarvet.

	Air	NS	15cm	30cm	45cm	60cm	SM
Mean	-6.04	-5.43	-5.58	-6.02	-6.36	-6.87	0.02
Standard Error	0.08	0.09	0.05	0.04	0.04	0.03	0.00
Median	-5.90	-5.46	-5.22	-5.55	-5.80	-6.33	0.00
Mode	-5.22	-6.21	-4.26	-4.26	-5.22	-5.96	0.00
Standard Deviation(s)	3.86	4.18	2.54	2.00	1.69	1.54	0.09
Sample Variance	14.93	17.48	6.47	4.02	2.85	2.37	0.01
Kurtosis	0.29	0.24	0.91	1.35	0.68	-0.05	57.92
Skewness	-0.34	-0.06	-0.86	-1.20	-1.11	-0.89	7.29
Range	23.48	25.80	14.34	11.26	8.14	7.04	1.06
Minimum	-18.50	-18.09	-14.30	-13.10	-11.93	-11.60	0.00
Maximum	4.98	7.71	0.04	-1.84	-3.79	-4.56	1.06

Average pressure recorded, seasonal minimum and maximum as well as seasonal ranges are shown in Table 31. A similarity can be seen in average pressure across the seasons, with summer (DJF) exhibiting the highest value and winter (JJA) the lowest average value. However, the highest maximum pressure is observed during autumn (MAM) which also records the lowest minimum, giving the largest range at 62hPa. Overall, the average pressures are high, which is to be anticipated on account of the fact that Antarctica is a desert environment where precipitation events and low-pressure systems which aren't frequent.

Table 31: Average, maximum, minimum and range for seasonal pressure at Vesleskarvet.

	Average	Max	Min	Range
DJF	888.6	903.3	870.9	32.4
MAM	883.0	912.0	850.0	62
JJA	875.0	892.2	854.6	37.6
SON	877.8	896.6	837.5	59.1
n= 5 years; 11 months				

The lowest average temperature observed for the study site occurs during the winter months (–24.4°C) and the highest average temperatures occur during summer (–7.8°C) (Table 32). All average seasonal temperature values are well below zero degrees Celsius. The highest range (27.6°C) in observed average hourly temperature values occurs during the winter months. The summer months, in contrast, show the lowest observed range of 21.5°C.

Table 32: Average, maximum, minimum and range for seasonal air temperature at Vesleskarvet. 2010.

	Average	**Max**	**Min**	**Range**
DJF	-7.8	1.6	-19.9	21.5
MAM	-18.4	-6.8	-31.9	25.0
JJA	-24.4	-11.8	-39.4	27.6
SON	-19.1	-6.5	-33.7	27.2
n= 5 years; 11 months				

Pearson's correlation at 95% ($\alpha = 0.05$, $p < 0.015$) significance was used to determine possible relationships between daily measurements of NST and the three climate parameters of ambient temperature, pressure and radiation. The Pearson's correlation coefficients are shown in Table 33. Despite a moderate correlation exhibited between active layer depth and mean summer air temperature (1 December 2009 – 28 February 2010) at Vesleskarvet (r=0.58), a strong relationship was found between mean summer air temperature and mean summer ground temperatures (Table 33). Correlations between air temperature and the ground thermal regimes ranged from r=0.56 to r=0.91 (Table 33). This was substantiated by GLM results in R (v 3.1.0.) which showed a highly statistically significant relationship ($p<0.001$) between air temperature and ground temperatures at a depth of 15cm (Figure 48). Coincidentally, the maximum thaw depth of the active layer for each year occurred when the soil temperature at 15cm reached its maximum at the 0°C isotherm.

Table 33: Coefficients of determination (r^2) and correlations (r) (in brackets) of 2010 summer (DJF) air temperature, radiation, and pressure with ground thermal temperatures.

	1cm	**15cm**	**30cm**	**45cm**	**60cm**
Air temperature °C	0.83 (0.91)	0.77 (0.87)	0.62 (0.78)	0.45 (0.67)	0.32 (0.56)
Radiation (kWh/m)	0.25 (0.50)	0.23 (0.48)	0.15 (0.38)	0.06 (0.23)	0.01 (0.10)
Pressure (hPa)	0.03 (0.19)	0.06 (0.25)	0.10 (0.32)	0.15 (0.39)	0.19 (0.43)

Compared to mean summer air temperature, the relationships of mean summer radiation and pressure with mean summer ground temperatures were much weaker (Table 33). The highest correlation with radiation was found to be near surface temperatures (r=0.5) (Table 33). Conversely, GLM results revealed a highly statistically significant relationship ($p < 0.001$) between radiation and ground temperatures at 30cm and 60cm (Figure 49).

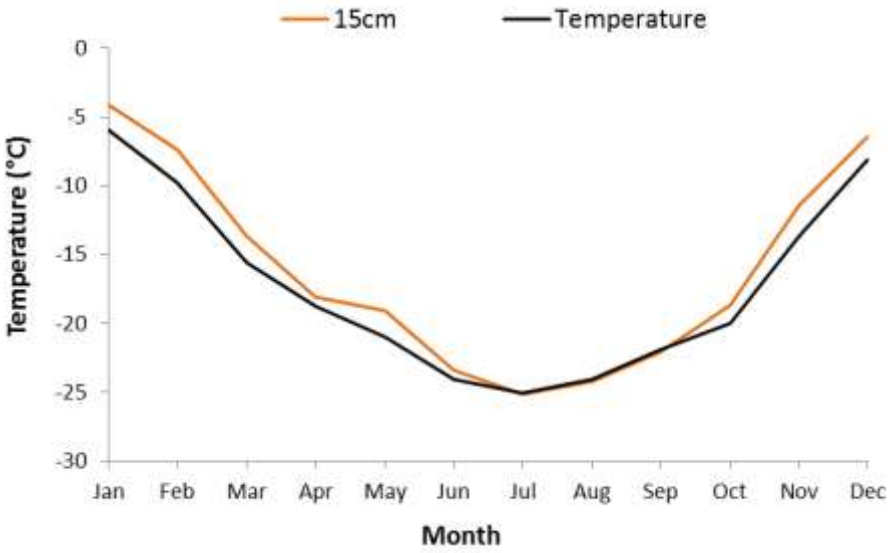

Figure 48: Mean monthly air temperature and ground temperature at 15cm depth, Vesleskarvet, 2010.

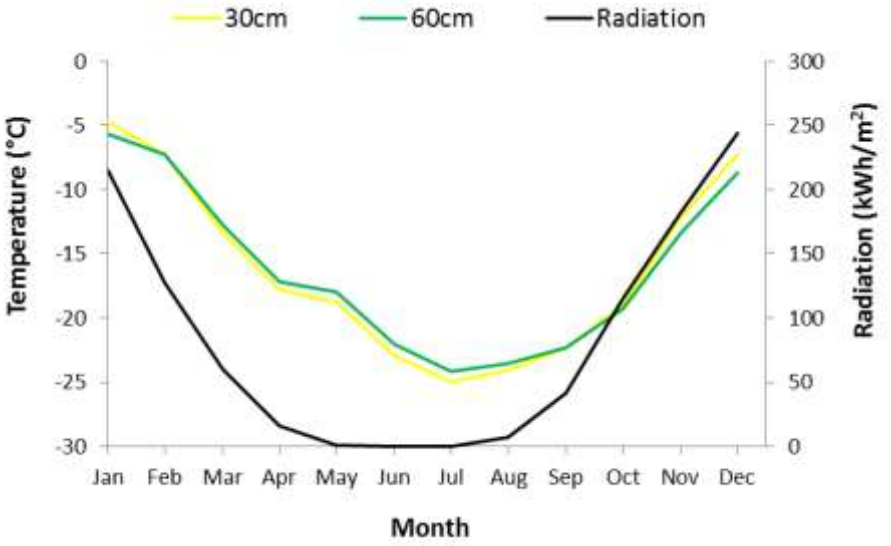

Figure 49: Mean monthly radiation and ground temperatures at 30cm and 60 cm depth, Vesleskarvet, 2010.

Air and near surface ground temperatures were found to have the strongest link with pressure according to GLM results ($p < 0.01$, Figure 50). Interestingly, the correlation between near surface temperature and pressure during May ($r=0.68$) and September ($r=0.63$) were notable in comparison to the other months which had correlations ranging between +0.41 and -0.01 (Table 34). This is attributable to the circumpolar trough (CPT) which is most pronounced during intermediate seasons (May and September) when it is furthest south (King & Turner, 1997). During maximum contraction of the CPT in early winter and spring, low pressure areas migrate towards the continent, bringing in a net transport of air which may account for the correlation found between

pressure and near surface temperatures at these times (King & Turner, 1997; van den Broeke, 2000a). Moreover, shifting westerlies, synchronous with the poleward migration of the CPT between June and September, result in the rapid advancement of sea ice (Meehl, 1991; Turner & Pendlebury, 2004; Bridgman & Oliver, 2006). Therefore, these results provide a foundation of the understanding that the southern annual oscillation has a significant role to play in the relationship between pressure, Antarctic near surface temperatures and the feedback mechanisms between sea-ice extents.

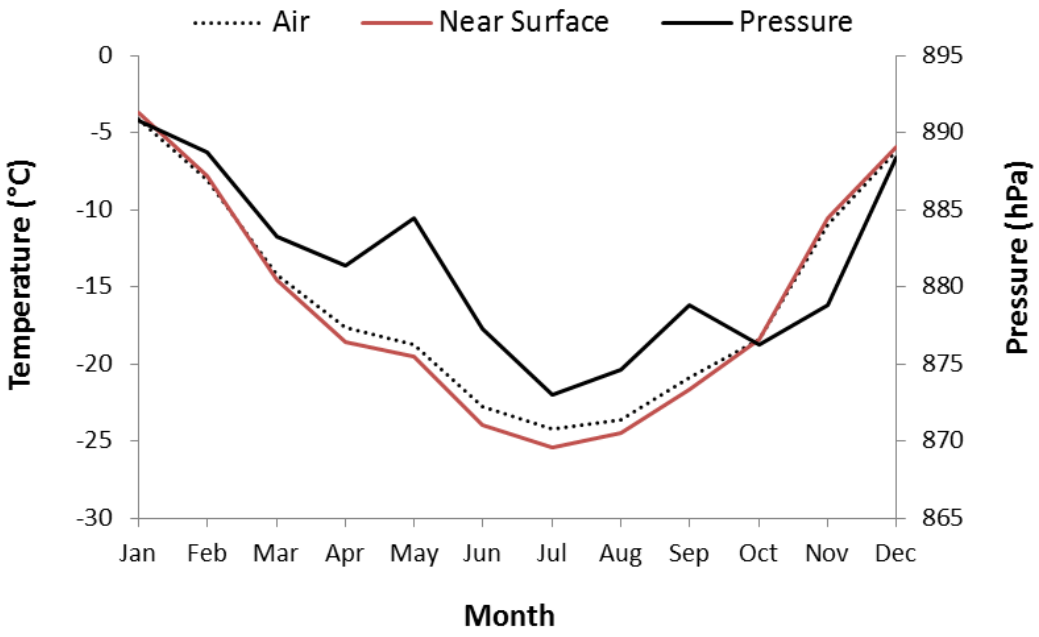

Figure 50: Mean monthly pressure, air temperature and NST at Vesleskarvet, 2010.

Table 34: Monthly correlation (r) between pressure and near surface ground temperatures at Vesleskarvet, 2010.

Month	Correlation (r)
Jan	-0.01
Feb	0.33
Mar	0.19
Apr	-0.07
May	0.69
Jun	0.27
Jul	0.41
Aug	-0.01
Sep	0.63
Oct	-0.3
Nov	-0.14
Dec	0.17

The ground thermal regimes during the winter period at Vesleskarvet (1 June–31 August 2010) showed weaker connections with air temperatures in comparison to summer (Table 35). This is substantiated by Zhang (2005) whom found higher correlations between air and ground surface temperatures during snow-free periods and a weakened correlation during snow-covered periods, particularly in winter. This is indicative of an active layer depth that is more responsive to summer rather than winter air temperatures. Radiation has a negligible relationship and significance with air temperatures as the presence of sunlight is non-existent in winter in the Antarctic (Table 35).

Table 35: Coefficients of determination (r^2) and correlations (r) (in brackets) of 2010 winter (JJA) air temperature, radiation, and pressure with ground thermal temperatures.

	1cm	15cm	30cm	45cm	60cm
Air temperature °C	0.93 (0.96)	0.68 (0.82)	0.45 (0.67)	0.19 (0.43)	0.10 (0.31)
Radiation (kWh/m)	0.01 (0.11)	0.01 (0.09)	0.01 (0.07)	0.00 (0.01)	0.00 (-0.04)
Pressure (hPa)	0.09 (0.30)	0.05 (0.22)	0.03 (0.18)	0.01 (0.12)	0.01 (0.09)

On closer inspection of the 2010/11 summer (Figure 51a), snowfall events are easily identifiable through the stabilization of ground temperatures over a short time series and the increase in near surface temperatures above air temperature due to insulation by snow cover . Thereafter, a progressive warming of the NST is apparent as the snow melts, leading to an increase in soil moisture content. The maxima soil moisture content is synchronous with spikes in near surface temperatures, with a time lag in soil moisture of roughly two hours from peaks in NST (Figure 52).

The ground temperatures from 6 to 12 December were warm in contrast to the period between 13 and 20 December. During this seven day storm period, two low pressure systems swept past the coast of WDML on 16 and 19 December 2010, potentially bringing snowfall which is evident by the stabilisation of ground temperatures. Near surface temperatures dip noticeably from 14 to 21 December. From the data, it is apparent that near surface temperatures follow ambient temperature conditions ($r^2 = 90$), with a time lag within a 24 hour period, consistent with the findings of Adlam *et al*. (2010), who suggested that soil temperatures respond to ambient temperatures within a 24-hour period. It is important to note that time lag within the 24 hour window will vary according to dependent variables such soil characteristics, soil moisture, snow characteristics, and the radiative regime.

A second noticeable storm event occurring between the 6 and 12 January 2011 could be linked with a large low pressure cell moving slightly to the east of the WDML coastline on 4 January, resulting in low pressures preceding snowfall events on 6 January 2011. Once again, snowfall associated with this cyclone led to the presence of soil moisture once air and ground temperatures peaked again (Figure 51). Low pressure events are associated with the position of the circumpolar trough (CPT) and although the CPT experiences storm activity in the Atlantic and Indian Ocean regions at

all times of year, it is less so during the Austral summer (Turner & Marshall, 2011). The link between fluctuations in ground temperatures and changes in atmospheric circulation can be elucidated by the seasonality of the Southern Annual Oscillation (SAO) (see Figure 54 and the accompanying discussion on pg.102).

a

b

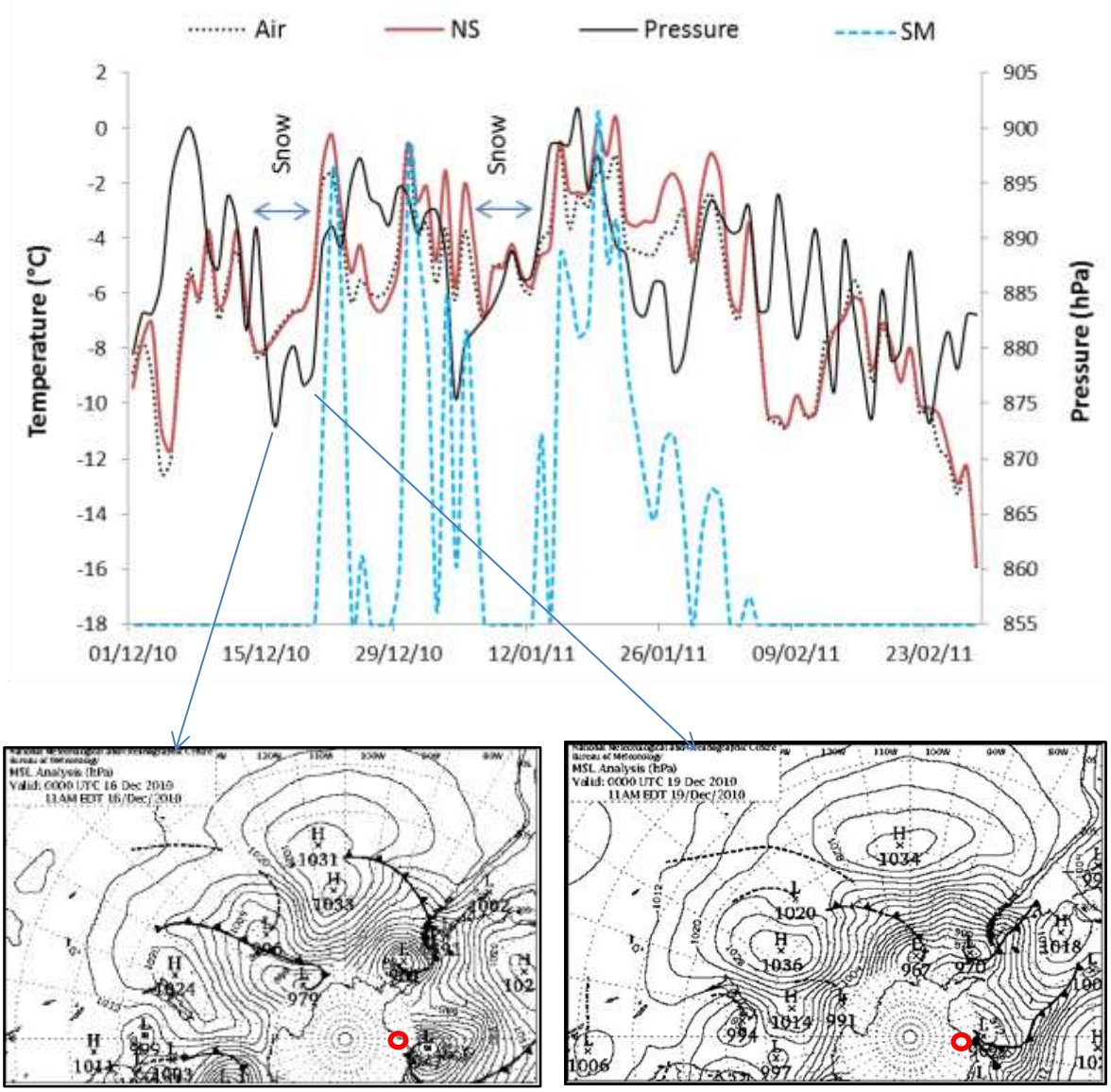

Figure 51: Daily air temperature, near surface temperature, atmospheric pressure and soil moisture for the 2010/11 summer (a) with accompanying synoptic charts from the Australian Bureau of Meteorology (b) (red circle indicates the study site location).

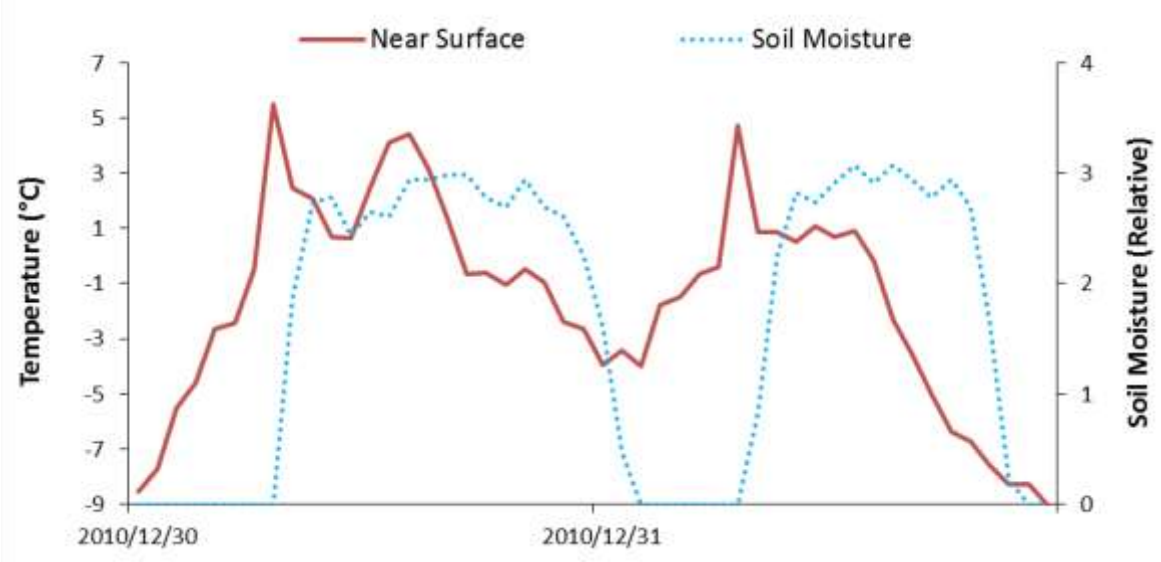

Figure 52: Near surface temperature and soil moisture on the 30-31st of December 2010.

van den Broeke (1998a and 1998b) studied the influence of the semi-annual oscillation (SAO) on near surface temperatures in Antarctica during 1957-79 and 1980-96 respectively. The second harmonic in pressure explains as much as 80% of the variance in surface pressure in the high southern latitudes (van den Broeke, 1998a). During the period of 1957-79, 68% of variance in the annual cycle of surface pressure at Vesleskarvet was attributed to the second harmonic, with an amplitude of 2.8hPa (van den Broeke, 1998a). However, van den Broeke (1998b) showed that during 1980-96 the variance decreased to 43% on account of a weakening SAO since the mid-1970s. The SAO undergoes a twice-yearly contraction and expansion, outlined in a brief bulleted summary below (Meehl, 1991; King & Turner, 1997; van den Broeke, 1998a):

- **December to March:** *CPT contracts and intensifies.*
- **February/March**: *CPT reaches equinoctial pressure maxima.*
- **March to June:** *CPT expands and weakens*.
- **June/July:** *CPT reaches solstitial pressure maxima*.
- **June to September:** *CPT contracts and intensifies.*
- **September/October:** *CPT reaches equinoctial pressure maxima.*
- **September-December:** *CPT expands and weakens*.
- **December/January:** *CPT reaches solstitial pressure maxima.*

From December to March and July to September, the CPT contracts and intensifies, leading to rapid cooling rates at Antarctic stations as the transport of warm air from lower latitudes is decreased (van den Broeke, 1998a; van den Broeke, 2000a). During February/March and September/October, the CPT reaches equinoctial pressure maxima driven by heightened baroclinity and westerly strength (King &Turner, 1997; van den Broeke, 1998a; Carleton, 2003). According to

van den Broeke (2000a), locally increased cloudiness and wind speed associated with strong baroclinity affects temperatures in these months. With the trough of minimum sea level pressure being farthest south and deepest during these transitional months, a higher frequency of precipitation events occur in response to cyclones moving and decaying closer to the coast (Meehl, 1991; King & Turner, 1997). Negative reversals (60cm warmer than NS) of ground temperature are seen from mid-February to mid-April and from mid-September to late September (Figure 54, pg. 101). This could be attributed to snow cover from increased cyclogenesis, compounded by a decreased net transport of air from lower latitudes to continental Antarctica.

From autumn to early winter, the north-west migration of the expanding and weakening CPT is accompanied by an amplification of the wave number-3 pattern of circulation around Antarctica (Meehl, 1991). This is manifested as a reversal of seasonal cooling in May, the by-product of increased meridional air exchange (net transport of air into the high latitudes) and pronounced surface temperature gradients (van den Broeke, 2000b). SANAE being situated in the troughs of the CPT, experiences a large change in temperature and small changes in pressure during from March to June on account of large scale circulation gaining a significant northerly component (van den Broeke, 1998a; van den Broeke, 2000b). This process directly links the SAO to Antarctic surface temperatures (i.e. there is a strong spatial contiguity between the second harmonics of pressure and temperature) (van den Broeke, 1998a). Therefore, we can see the effects of the expanding and weakening CPT from March to June with a positive reversal (NS warmer than 60cm) of ground temperatures occurring from mid-April to mid-May (Figure 54) and by the May peak in temperatures on Figure 53 which was on average 1.7°C warmer than June.

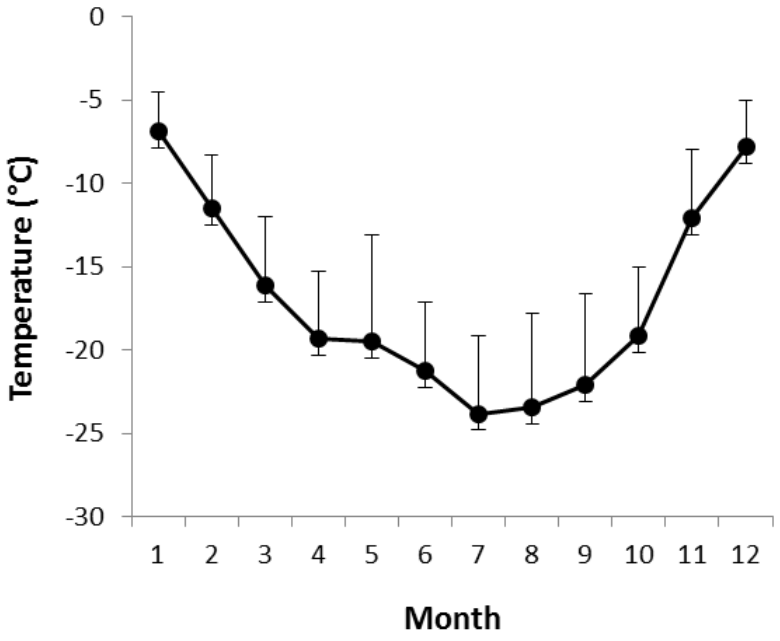

Figure 53: Annual cycle of temperature and standard deviations measured by the SAWS weather station at Vesleskarvet, based on six years of measurements (2009-2014).

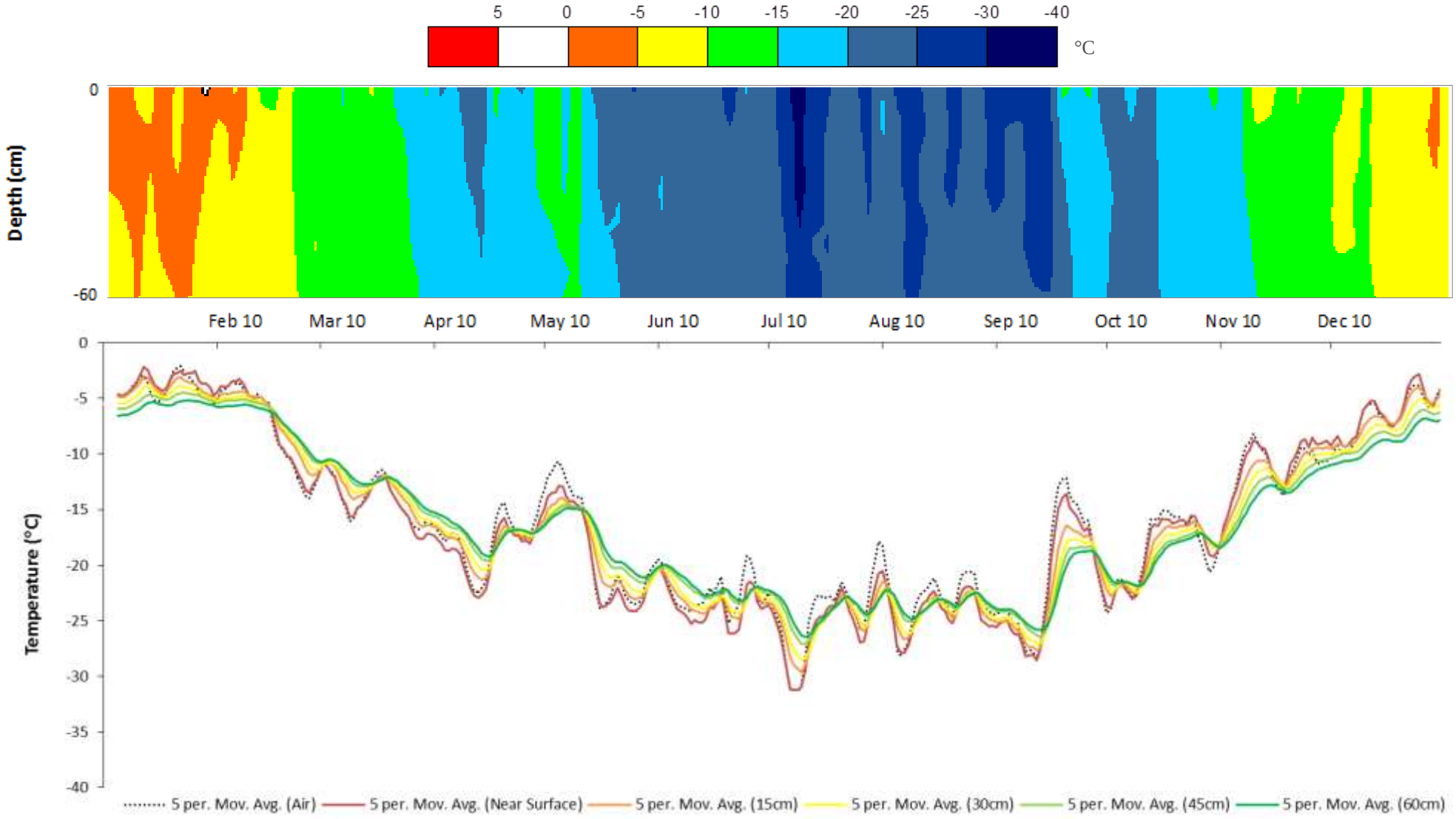

Figure 54: Surfer plot of temperature with depth accompanied by a 5-day moving average of daily ground temperatures at Vesleskarvet, 2010.

The trough of minimum sea level pressure is farthest north and weakest in June which is reflected by surface pressure maxima around the Antarctic coast (Meehl, 1991; King & Turner, 1997; van den Broeke, 1998a; Carleton, 2003). A study conducted by van den Broeke and van Lipzig (2003) on the near surface (6-7m) wind field in Antarctica during July revealed that the katabatic pressure gradient force (PGF) increases from the interior toward the coast, reaching maxima over steep coastal slopes. However, the narrow ice shelves fringing the coast of DML are characterised by a small surface slope which is reflected by a small katabatic PGF. A thermal wind PGF dominates over katabatic winds in DML, induced by cold air accumulation over the nearly flat ice shelves. Therefore, although the easterly near surface winds in DML are comparable in magnitude and direction to katabatic winds, they are mainly forced by a large scale pressure gradient reaching speeds in excess of $10ms^{-1}$ (van den Broeke & van Lipzig, 2003). The result can be seen by the deepest dips of temperature in July, visualised by the contouring of temperatures in Figure 54.

The reversal in ground temperatures becomes negative (60cm warmer than NST) in mid-May, lasting until early September (Figure 54), which is indicative of the net balance of longwave radiation exceeding the insulating effect of the snow cover (Guglielmin e*t al.*, 2014b). The effects of snow cover are not apparent (NST lower than air temperature), due to the proximity and immediate response of the NST sensor to the surface. Lacking solar radiation in the winter months increases the temperature disparity between the surface of the earth and the highest temperature within the lower troposphere, leading to strengthened inversions (King &Turner, 1997).

The flatness of the Fimbul ice shelf bordering Vesleskarvet prohibits the development of katabatics, further facilitating the development of a strong temperature inversion at the surface (van den Broeke, 2000a). This could be augmented by the distance of Vesleskarvet from the plateau, as well as the height of the Ahlmannryggen which provides shelter from harsh katabatic winds. According to King and Turner (1997), the surface temperature inversion can reach up to 10°C when accompanied by low wind speeds and low atmospheric moisture content. The amplitude of the second harmonic in temperature is susceptible to the strength of the inversion in winter. As mentioned previously, inversions during winter are sensitive to disturbance such as wind speed which enhances variability in Antarctic NST, creating a positive correlation between mean temperature and wind speed/cloudiness (van den Broeke, 2000c). This elucidates the low annual mean temperature experienced at Vesleskarvet (ca −16 °C), which is comparable with other East Antarctic ice shelf stations (such as Halley and Neumayer) (van den Broeke, 2000c). The amplitude of the second harmonic in surface temperatures is underpinned by station position in terms of continentality and latitude. Because SANAE is located close to an ice shelf, latitude is the dominant process whereby inter-annual temperature variability can be linked to variability in cloudiness and wind speed particularly for the winter months (van den Broeke, 2000c).

4.3. Objective 3: ^{137}Cs Tracing

Underpinned by fallout history and known half-life, the vertical and horizontal movements of sediment from decadal timescales and more, may be conjectured using the topographic distribution of ^{137}Cs (Klaminder *et al*., 2014). Similarly to Klaminder *et al*. (2014), the purpose of this objective is to prove the hypothesis that ^{137}Cs activity increases from the inner domain of the sorted circle to the coarse boundary. Additionally, to prove that ^{137}Cs activity is higher on terrace bases's compared to their middles. Although Slettfjell is not one of the four focal nunataks used in this dissertation, ^{137}Cs sampling has been done to support the initial findings done by Meiklejohn (2012) in the Initial Environmental Evaluation. The sample numbers and corresponding names are displayed in Table 36 which also indicates the landform type.

Table 36: Legend of sample numbers, samples and corresponding landforms used in ^{137}Cs analysis.

	Sample	Landform
1	Flårjuven M1	Terrace
2	Flårjuven B1	Terrace
3	Flårjuven M4	Terrace
4	Flårjuven B4	Terrace
5	Flårjuven M7	Terrace
6	Flårjuven B7	Terrace
7	Flårjuven Centre	Sorted Circle
8	Flårjuven Crack	Sorted Circle
9	Robertskollen Centre	Sorted Circle
10	Robertskollen Crack	Sorted Circle
11	Slettfjell Centre	Sorted Circle
12	Slettfjell Crack	Sorted Circle

Figure 55 shows ^{137}Cs activity plotted against specific surface area (SSA). This is necessary as tracers have a higher affinity for the fine earth fraction, providing a linear relationship between particle size and tracer quantity. The diamond shapes represent the terraces at Flårjuven, whilst the circles represent the sorted circles at the various nunataks. The samples with a detectable amount of ^{137}Cs follow a straight line, indicating that particle size may be a major determinant in ^{137}Cs abundance. Samples 3, 6 and 9 (Flårjuven M4, Flårjuven B7 and Robertskollen centre respectively) do not have any detectable ^{137}Cs activity, despite having the largest percentage of fines (Figure 55; Figure 56). Similarly, samples 1 and 11 (Flårjuven M1 and Slettfjell Centre) have the next lowest ^{137}Cs abundance (Figure 57) despite a moderate amount of fines present (Figure 56). This means that ^{137}Cs activities at these sites are not dependent on the amount of fines.

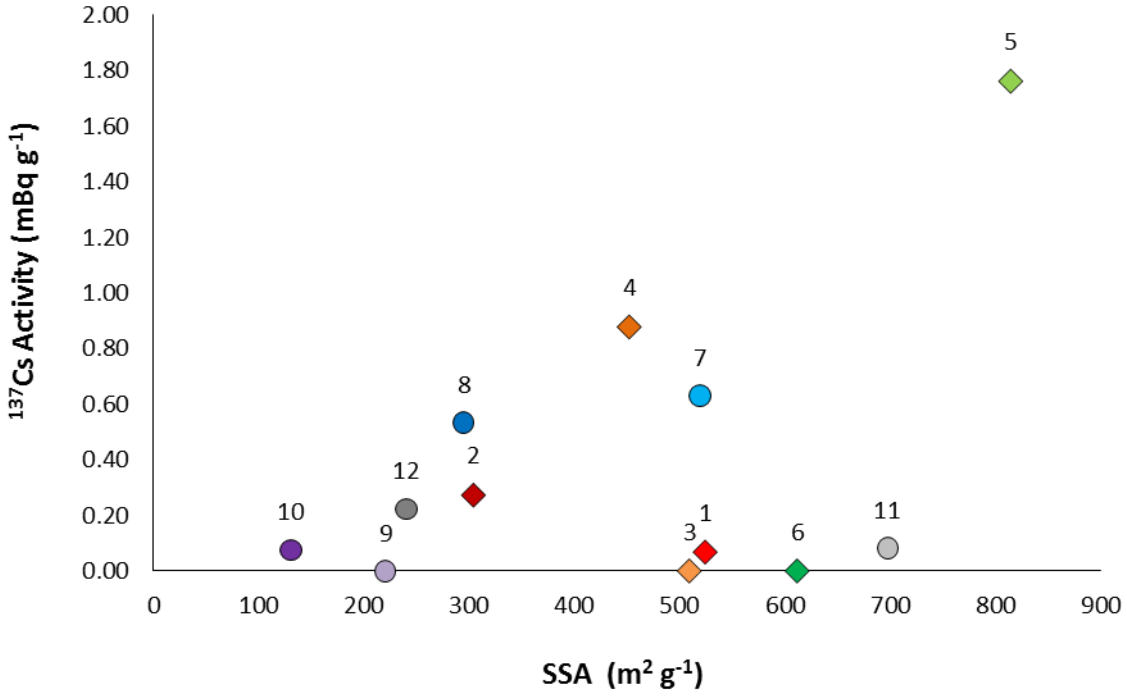

Figure 55: ^{137}Cs Activity plotted against specific surface area for the 12 sample sites.

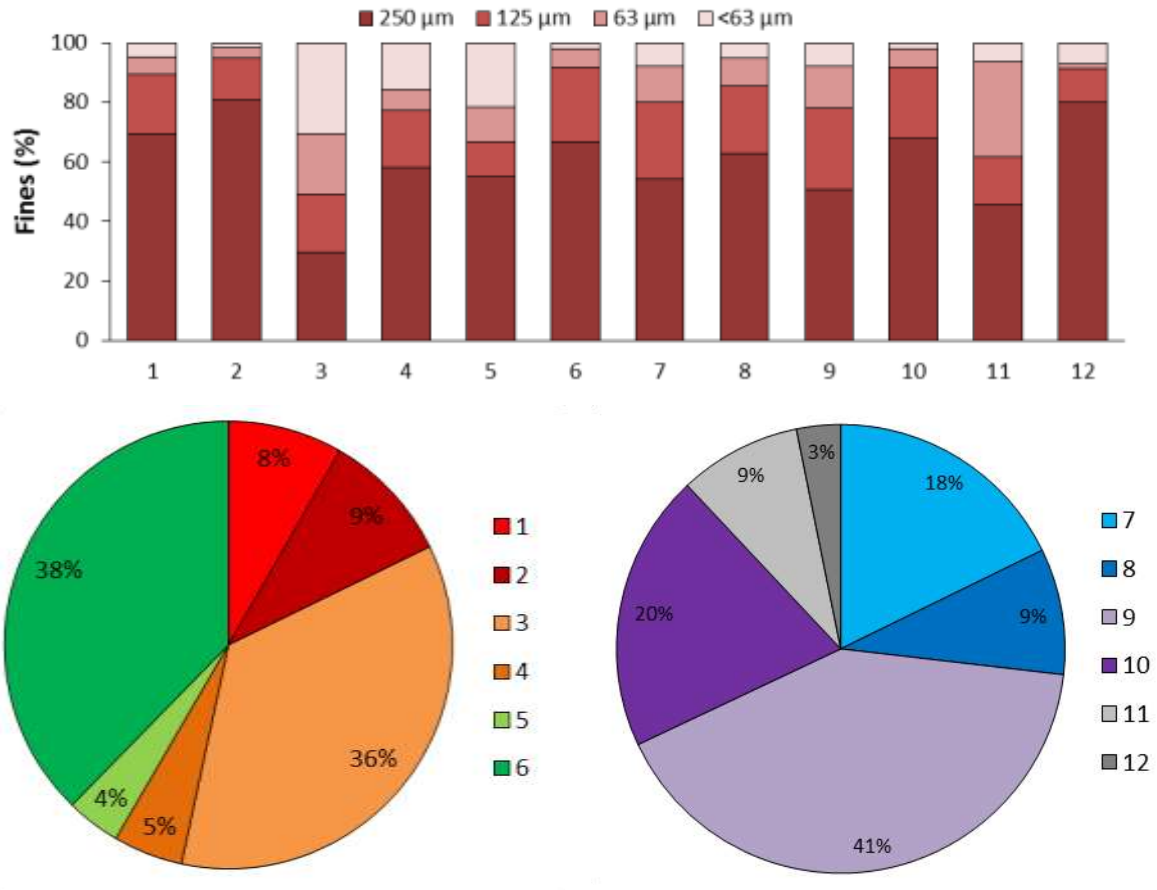

Figure 56: Proportion of fines (%) and fines as a proportion of total sediment sample for terraces (1-6) and sorted circles respectively (7-12).

For the terraces, all bases had lower elevations than the middles except for sample 2 which formed an elevated toe being the last and lowest terrace on the slope. Flårjuven M1, B1, M4 and B4 (samples 1,2,3,4 respectively) showed the ideal pattern of having higher ^{137}Cs abundance at the base of the terrace (Table 36). Samples 3 and 6 were most likely covered by snow during the radioactive fallout period, indicating that the terraces have not been active since before that time. It is also possible that Flårjuven M1 (sample 1, part of the bottom-most terrace set), was also snow covered during the radioactive fallout period, acquiring ^{137}Cs subsequent to the melting of snow over consecutive seasons. Alternatively and more possibly at Flårjuven M1, wind may have blown fines down from the top terraces, consequently introducing trace amounts of ^{137}Cs to the proportion of fines already present at the site that may have been previously buried under snow during fallout.

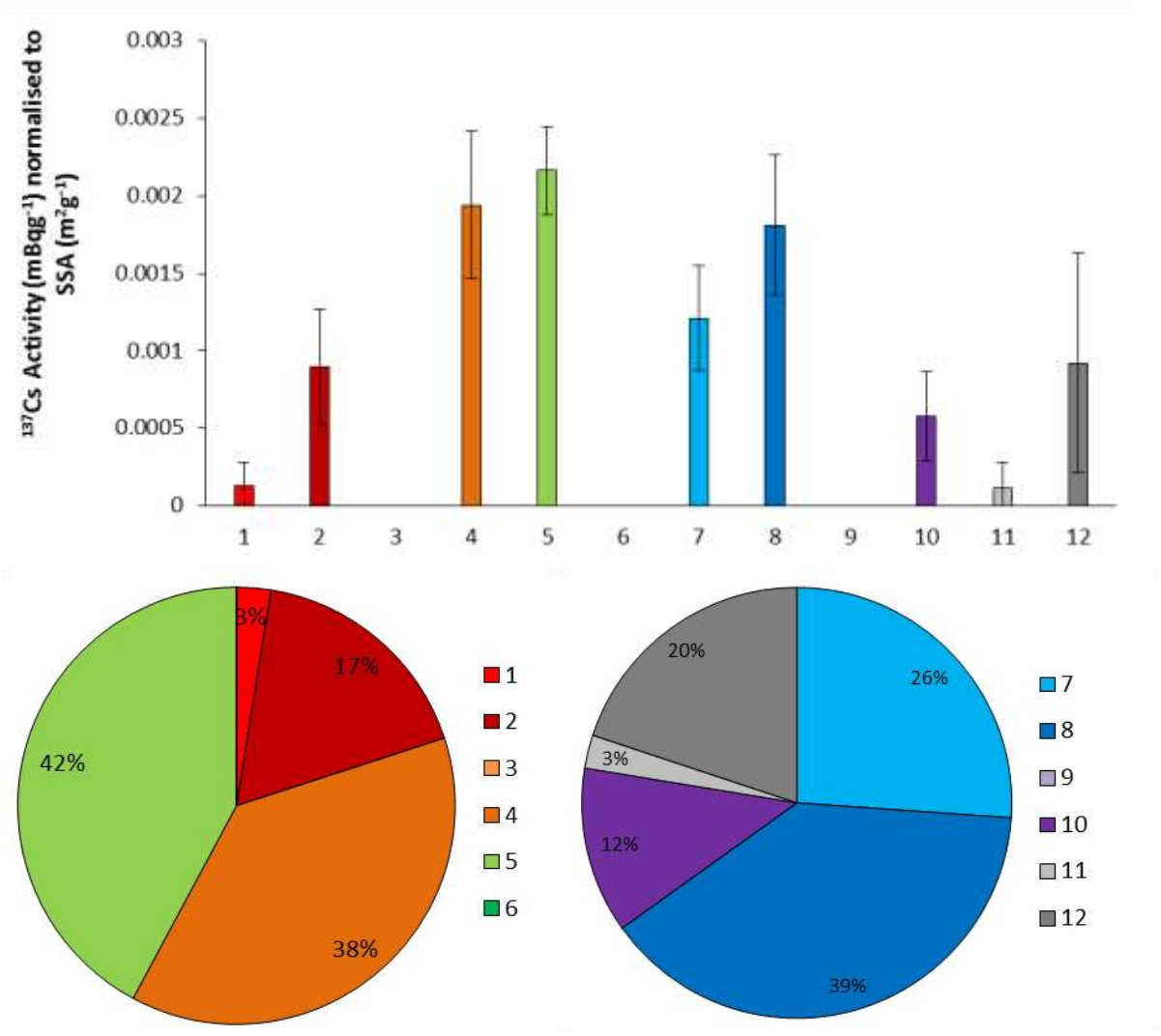

Figure 57: ^{137}Cs Activity normalised to SSA for terraces (1-6) and sorted circles respectively (7-12).

Samples 11 and 12 are the centres and cracks respectively of the sorted circles found at Slettfjell. From Figure 57 it is clear that the centre has a lower ^{137}Cs concentration than the crack. This is substantiated by the initial findings by Meiklejohn (2012), where a concentration of ^{137}Cs was found in the coarse boundaries of sorted circles on the Slettfjell nunatak. The sorted circle centres of Flårjuven and Robertskollen (samples 7 and 9 respectively) also show lower ^{137}Cs than the cracks (samples 8 and 10). This is concurrent with the cryoturbation model as smaller amounts of ^{137}Cs are expected to be found in the centres in comparison with the edges, whereby movement of material from the fine centres towards coarse boundaries occurs (Warburton, 2013). The results indicate that the sorted circles at Robertskollen are the most active, followed by Slettfjell and then those at Flårjuven as the centre at Flårjuven still holds higher amounts of ^{137}Cs, indicating that it has been more recently active that the other two.

Overall, the results show that surficial ^{137}Cs activities are heterogeneous across the nunataks, as well as within the patterned ground features themselves. The sorted circles (samples 7- 12) exhibited a higher abundance of ^{137}Cs in the outer domain in comparison to the inner domain, as materials in the centre are eroded and deposited in the outer domain which is supplemented by subduction. This occurs on decadal to centennial timescale (Klaminder *et al*., 2014). Gaspar *et al*. (2013) highlighted the roles of erosion and deposition within the expressions of patterned ground, each linked with exhausted and enhanced levels of ^{137}Cs respectively. Once again, the amount of ^{137}Cs in conjunction with the disparity between activity in the centre and the crack differed substantially for each nunatak. This is potentially due to the presence of snow cover. Slettfjell has the flattest top which encourages snow accumulation, influencing the amount of fallout to settle on the sediment surface during that time, therefore, explaining overall low amounts of ^{137}Cs on this nunatak in comparison with the others. The sorted circles at Flårjuven exhibited the highest difference in ^{137}Cs activity between the circle centre and its boundary, followed by Slettfjell and then Robertskollen which holds an undetectable ^{137}Cs reading in the centre.

From the results, it seems logical to infer that materials containing measurable ^{137}Cs were therefore existent at or close to the soil surface during majority of the atmospheric fallout between 1958 and 1971 (Jelinski, 2013). Whilst, the absence of ^{137}Cs in materials is interpreted as being buried during the same time period and undergone subsequent exhumation. This suggests an upward movement of buried sediment in the centre of the sorted circles through subduction over the past 40 years or less (Jelinski, 2013). The cryoturbation process results in a loss of ^{137}Cs in the centres. Nevertheless it is important to consider other potential contributing factors to lower ^{137}Cs concentrations in the centres, such as differential deposition of the radiogenic isotopes across microtopography during fallout and wind erosion from the elevated centres (Jelinski, 2013).

4.4. Objective 4: Spatial Distribution of Active Layer Related Landforms

4.4.1. Vesleskarvet

Polar environments are often characterised by patterned ground related to cyclic freezing and thawing whereby temperature induces volume changes in sediments (Humlum & Christiansen, 2008). According to Kessler and Werner (2003), these patterned ground features comprise of circles, polygons, and sorted stripes on hillslopes (terraces). Figure 58 show the number of potential freeze thaw events (PFTE) in the near surface soil layer (1cm depth) at the four different sites. Nonshøgda shows an anomalously high amount of PFTE during 2013 due to the construction of a hut in the vicinity of the logger which introduced artificial moisture inputs and therefore a higher thermal diffusivity of the sediments. The other three bars are shaded due to incomplete datasets and are therefore not an accurate representation of the PFTE during the year. Overall from Figure 58 it is clear that Robertskollen and Flårjuven experience the most PFTE in the uppermost layer of sediment, followed by Vesleskarvet and then Nonshøgda. These results are reflected by the amount and types of patterned ground/periglacial landforms at the four different sites which are depicted in the landform maps below (Figure 59-70).

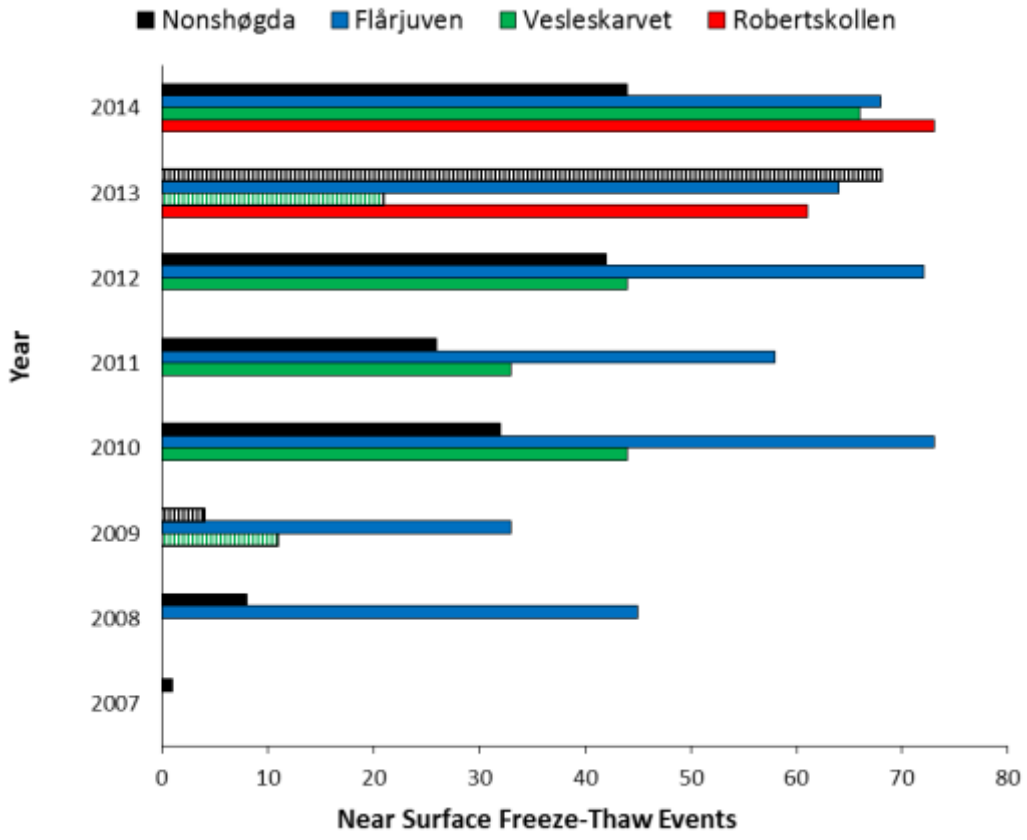

Figure 58: Yearly freeze-thaw events in the top 1cm of sediment at each study site (shaded bars indicate years with missing or inaccurate data and should be interpreted with caution).

Majority of the periglacial landforms depicted below were too small to be accurately represented by the LANDSAT imagery available, which has a maximum resolution of 30m. Therefore, it was necessary to create multiple maps of one nunatak to accurately display the landforms at a small scale. Moreover, the purpose of the maps is to show the type and relative abundance of landforms at each study site. Therefore, it is pertinent to note that only the landforms recorded during the fieldwork seasons are displayed and are not representative of the absolute abundance or coverage of the landform types. For instance, the maps indicating polygons only reveal the recorded and measured polygons which are amongst many within a polygon field. The Northern Buttress of Vesleskarvet is characterised by sorted circles and semi-circles (sorted circles that have formed partially under a rock, giving rise to a half circle) with an average (n=39) a-axis of ca. 32cm and b-axis of ca. 22cm. They are located in a depression which facilitates the accumulation of snow; subsequently, the presence of snow in close proximity to the circles has been noted in conjunction with the visual presence of soil moisture in the fine domain at the surface.

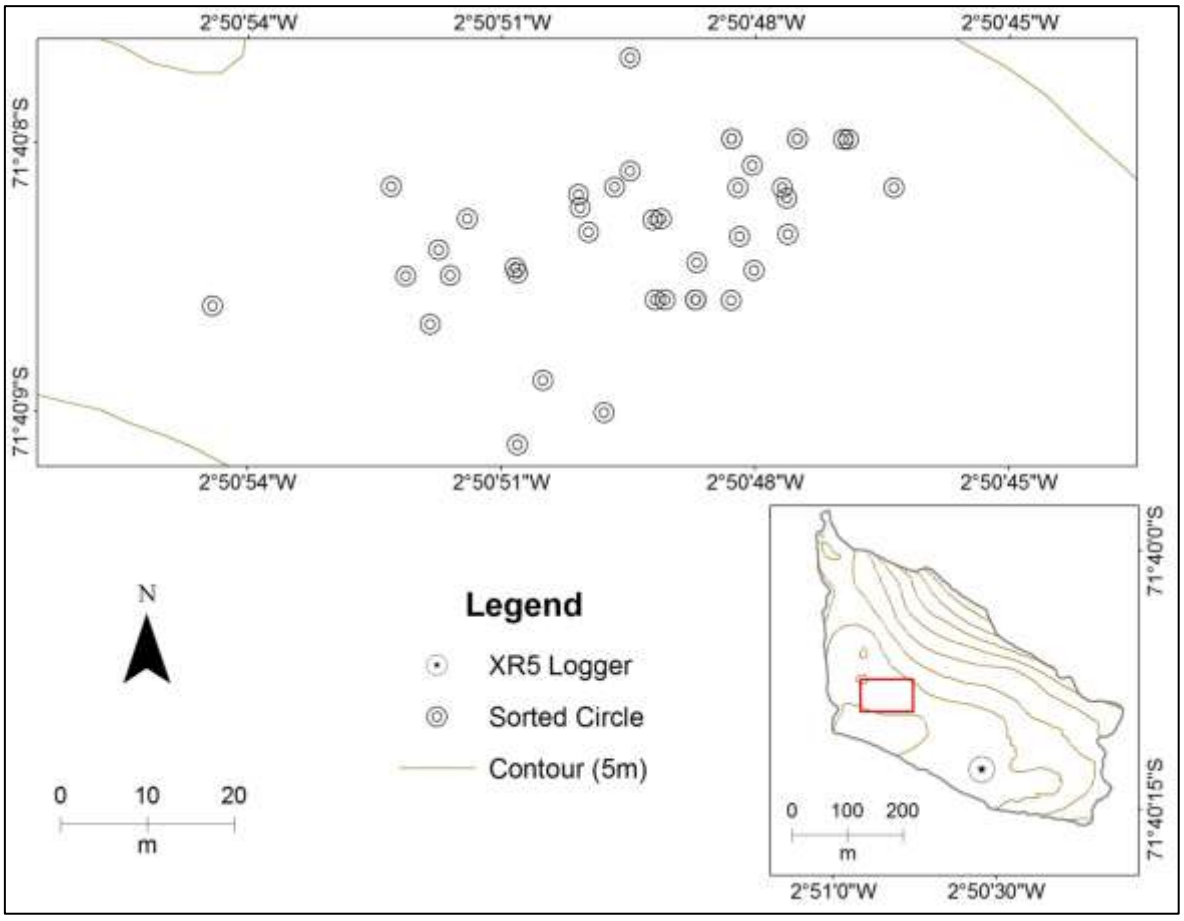

Figure 59: Sorted circles at Vesleskarvet.

4.4.2. Flårjuven

As evident from figures 60-64, Flårjuven is characterised by a wide range of periglacial landforms indicative of an active layer at multiple locations across the nunatak. On the northeastern flank of the nunatak, multiple terraces were extended from a high elevation all the way through to a depression where a network of polygons was found (Figure 60). Scott (2014) found that the polygons (n=31) have a mean area of 44.68m² and the terraces (n=7) have a mean area of 183.28m². Standard deviations of 66 and 25 for the terraces and polygons respectively reveal a large the variability in landform size (Scott, 2014).

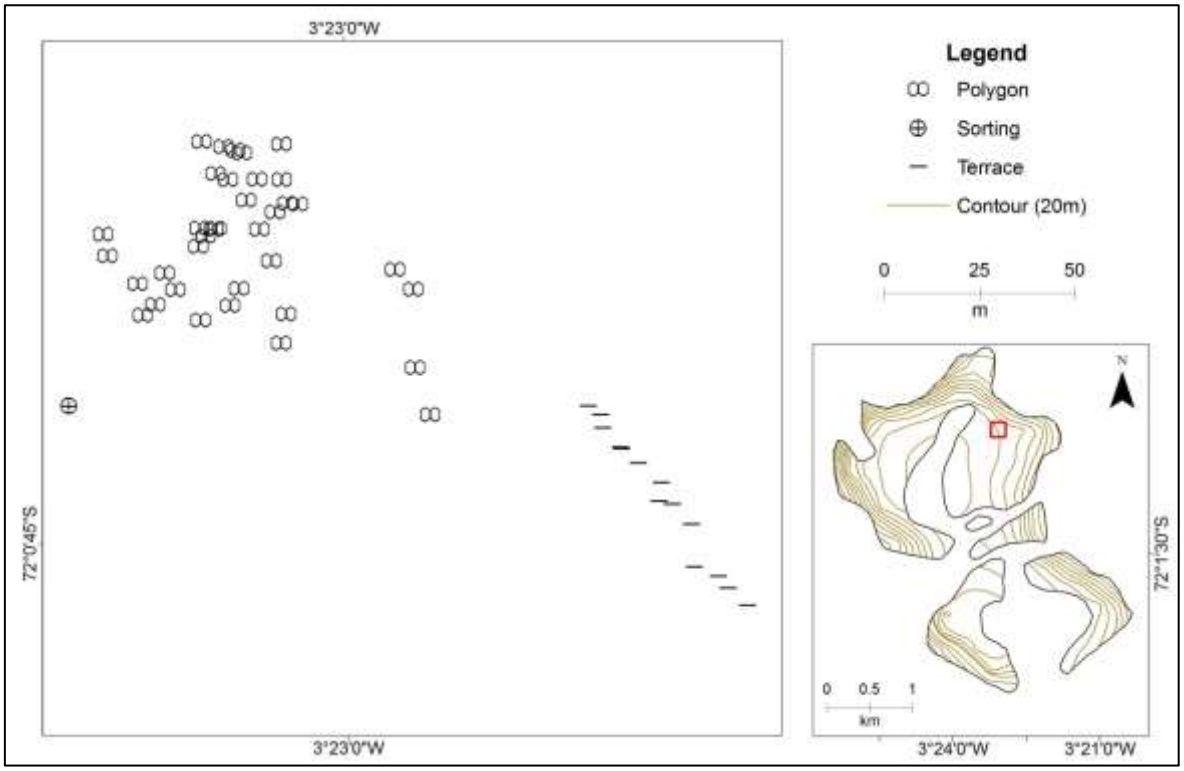

Figure 60: Flårjuven landforms 1.

Terraces were also documented on the north-western side of Flårjuven (n=8), accompanied by contraction cracks (n=1), sorted circles (n=4) and sorting (n=5) pre-emptive of a patterned ground feature (Figure 61). Sorting (n=5), sorted circles (n=3), soilfluction lobes (5), stripes (n=1), terraces (n=1) and contraction cracks (n=2) were found elsewhere on Flårjuven too. Most importantly was the proximity of sorted circles and sorting in close proximity to the PACE XR-5 logger (Figure 62).

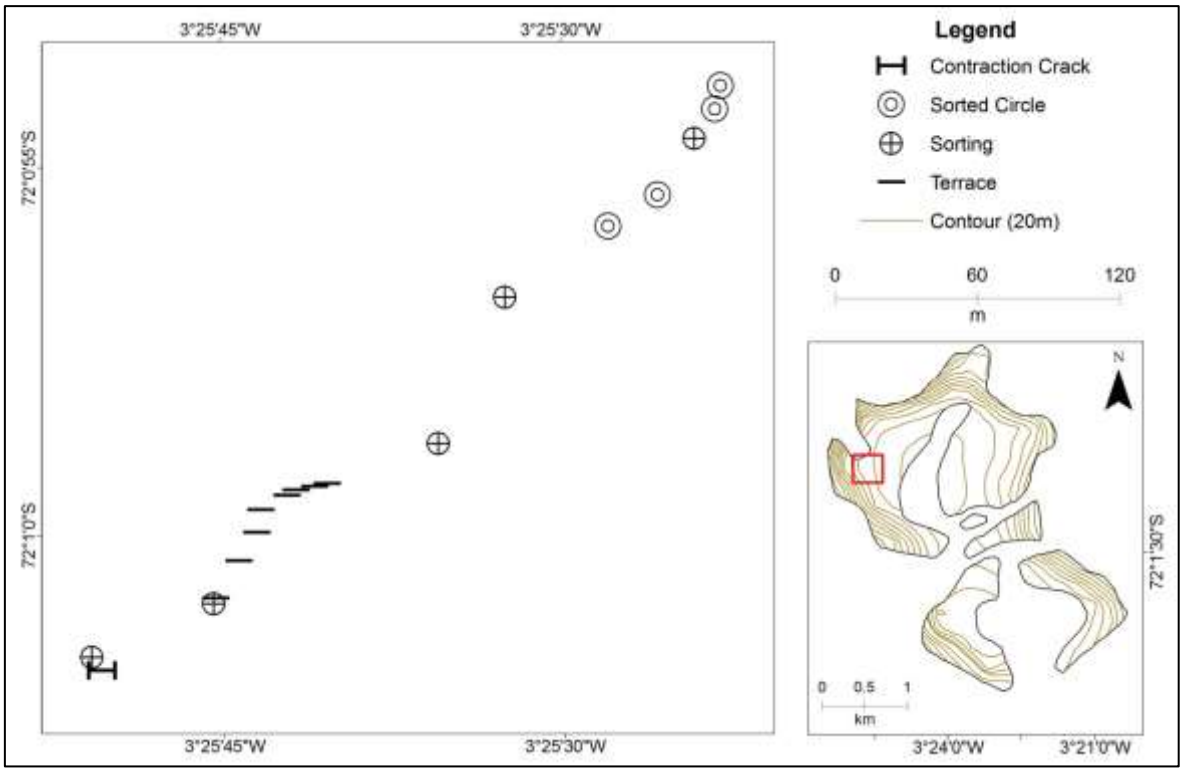

Figure 61: Flarjuven landforms 2.

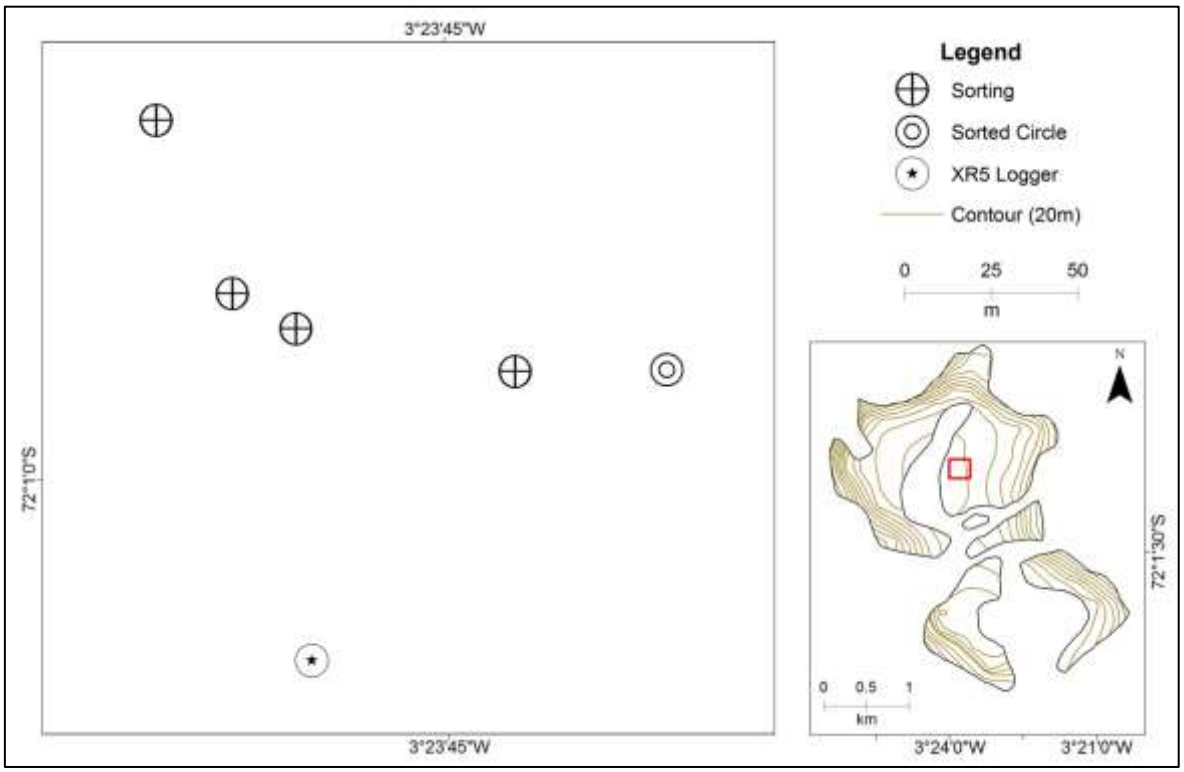

Figure 62: Flarjuven landforms 3

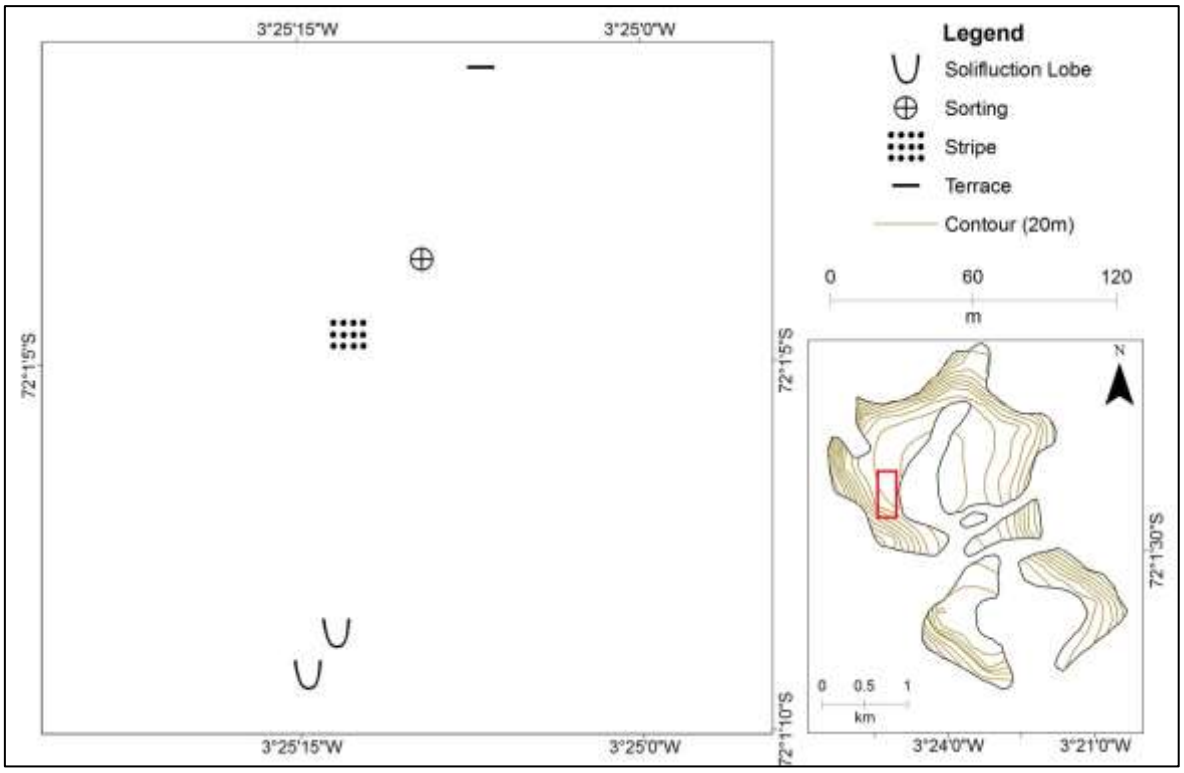

Figure 63: Flarjuven landforms 4.

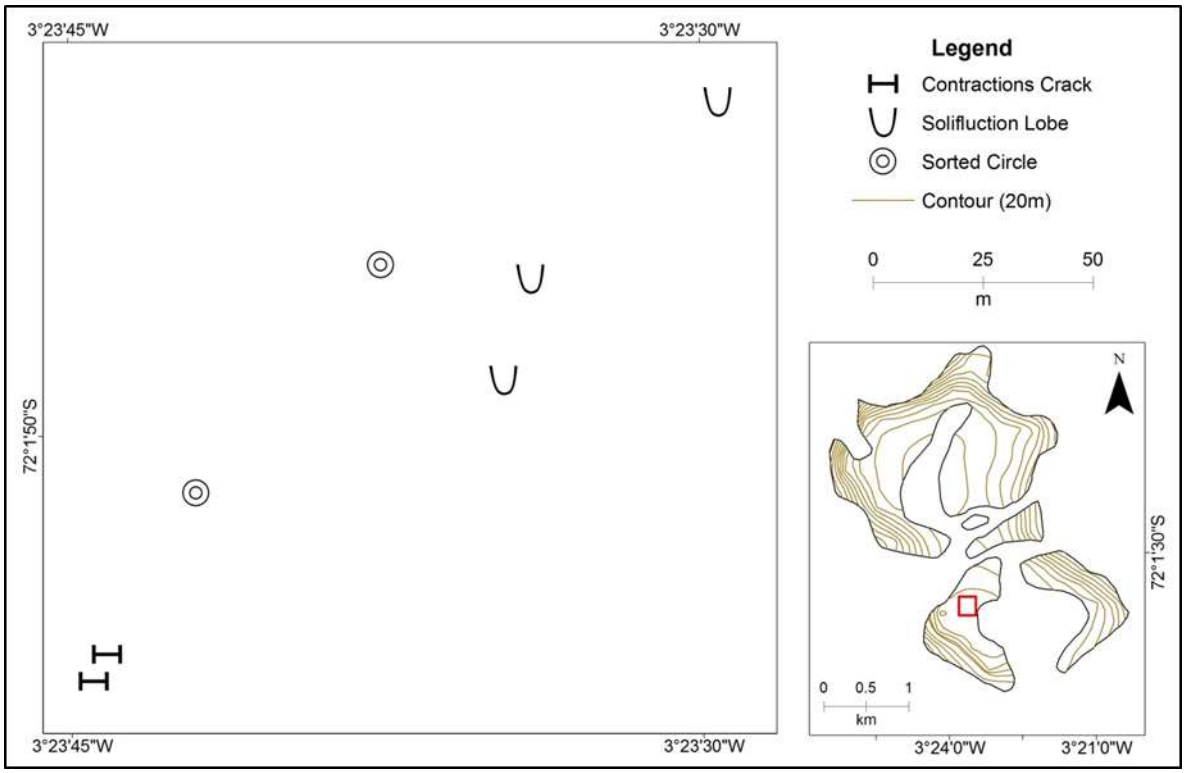

Figure 64: Flarjuven landforms 5.

4.4.3. Robertskollen

Similarly to Flårjuven, sorted circles (n=4) were also found in the vicinity of the logger. Although not shown in Figure 65, the logger itself is situated within the centre of a sorted circle. Other landforms found at Robertskollen include contraction cracks (n=3), stripes (n=1), and mudboils (n=1), the latter of which were located at the base of boulders with an abundance of snow present (Figure 66).

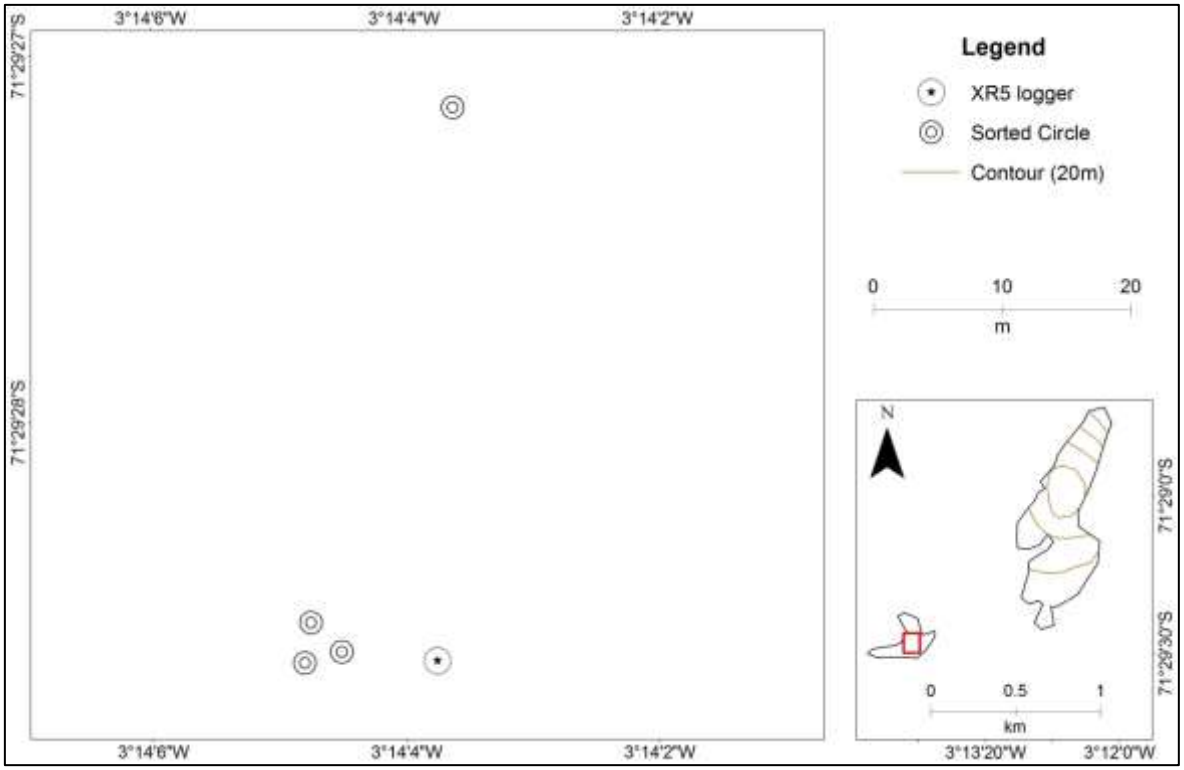

Figure 65: Robertskollen landforms 1.

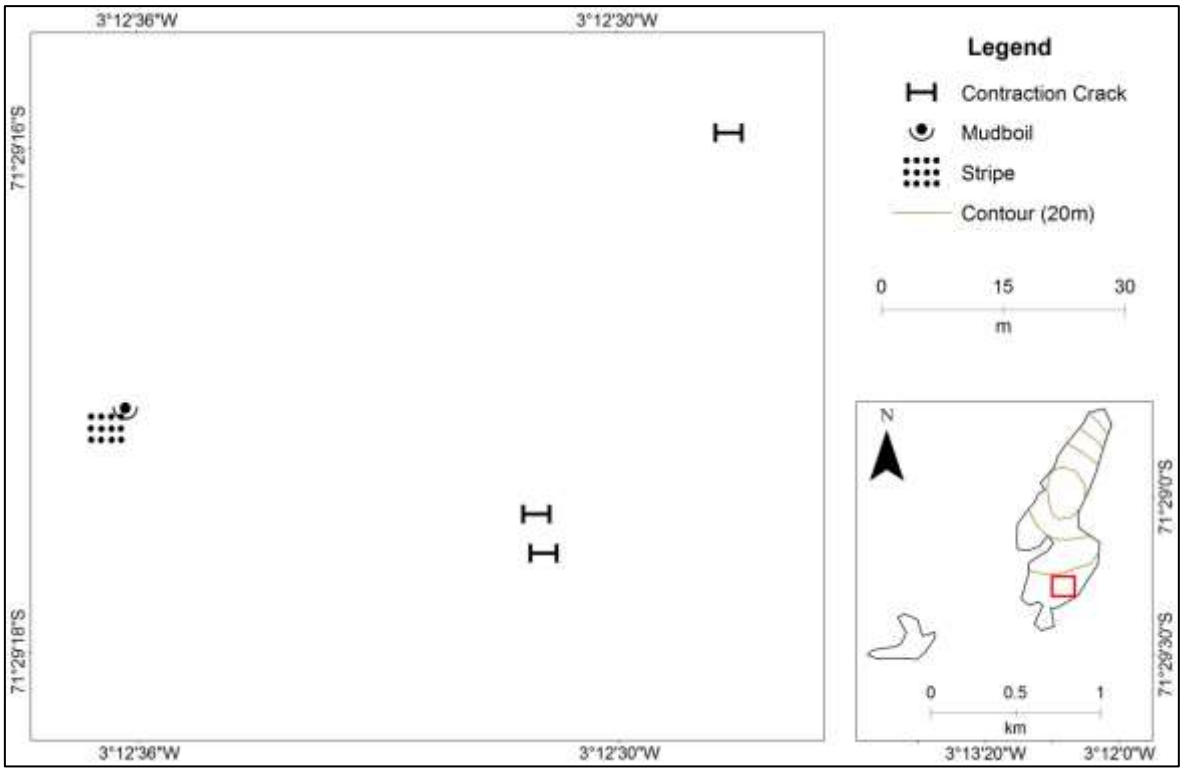

Figure 66: Robertskollen landforms 2.

4.4.4. Jutulsessen

Rock glaciers (Figure 67), polygons (Figure 68 & Figure 69) and terraces (Figure 70) have been identified in the Jutulsessen, Antarctica. Rudolph (2015) has identified and characterised five rock glaciers in the Jutulsessen, which are depicted in Figure 67 below. It remains uncertain as to whether these rock glaciers are active, dormant or relict. Nonetheless, they are characteristic features of a periglacial environment as majority of rock glaciers cited in literature are underlain by permafrost (French, 2007). Another characteristic feature of permafrost driven landscapes are polygons which are found in abundance in the Jutulsessen, and have even been observed on the lower reaches of Grjotyøra and Vassdalen rock glaciers. Hansen *et al*. (2014) conducted an investigation into the morphology and dynamics of polygons at Mimelia in the Jutulsessen (Figure 69) and found that they have an average diameter of 12m, vary greatly in size, and occur on slopes ranging from 8°- 27°. Trenches dug into the well-developed troughs of the polygons revealed that they are of the sand wedge variety. This was also found for other sites (i.e. Nonshøgda; pers.obs). Additionally, secondary cracking on the surface of primary polygons observed on the Mimelia polygons (Hansen *et al*., 2014) were also observed for other polygon fields in the Jutulsessen (pers.obs). Overall, polygon development was attributed to thermal contraction and analysis of shape indicated that the polygon field may be approaching maturity (Hansen *et al*., 2014). Conversely, it may be the opposite as secondary processes acting on the polygon field may indicate that the polygons are well past maturity as revealed by Bockheim *et al* (2009).

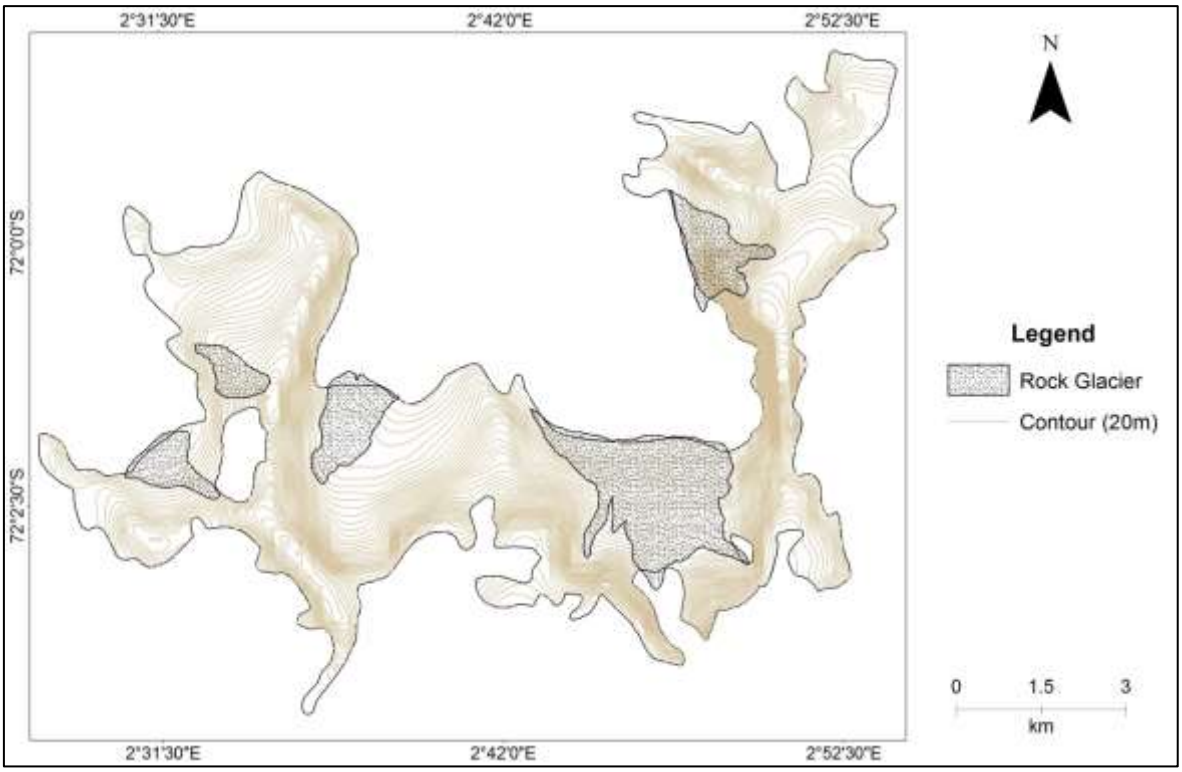

Figure 67: Rock glaciers in the Jutulsessen (adapted from Rudolph, 2015).

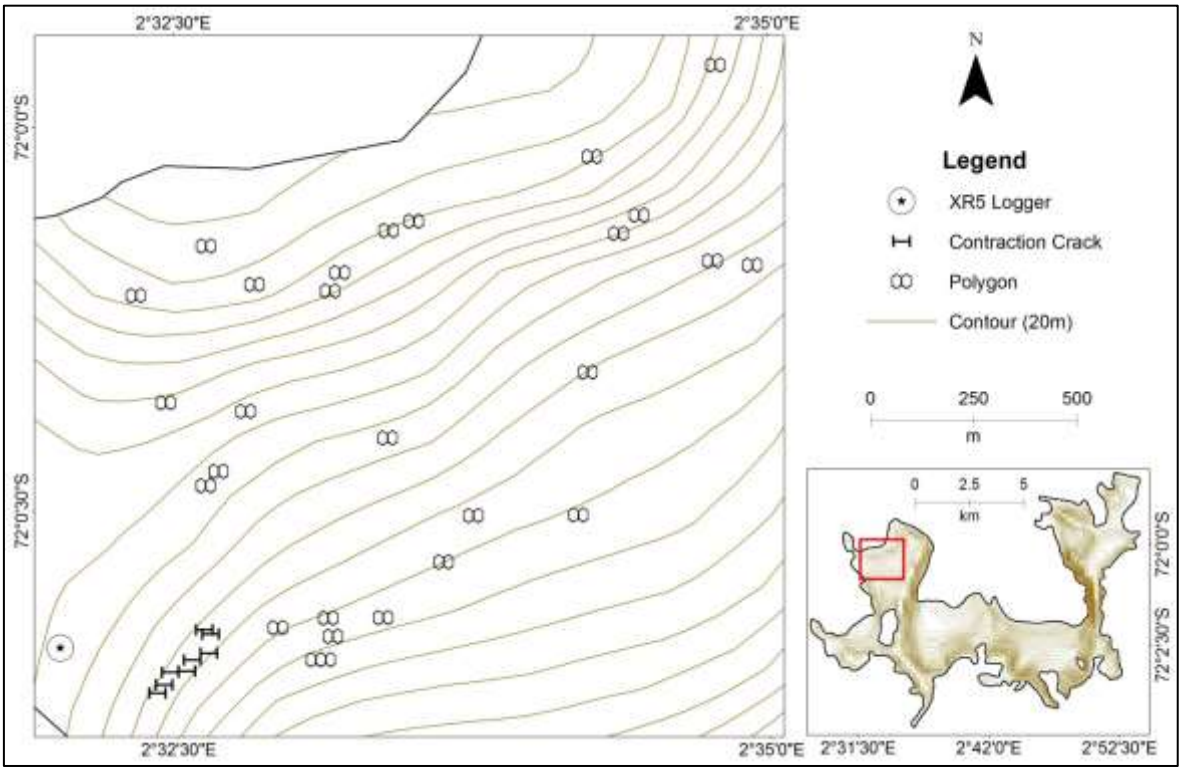

Figure 68: Polygons at Nonshøgda in the Jutulsessen.

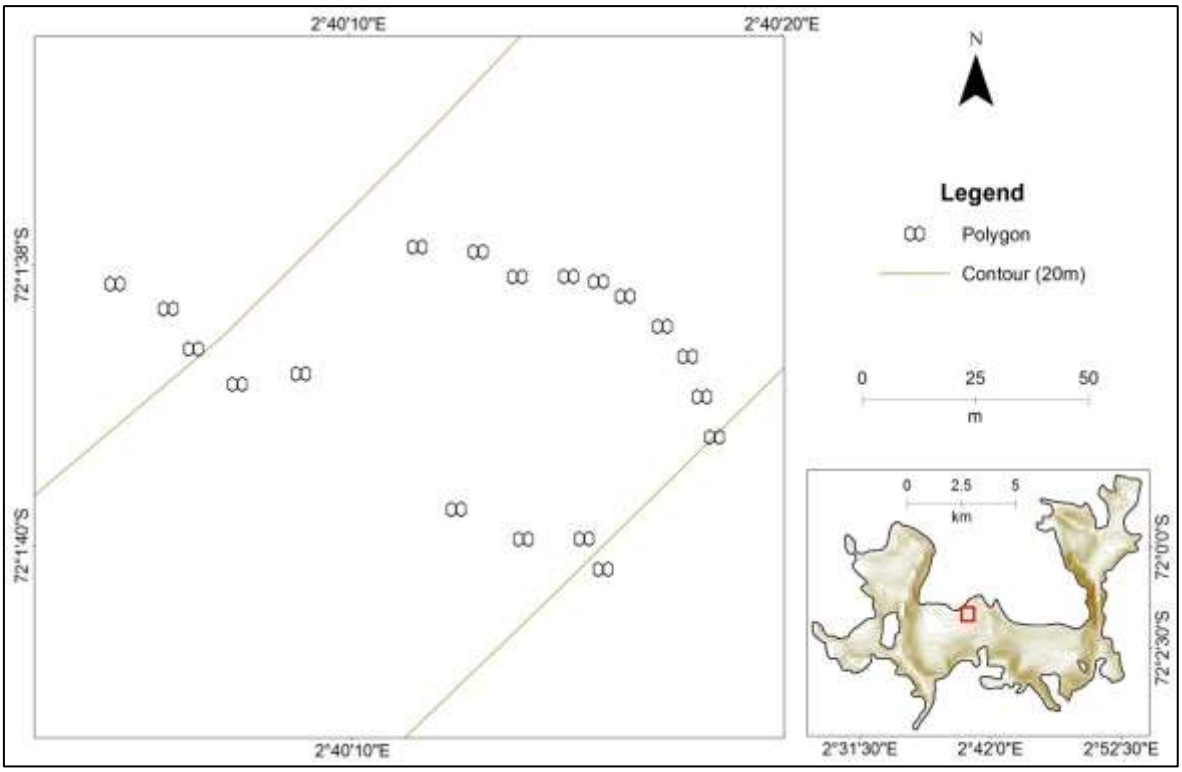

Figure 69: Polygons at Mimelia in the Jutulsessen.

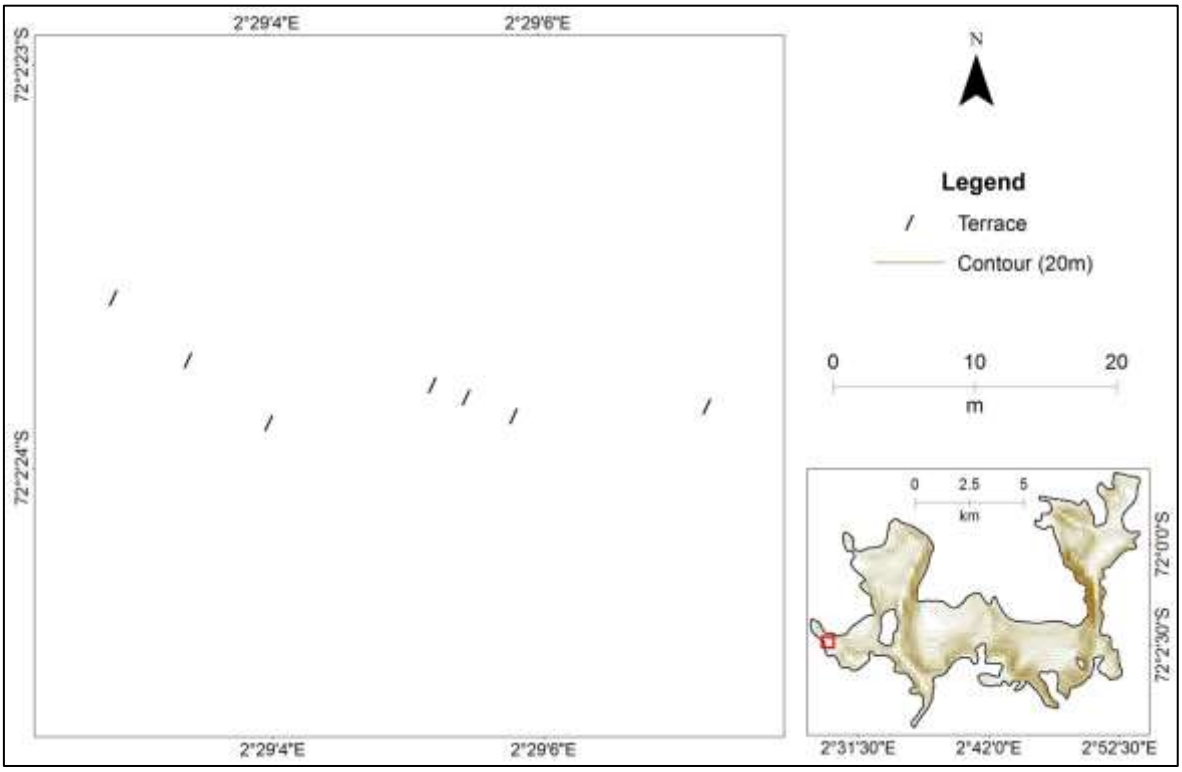

Figure 70: Terraces at Klovningen in the Jutulsessen.

CHAPTER 5: Synthesis, Conclusion and Recommendations

This dissertation is concluded with a synthesis of main results of the four objectives (listed under Aims and Objectives, pg.6), followed by project limitations. Lastly, recommendations and concluding remarks are provided.

5.1. Synthesis

Table 37: Synthesis of air temperature, sediment and active layer indices given in descending order (Black = Nonshøgda, Blue = Flårjuven, Green = Vesleskarvet, Red = Robertskollen).

Measurement	***Descending order***			
ALD (cm)	**58**	**24**	**18**	**16**
Alt. (masl)	**1283**	**1278**	**848**	**468**
Bulk Density (g/cm-3)	**2.04**	**1.97**	**1.83**	**1.69**
Distance to shelf (m)	**220**	**174**	**140**	**120**
Landforms types (n)	**7**	**4**	**4**	**1**
MAAT (°C)	**-13.79**	**-15.88**	**-17.7**	**-18.85**
nf (°C.day)	**1.01**	**0.98**	**0.96**	**0.94**
PFTE (n)	**67**	**61**	**36**	**36**
Phi Sorting (ϕ)	**3.3**	**2**	**1.5**	**1.5**
Porosity (St)	**0.36**	**0.31**	**0.26**	**0.23**
Range Air (°C)	**58.55**	**47.55**	**43.68**	**38.67**
Range NST (°C)	**59.12**	**52.02**	**48.87**	**42.3**
Surface Offest (°C)	**0.76**	**0.75**	**0.38**	**-0.28**
Std.dev. Air (*s*)	**5.39**	**4.06**	**3.93**	**3.63**
Thaw hours (n)	**1165**	**364**	**236**	**237**
TSI (°C.day)	**2750**	**1998**	**1930**	**1165**
VWC (cm3/cm3)	**0.15**	**0.06**	**0.03**	**0**

Nonshøgda is characterised by the highest altitude and furthest distance from the coast. This is reflected by the highest range and standard deviation in air temperature as temperature extremes increase as distance from the coast increases (Table 37). The soils at Nonshøgda are the most poorly sorted of all the sites, and have the lowest VWC which is reflected by high bulk density and low porosity values. Nonshøgda has the least amount of PFTE, which is reflected by it having the least soil moisture in the near surface soil layer of all the sites, as well as a lack of active layer related landforms. Ultimately, the active layer at Nonshøgda is influenced mostly by radiation and a thin snow cover, which is supported by the SO, *nf* and low TSI. Consequently, it is also the site that has experienced the most warming in NST over the study period, potentially a consequence of increasing solar radiation. The results in Table 37 indicate that Nonshøgda is a more permafrost-dominated landscape, visualised through the abundance of PPG and rock glaciers.

The sand-wedge polygons characteristic of Nonshøgda is associated with cold air temperatures, strong winds, and an absence of moisture which permit the filling of fractures by wind-blown sediments. A thin snow cover, advocated by the SO and *nf* values, provides the ideal ratio between air temperature and ground temperature to facilitate cracking which have been shown to originate at the top of permafrost (French, 2007).

Flårjuven is the most similar to Nonshøgda, being the second highest and furthest from the coast, with the next highest standard deviation in air temperature (Table 37). It has the lowest MAAT which is a function of its altitude and topography. Contrary to Nonshøgda, it has the second highest amount of PFTE which is substantiated by it having the second highest soil moisture, amount of thaw hours and TSI which is reflected by the highest range in NS temperatures. These indices underpin the wide variety of landforms present at Flårjuven, which are also consistent with the highest porosity and lowest bulk density values of all the sites (Table 37). ^{137}Cs tracing has revealed landforms in WDML to be currently active, particularly those associated with cryoturbation which is favoured by soil moisture and a large number of freeze-thaw cycles, such as at Flårjuven and Robertskollen (Navas *et al*., 2005). Snow plays a large role on Flårjuven judging by the disparity between air and NST given by the *nf* and SO. However, air temperature and soil moisture inputs from the abundance of snow alter the thermal conductivity within the active layer, validating the active layer depth displayed at Flårjuven despite its high altitude (Adlam *et al*., 2010; Ikard *et al*., 2009).

Of all the sites, Robertskollen has the lowest altitude and is the closest to the Fimbul Ice shelf which is seen in the high MAAT, low air temperature range and standard deviation in air temperature (Table 37). Moreover, it also has the most PFTE of all the sites, underpinned by the highest thaw hours, deepest active layer and second highest TSI. In contradiction to this is the extremely low VWC measured in the near surface layer. Personal observations reveal Robertskollen to be one of the more moist sites, which is evidenced by the abundance of plant diversity and the presence of mudboils. Mudboils are associated with late summer when active layer thickness has reached maximum extent and saturation by thawing of the ice-rich layer (French, 2007). It is, therefore, hypothesized that the active layer at Robertskollen is governed by topography and heat transfer through sub-surface hydrology, explaining the deficit in soil moisture in the near surface layer which probably sublimates due to the higher MAAT (Conovitz *et al*., 2006; Adlam *et al*., 2010). The *nf* indicates that air and NST are very similar, whilst the SO shows that the GST is slightly higher than air temperature which could be attributed to the insulating properties snow (particularly during winter) (Table 37). The occurrence of late-lying snow patches create more favourable conditions for lichen, moss, and algae at Robertskollen (Guglielmin *et al*., 2012b), particularly in conjunction with warmer temperatures as validated by the thermal indices.

Similarly to Robertskollen, the lower altitude and closer distance to the coast exhibited by Vesleskarvet is seen by the second highest and second lowest MAAT and standard deviation in air temperature respectively. Conversely, Vesleskarvet reveals characteristics more in line with the higher altitude site of Nonshøgda, such as a similar active layer depth, amount of PFTE, and thaw hours. This is manifested through a high *nf* and a negative SO which shows that soil temperatures are colder than air temperature on an annual basis. Although this suggests the absence of an insulating snow cover, it is probably due to the ameliorating properties of the overlying block field which could be protecting the active layer from deepening in response to air temperatures, leading to a shallower active layer depth with less variation than the other sites. Although the presence of snow is not supported by the indices, it has been personally observed and is evidenced by the highest VWC of all the sites, which in turn is exhibited by an abundance of sorted circles. Statistical analysis revealed that the active layer at Vesleskarvet is governed by air temperature which was found to have the highest correlation, followed by incoming radiation and then pressure during summer. The seasonality of each parameter was reflected by the depth in the active layer with which they exhibited the strongest correlation. Moreover, a link between near surface temperatures and pressure has been identified, whereby the months of May and September show the most significant correlations. This has a considerable relevance to the Semi-Annual Oscillation which experiences a transitional period during these times, at the same time underpinning a potential underlying relationship between pressure, sea-ice extent and active layer dynamics in continental Antarctica.

5.2. Recommendations and Concluding Remarks

The data recorded in this study provide a foundation for active layer studies in WDML, Antarctica, forming part of a growing database with valuable site description metadata. However, the short record of data (maximum of eight years at Nonshøgda and minimum of two years at Robertskollen) prohibits long-term interpretation of trends. Further limitations are attributed to incomplete records as a result of equipment malfunction, particularly during the year 2013, giving inaccurate readings for air temperature at Flårjuven, air and near surface temperature data at Vesleskarvet, and data from the entire array for Nonshøgda from June to December. This had implications for data analysis as 2013 was identified as being an anomalously warm year as pointed out by recent literature. Therefore, to compensate for the failure rate of these loggers due to the harsh conditions experienced over the Antarctic winter, it is recommended that more loggers should be set up at each site. Not only will this act as a failsafe, but can also be used to interpolate the active layer regime experienced across an entire nunatak and the implications this could have on permafrost continuity and longevity over time due to climate change.

Also pertaining to the analysis of active layer dynamics, no records of snow depth or precipitation exist for WDML, Antarctica. The lack of which limits a more in depth characterisation of the active layer in this sparsely studied region. It is therefore recommended iButton temperature loggers be installed at fixed heights along the pole of the air temperature sensor in order to determine the evolution of snow cover during the winter (Lewkowicz, 2008). Wind speed and direction data is also required in the monitoring of the ground thermal regime as they have been found to influence ground temperatures substantially (Guglielmin *et al*., 2003; Adlam *et al*., 2010; Guglielmin *et al*., 2011). Although Meteonorm was used to obtain radiation data, the values are stochastically interpolated and are not a true reflection of the absolute incoming solar radiation values received at each logging site. Therefore, the implementation of a pyronometer is necessary to measure site-specific radiation for each borehole. Largely, it is worthwhile establishing a small-automated weather station at each permafrost borehole site. It is also recommended that all boreholes in WDML be standardised and extend to 2m in order to capture a complete depth profile of the active layer, particularly in the case of Robertskollen. It is pertinent to note, that at sites with such a high incidence of freeze thaw cycles as seen by the relatively warm climate of Robertskollen, that the issue of equipment heave is a reality. During the 2014/15 take-over, the soil moisture sensor at Robertskollen required readjustment. Therefore, it is important to closely monitor the effects of heave during fieldwork seasons to ensure the loggers are logging at the correct depth.

On the same note, the placement of the soil moisture tines parallel to the near surface layer encourages displacement by freeze thaw activity. It is thus recommended that the sensors be inserted vertically according to Cobos and Chambers (2009) application note. A vertical insertion into the soil will also eliminate incorrect readings of the soil moisture sensor due to air gaps and pooling of moisture. Variability brought about by temperature fluctuation, particularly due to the shallow burial of the EC-5 soil moisture sensor, can be rectified with the use of a multiplier for temperature at the probe surface (Campbell, 2006). It is also advised to install soil moisture sensors in an array along the entire soil profile from the surface to the top of the permafrost (TTOP), in order to determine the rate at which available thermal energy is transferred between soil layers which in turn regulates the soil temperature regime and depth of thaw (Ikard *et al*., 2009). Additionally, Seybold *et al*. (2010) found the largest water contents near the ice-cemented permafrost which could be a reality for the study sites. Overall defining the non-linear interaction between temperature and soil moisture availability in WDML, as well as the whole of the continent, will further elucidate the impacts of climate change (Ikard *et al.*, 2009).

In terms of ^{137}Cs analysis, the dataset chosen was not large enough to provide a complete representation of ^{137}Cs distribution or concentrations across landform features. Therefore, a larger sample number is required in order to substantiate conclusions. Additionally, the sampling strategy

of ^{137}Cs needs to be improved, particularly for Antarctic mineral soils which were found to be very dry. A core rather than surficial samples are required, particularly for cryoturbation processes such as the methods used by Jelinski (2013).

Although the landform maps created in line with objective four were useful in showing the spatial distribution of active layer related processes, more in depth geomorphological mapping of nunataks in WDML are required. Points showing the position of a feature on a nunatak require expansion through the use of a DGPS, which would increase positional accuracy and allow for the creation of DEMs etc. The landform database requires augmentation through a detailed fieldwork analysis if landforms, including the documentation of orientation, dip, aspect and dimensions. Furthermore, the use of unmanned aerial vehicles (UAV) is recommended as a tool to remedy the lack of fine scale resolution imagery available in WDML for the large-scale mapping of small landforms such as patterned ground. Scott (2014) promoted the use of UAVs to take aerial photographs of the landscape which can subsequently be used in creating 3D models and ultra-high resolution geomorphological maps, as well as conducting post fieldwork landscape feature analysis.

Despite the few limitations and recommendations listed above, this study has contributed to answering question 42 posed by the SCAR Horizon Scan in Kennicutt *et al*. (2014b). This was done by exploring the dynamics of permafrost, the active layer and water availability in WDML soils over six consecutive summers (starting 2007/08 and ending 2013/14), providing a foundation for future research. Aside from Nonshøgda, no trend of increasing active layer depth was apparent. Although altitude influenced MAAT, active layer depth failed to show clear altitudinal gradients. This could be due to other influencing factors such as the presence of block deposits, differing topography, sediment characteristics, snow cover depth and moisture availability. Soil moisture values confirmed the presence of dry permafrost in WDML with inherently low GMC values.

The aforementioned factors substantiate the main findings of a variable active layer depth, whereby inter annual variability was expressed in both the timing and depth of maximum thaw, which was further facilitated by between-summer variability in mean summer air temperatures. Moreover, all sites shared similarities in experiencing minima and maxima in active layer depths, such as the anomalously warm summer of 2012/13. Climate parameters including temperature, pressure and radiation were found to influence the active layer at different depths, further elucidating the roles of teleconnections on ground thermal regimes such as the SAO and SAM. This reveals the dynamic coupling between the ground and atmosphere, particularly the role that synoptic events play in yielding geomorphic responses through the ground which are quantifiable through freeze-thaw events and subsequently periglacial landforms. Overall, the ground-atmosphere link requires further investigation, which, by extension will aid in the elucidation of potential impacts of climate change on ecosystems and biochemical cycles.

CHAPTER 6: Reference List

Adlam, L.S., Balks, M.R., Seybold, C.A. and Campbell, D.I. 2010. Temporal and spatial variation in active layer depth in the McMurdo Sound Region, Antarctica. *Antarctic Science*, 22: 45-52.

Almeida, I.C.C., Schaefer, C.E.G.R., Fernandes, R.B.A., Pereira, T.T.C., Nieuwendam, A. and Pereira, A.B. 2014. Active layer thermal regime at different vegetation covers at Lions Rump, King George Island, maritime Antarctica. *Geomorphology*, 225: 36–46.

Anisimov, O., Fitzharris, B., Hagen, J.O., Jeffries, R., Marchant, H., Nelson, F.E., Prowse, T. and Vaughan, D.G. 2001. Polar regions (Arctic and Antarctic). *In Climate change: Impacts, adaptation, and vulnerability, the Contribution of Working Group II of the Intergovernmental Panel on Climate Change, Third Assessment Review*. Cambridge: Cambridge University Press. p. 801–841.

Ashman, M.R. and Puri, G. 2002. *Essential soil science: A clear and concise introduction to soil science*. Oxford: Blackwell Publishing.

Atkinson, P.M., German, S.E., Sear, D.A. and Clark, M.A. 2003. Exploring the relations between riverbank erosion and geomorphological controls using geographically weighted logistic regression. *Geographical Analysis*, 35: 58-82.

ATS. 1959. *The Antarctic Treaty*. Washington, D.C.: Secretariat of the Antarctic Treaty, December 1 1959.

Ball, B.A., Barrett, J.E., Gooseff, M.N., Virginia, R.A. and Wall, D.H. 2011. Implications of meltwater pulse events for soil biology and biogeochemical cycling in a polar desert. *Polar Research*, 30: 1–10

Bandoro, J., Solomon, S., Donohoe, A., Thompson, D.W.J. and Santer, B.D. 2014. Influences of the Antarctic ozone hole on southern hemispheric summer climate change. *Journal of Climate*, 27: 6245–6264.

Bargagli, R. 2005. *Antarctic ecosystems: Environmental contamination, climate change, and human impact*. Berlin: Springer-Verlag.

Barry, R.G. and Yew Gan, T. 2011. *The global cryosphere: Past, present, and future*. Cambridge: Cambridge University Press.

Barsch, D. 1993. Periglacial geomorphology in the 21st century. *Geomorphology*, 7: 141–163.

Berthling, I., Schomacker, A. and Benediktsson, Í.Ö. 2013. The glacial and periglacial research frontier: Where from here? *In* Giardino, R. and Harbor, J. (eds.). *Treatise on Geomorphology*. London: Elsevier Inc. p. 479-498.

Black, R. 1976. Periglacial features indicative of permafrost : Ice and soil wedges. *Quaternary Research*, 6: 3–26.

Block, W. 1994. Terrestrial ecosystems : Antarctica. *Polar Biology*, 14: 293–300.

Blott, S.J. and Pye, K. 2006. Particle size distribution analysis of sand-sized particles by laser diffraction: An experimental investigation of instrument sensitivity and the effects of particle shape. *Sedimentology*, 53: 671–685.

Bluman, A.G. 2009. *Elementary statistics: A step by step approach* (7ed.). New York: McGraw-Hill.

Bockheim, J.G. 1995. Permafrost distribution in the southern circumpolar region and its relation to the environment: A review and recommendations for further research. *Permafrost and Periglacial Processes*, 6: 27–45.

Bockheim, J.G. 2002. Landform and soil development in the McMurdo Dry Valleys, Antarctica: A regional synthesis. Arctic, *Antarctic and Alpine Research*, 34: 308–317.

Bockheim, J.G. 2007. Importance of cryoturbation in redistributing organic carbon in permafrost-affected soils. *Soil Science Society of America Journal*, 71: 1335-1342.

Bockheim, J.G. 2014. Distribution, properties and origin of viscous-flow features in the McMurdo Dry Valleys, Antarctica. *Geomorphology*, 204: 114–122.

Bockheim, J.G. and Hall, K.J. 2002. Permafrost, active-layer dynamics and periglacial environments of continental Antarctica. *South African Journal of Science*, 98: 82–90.

Bockheim, J.G. and Tarnocai, C. 1998a. Nature, occurrence and origin of dry permafrost. *In Proceedings of the 7th International Conference on Permafrost*. Yellowknife, Northwest Territories, Canada, June 23-27, 1998. p. 57-64.

Bockheim, J.G. and Tarnocai, C. 1998b. Recognition of cryoturbation for classifying permafrost-affected soils. *Geoderma*, 81: 281–293.

Bockheim, J.G., Campbell, I.B. and McLeod, M. 2007. Permafrost distribution and active-layer depths in the McMurdo Dry Valleys, Antarctica. *Permafrost and Periglacial Processes*, 18: 217–227.

Bockheim, J.G., Kurz, M.D., Soule, S.A. and Burke, A. 2009. Genesis of active sand-filled polygons in lower and central Beacon. *Permafrost and Periglacial Processes*, 20: 295–308.

Bockheim, J.G., Vieira, G., Ramos, M., López-Martínez, J., Serrano, E., Guglielmin, M., Wilhelm, K. and Nieuwendam, A. 2013. Climate warming and permafrost dynamics in the Antarctic Peninsula region. *Global and Planetary Change*, 100: 215–223.

Boelhouwers, J.C. and Hall, K. 2002. Periglacial and permafrost research in the southern hemisphere. *South African Journal of Science*, 98: 46.

Bogena, H.R., Huisman, J.A., Oberdörster, C. and Vereecken, H. 2007. Evaluation of a low-cost soil water content sensor for wireless network applications. *Journal of Hydrology*, 344: 32–42.

Bothale, R.V., Rao, P.V.N., Dutt, C.B.S. and Dadhwal, V.K. 2014. Dynamics of surface melting over Amery and Ross ice shelf in Antarctic using OSCAT Data. *In Proceedings of the ISPRS Technical Commission VIII Symposium*. Hyderabad, India, December 9-12, 2014. p. 505–509.

Bridgman, H.A. and Oliver, J.E. 2006. *The global climate system: Patterns, processes, and teleconnections*. New York: Cambridge University Press.

Briggs, D. J. 1977a. *Sources and methods in geography – Sediments*. London: Butterworths & Co. Ltd.

Briggs, D. J. 1977b. *Sources and methods in geography – Soils*. London: Butterworths & Co. Ltd.

Burn, C.R. 1998. The active-layer: Two contrasting definitions. *Permafrost and Periglacial Processes,* 9: 411-416.

Campbell, C.S. 2006. Response of the ECH_2O soil moisture sensors to temperature variation. Application Note, *Decagon Devices Inc*., Pullman, Wash. p. 1-5.

Campbell, C.S. 2009. Frequently asked questions about soil moisture sensors. Application note, *Decagon Devices, Inc*., Pullman, Wash. p. 1- 4.

Campbell, I.B. and Claridge, G.G.C. 2006. Permafrost properties, patterns and processes in the Transantarctic mountains region. *Permafrost and Periglacial Processes*, 17: 215–232.

Cannone, N. and Guglielmin, M. 2009. Influence of vegetation on the ground thermal regime in continental Antarctica. *Geoderma,* 151: 215–223.

Cannone, N. and Guglielmin, M. 2010. Relationships between periglacial features and vegetation development in Victoria Land, continental Antarctica. *Antarctic Science*, 22: 703–713.

Cannone, N., Ellis Evans, J.C., Strachan, R. and Guglielmin, M. 2006. Interactions between climate, vegetation and the active layer in soils at two maritime Antarctic sites. *Antarctic Science*, 18: 323–333.

Cannone, N., Wagner, D., Hubberten, H.W. and Guglielmin, M. 2008. Biotic and abiotic factors influencing soil properties across a latitudinal gradient in Victoria Land, Antarctica. *Geoderma*, 144: 50–65.

Carleton, A.M. 2003. Atmospheric teleconnections involving the southern ocean. *Journal of Geophysical Research*, 108: 1–15.

Carter, M.R. and Gregorich, E.G. 2006. *Soil sampling and methods of analysis* (2ed.). New York: Taylor and Francis Group.

Cassano, J.J. 2013. Climate of extremes. *In* Walton, D.W.H. (ed.). *Global science from a frozen continent*. New York: Cambridge University Press. p. 102-136.

Chang, M., Jamieson, S.S.R., Bentley, M.J. and Stokes, C.R. 2015. The surficial and subglacial geomorphology of Western Dronning Maud Land, Antarctica. *Journal of Maps*. 1–12.

Chesworth, W. 2008. *Encyclopaedia of soil science*. New York: Springer.

Chown, S.L., Clarke, A., Fraser, C.I., Cary, S.C., Moon, K.L. and McGeoch, M.A. 2015. The changing form of Antarctic biodiversity. *Nature*, 522: 431–438.

Christiansen, H.H., Etzelmüller, B., Isaksen, K., Juliussen, H., Farbrot, H., Humlum, O., Johansson, M., Ingeman-Nielsen, T., Kristensen, L., Hjort, J., Holmlund, P., Sannel, A.B.K., Sigsgaard, C., Åkerman, H.J., Foged, N., Blikra, L.H., Pernosky, M.A. and Ødegård, R.S. 2010. The thermal state of permafrost in the Nordic area during the International Polar Year 2007-2009. *Permafrost and Periglacial Processes*, 21: 156–181.

Christopherson, R.W. 2009. *Geosystems: An introduction into physical geography* (7ed.). USA: Pearson Education, Inc.

Church, M. 2010. The trajectory of geomorphology. *Progress in physical geography*, 34: 265–286.

Church, M. 2013. Refocusing geomorphology: Field work in four acts. *Geomorphology*, 200: 184–192.

Claridge, G.G.C., Campbell, I.B. and Balks, M.R. 1999. Movement of salts in Antarctic soils : Experiments using lithium chloride. *Permafrost and Periglacial Processes*, 10: 223–233.

Cobos, D. and Chambers, C. 2009. Calibrating ECH_2O soil moisture sensors. Application note, *Decagon Devices, Inc*., Pullman, Wash. p. 1-4.

Collins, A.L. Walling, D.E. and Leeks, G.J.L. 1997. Source type ascription for fluvial suspended sediment based on a quantitative composite fingerprinting technique. *Catena*, 29 (1): 1-27.

Conovitz, P.A., MacDonald, L.H. and McKnight, D.M. 2006. Spatial and temporal active layer dynamics along three glacial meltwater streams in the McMurdo Dry Valleys, Antarctica. *Arctic, Antarctic and Alpine Research*, 38: 42–53.

Convey, P., Brandt, A. and Nicol, S. 2013. Life in a cold environment. *In* Walton, D.W.H. (ed.). *Global science from a frozen continent*. New York: Cambridge University Press. p.161-210.

Dallmann, W.K., Austrheim, H., Bucher-nurminen, K. and Ohta, Y. 1990. *Geology around the Norwegian Antarctic station "Troll", Jutulsessen, Dronning Maud Land*. Oslo: Norsk Polarinstitutt. p. 1-37.

Das, B. 2002. *Soil mechanics laboratory manual* (6ed.). New York: Oxford University Press.

de Pablo, M.A., Blanco, J.J., Molina, A., Ramos, M., Quesada, A. and Vieira, G. 2013. Interannual active layer variability at the Limnopolar Lake CALM site on Byers Peninsula, Livingston Island, Antarctica. *Antarctic Science*, 25: 167–180.

Diniz-Filho, J.A.F., Bini, L.M. and Hawkins, B.A. 2003. Spatial autocorrelation and red herrings in geographical ecology. *Global Ecology and Biogeography*, 12: 53 – 64.

Di Stefano, C. Ferro, V. and Mirabile, S. 2010. Comparison between grain-size analyses using laser diffraction and sedimentation methods. *Biosystems Engineering*, 106 (2): 205-215.

Dwight, R.A. 2014. *Geomorphic and ambient environmental impacts on lichen distribution on two inland nunataks in Western Dronning Maud Land, Antarctica*. MSc Dissertation. Grahamstown: Rhodes University.

Farbrot, H., Hipp, T.F., Etzelmüller, B., Isaksen, K., Ødegård, R.S., Schuler, T.V. and Humlum, O. 2011. Air and ground temperature variations observed along elevation and continentality gradients in southern Norway. *Permafrost and Periglacial Processes*, 22: 343–360.

Farbrot, H., Isaksen, K., Etzelmüller, B. and Gisnås, K. 2013. Ground thermal regime and permafrost distribution under a changing climate in northern Norway. *Permafrost and Periglacial Processes*, 24: 20–38.

Feuillet, T., Mercier, D., Decaulne, A. and Cossart, E. 2012. Classification of sorted patterned ground areas based on their environmental characteristics (Skagafjörður, Northern Iceland). *Geomorphology*, 139-140: 577-587

Fogt, R.L. and Bromwich, D.H. 2006. Decadal variability of the ENSO teleconnection to the high-latitude South Pacific Governed by coupling with the Southern Annular Mode*. *Journal of Climate*, 19: 979–998.

Foster, I.D.L., Boardman, J. and Keay-Bright, J. 2007. Sediment tracing and environmental history for two small catchments, Karoo Uplands, South Africa. *Geomorphology*, 90: 126–143.

Francesca, V., Osvaldo, F., Stefano, P. and Paola, R.P. 2010. Soil moisture measurements: A comparison of instrumentation performances. *Journal of Irrigation and Drainage Engineering*, 136: 81–89.

French, H. 2007. *The periglacial environment* (3ed.). Sussex, England: John Wiley & Sons Ltd.

French, H. and Guglielmin, M. 2000. Frozen ground phenomena in the vicinity of Terra Nova Bay. Northern Victoria Land, Antarctica: A preliminary report. *Geografiska Annaler, Series A*, 82: 513–526.

French, H. and Thorn, C.E. 2006. The changing nature of periglacial geomorphology. *Géomorphologie: relief, processus, environnement*, 3: 165–173.

French, W.J.R. and Burns, G.B. 2004. The influence of large-scale oscillations on long-term trend assessment in hydroxyl temperatures over Davis, Antarctica. *Journal of Atmospheric and Solar-Terrestrial Physics*, 66: 493–506.

Gaspar, L., Navas, A., Walling, D.E., Machín, J. and Gómez Arozamena, J. 2013. Using ^{137}Cs and $^{210}Pb_{ex}$ to assess soil redistribution on slopes at different temporal scales. *Catena*, 102: 46–54.

Gilmore, G.R. 2008. *Practical gamma-ray spectrometry* (2ed.). West Sussex, England: John Wiley & Sons Ltd.

Godfrey, M.J., Bannister, M.T., Nobes, D.C. and Sletten, R.S. 2008. 3D time-lapse imaging of polygonal patterned ground in the McMurdo Dry Valleys of Antarctica. *In Proceedings of the 12th International Conference on Ground Penetrating Radar*. Birmingham, UK, June 16-19, 2008.

Gong, D. and Wang, S. 1999. Definition of Antarctic Oscillation index. *Geophysical Research Letters*, 26: 459–462.

Gray, A.B. Pasternack, G.B. and Watson, E.B. 2010. Hydrogen peroxide treatment effects on the particle size distribution of alluvial and marsh sediments. *The Holocene*, 20 (2): 293-301.

Grosch, E.G., Bisnath, A., Frimmel, H.E. and Board, W.S. 2007. Geochemistry and tectonic setting of mafic rocks in Western Dronning Maud Land, East Antarctica: Implications for the geodynamic evolution of the proterozoic Maud Belt. *Journal of the Geological Society, London*. 164: 465-475.

Guglielmin, M. 2004. Observations on permafrost ground thermal regimes from Antarctica and the Italian Alps, and their relevance to global climate change. *Global and Planetary Change*, 40: 159–167.

Guglielmin, M. 2006. Ground surface temperature (GST), active layer and permafrost monitoring in continental Antarctica. *Permafrost and Periglacial Processes*, 17: 133–143.

Guglielmin, M. 2012. Advances in permafrost and periglacial research in Antarctica: A review. *Geomorphology*, 155-156: 1–6.

Guglielmin, M. and Cannone, N. 2012. A permafrost warming in a cooling Antarctica? *Climatic Change*, 111: 177–195.

Guglielmin, M. and Vieira, G. 2014. Permafrost and periglacial research in Antarctica: New results and perspectives. *Geomorphology*, 225: 1–3.

Guglielmin, M., Balks, M.R., Adlam, L.S. and Baio, F. 2011. Permafrost thermal regime from two 30-m deep boreholes in Southern Victoria Land, Antarctica. *Permafrost and Periglacial Processes*, 22: 129–139.

Guglielmin, M., Balks, M. and Paetzold, R. 2003. Towards an Antarctic active layer and permafrost monitoring network. *In Proceedings of the 8th International Conference on Permafrost*. Zurich, Switzerland, July 21-25, 2003. p. 337-341.

Guglielmin, M., Dalle Fratte, M. and Cannone, N. 2014a. Permafrost warming and vegetation changes in continental Antarctica. *Environmental Research Letters*, 9: 1-14.

Guglielmin, M., Ellis Evans, C.J. and Cannone, N. 2008. Active layer thermal regime under different vegetation conditions in permafrost areas. A case study at Signy Island (Maritime Antarctica). *Geoderma*, 144: 73–85.

Guglielmin, M., Worland, M.R., Baio, F. and Convey, P. 2014b. Permafrost and snow monitoring at Rothera Point (Adelaide Island, Maritime Antarctica): Implications for rock weathering in cryotic conditions. *Geomorphology*, 225: 47–56.

Guglielmin, M., Worland, M.R. and Cannone, N. 2012. Spatial and temporal variability of ground surface temperature and active layer thickness at the margin of maritime Antarctica, Signy Island. *Geomorphology*, 155-156: 20–33.

Haeberli, W., Hallet, B., Arenson, L., Elconin, R., Humlum, O., Kaab, A., Kaufmann, V., Ladanyi, B., Matsuoka, N., Springman, S. and Vonder Muhll, D. 2006. Permafrost creep and rock glacier dynamics. *Permafrost and Periglacial Processes*, 17: 189–214.

Hall, K. 2013. Mechanical weathering in cold regions. *In* Giardino, R. and Harbor, J. (eds.). *Treatise on Geomorphology*. London: Elsevier Inc. p. 259-272.

Hallet, B., Sletten, R. and Whilden, K. 2011. Micro-relief development in polygonal patterned ground in the Dry Valleys of Antarctica. *Quaternary Research*, 75: 347–355.

Hansen, C.D. 2013. *The characterization of an openwork block deposit, Northern Buttress, Vesleskarvet, Dronning Maud Land, Antarctica*. MSc Dissertation. Grahamstown: Rhodes University.

Hansen, C.D., Meiklejohn, K.I., Nel, W., Loubser, M.J. and Van Der Merwe, B.J. 2013. Aspect-controlled weathering observed on a blockfield in Dronning Maud Land, Antarctica. *Geografiska Annaler, Series A*, 95(4): 305–313.

Hansen, G., Aspmo, K., Berg, T., Edvardsen, K., Fiebig, M., Kallenborn, R., Krognes, T., Lunder, C., Stebel, K., Schmidbauer, N., Solberg, S. and Yttri, K.E. 2009. Atmospheric monitoring at the Norwegian Antarctic Station Troll: Measurement programme and first results. *Polar Research*, 28: 353–363.

Harris, K.J., Carey, A.E., Lyons, W.B., Welch, K.A. and Fountain, A.G. 2007. Solute and isotope geochemistry of subsurface ice melt seeps in Taylor Valley, Antarctica. *Geological Society of America Bulletin*, 119: 548–555.

Harris, S.A. and Pedersen, D. 1998. Thermal regimes beneath coarse blocky materials. *Permafrost and Periglacial Processes*, 9: 107–120.

Hedding, D.W. 2006. *Geomorphology and geomorphological responses to climate change in the interior of sub-Antarctic Marion Island*. MSc Dissertation. Pretoria: University of Pretoria.

Hjort, J. and Luoto, M. 2009. Interaction of geomorphic and ecologic features across altitudinal zones in a subarctic landscape. *Geomorphology*, 112: 324–333.

Huggett, R.J. 2011. Fundamentals of Geomorphology (3ed.). USA: Routledge.

Hughes, P. 2013. Quaternary-pleistocene glacial and periglacial environments. *In* Giardino, R. and Harbor, J. (eds.). *Treatise on Geomorphology*. London: Elsevier Inc. p. 30–44.

Humlum, O. and Christiansen, H.H. 2008. Lowland periglacial research : A review of published advances 2003 – 2007. *Permafrost and Periglacial Processes*, 19: 211–235.

Ikard, S.J., Gooseff, M.N., Barrett, J.E. and Takacs-Vesbach, C. 2009. Thermal characterisation of active layer across a soil moisture gradient in the McMurdo Dry Valleys, Antarctica. *Permafrost and Periglacial Processes*, 20: 27–39.

IPA. 2012. Global terrestrial network on permafrost (GTN-P): Strategy and implementation plan 2012-2016.

Ishikawa, M. 2003. Thermal regimes at the snow–ground interface and their implications for permafrost investigation. *Geomorphology*, 52: 105–120.

Jelinski, N.A. 2013. Cryoturbation in the Central Brooks Range, Alaska. *Soil Horizons*, 54: 1–7.

Kachanoski, R. 1993. Estimating soil loss from changes in soil cesium-137. *Journal of Soil Science*, 73: 629–632.

Kärkäs, E. 2004. Meteorological conditions of the Basen Nunatak in Western Dronning Maud Land, Antarctica, during the Years 1989-2001. *Geophysica*, 40: 39–52.

Karunaratne, K.C. 2002. *N-Factors and the relationships between air and surface temperatures in discontinuous permafrost near Mayo, Yukon Territory*. Dissertation. Ontario: Carleton University.

Karunaratne, K.C. and Burn, C.R. 2004. Relations between air and surface temperature in discontinuous permafrost terrain near Mayo, Yukon Territory. *Canadian Journal of Earth Sciences*, 41: 1437–1451.

Kennedy, A.D. 1993. Water as a limiting factor in the Antarctic environment : a biogeographical synthesis. *Arctic and Alpine Research*, 25: 308–315.

Kennicutt, M.C., Chown, S.L., Cassano, J.J., Liggett, D., Massom, R., Peck, L.S., Rintoul, S.R., Storey, J.W.V., Vaughan, D.G., Wilson, T.J. and Sutherland, W.J. 2014a. Polar research: Six priorities for Antarctic Science. *Nature*, 512, 23-25.

Kennicutt, M.C., Chown, S.L., Cassano, J.J., Liggett, D., Peck, L.S., Massom, R., Rintoul, S.R., Storey, J., Vaughan, D.G., Wilson, T.J., Allison, I., Ayton, J., Badhe, R., Baeseman, J., Barrett, P.J., Bell, R.E., Bertler, N., Bo, S., Brandt, A., Bromwich, D., Cary, S.C., Clark, M.S., Convey, P., Costa, E.S., Cowan, D., Deconto, R., Dunbar, R., Elfring, C., Escutia, C., Francis, J., Fricker, H.A., Fukuchi, M., Gilbert, N., Gutt, J., Havermans, C., Hik, D., Hosie, G., Jones, C., Kim, Y.D., Le Maho, Y., Lee, S.H., Leppe, M., Leitchenkov, G., Li, X., Lipenkov, V., Lochte, K., López-Martínez, J., Lüdecke, C., Lyons, W., Marenssi, S., Miller, H., Morozova, P., Naish, T., Nayak, S., Ravindra, R., Retamales, J., Ricci, C.A., Rogan-Finnemore, M., Ropert-Coudert, Y., Samah, A.A., Sanson, L., Scambos, T., Schloss, I.R., Shiraishi, K., Siegert, M.J., SimÃes, J.C., Storey, B., Sparrow, M.D., Wall, D.H., Walsh, J.C., Wilson, G., Winther, J.G., Xavier, J.C., Yang, H. and Sutherland, W.J. 2014b. A roadmap for Antarctic and Southern Ocean Science for the next two decades and beyond. *Antarctic Science*, 27, 3-18.

Kessler, M.A. and Werner, B.T. 2003. Self-organization of sorted patterned ground. *Science*, 299: 380–383.

King, J. and Turner, J. 1997. *Antarctic meteorology and climatology*. New York: Cambridge University Press.

Klaminder, J., Yoo, K., Olid, C., Ramebäck, H. and Vesterlund, A. 2014. Using short-lived radionuclides to estimate rates of soil motion in frost boils. *Permafrost and Periglacial Processes*, 25: 184–193.

Klene, A.E., Nelson, F.E., Shiklomanov, N.I. and Hinkel, K.M. 2001. The N-Factor in natural landscapes: Variability of air and soil-surface temperatures, Kuparuk River Basin, Alaska, U.S.A. *Arctic, Antarctic and Alpine Research*, 33: 140–148.

Koiter, A.J. Owens, P.N. Petticrew, E.L. and Lobb, D.A. 2013. The behavioural characteristics of sediment properties and their implications for sediment fingerprinting as an approach for identifying sediment sources in river basins. *Earth-Science Reviews,* 125: 24-42.

Lacelle, D. and Vasil'chuk, Y.K. 2013. Recent progress (2007-2012) in permafrost isotope geochemistry. *Permafrost and Periglacial Processes*, 24: 138–145.

Lacelle, D., Lapalme, C., Davila, A.F., Pollard, W., Marinova, M., Heldmann, J. and McKay, C.P. 2015. Solar radiation and air and ground temperature relations in the cold and hyper-arid Quartermain Mountains, McMurdo Dry Valleys of Antarctica. *Permafrost and Periglacial Processes*. DOI: 10.1002/ppp.1859.

Lee, J.E., Le Roux, P.C., Meiklejohn, K.I. and Chown, S.L. 2013. Species distribution modelling in low-interaction environments: Insights from a terrestrial Antarctic system. *Austral Ecology*, 38: 279–288.

Levy, J.S., Head, J.W. and Marchant, D.R. 2008. The role of thermal contraction crack polygons in cold-desert fluvial systems. *Antarctic Science*, 20: 565–579.

Levy, J.S., Marchant, D.R. and Head, J.W.I. 2006. Distribution and origin of patterned ground on Mullins Valley debris-covered glacier, Antarctica: The Roles of Ice Flow and Sublimation. *Antarctic Science*, 18: 385–397.

Lewkowicz, A.G. 2008. Evaluation of miniature temperature-loggers to monitor snowpack evolution at mountain permafrost sites, Northwestern Canada. *Permafrost and Periglacial Processes*, 19: 323-331.

Ling, F. and Zhang, T. 2003. Impact of the timing and duration of seasonal snow cover on the active layer and permafrost in the Alaskan Arctic. *Permafrost and Periglacial Processes*, 14: 141–150.

Loveland, P.J. and Whalley, W.R. 2000. Particle size analysis. *In* Smith, K.A. and Mullins, C.E. (ed.). *Soil and environmental analysis*. (2ed.). USA: Marcel Dekker, Inc. p. 281 314.

Mabit, L., Benmansour, M. and Walling, D.E. 2008. Comparative advantages and limitations of the fallout radionuclides ^{137}Cs, ^{210}Pbex And ^{7}Be for assessing soil erosion and sedimentation. *Journal of Environmental Radioactivity*, 99: 1799–1807.

Marchenko, S. and Etzelmüller, B. 2013. Permafrost: Formation and distribution, thermal and mechanical properties. *In* Giardino, R. and Harbor, J (eds.). *Treatise on Geomorphology*. London: Elsevier Inc. p. 202-222.

Marmion, M., Hjort, J., Thuiller, W. and Luoto, M. 2008. A comparison of predictive methods in modelling the distribution of periglacial landforms in Finnish Lapland. *Earth Surface Processes and Landforms,* 33(14): 2241–2254.

Marshall, D.J., Crafford, J., Krynauw, J., Drummond, A. and Newton, I. 1995. The biology, physico-chemistry and geology of a nunatak pond at Valterkultun, Western Dronning Maud Land, Antarctica. *South African Journal of Antarctic Research*, 25: 9–16.

Marshall, G.J. 2007. Half-century seasonal relationships between the Southern Annular Mode and Antarctic temperatures. *International Journal of Climatology*, 27, 373–383.

Masson-Delmotte, V. 2013. Ice with everything. *In* Walton, D.W.H (ed.). *Global Science from a frozen continent*. New York: Cambridge University Press. p. 67-101.

Matsuoka, N. 2001. Solifluction rates, processes and landforms: A Global Review. *Earth-Science Reviews*, 55: 107–134.

McCraw, J.D. 1967. Some surface features of McMurdo Sound Region, Victoria Land, Antarctica. *New Zealand Journal of Geology and Geophysics*, 10: 394–417.

McLeod, M., Bockheim, J.G. and Balks, M.R. 2008. Glacial geomorphology, soil development and permafrost features in central-upper Wright Valley, Antarctica. *Geoderma*, 144: 93–103.

Meehl, G.A. 1991. A reexamination of the mechanism of the Semiannual Oscillation in the southern hemisphere*. *Journal of Climate*, 4: 911–926.

Meiklejohn, K.I. 2012. Initial environmental evaluation – Landscape processes in Antarctic ecosystems. Department of Environmental Affairs, South Africa.

Meiklejohn, K.I., Matcher, G., Dwight, R. and Scott, D. 2014. South African National Antarctic Programme takeover report: 2012/2013 annual relief voyage to SANAE IV.

Michel, R.F.M., Schaefer, C.E.G.R., Poelking, E.L., Simas, F.N.B., Fernandes Filho, E.I. and Bockheim, J.G. 2012. Active layer temperature in two cryosols from King George Island, Maritime Antarctica. *Geomorphology*, 155-156: 12–19.

Mikulecky, D.C. 2001. The emergence of complexity : science coming of age or science growing old ? *Computers and Chemistry*, 25: 341–348.

Millar, S. 2013. Mass movement processes in the periglacial environment. *In* Giardino, R. and Harbor, J. (eds.). *Treatise on Geomorphology*. London: Elsevier Inc. p. 374–391.

Miller, H.J. 2004. Tobler's first law and spatial analysis. *Annals of the Association of American Geographers*, 94(2): 284–289.

Muller, S.W. 1947. P*ermafrost or permanently frozen ground and related engineering problems*. Edwards, Ann Arbor, MI.

Murray, A.B., Lazarus, E., Ashton, A., Baas, A., Coco, G., Coulthard, T., Fonstad, M., Haff, P., McNamara, D., Paola, C., Pelletier, J. and Reinhardt, L. 2009. Geomorphology, complexity, and the emerging science of the Earth's surface. *Geomorphology*, 103: 496–505.

Navas, A., Soto, J. and López-Martínez, J. 2005. Radionuclides in soils of Byers Peninsula, South Shetland Islands, Western Antarctica. *Geoderma*, 62: 809–816.

Noone, D., Turner, J. and Mulvaney, R. 1999. Atmospheric signals and characteristics of accumulation in Dronning Maud Land, Antarctica. *Journal of Geophysical Research*, 104: 191–211.

Orheim, O. 2013. Managing the frozen commons. *In* Walton, D.W.H. (ed.). *Global science from a frozen continent*. New York: Cambridge University Press. p. 273-300.

Pavelsky, T.M., Boé, J., Hall, A. and Fetzer, E.J. 2011. Atmospheric inversion strength over polar oceans in winter regulated by sea ice. *Climate Dynamics*, 36: 945–955.

PermaNet, 2011. *Guidelines for monitoring GST – Ground surface temperature (v3)*. [Online]. Available: www.permanet-alpinespace.eu/archive/pdf/GST.pdf [20/02/2015].

Pulley, S.J. 2014. Exploring fine sediment dynamics and the uncertainties associated with sediment fingerprinting in the Nene River Basin, UK. PhD Dissertation. UK: University of Northampton.

Rafferty, J.P. 2011. *Glaciers, sea ice, and ice formation*. New York: Britannica Educational Publishing.

Ramos, M. and Vieira, G. 2003. Active layer and permafrost monitoring in Livingston Island, Antarctic. First results from 2000 to 2001. *In* Phillips, M., Springman, S.M., and Arenson, L. (eds.), *Proceedings of the 8th International Conference on Permafrost*. Zurich, Switzerland: Balkema Publishers. p. 929–933.

Ramos, M., Vieira, G., Blanco, J.J., Gruber, S., Hauck, C., Hidalgo, M.A. and Tomé, D. 2008. Active layer temperature monitoring in two boreholes in Livingston Island, maritime Antarctic: First results for 2000–2006. *In* Kane, D., Hinkel, K. (eds.), *Proceedings of the 9th International Conference on Permafrost.* Fairbanks, Alaska: University of Alaska Press. p. 1463–1467.

Ramos, M., Vieira, G., Gruber, S., Blanco, J.J., Hauck, C., Hidalgo, M.A., Tomé, D., Neves, M. and Trindade, A. 2007. Permafrost and active layer monitoring in the maritime Antarctic : Preliminary results from CALM sites on Livingston and Deception Islands. *In Proceedings of the 10th International Symposium on Antarctic Earth Sciences*. U.S. Geological Survey and The National Academies, USGS OF-2007-1047, Short Research Paper 070.

Reijmer, C.H. and van den Broeke, M.R. 2001. Moisture source of precipitation in Western Dronning Maud Land, Antarctica. *Antarctic Science*, 13: 210–220.

Remund, J., Müller, S., Kunz, S., Hugenin-Landl, B., Schmid, C. and Schilter, C. 2014. *Meteonorm Handbook Part I : Software*. Version 7. Switzerland: Meteotest. p. 1-58.

Ridefelt, H. and Boelhouwers, J. 2006. Observations on Regional variation in solifluction landform morphology and environment in the Abisko Region, Northern Sweden. *Permafrost and Periglacial Processes*, 17: 253–266.

Riseborough, D., Shiklomanov, N.I., Etzelmüller, B., Gruber, S. and Marchenko, S. 2008. Recent advances in permafrost modelling. *Permafrost and Periglacial Processes*, 19: 137–156.

Romanovsky, V.E., Drozdov, D.S., Oberman, N.G., Malkova, G.V., Kholodov, A.L., Marchenko, S.S., Moskalenko, N.G., Sergeev, D.O., Ukraintseva, N.G., Abramov, A.A., Gilichinsky, D.A. and Vasiliev, A.A. 2010a. Thermal state of permafrost in Russia. *Permafrost and Periglacial Processes*, 21: 136–155.

Romanovsky, V.E., Smith, S.L. and Christiansen, H.H. 2010b. Permafrost thermal state in the polar northern hemisphere during the International Polar Year 2007-2009: a Synthesis. *Permafrost and Periglacial Processes*, 21: 106–116.

Rosenbaum, U., Huisman, J.A., Weuthen, A., Vereecken, H. and Bogena, H.R. 2010. Sensor-to-sensor variability of the ECH2O EC-5, TE, and 5TE sensors in dielectric Liquids. *Vadose Zone Journal*, 9: 181-186.

Rudolph, E.M. 2015. *Surface characteristics of rock glaciers in the Jutulsessen, Dronning Maud Land, Antarctica*. MSc Dissertation. Grahamstown: Rhodes University.

Russell, A. and McGregor, G.R. 2010. Southern hemisphere atmospheric circulation: impacts on Antarctic climate and reconstructions from Antarctic ice core data. *Climatic Change*, 99: 155–192.

Ryan, P.G., Watkins, B., Smith, R., Dastyeh, H., Eicker, A., Foissner, W., Heafwole, H., Miller, W. and Thompson, G. 1989. Biological survey of Robertskollen, Western Dronning Maud Land: Area description and preliminary species lists. *South African Journal of Antarctic Research*, 19: 10–20.

SANAP. 2009. *South African National Antarctic Program (SANAP) safety manual for participants*. Pretoria: Department of Environmental Affairs.

Santamarina, J.C., Klein, K.A, Wang, Y.H. and Prencke, E. 2002. Specific surface: Determination and relevance. *Canadian Geotechnical Journal*, 39: 233–241

SASCAR. 1984. *South African Antarctic Earth Science Research Programme*. South African National Scientific Programmes Report, 81. Pretoria.

SCAR. 2010. [Online]. *Scientific Committee on Antarctic Research*. [Online]. Available: http://www.scar.org/about/. [9/03/2014].

Schneider, D.P., Steig, E.J. and Comiso, J.C. 2004. Recent climate variability in Antarctica from satellite-derived temperature data. *Journal of Climate*, 17: 1569–1583

Scott, D.A. 2014. *On active layer processes and landforms in Western Dronning Maud Land, Antarctica*. MSc Dissertation. Grahamstown: Rhodes University.

Selby, M.J. 1971. Some solifluction surfaces and terraces in the ice-free valleys of Victoria Land, Antarctica. *New Zealand Journal of Geology and Geophysics*, 14: 469–476.

Seybold, C. A., Balks, M.R. and Harms, D.S. 2010. Characterization of active layer water contents in the McMurdo Sound region, Antarctica. *Antarctic Science*, 22: 633–645.

Sexton, D.M.H. 2001. The effect of stratospheric ozone depletion on the phase of the Antarctic Oscillation. *Geophysical Research Letters*, 28: 3697–3700.

Shiklomanov, N.I., Nelson, F.E., Streletskiy, D.A., Hinkel, K.M. and Brown, J. 2008. The Circumpolar Active Layer Monitoring (CALM) Program: Data collection, management, and dissemination strategies. *In Proceedings of the 9th International Conference on Permafrost*. Fairbanks, Alaska, 29 June–3 July, 2008. p. 1–6.

Singh, V.P., Singh, P. and Haritashya, U.K. (eds.). 2011. *Encyclopaedia of snow, ice and glaciers*. Netherlands: Springer.

Sletten, R.S., Hallet, B. and Fletcher, R.C. 2003. Resurfacing time of terrestrial surfaces by the formation and maturation of polygonal patterned ground. *Journal of Geophysical Research*, 108: 1-10.

Smith, S.L., Romanovsky, V.E., Lewkowicz, A.G., Burn, C.R., Allard, M., Clow, G.D., Yoshikawa, K. and Throop, J. 2010. Thermal state of permafrost in North America: A contribution to the International Polar Year. *Permafrost and Periglacial Processes*, 21: 117–135.

Speden, I.G. 1960. Post-glacial terraces near Cape Chocolate, McMurdo Sound, Antarctica. *New Zealand Journal of Geology and Geophysics*, 3: 203–217.

Stammerjohn, S.E., Martinson, D.G., Smith, R.C., Yuan, X. and Rind, D. 2008. Trends in Antarctic annual sea ice retreat and advance and their relation to El Niño–Southern Oscillation and Southern Annular Mode variability. *Journal of Geophysical Research*, 113: 1–20.

Summerhayes, C.P. 2013. Scientists together in the cold. *In* Walton, D.W.H. (ed.). *Global science from a frozen continent*. New York: Cambridge University Press. p. 253-272.

Till, R. 1985. *Statistical methods for the earth scientist – an introduction.* London: MacMillian Education Ltd.

Trenberth, K.., Jones, P.D., Ambenje, P., Bojariu, R., Easterling, D., Tank, A.K., Parker, D., Rahimzadeh, F., Renwick, J.A., Rusticucci, M., Soden, B., Zhai, P. 2007. Observations: Surface and Atmospheric Climate. *In* Solomon, S., Qin, D., Manning, M., Chen, Z., Marquis, M., Averyt, K.., Tignor, M., Miller, H.L. (eds.). *Climate Change 2007: The Physical Science Basis. Contribution of the Working Group 1 to the Fourth Assessment Report of the Intergovernmental Panel on Climate Change*. Cambridge, United Kingdom and New York, USA: Cambridge University Press. p. 236-336.

Turner, J. 2004. The El Niño–Southern Oscillation and Antarctica. *International Journal of Climatology*, 24: 1–31.

Turner, J. and Marshall, G.J. 2011. *Climate change in the polar regions*. Cambridge: Cambridge University Press.

Turner, J. and Pendlebury, S. (eds.). 2004. *The international Antarctic weather forecasting handbook.* Cambridge: British Antarctic Survey.

Turner, J., Bindschadler, R.A., Convey, P., di Prisco, G., Fahrbach, E., Gutt, J., Hodgson, D.A., Mayewski, P.A. and Summerhayes, C.P. 2009. *Antarctic climate change and the environment*. Cambridge, UK: Scientific Committee for Antarctic Research. p. 1-526.

van den Broeke, M.R. 1998a. The Semi-Annual Oscillation and Antarctic climate. Part 1: Influence on near surface temperatures (1957–79). *Antarctic Science*, 10: 175–183.

van den Broeke, M.R. 1998b. The Semi-Annual Oscillation and Antarctic climate. Part 2 : Recent changes. *Antarctic Science*, 10: 184–191.

van den Broeke, M.R. 2000a. The Semi-Annual Oscillation and Antarctic climate. Part 3 : The role of near-surface wind speed and cloudiness. *International Journal of Climatology*, 20: 117–130.

van den Broeke, M.R. 2000b. The Semi-Annual Oscialltion and Antarctic climate. Part 4: A note on sea ice cover in the Amundsen and Bellingshausen Seas. *International Journal of Climatology*, 20: 455–462.

van den Broeke, M.R. 2000c. On the interpretation of Antarctic temperature trends. *Journal of Climate*, 13: 3885–3891.

van den Broeke, M.R. 2000d. The Semi-Annual Oscillation and Antarctic climate, Part 5: Impact on the annual temperature cycle as derived from NCEP/NCAR re-analysis. *Climate Dynamics*, 16:369-377

van den Broeke, M.R. and van Lipzig, N.P.M. 2003. Factors controlling the near-surface wind field in Antarctica*. *Monthly Weather Review*, 131: 733–743.

Vieira, G., Bockheim, J., Guglielmin, M., Balks, M., Abramov, A.A., Boelhouwers, J., Cannone, N., Ganzert, L., Gilichinsky, D.A., Goryachkin, S., López-Martínez, J., Meiklejohn, I., Raffi, R., Ramos, M., Schaefer, C., Serrano, E., Simas, F., Sletten, R. and Wagner, D. 2010. Thermal state of permafrost and active-layer monitoring in the Antarctic: Advances during the International Polar Year 2007-2009. *Permafrost and Periglacial Processes*, 21: 182–197.

Vieira, R., Hinata, S., da Rosa, K.K., Zilberstein, S. and Simoes, J.C. 2012. Periglacial features in Patriot Hills, Ellsworth Mountains, Antarctica. *Geomorphology*, 155-156: 96–101.

Walford, N. 2011. Practical statistics for Geographers and Earth Scientists. UK: John Wiley & Sons Ltd.

Wallbrink, P.J. Olley, J.M. and Roddy, B.P. (1997) *Quantifying the redistribution of soils and sediments within a post-harvested forest coupe near Bombala, New South Wales, Australia.* Technical Report 7/97.

Walton, D.W.H. 2013. *Antarctica: Global science from a frozen continent*. New York: Cambridge University Press.

Warburton, J. 2013. Patterned ground and polygons. *In* Giardino, R. and Harbor, J (eds.). *Treatise on Geomorphology*. London: Elsevier Inc. p. 298–312.

Weiss, N.A. 2012. Introductory statistics (9ed.). Boston, USA: Pearson Education Inc.

Wilhelm, K.R., Bockheim, J.G. and Kung, S. 2015. Active layer thickness prediction on the western Antarctic Peninsula. *Permafrost and Periglacial Processes*, 1845–1857.

Williams, M.W., Knauf, M., Cory, R., Caine, N. and Liu, F. 2007. Nitrate content and potential microbial signature of rock glacier outflow, Colorado Front Range. *Earth Surface Processes and Landforms*, 32(7): 1032-1047.

Williams, P.J. and Smith, M.W. 1989. *The frozen earth: Fundamentals of geocryology*. Cambridge: Cambridge University Press.

Wynn-Williams, D.D. 1990. Microbial colonization processes in Antarctic fellfield soils: An experimental overview. *Polar Biology*, 3: 164–178.

Yershov, E.D. 1998. *General geocryology*. Cambridge: Cambridge University Press.

Zhang, T., Frauenfeld, O.., Serreze, M.C., Etringer, A., Oelke, C., McCreight, J., Barry, R.G., Gilichinsky, D., Yang, D., Ye, H., Ling, F. and Chudinova, S. 2005. Spatial and temporal variability in active layer thickness over the Russian Arctic drainage basin. *Journal of Geophysical Research*, 110: 1–14.

Zhang, T., Osterkamp, T.E. and Stamnes, K. 1996. Influence of the depth hoar layer of the seasonal snow cover on the ground thermal regime. *Water Resources Research*, 32(7): 2075–2086.

APPENDIX A: Soil Moisture Calibrations

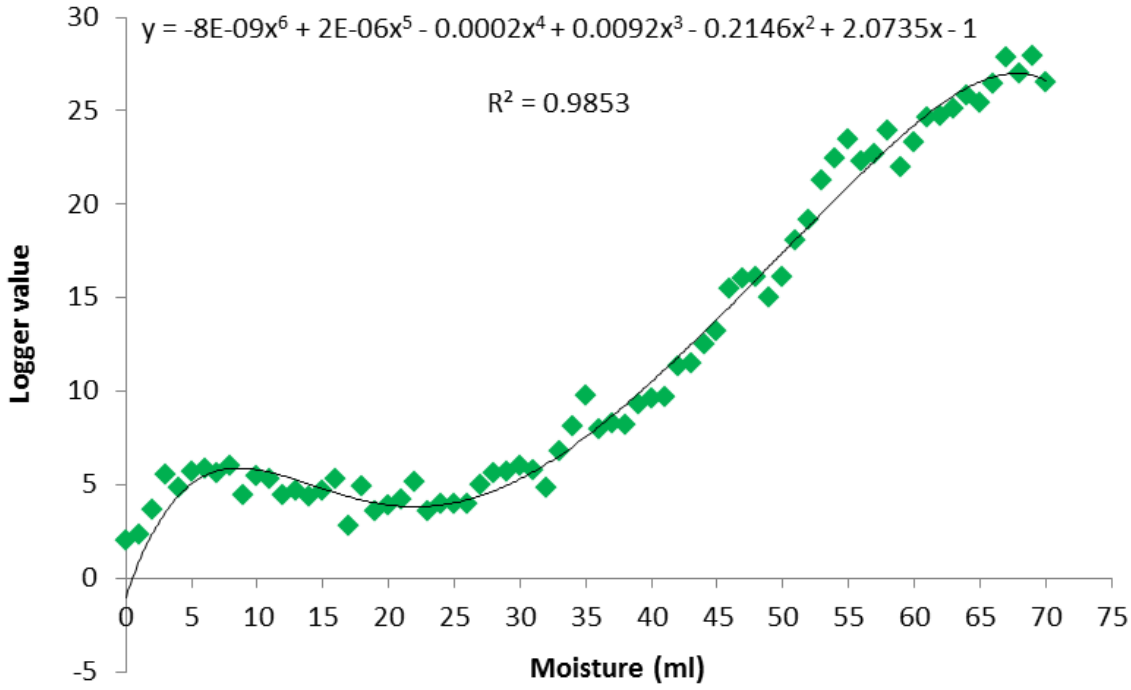

Figure 71: Soil specific moisture calibration polynomial, Vesleskarvet

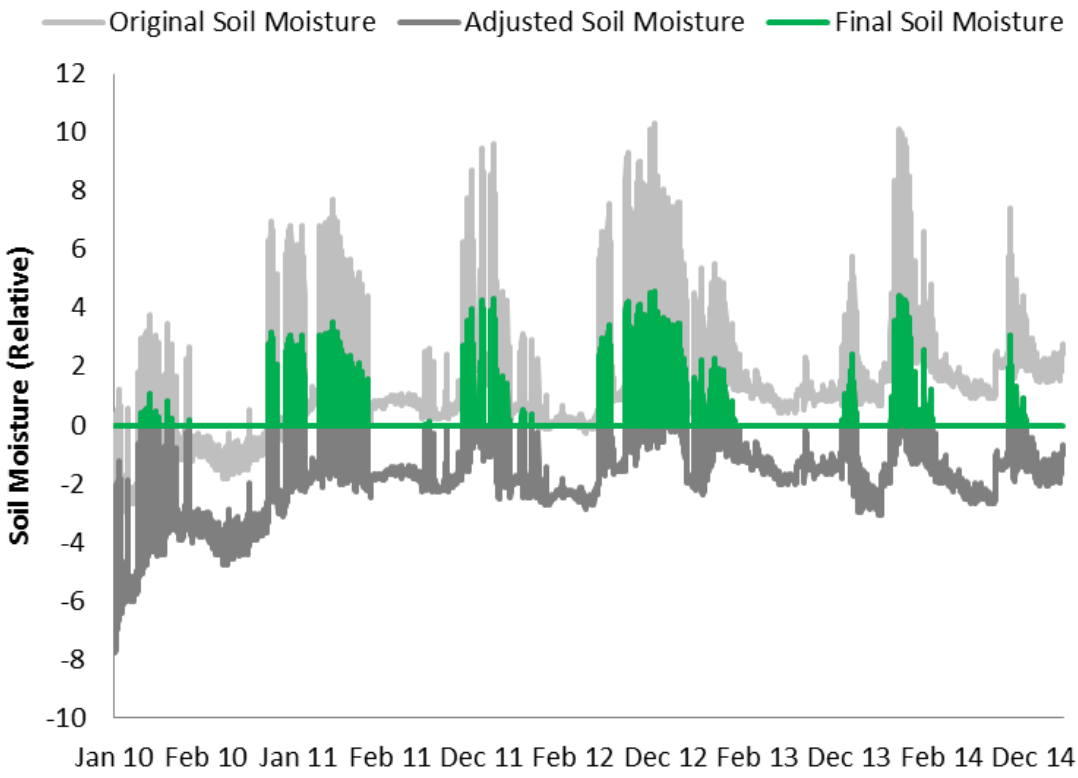

Figure 72: Original, adjusted and final soil moisture values for Vesleskarvet.

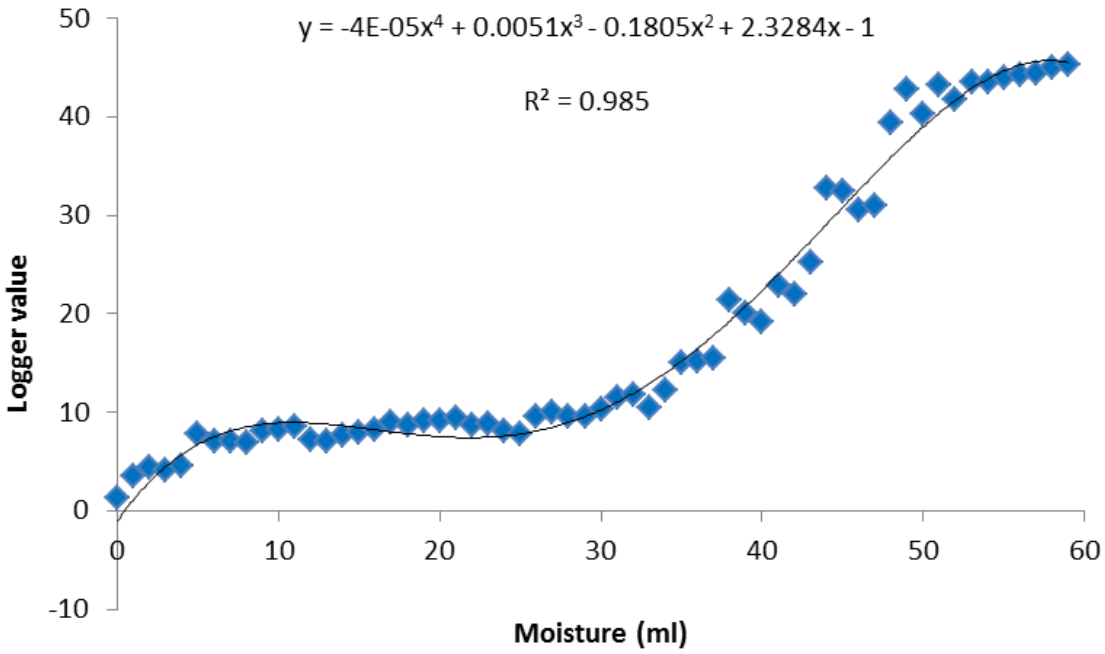

Figure 73: Soil specific moisture calibration polynomial, Flårjuven

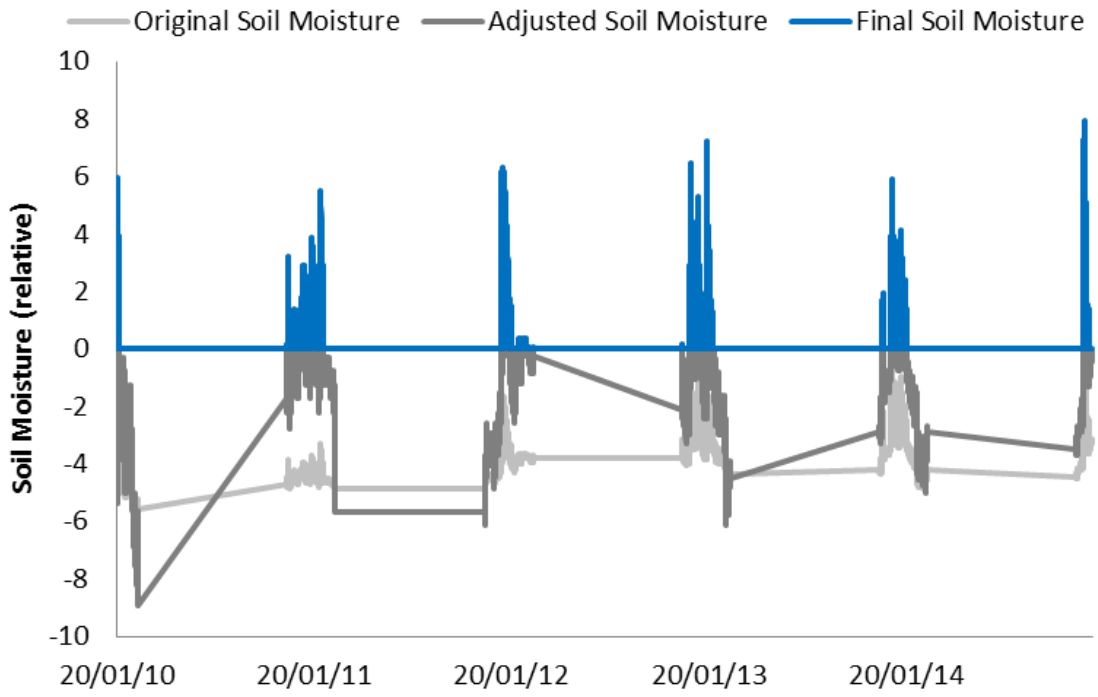

Figure 74: Original, adjusted and final soil moisture values for Flårjuven.

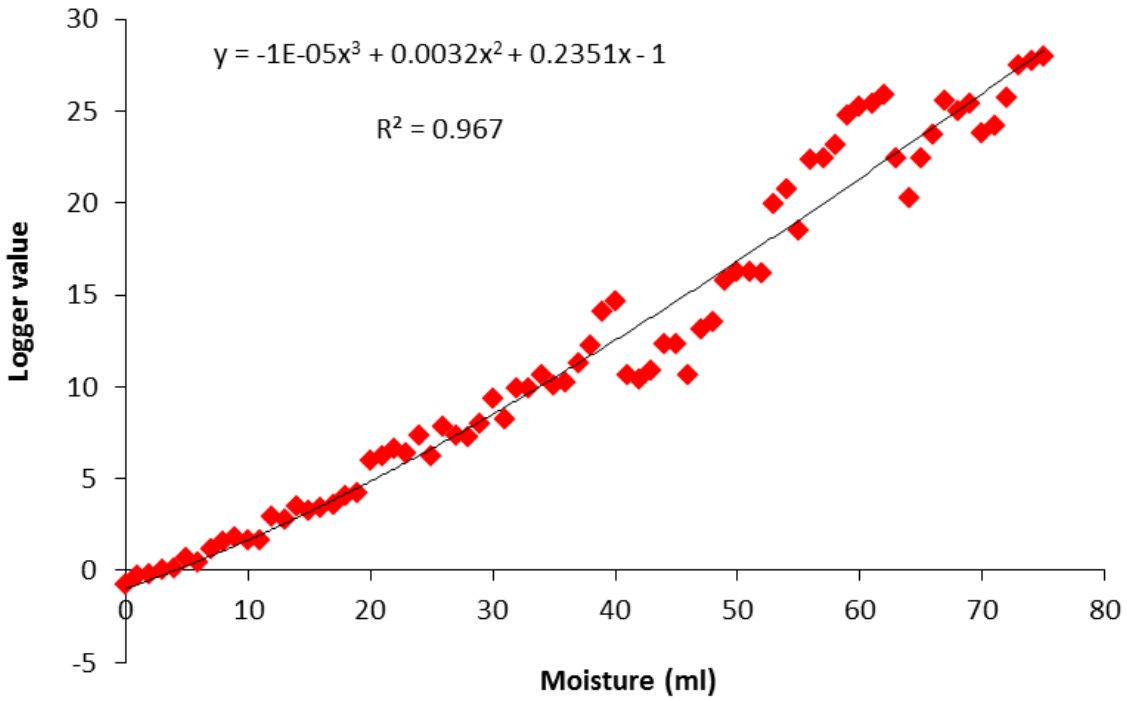

Figure 75: Soil specific moisture calibration polynomial, Robertskollen

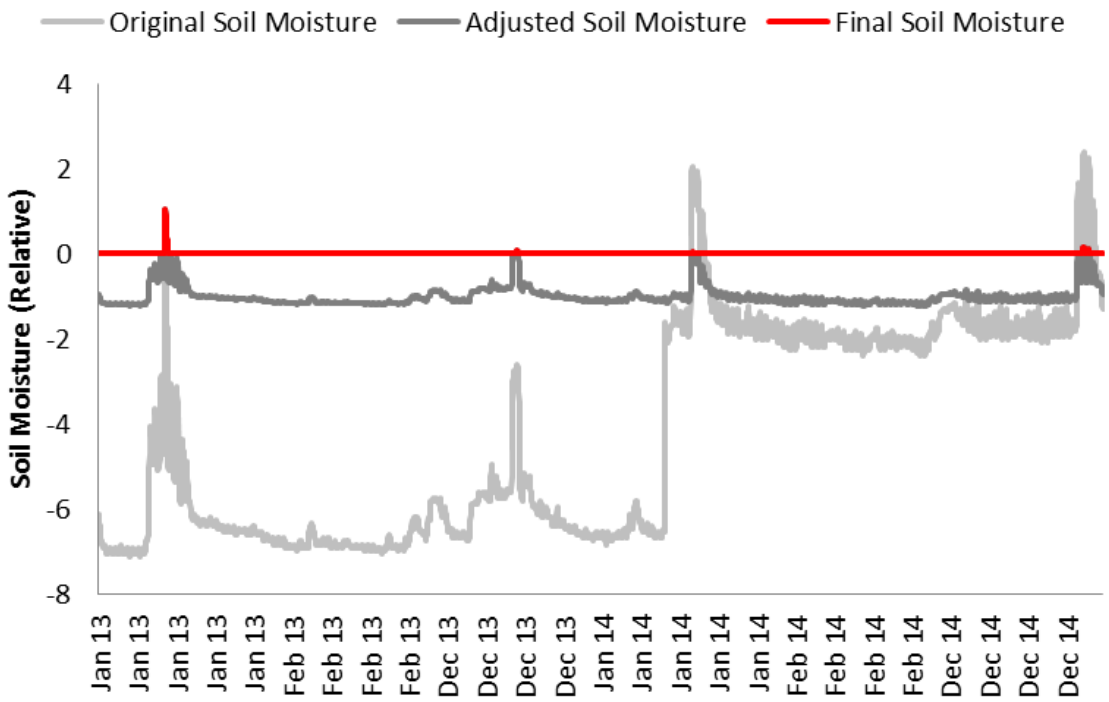

Figure 76: Original, adjusted and final soil moisture values for Robertskollen.

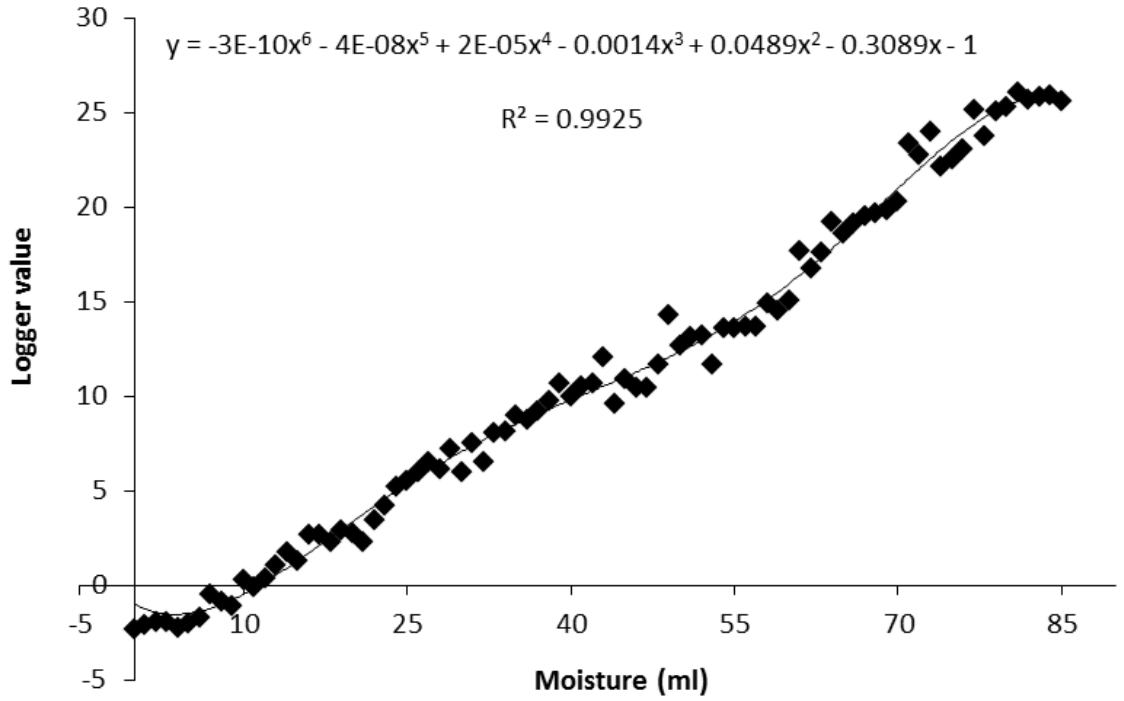

Figure 77: Soil specific moisture calibration polynomial, Nonshøgda

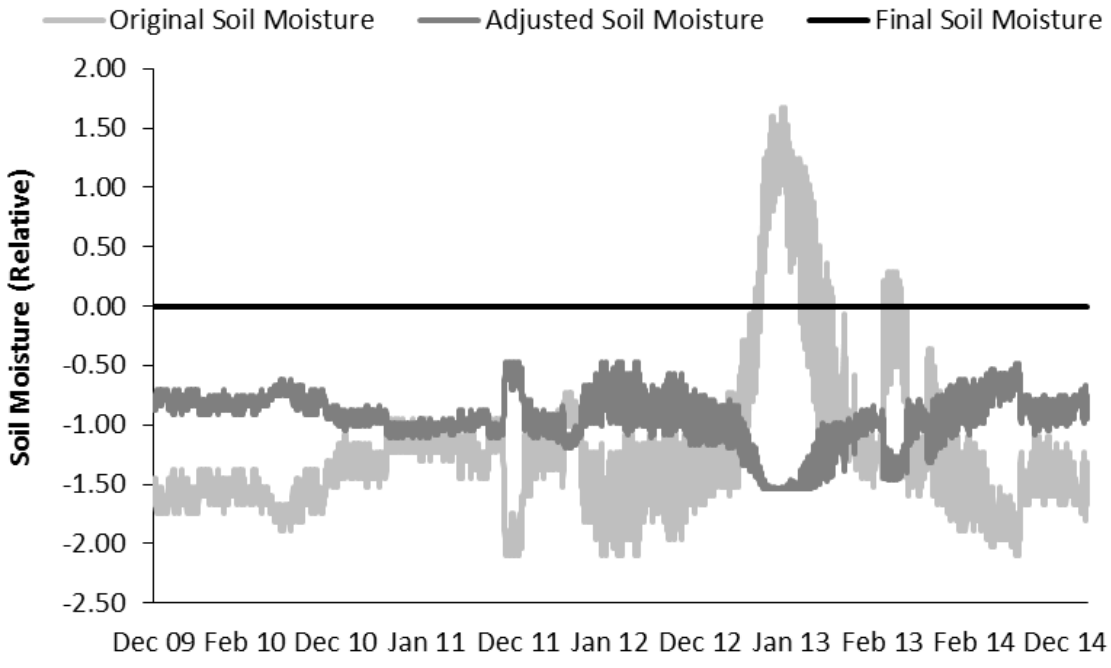

Figure 78: Original, adjusted and final soil moisture values for Nonshøgda

APPENDIX B: Statistical Descriptions, Ranges and Classes

Table 38: Descriptive terms and ranges used for skewness classes (Hansen, 2013)

Description	Range
Highly negatively skewed	<-1.62
Negatively skewed	-1.0 – -1.62
Moderately negatively skewed	-0.3 – -1.0
Finely negatively skewed	-0.3 – -0.1
Symmetrical	-0.1 – 0.1
Finely positively skewed	0.1 – 0.3
Positively skewed	0.3 – 1.0
Very positively skewed	1.0 – 1.62
Highly positively skewed	>1.62

Table 39: Descriptive terms and ranges used for correlation coefficients (Hansen, 2013)

Description	Range
Perfect downhill linear relationship	–1
Strong downhill linear relationship	–0.70
Moderate downhill linear relationship	–0.50
Weak downhill linear relationship	–0.30
No linear relationship	0
Weak uphill linear relationship	0.30
Moderate uphill linear relationship	0.50
Strong uphill linear relationship	0.70
Perfect uphill linear relationship	1

Table 40: Size grades of sedimentary particles (Briggs, 1977b)

Phi size (ø)	Millimetres (mm)	Micrometres (µm)	Wentworth grade
-6.0	64	64000	Cobbles 60.0mm
-5.5 -5.0 -4.5	44.8 32 22.4	448000 32000 22400	Coarse gravel 20.0mm
-4.0 -3.5 -3.0	16 11.2 8	16000 11200 8000	Medium gravel 6.0mm
-2.5 -2.0 -1.5 -1.0	5.6 4 2.8 2	5600 4000 2800 2000	Fine gravel 2.0mm
-0.5 0.0 0.5	1.4 1 0.71	1400 1000 710	Coarse sand 0.6mm
1.0 1.5 2.0	0.5 0.355 0.25	500 355 250	Medium sand 0.2mm
2.5 3.0 3.5 4.0	0.18 0.125 0.090 0.063	180 125 90 63	Fine sand 0.06mm
4.5 5.0 5.5	0.045 0.032 0.023	45 32 23	Coarse silt 0.02mm
6.0 6.5 7.0	0.016 0.032 0.008	16 11 8.0	Medium silt 0.006mm
7.5 8.0 8.5	0.0055 0.004 0.00275	5.5 4.0 2.75	Fine silt 0.002mm
9.0 9.5 10.0	0.002 0.00138 0.001	2.0 1.38 1.0	Clay

Table 41: Descriptive terms and ranges used for sediment sorting classes (Briggs, 1977b).

Description	Range
Very well sorted	<0.35
Well sorted	0.35 – 0.50
Moderately well sorted	0.50 – 0.70
Moderately sorted	0.70 – 1.00
Poorly sorted	1.00 – 2.00
Very poorly sorted	2.00 – 4.00
Extremely poorly sorted	> 4.00

APPENDIX C: Surfer Plots

Table 42: Vesleskarvet yearly active layer temperature vs depth profiles

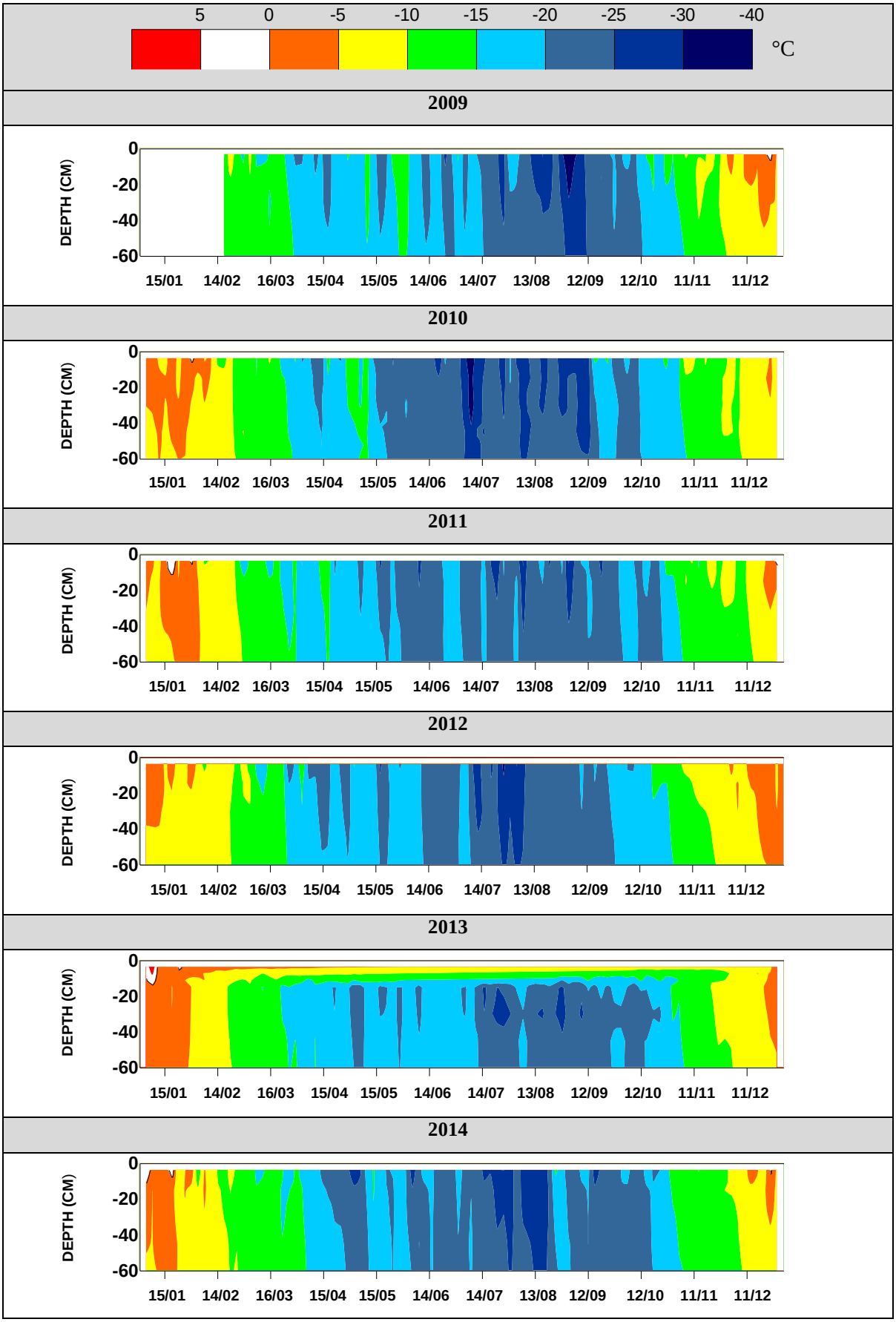

Table 43: Vesleskarvet summer active layer temperature vs depth profiles

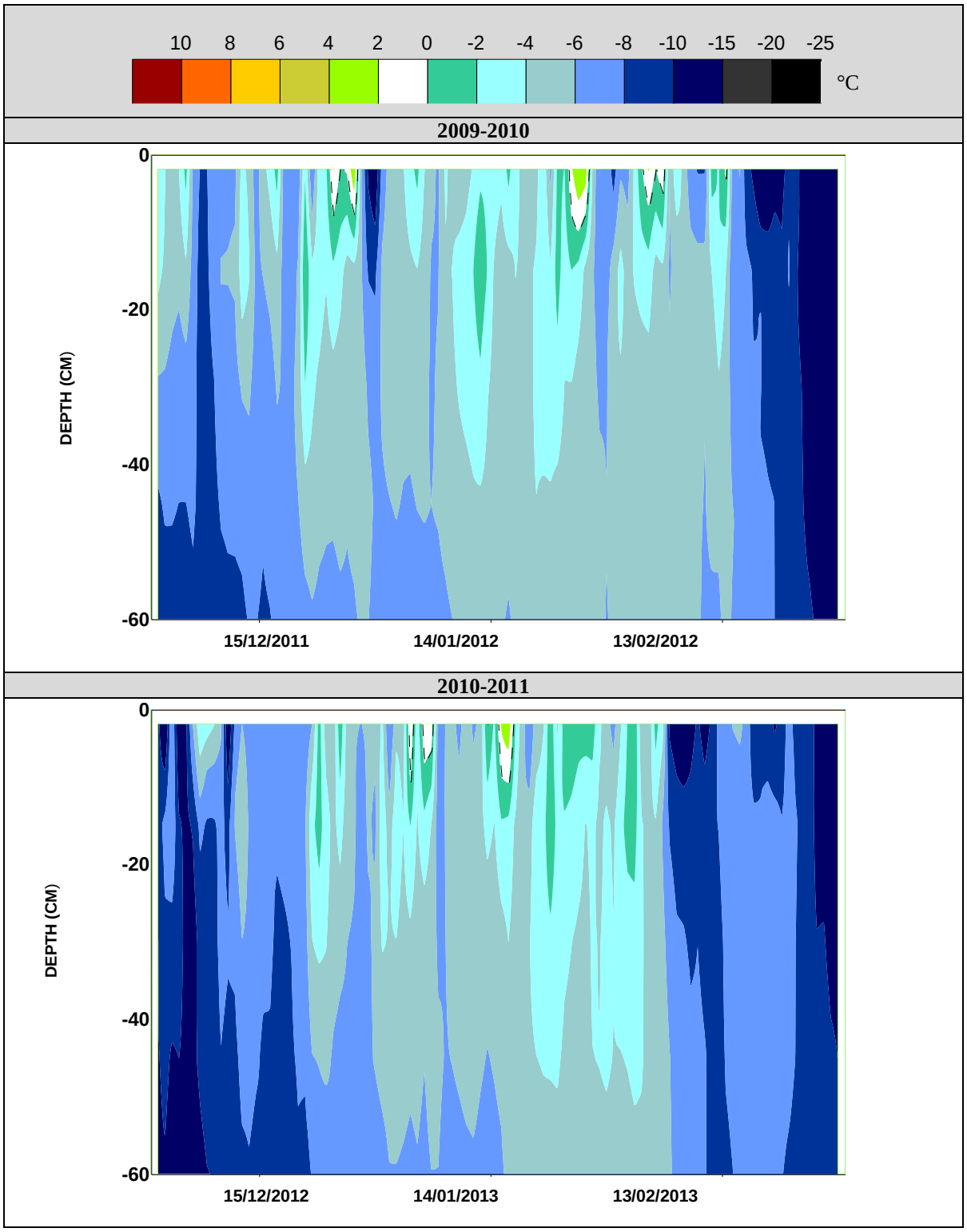

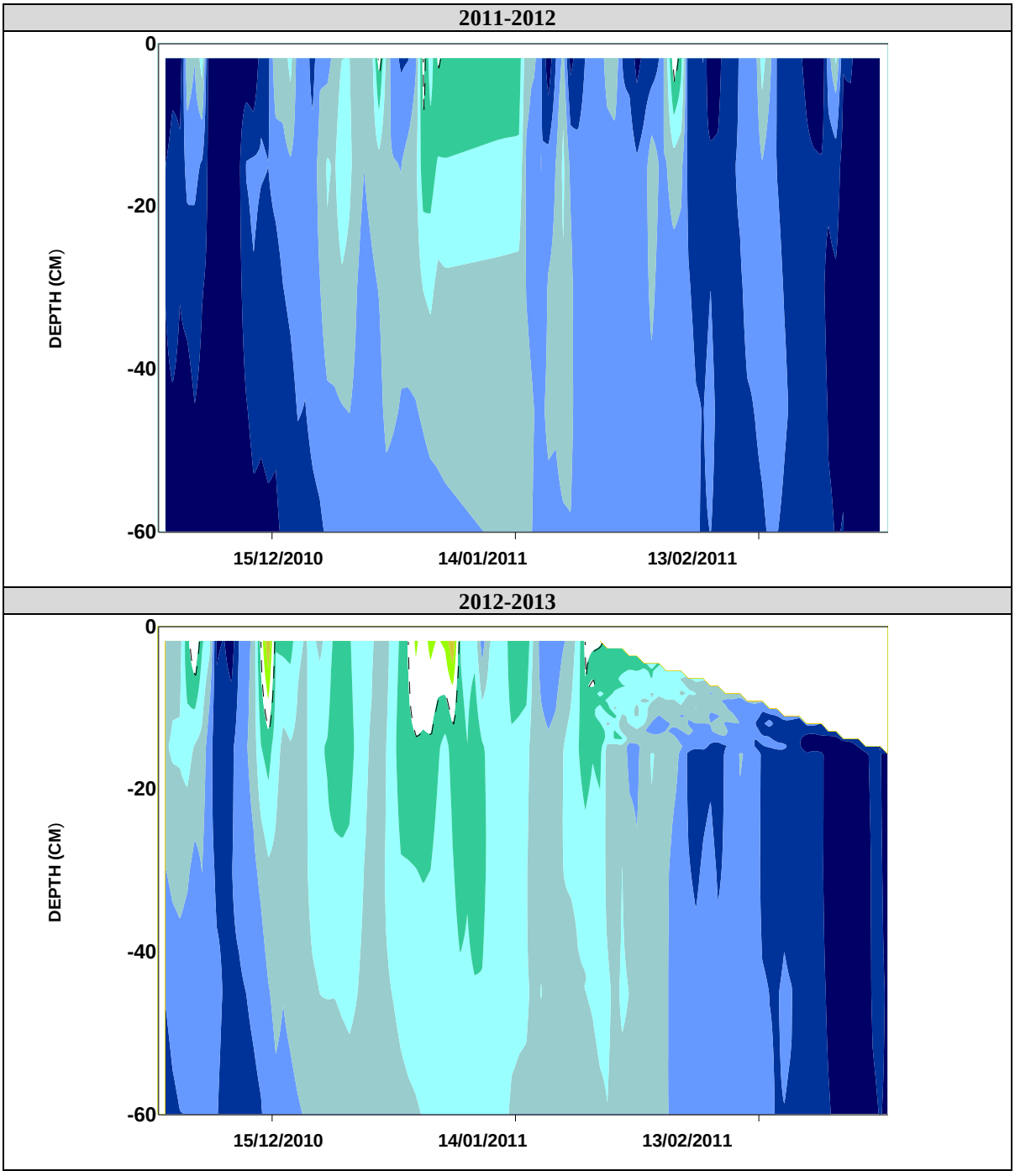
2011-2012
0
-20
-40
-60
DEPTH (CM)
15/12/2010
14/01/2011
13/02/2011
2012-2013
0
-20
-40
-60
DEPTH (CM)
15/12/2010
14/01/2011
13/02/2011

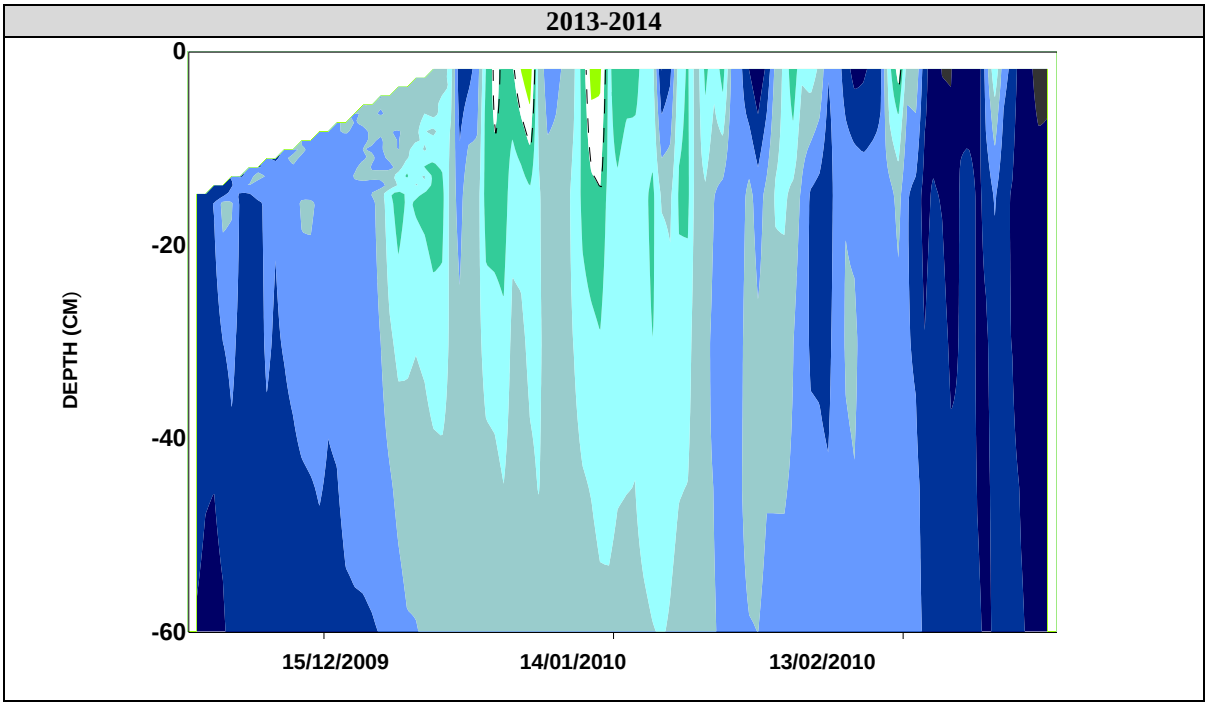
2013-2014
0
-20
-40
-60
DEPTH (CM)
15/12/2009
14/01/2010
13/02/2010

Table 44: Flårjuven yearly active layer temperature vs depth profiles

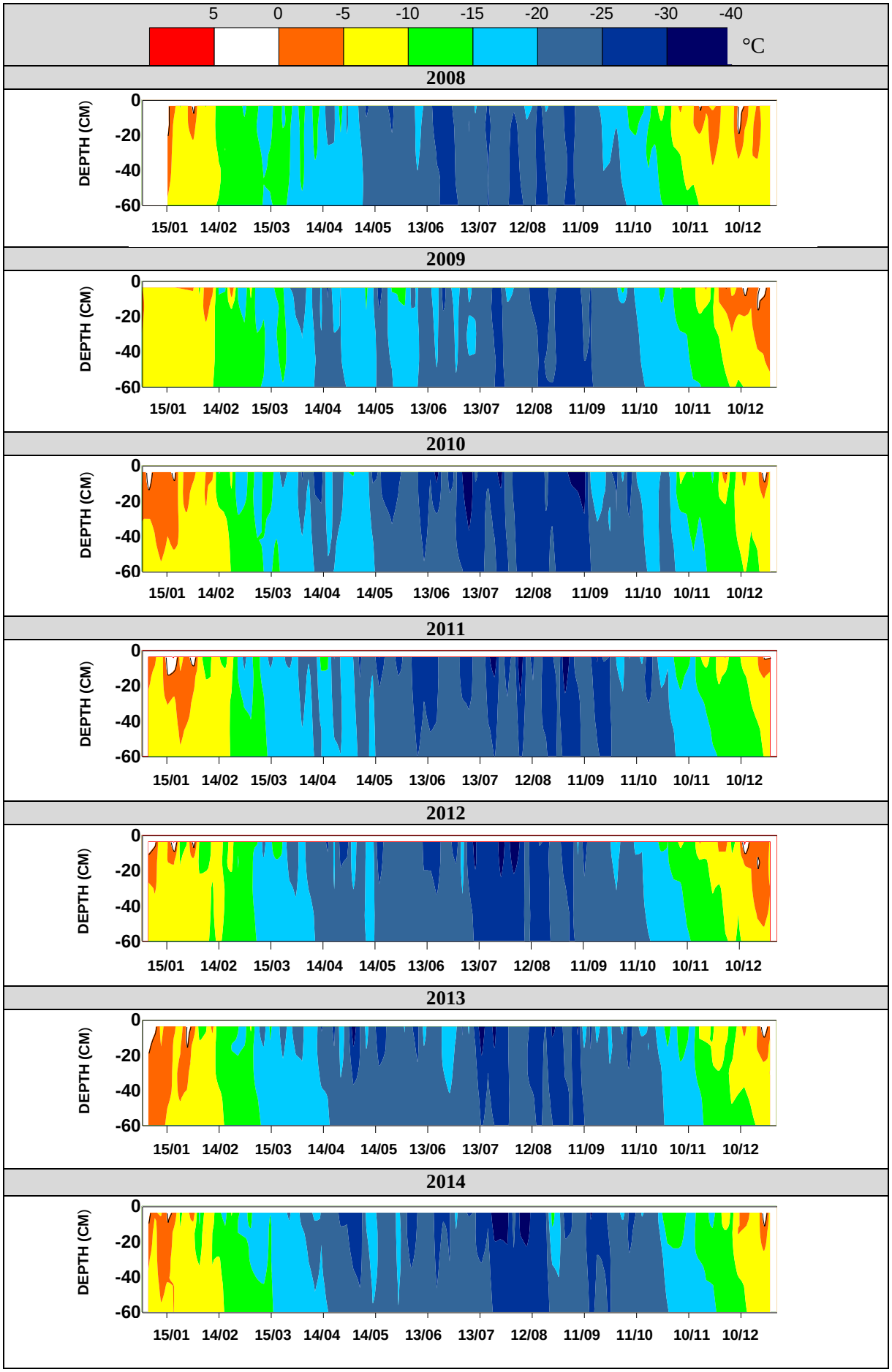

Table 45: Flårjuven summer active layer temperature vs depth profiles

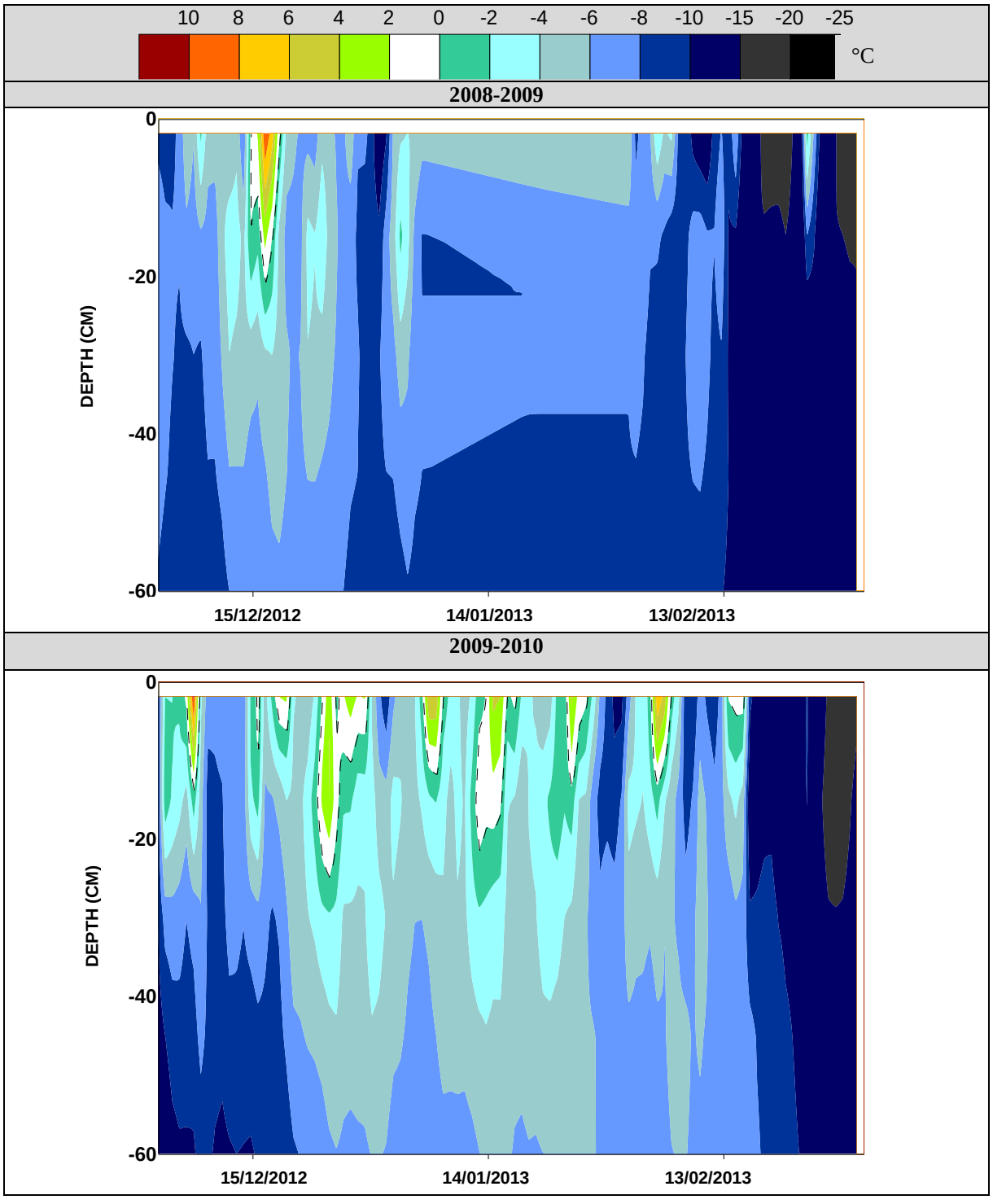

2010-2011

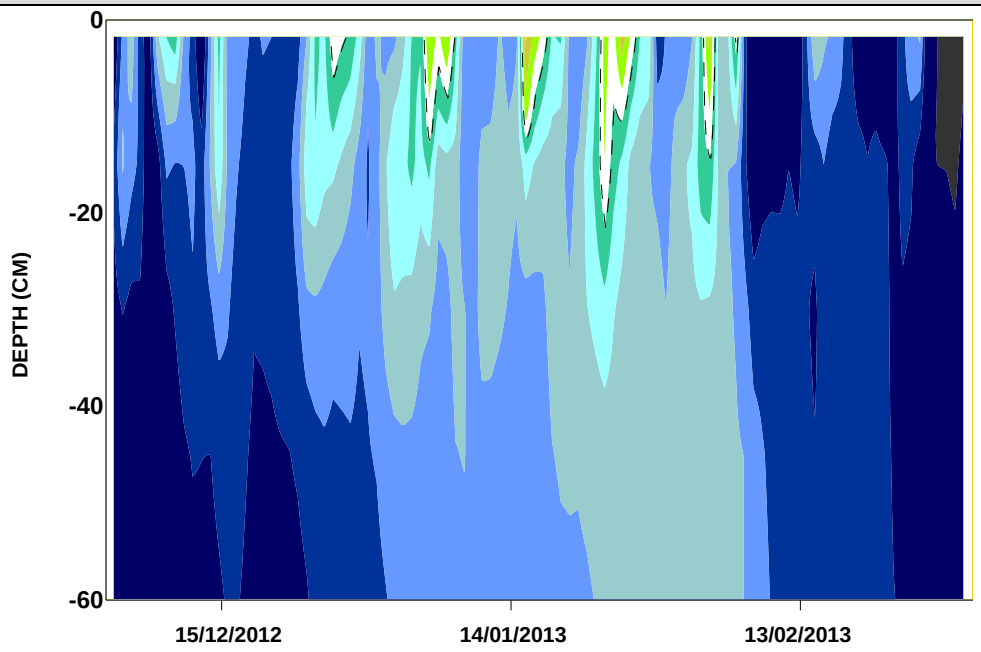

2011-2012

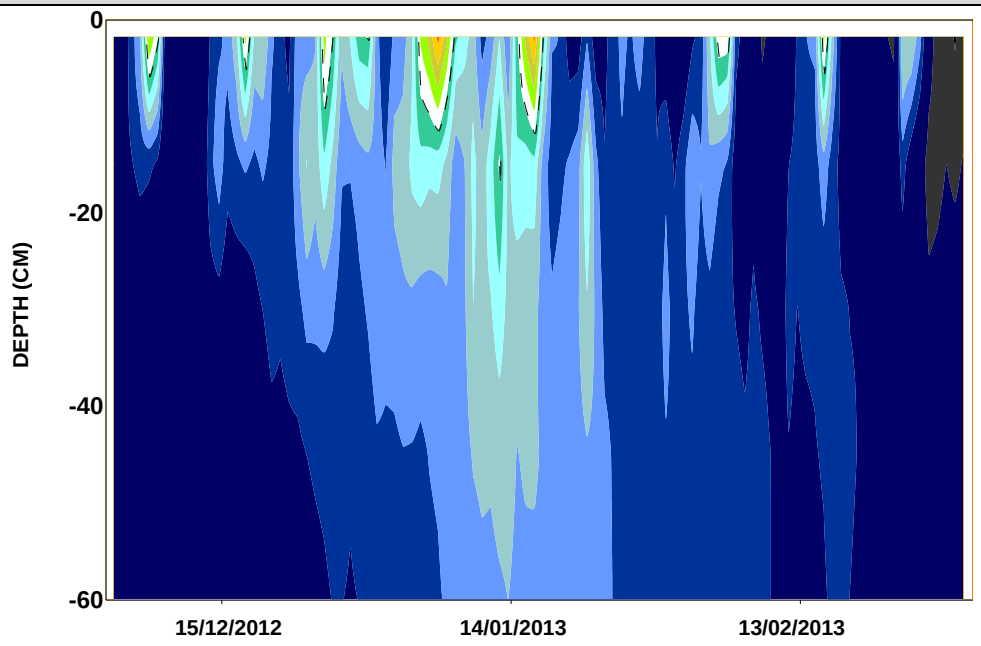

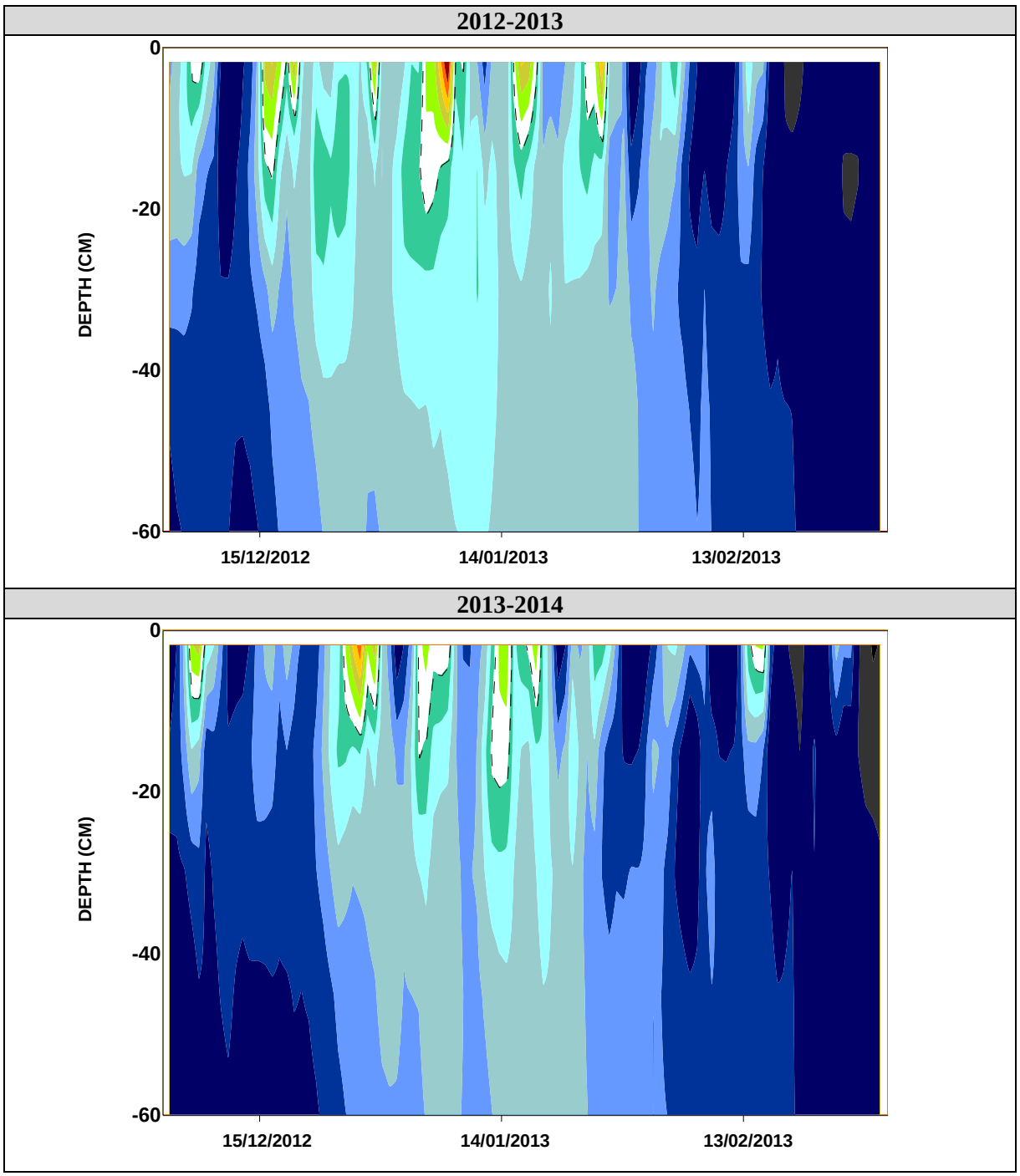
2012-2013
0
-20
-40
-60
DEPTH (CM)
15/12/2012
14/01/2013
13/02/2013
2013-2014
0
-20
-40
-60
DEPTH (CM)
15/12/2012
14/01/2013
13/02/2013

Table 46: Robertskollen yearly active layer temperature vs depth profiles

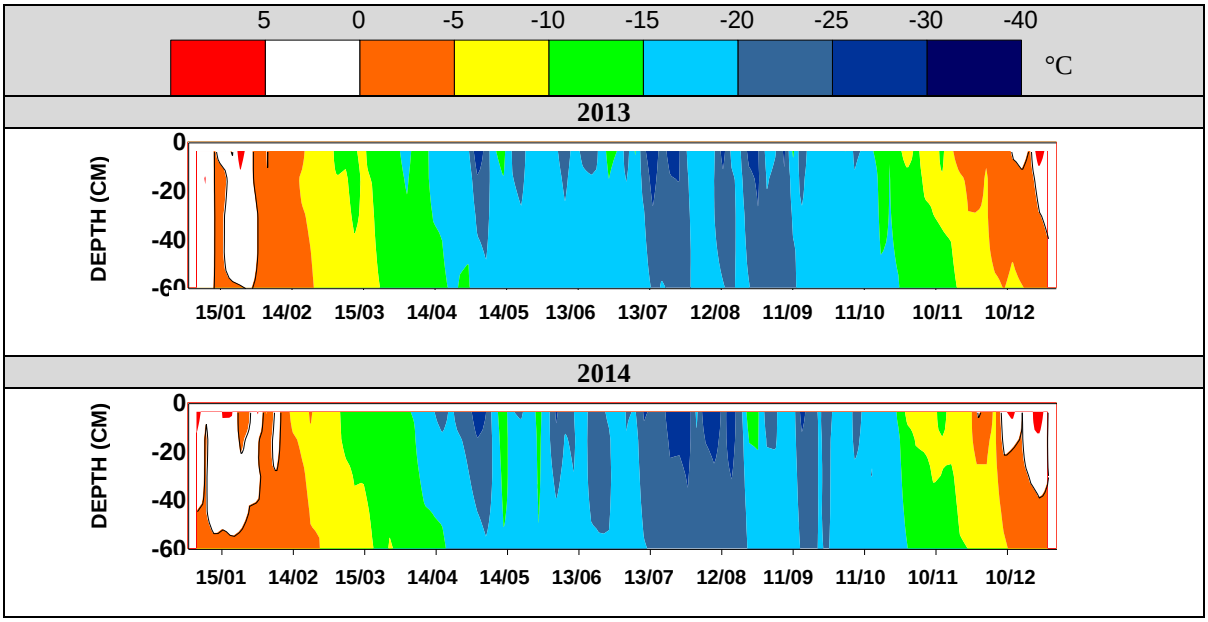

Table 47: Robertskollen summer active layer temperature vs depth profiles

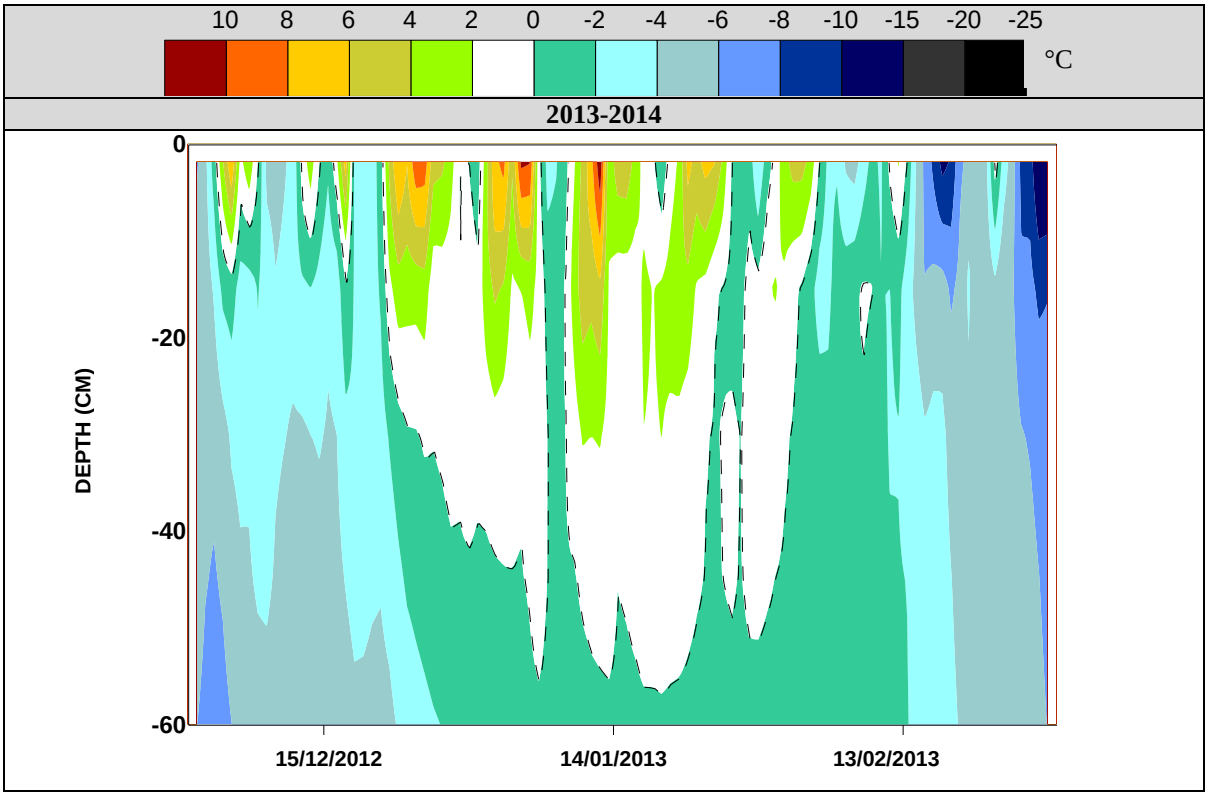

Table 48: Nonshøgda yearly active layer temperature vs depth profiles

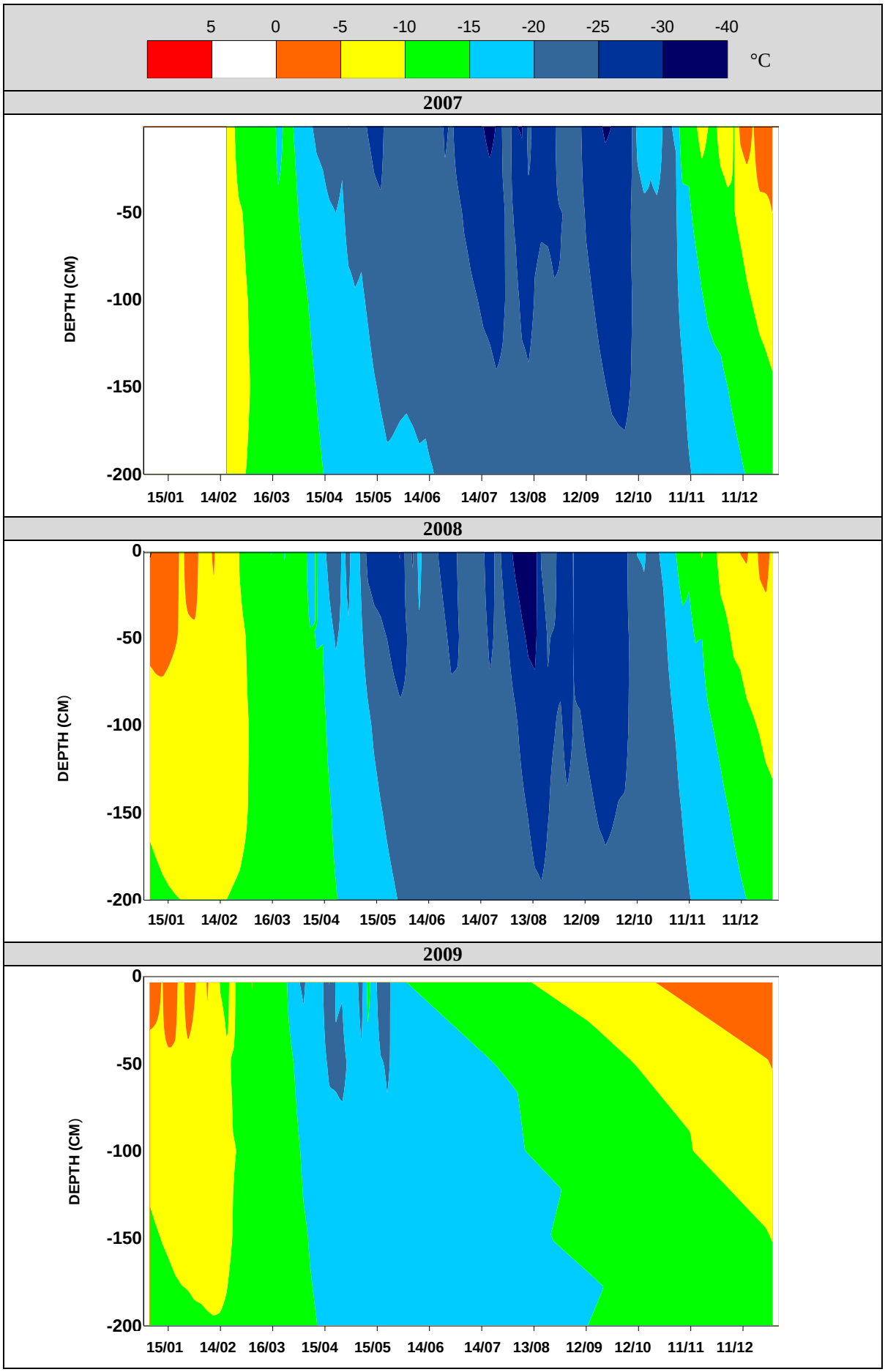

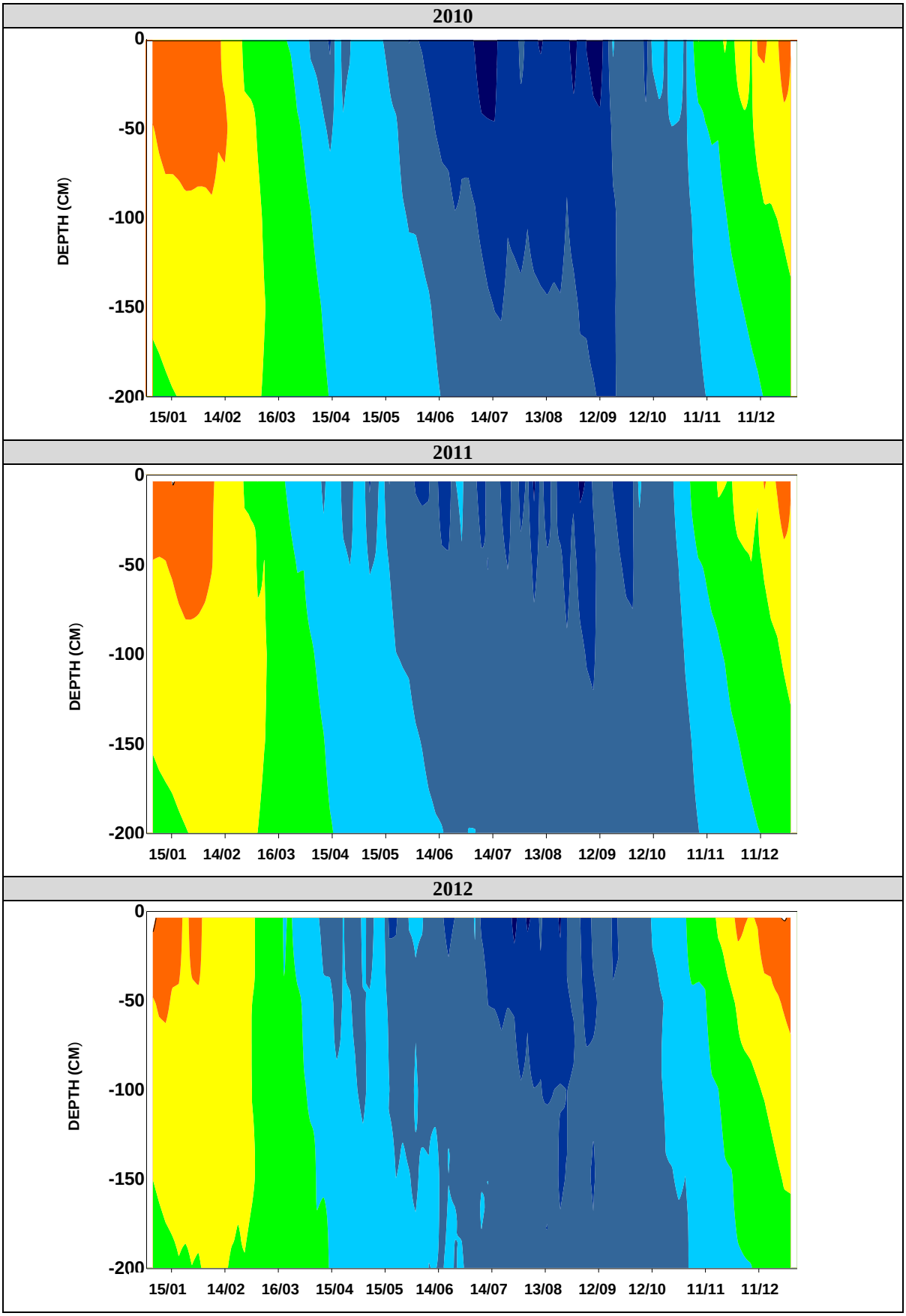
2010
0
-50
-100
-150
-200
DEPTH (CM)
15/01
14/02
16/03
15/04
15/05
14/06
14/07
13/08
12/09
12/10
11/11
11/12
2011
0
-50
-100
-150
-200
DEPTH (CM)
15/01
14/02
16/03
15/04
15/05
14/06
14/07
13/08
12/09
12/10
11/11
11/12
2012
0
-50
-100
-150
-200
DEPTH (CM)
15/01
14/02
16/03
15/04
15/05
14/06
14/07
13/08
12/09
12/10
11/11
11/12

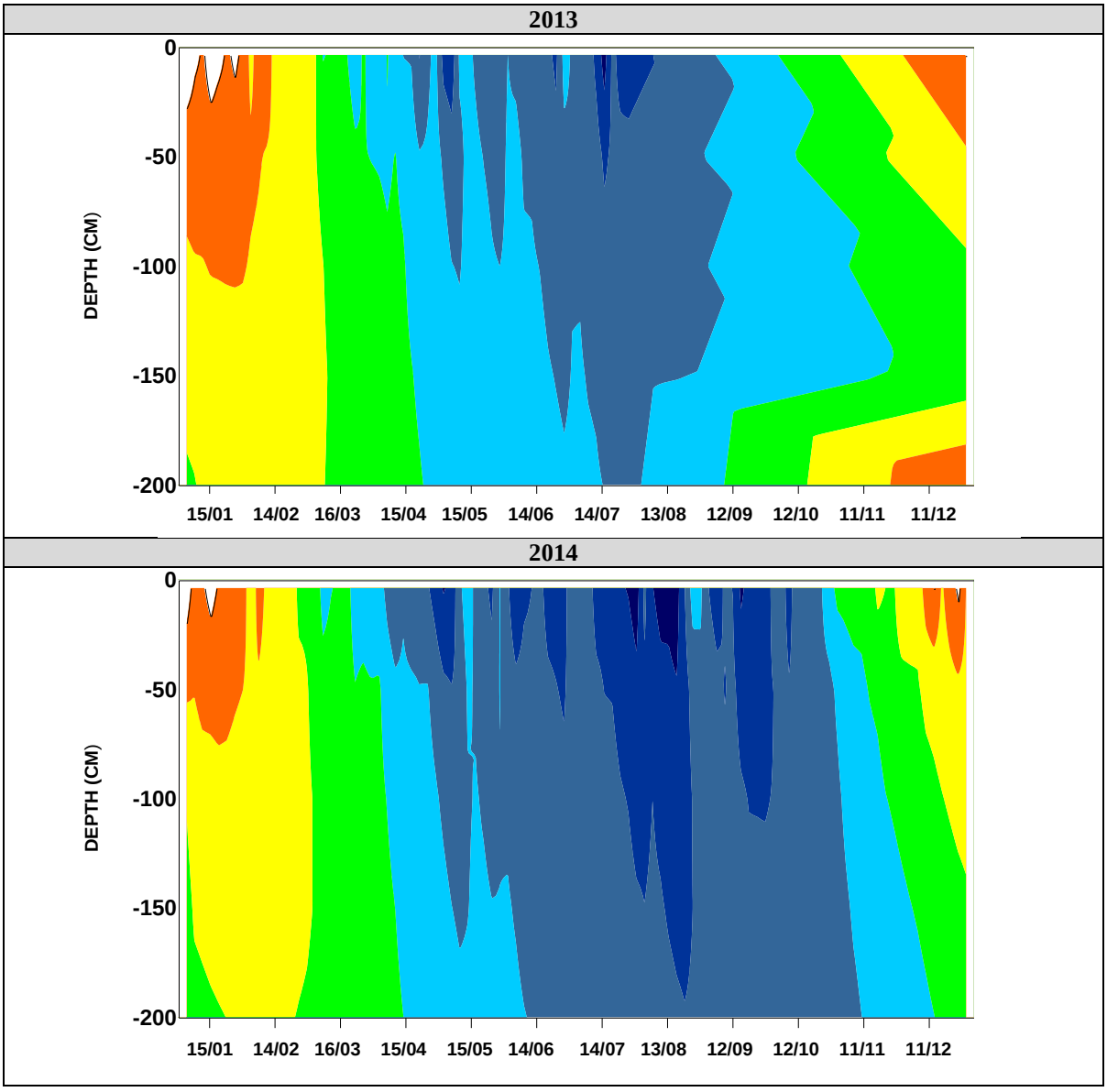
2013
0
-50
-100
-150
-200
DEPTH (CM)
15/01
14/02
16/03
15/04
15/05
14/06
14/07
13/08
12/09
12/10
11/11
11/12
2014
0
-50
-100
-150
-200
DEPTH (CM)
15/01
14/02
16/03
15/04
15/05
14/06
14/07
13/08
12/09
12/10
11/11
11/12

Table 49: Nonshøgda summer active layer temperature vs depth profiles, 200cm vs 50cm

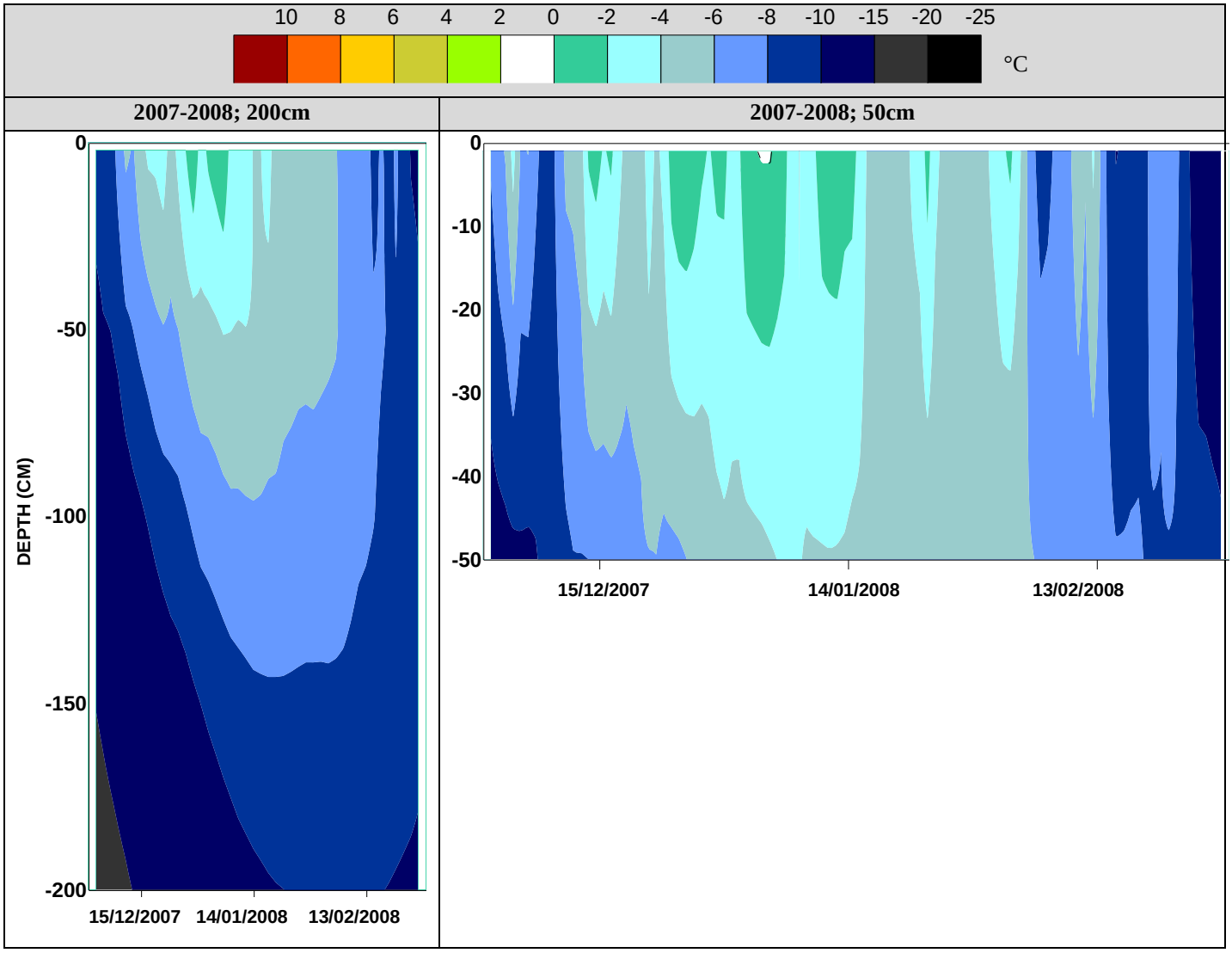

2008-2009; 200cm	2008-2009; Summer 50cm
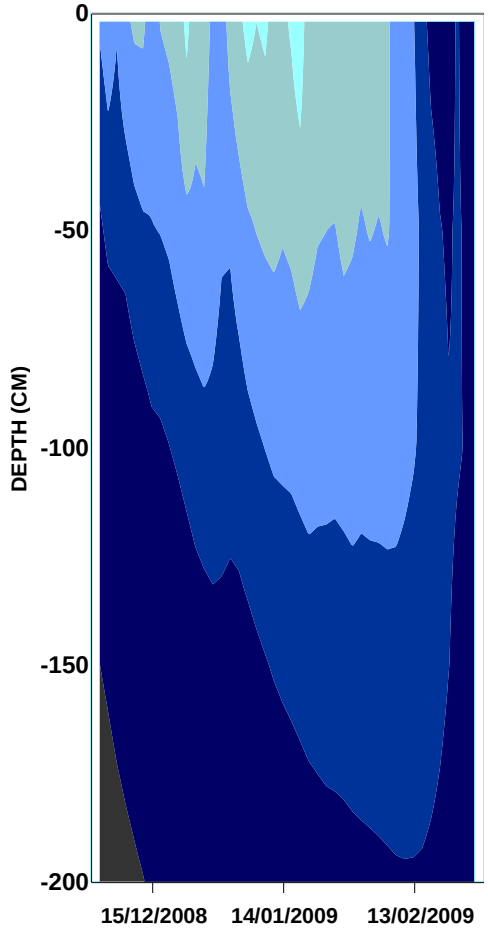	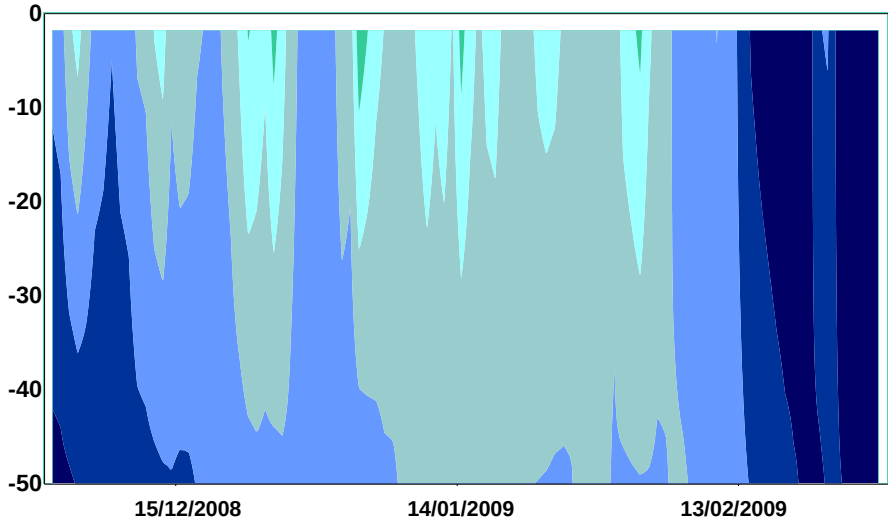

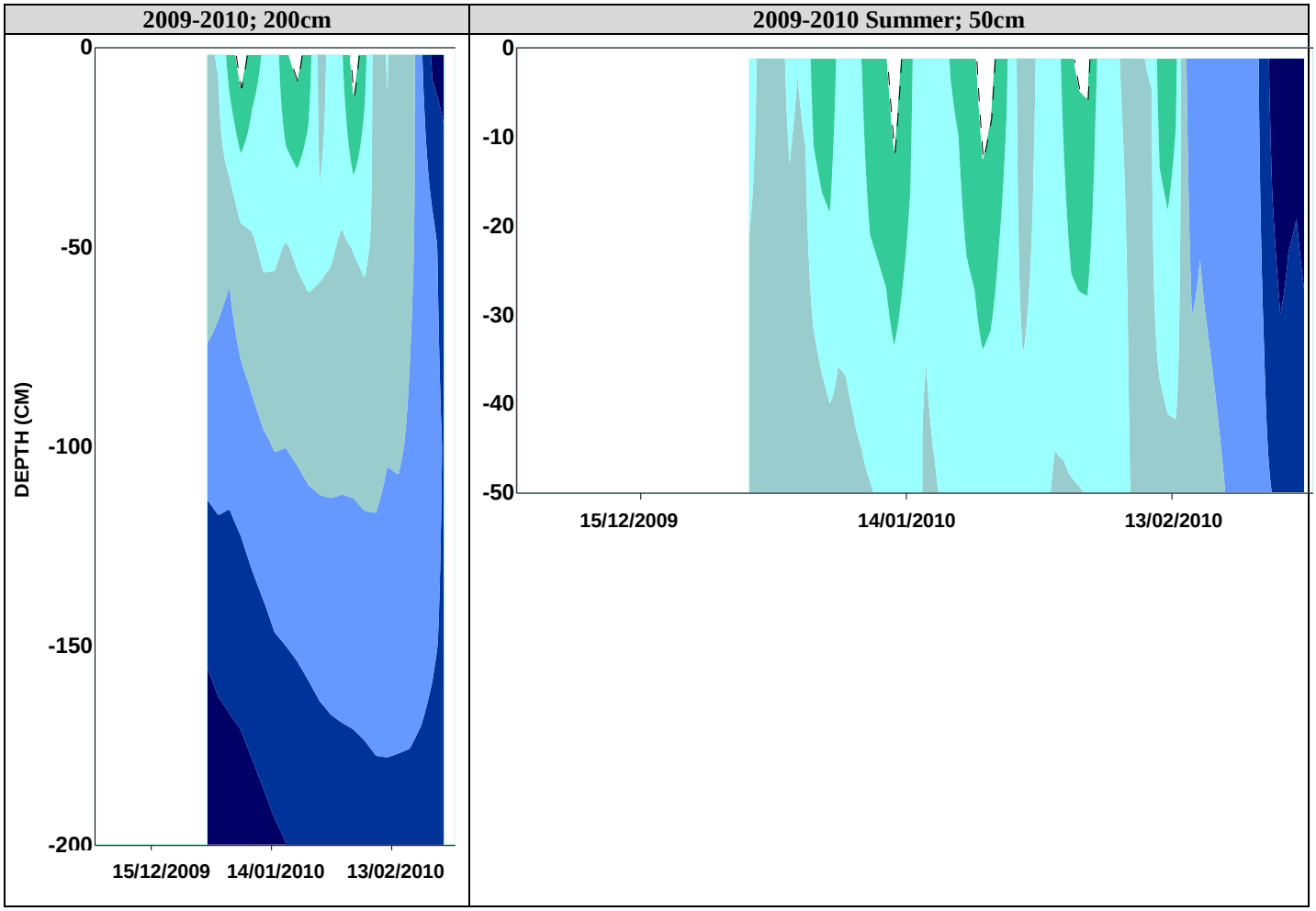
2009-2010; 200cm
2009-2010 Summer; 50cm
DEPTH (CM)
0
-50
-100
-150
-200
15/12/2009
14/01/2010
13/02/2010
0
-10
-20
-30
-40
-50
15/12/2009
14/01/2010
13/02/2010

2010-2011; 200cm	2010-2011; 50cm
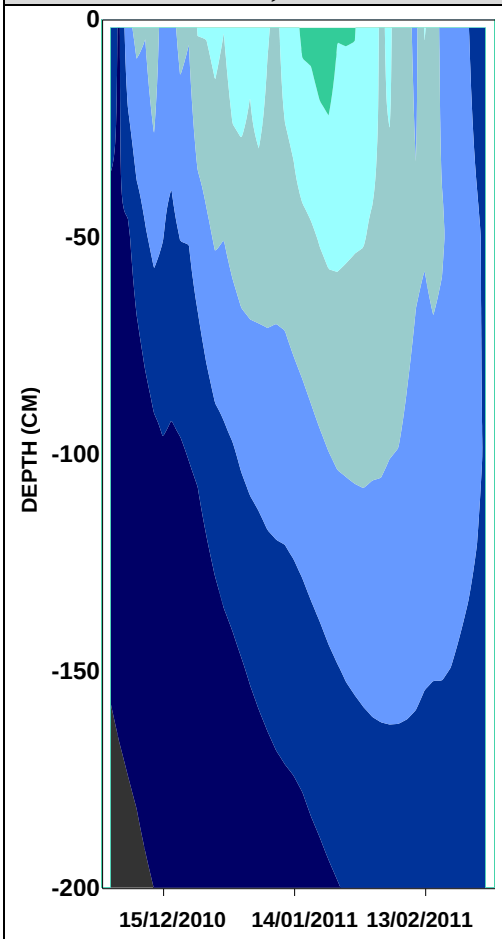	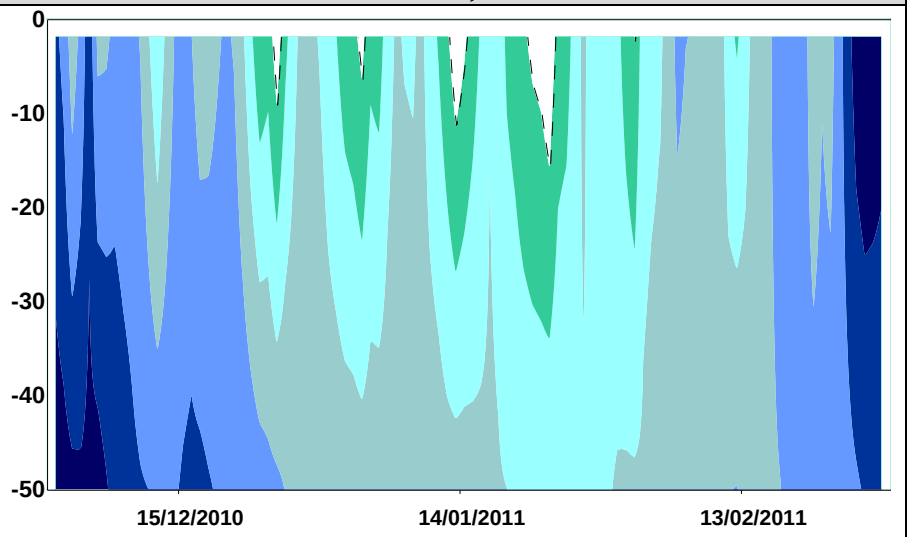

2011-2012; 200cm	2011-2012; 50cm
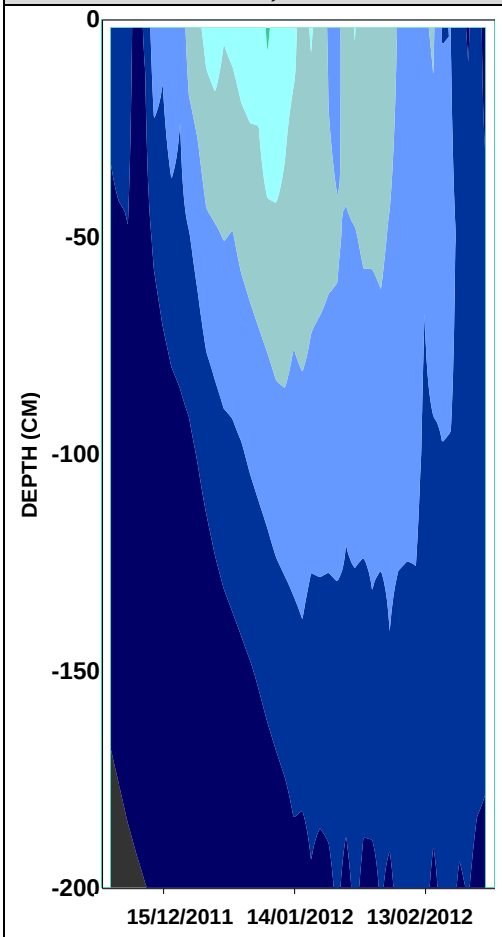	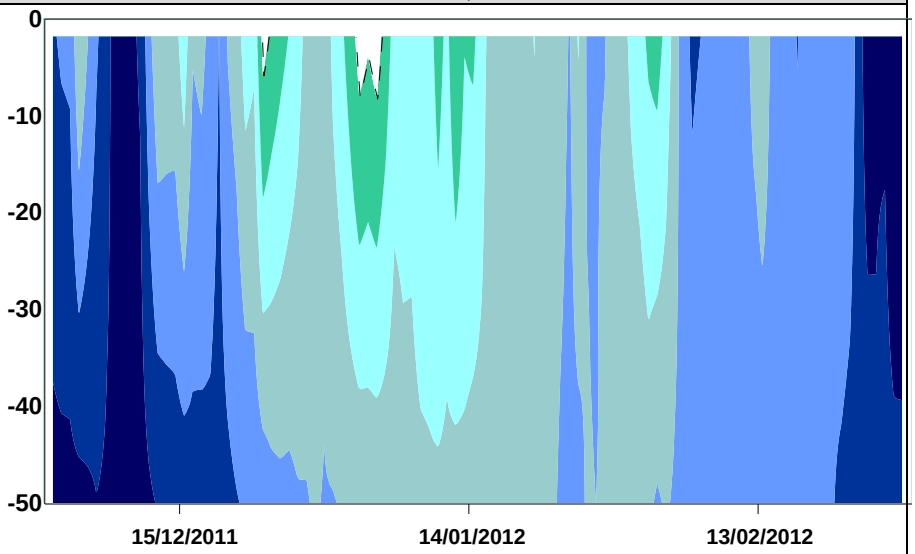

2012-2013; 200cm	2012-2013; 50cm
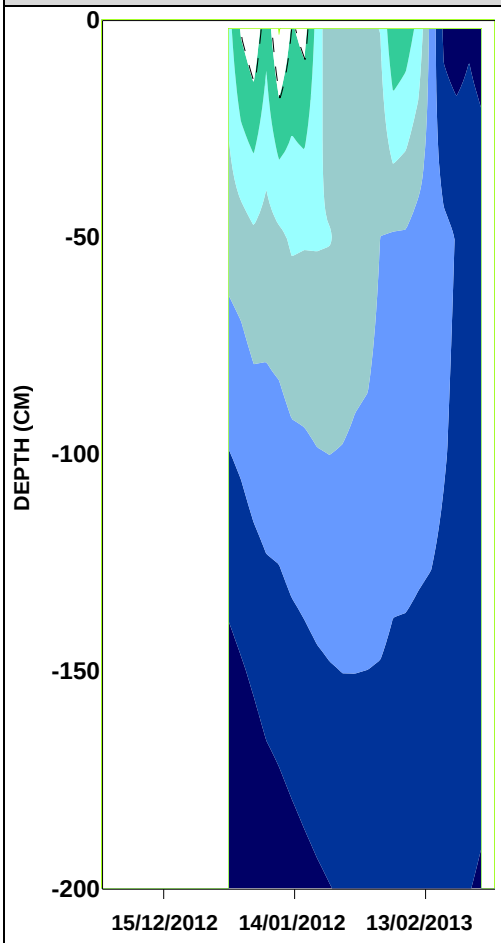	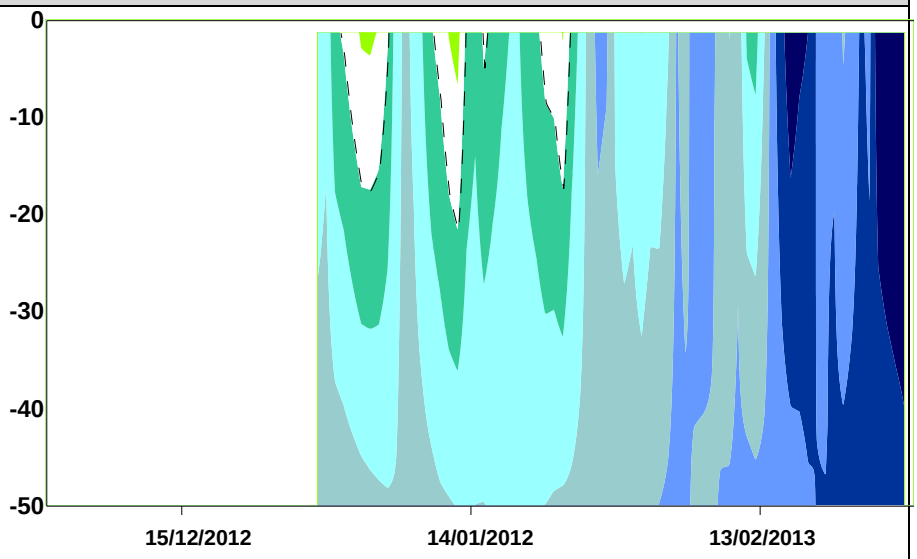

2013-2014; 200cm	2013-2014; 50cm